uOttawa

L'Université canadienne
Canada's university

FACULTÉ DES ÉTUDES SUPÉRIEURES ET POSTDOCTORALES

uOttawa

L'Université canadienne
Canada's university

FACULTY OF GRADUATE AND POSTDOCTORAL STUDIES

Selena Sagan

AUTEUR DE LA THÈSE / AUTHOR OF THESIS

Ph.D. (Microbiology and Immunology)

GRADE / DEGREE

Department of Biochemistry, Microbiology and Immunology

FACULTÉ, ÉCOLE, DÉPARTEMENT / FACULTY, SCHOOL, DEPARTMENT

Development of Protein- and RNA-based Tools for Studying Small RNAs Using *Tombusvirus* p19 and Native RNA Microarrays

TITRE DE LA THÈSE / TITLE OF THESIS

J. Pezachi

DIRECTEUR (DIRECTRICE) DE LA THÈSE / THESIS SUPERVISOR

N. Goto

CO-DIRECTEUR (CO-DIRECTRICE) DE LA THÈSE / THESIS CO-SUPERVISOR

EXAMINATEURS (EXAMINATRICES) DE LA THÈSE / THESIS EXAMINERS

J. Côté

K. Dimock

I. MacRae

S. Sad

Gary W. Slater

Le Doyen de la Faculté des études supérieures et postdoctorales / Dean of the Faculty of Graduate and Postdoctoral Studies

Development of Protein- and RNA-based Tools for Studying Small RNAs Using *Tombusvirus* p19 and Native Target RNA Microarrays

Selena M. Sagan

Thesis submitted to the
Faculty of Graduate and Postdoctoral Studies
In partial fulfillment of the requirements for the
PhD degree in Microbiology & Immunology

Department of Biochemistry, Microbiology & Immunology
Faculty of Medicine
University of Ottawa

Your file Votre référence
ISBN: 978-0-494-61384-9
Our file Notre référence
ISBN: 978-0-494-61384-9

Abstract

Over the past decade, small RNAs have emerged as important regulators of eukaryotic messenger RNAs (mRNAs). Short-interfering RNAs (siRNAs) and microRNAs (miRNAs) participate in 'RNA silencing' pathways that regulate transcription, chromatin structure, genome integrity, translation, and mRNA stability. Both types of small RNAs can be functionally equivalent, but they are distinguished by their origin. Herein, novel protein- and RNA-based tools for studying RNA silencing and small RNAs are described.

Detection, purification, and quantification of small RNAs is important for gaining an understanding of the roles of RNA silencing pathways in eukaryotic organisms. This thesis describes the development of the tombusviral p19 protein, which is a suppressor of RNA silencing, as a tool to study small RNAs. The siRNA-binding properties of the p19 protein *in vitro* were investigated and an assay for high-throughput siRNA detection and quantification was developed. Furthermore, a small molecule library was screened to identify small molecule inhibitors of the p19-siRNA interaction. These studies identified small molecules that act as potent inhibitors of the p19-siRNA interaction by alkylation of cysteine residues. Mutagenesis revealed novel postulates regarding the role of cysteine residues within the p19 protein. The specificity of p19-small RNA interactions was also investigated using fluorescence-based techniques in order to determine the affinity of p19 for irregularly-structured small RNAs. Differential binding affinities of p19 to canonical and irregularly structured small RNAs has implications for the use of p19 as a tool for detection, purification and quantification of small RNAs *in vitro* and in diverse eukaryotic organisms.

In addition to developing protein-based tools to study small RNAs, we also wanted to investigate the effects of target site accessibility on the design of highly effective siRNAs. Thus, the importance of target site accessibility in the design of effective siRNAs against highly-structured targets was investigated using the Hepatitis C virus (HCV) RNA genome as a model. Since siRNA knockdown is hampered by target site accessibility, and current computational approaches are not yet able to reliably predict accessibility for large target RNAs, an *in vitro* screening approach for target site accessibility was developed. Native HCV target RNA microarrays were used to predict the potency of small RNAs directed against the HCV replicon RNA genome. This technique could be useful for the identification of novel, highly potent siRNA target sites within the large, highly-structured HCV RNA genome. Our results suggest that the highly-structured nature of the HCV RNA genome may impede the design of highly-effective siRNA-based inhibitors for this important human pathogen. In addition, the methodology described here could be extended to other systems, including the highly-structured genomes of other human pathogens.

Acknowledgements

To begin, I would like to express my sincere gratitude to my supervisors Dr. Natalie Goto and Dr. John Paul Pezacki, who guided me through my graduate studies. You both have had a great influence on my development. I thank Natalie for taking a chance on an unknown kid and for providing me with many helpful suggestions when I seemed to have reached my wits end. I thank John for his guidance, encouragement and unwavering support over the past five years. Without a doubt, his mentorship has been invaluable to my growth as a scientist. John provided me with an incredible environment in which to flourish as he encouraged and supported my independent research ideas from day one. I also very much appreciated his insights during our discussions (scientific and otherwise) which always gave me much to think about. His incredible mentorship always made me feel that I was a peer rather than a trainee; and this was appreciated more than he will ever know. It is this that I take with me, along with his contagious enthusiasm and excitement for science.

I am also very grateful to all of my colleagues at the NRC with whom I have had the pleasure of working with over the past five years. I would like to extend thanks to Mauro Tomietto and Dr. Zygmunt Jakubek for their help with AFM and fluorescence polarization, respectively. I am truly grateful to Yanouchka Rouleau who helped me perform some of my first experiments in the lab, and who, together with Sylvie Bélanger and Dr. Angela Tonary, was always around to discuss results with (good, bad or otherwise). I am indebted to Dr. Roger Koukiekolo whom I set up some of the first p19 experiments with, and Christian Luebbert, without whom I never would have gotten anywhere with microarrays. I am especially thankful for my interactions with Jenny

Cheng. Without her savvy hands, novel insights, patience, friendship and laughter, I may not have gotten through the latter half of this degree. We made a wonderful team (are you sure you don't want to come with me? ☺). For their friendship and willingness to provide new insights into my research (especially if it was over beers), my sincerest thanks go to Matthew Noestheden and Dr. David 'Council Chambers' Kennedy. To all the other graduate students, TOs, post-docs, and undergraduates I have had the pleasure of working with, thank you for providing an exceptional environment in which to learn and grow. Thanks also to my colleagues at the University of Ottawa, especially Dr. Ken Dimock and my advisory committee members, Dr. Kathryn Wright and Dr. Daniel Figeys. Their knowledge and guidance was much appreciated.

My family have been immensely supportive over the course of my education, even when they had more important things to deal with. My parents (John and Debra) and sister (Melissa) have always believed in my potential and encouraged me in all my pursuits, even when I didn't believe in myself. In addition, my extended family (especially Uncle Nick) has given me much confidence and always whole-heartedly supported my endeavours. Thank you all for your support in the good times and especially during the bad ones.

Finally, I would also like to acknowledge Chris for his patience and support. Your passion and enthusiasm in your own pursuits encouraged me to pursue my own with fervour. Thank you for being a part of my life.

Table of Contents

List of Abbreviations

AC	Acoustic
ADK	Adenosine kinase
ADP	Adenosine Diphosphate
AFM	Atomic Force Microscopy
AGO	Argonaute
ARM	Arginine-Rich Motif
ATP	Adenosine Triphosphate
bp	Base Pair
BSA	Bovine Serum Albumin
BV	Bunyavirus
BVDV	Bovine Viral Diarrhoea Virus
CaM	Calmodulin
CD	Circular Dichroism
cDNA	complementary DNA
CIRV	Carnation Italian Ringspot Virus
Cj	*Campylobacter jejuni*
CP	Coat Protein
CSFV	Classical Swine Fever Virus
CSK	Carboxyl-terminal Src Kinase
CTP	Cytidine Triphosphate
Cy3	Cyanine-3
Cy5	Cyanine-5
DCL	Dicer-Like
DHV	Duck Hepatitis Virus
DMEM	Dulbecco's Modified Eagle Medium
DNA	Deoxyribonucleic Acid
dsRNA	Double-Stranded RNA
DTT	Dithiothreitol
EDTA	Ethylenediaminetetraacetic Acid
E_m	Emission

EMCV	Encephalomyocarditis Virus
EMSA	Electrophoretic Mobility Shift Virus
Entero C	Enterovirus Species C
ERI-1	Enhanced RNAi-1
E_x	Excitation
FBS	Fetal Bovine Serum
FCV	Feline Calicivirus
FHV	Flock House Virus
FMDV	Foot-and-Mouth Disease Virus
FRET	Förster Resonance Energy Transfer
GFP	Green Fluorescent Protein
GST	Glutathione-S-transferase
hAGO	Human AGO
HAV	Hepatitis A Virus
HBV	Hepatitis B Virus
HCV	Hepatitis C Virus
HEV	Hepatitis E Virus
HGV/GBV-C	Hepatitis G Virus/GB Virus C
His-tag	Histidine Tag
HIV-1	Human Immunodeficiency Virus-1
HRP	Horse-Radish Peroxidase
HRV	Human Rhinovirus
Huh-7	Human Hepatoma Cell Line
IFN	Interferon
IgG	Immunoglobulin G
IPTG	Isopropyl β-D-1-Thiogalactopyranoside
IRES	Internal Ribosome Entry Site
IVT	*In Vitro* Transcription
JEV	Japan Encephalititis Virus
kb	Kilobase
K_d	Dissociation Constant
kDa	Kilodalton

LNA	Locked Nucleic Acid
MALDI	Matrix-Assisted Laser Desorption/Ionization
MALDI-TOF	Matrix-Assisted Laser Desorption/Ionization Time-of-Flight
MCS	Multiple Cloning Site
MFE	Minimum Free Energy
MFED	MFE Difference
miRNA	MicroRNA
MNV	Murine Norovirus
mRNA	Messenger RNA
MS	Mass Spectrometry
N/A	Not Available
NCR	Non-Coding Region
NEM	*N*-ethylmaliemide
Neo^R	Neomycin Resistance
Ni^{2+}-NTA	Nickel-Nitrilotriacetic Acid
NS	Non-Structural
nt	Nucleotide
NTP	Nucleotide Triphosphate
NW	New World
OG	Ocean Group
ORF	Open Reading Frame
OW	Old World
p19	19 kDa Protein
PAGE	Polyacrylamide Gel Electrophoresis
PBS	Phosphate Buffered Saline
PCR	Polymerase Chain Reaction
PDB	Protein Database
PFV-1	Primate Foamy Virus-1
P_i	Inorganic Phosphate
PKR	Protein Kinase R
pre-miRNA	Precursor miRNA
pri-miRNA	Primary miRNA

PV	Poliovirus
PVDF	Polyvinylidene Difluoride
RAKE	RNA-primed Array-based Klenow Enzyme
RdRp	RNA-dependent RNA Polymerase
rgsCaM	Regulator of Gene Silencing CaM
RIG-I	Retinoic Acid Inducible Gene-I
RISC	RNA-Induced Silencing Complex
RNA	Ribonucleic Acid
RNAi	RNA Interference
RSV	Respiratory Syncytial Virus
RT-qPCR	Real-time quantitative PCR
SDS	Sodium Dodecyl Sulfate
SE	Standard Error
shRNA	Short-hairpin RNA
siRNA	Short-interfering RNA
SL	Stem-loop
SodI	Superoxide Dismutase 1
ssRNA	Single-stranded RNA
TBE	Tris-Borate-EDTA
TBEV	Tick-borne Encephalitis Virus
TCEP	Tris(2-carboxyethyl)phosphine
TEV	Tobacco Etch Virus
UTP	Uridine Triphosphate
UV	Ultraviolet
VA RNA	Virus-Associated RNA
VSR	Viral Suppressor of RNA Silencing
WEL-1	Werner Exonuclease-like 1
WT	Wild-type
Xlrbpa	*Xenopus laevis* RNA Binding Protein A
YFV	Yellow Fever Virus

List of Figures

List of Tables

Chapter 1: Introduction

1.1 Introduction

RNA silencing is an evolutionarily conserved pathway for potent and sequence-specific silencing of gene expression mediated by double-stranded RNA (dsRNA) (1). RNA silencing has become a standard tool in molecular biology for assessing gene function and it is being pursued aggressively for its therapeutic potential (2). Despite the importance of this pathway for molecular biology and medicine, the underlying mechanisms of RNA silencing are not yet fully understood. The experimental detection, quantification, purification and characterization of small RNAs are crucial to the study of RNA silencing pathways and their small RNA mediators. There is thus a need for development of new tools to study protein-RNA and RNA-RNA interactions important for RNA silencing. Herein, the current knowledge regarding the mechanisms of RNA silencing (in plants, invertebrates, and mammalian cells) and the available tools for studying RNA silencing and small RNAs is reviewed. The limitations of current approaches are highlighted and the need for new methodologies is discussed.

1.2 RNA Silencing

RNA silencing is an evolutionarily conserved pathway whereby dsRNA sequence-specifically suppresses the expression of a target gene(s) (1). Although the structures and mechanisms of plant, invertebrate and mammalian RNA silencing pathways differ substantially, the key components of the pathways are homologous and will be described herein. In all eukaryotes, RNA silencing is triggered by the accumulation of dsRNA in the cytoplasm. The dsRNA is cleaved into small RNA duplexes by an ATP-dependent, RNase III-like nuclease called Dicer (invertebrates,

mammals) or Dicer-like (DCL, plants) (3). The small RNA duplexes, which are the mediators of RNA silencing, are typically characterized by their short length [~21-25 nucleotides (nt)], 3' 2-nt overhanging ends, 3'-hydroxyl groups, and 5'-phosphate groups (4, 5). These small RNAs are then assembled into an RNA-induced silencing complex (RISC) which contains an Argonaute (AGO) protein (4, 6). Multiple AGO proteins exist in plants, invertebrates and mammalian cells. In mammals, there are four AGO proteins (AGO1 to AGO4) all of which may be found at the center of the RISC. Mammalian AGO1 has been implicated in heterochromatin silencing (7, 8); and AGO2, which is the only cleavage competent mammalian AGO protein, has been shown to participate in microRNA (miRNA)-mediated repression as well as the short-interfering RNA (siRNA) pathway (discussed in more detail below) (9-11). However, the roles of AGO3 and AGO4 in RNA silencing remain unclear.

The AGO protein of the RISC unwinds the small RNA duplex, and one strand of the small RNA is used as a guide to target homologous RNA. The thermodynamic stability at the ends of the small RNA duplex determines which strand is incorporated into RISC; with the incorporated strand being less tightly paired to its complement at its 5' end (12-14). Of the two strands, the strand incorporated into RISC is termed the 'guide' strand and the other strand, the 'passenger' strand, rapidly undergoes degradation by exonucleases (15, 16). The whole process culminates with either cleavage, translation inhibition, or accelerated deadenylation of the homologous target RNA, the outcome being determined by the degree of base complementarity between the small RNA and its target RNA (14, 17, 18) (Figure 1.1).

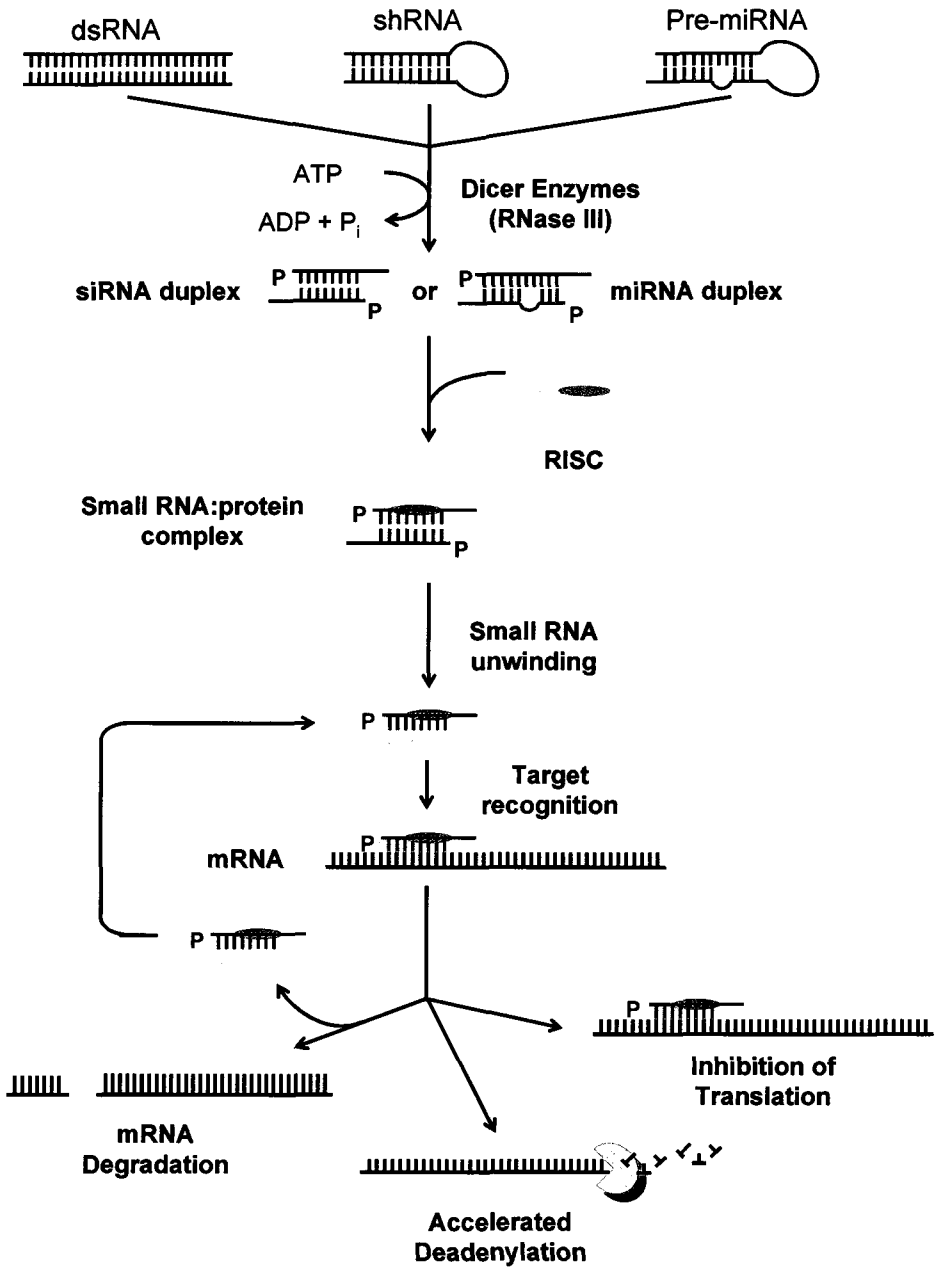

Figure 1.1 The RNA silencing pathway. RNA silencing is triggered by the accumulation of dsRNAs in the cytoplasm. DsRNAs are cleaved by Dicer enzymes into small RNA duplexes (siRNAs and miRNAs) generally characterized by their short length, 3' 2-nt overhanging ends, and 5' phosphate groups. The small RNA duplexes are then incorporated into the RISC which unwinds the small RNA duplex and uses one strand to target complementary mRNAs for degradation, translational inhibition, or accelerated deadenylation.

Over the past decade, small RNAs and the RNA silencing pathway have emerged as important regulators of eukaryotic messenger RNAs (mRNAs). Small RNAs participate in RNA silencing pathways that regulate diverse cellular activities including transcription, chromatin structure, genome integrity, translation, and mRNA stability (19). The two main classes of small RNAs: siRNAs and miRNAs, can be functionally equivalent, but they are distinguished by their origin.

1.2.1 Short-interfering RNAs (siRNAs)

siRNAs are derived from exogenous dsRNA, or are transcribed from transposable elements and other types of inverted repeats in the genome of eukaryotic cells. In plants and invertebrates (but not humans), siRNAs can be derived from viral dsRNA intermediates or can be formed by endogenous RNA-dependent RNA polymerases (RdRp) capable of converting single-stranded RNAs (ssRNAs) into dsRNA (20-24). Specialized classes of siRNAs are also involved in maintaining genome integrity in plants, invertebrates and mammals by silencing transcription from undesired loci in the genome (e.g. retrotransposons and inverted repeat sequences) (25-27). In addition, short hairpin RNAs (shRNAs) and synthetic siRNAs can be introduced into the cell and are able to enter the RNA silencing pathway and silence the expression of a target gene(s).

siRNAs are typically perfectly complementary to their RNA targets and hence exert their effects by RISC-mediated target RNA cleavage (14). Extensive pairing between the siRNA and its RNA target results in cleavage of a single phosphodiester bond in the target RNA, between nt 10 and 11 of the small RNA guide (28). In mammals, AGO2 is the only AGO protein able to mediate target cleavage and, together with the

siRNA guide, represents a minimal cleavage-competent RISC (11, 14, 17). Human AGO2-mediated target cleavage is a multiple-turnover reaction, with the siRNA-RISC guiding cleavage of hundreds of target RNAs (14, 17) (Figure 1.1). The cleavage products are subsequently degraded by 3' and 5' exonucleases in the cytoplasm since the resultant RNA cleavage products lack the stabilizing 5' cap or poly(A) tail (29). In plants, an amplification system is in place whereby an RdRp amplifies the siRNA signal and a longer class of siRNAs are produced, approximately 24 to 26-nt in length, that are able to spread from cell-to-cell and over long distances via vascular-mediated transport (30). Mobile silencing signals have also been demonstrated to occur in *C. elegans* (31, 32); however, to date, no cellular RdRp has been identified in mammalian cells. Today, siRNAs are widely used to silence the expression of target genes by transfection of synthetic shRNA-vectors or siRNAs complementary to the gene(s) of interest. This is a widely used technique to assess gene function and also has the potential to be used to silence disease-relevant targets, such as viruses or oncogenes.

1.2.2 MicroRNAs (miRNAs)

miRNAs have been identified in all metazoa studied to date. They are endogenous non-coding RNAs that are expressed in a developmentally-regulated and tissue-specific manner, and are predicted to regulate at least one-third of all human genes (33-36). In contrast to siRNAs, miRNAs are generally encoded by their own, distinct genes; in single or clustered transcription units (37-39). Typically, miRNAs are transcribed by RNA polymerase II as large, stem-loop precursor RNAs called primary miRNAs (pri-miRNAs) (39). Pri-miRNAs are processed in the nucleus by an RNase III-like enzyme, Drosha

(invertebrates, mammals) or DCL1 (plants), into highly structured ~70-nt precursor miRNAs (pre-miRNAs) (40). These pre-miRNAs are then exported to the cytoplasm via the nuclear receptor exportin-5 where they are further processed by Dicer (invertebrates, mammals) or DCL (plants) into ~21-nt mature miRNAs (41-43) (Figure 1.2). Alternatively, a class of miRNAs termed 'mirtrons' are derived from introns of spliced mRNAs that mimic the structural features of pre-miRNAs, and hence enter the miRNA processing pathway without Drosha-mediated cleavage (44) (Figure 1.2). Like siRNAs, the resultant miRNA molecules are asymmetrically assembled into RISC, which guides them to their RNA target(s). Computational algorithms that combine thermodynamic modeling of RNA-RNA interactions and comparative sequence analysis have been used to predict miRNA target sites in the genomes of a number of eukaryotic organisms (45-60). These have demonstrated that plant miRNAs are typically directed against the open reading frame (ORF) of their target genes (45, 49, 50, 56, 61, 62). In contrast, invertebrate and mammalian miRNAs are typically directed against the 3' non-coding region (NCR) of their target RNAs, often with multiple miRNAs coordinating to control the expression of a single gene (46-48, 51-55, 57-60). Table 1.1 summarizes and contrasts the features of the siRNA and miRNA pathways in plants, invertebrates and mammals (Table 1.1).

Mammalian miRNAs are often only partially complementary to their RNA targets and can contain mismatches, gaps and G:U basepairs at different positions (52, 57-59). The bulk of the binding specificity for these miRNA-RISC complexes is provided by a mere 7-nt of the 21-nt miRNA, specifically nt 2-8 numbered from the 5' end, referred to as the 'seed sequence' (47). This small region of complementarity required for binding to

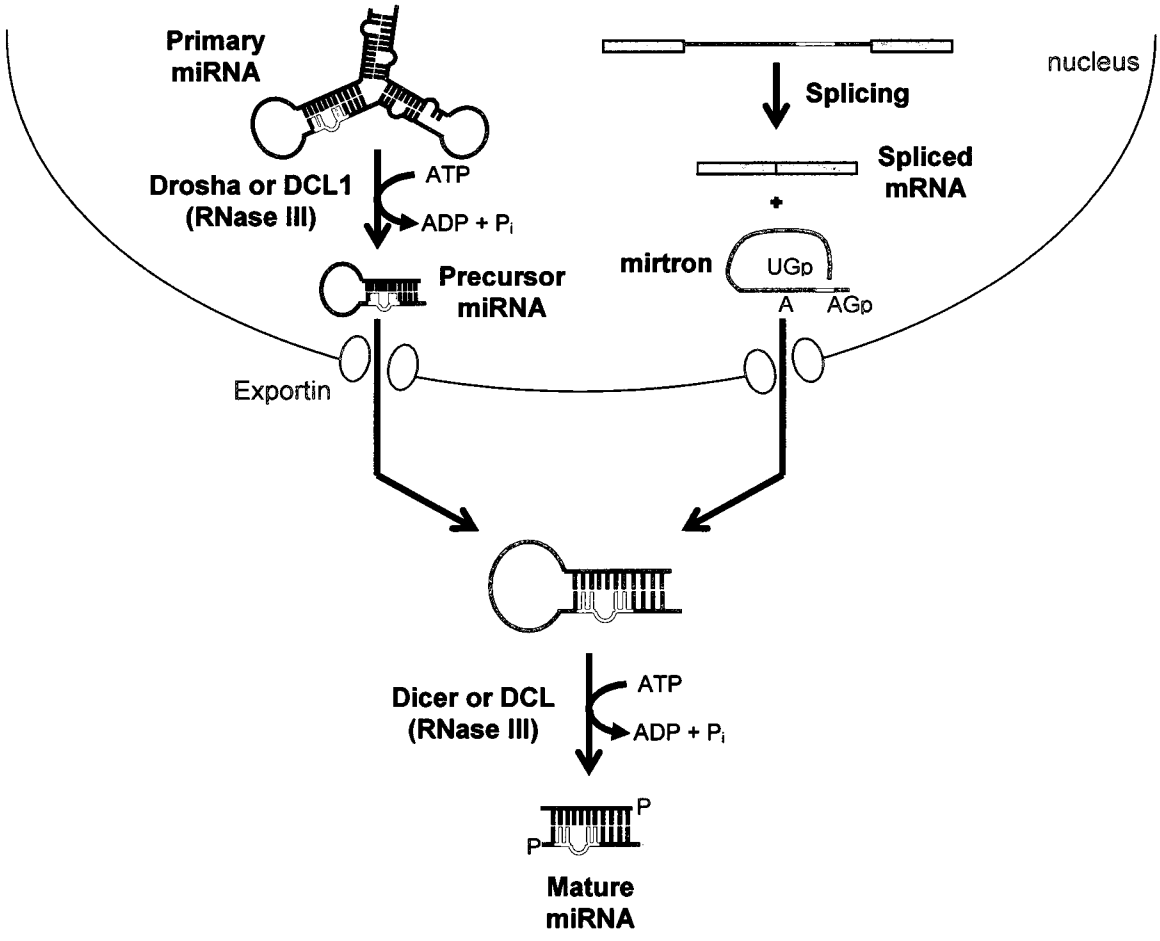

Figure 1.2 Biogenesis of miRNAs. MicroRNAs typically arise through transcription of highly structured RNA polymerase II transcripts called pri-miRNAs. Pri-miRNAs are then converted to approximately 70-nt stem-loop pre-miRNAs by the nuclear RNase III enzymes, Drosha or DCL1. Alternatively, miRNAs can arise from introns during splicing. Termed mirtrons, these miRNA precursors are able to bypass Drosha- or DCL1-mediated cleavage. Both types of miRNA precursors (pre-miRNAs and mirtrons) are exported to the cytoplasm by the nuclear receptor exportin-5 and are converted into mature miRNAs by the cytoplasmic RNase III enzyme Dicer or DCL. The mature miRNAs are then able to enter the RNA silencing pathway.

Table 1.1 A comparison of the siRNA and miRNA pathways in plants, invertebrates and mammals.[1]

	Plants	**Invertebrates**	**Mammals**
siRNA pathway			
Precursor	dsRNA	dsRNA	dsRNA
Source	viruses, transposons, repeat elements	viruses, transposons, repeat elements	transposons, repeat elements
dsRNA duplex	strand symmetry	strand symmetry	strand symmetry
Biogenesis	Dicer-like	Dicer	Dicer
Degree of complementarity to target	high	high	high
Mechanism of repression	cleavage	cleavage	cleavage
Amplification/systemic silencing	yes	yes (*C. elegans*)	no
Function	innate immunity, genome integrity	innate immunity, genome integrity	genome integrity
miRNA pathway			
Precursor	stem-loop RNA	stem-loop RNA	stem-loop RNA
Source	intergenic regions (mostly), introns	intergenic regions, introns	intergenic regions, introns
dsRNA duplex	strand assymetry	strand assymetry	strand assymetry
Biogenesis	Dicer-like	Drosha, Dicer	Drosha, Dicer
Degree of complementarity to target	high	partial, relatively low	partial, relatively low
Mechanism of repression	cleavage (generally)	translational repression	translational repression, accelerated deadenylation
Function	regulation of gene expression	regulation of gene expression	regulation of gene expression
Location of miRNA targets	open reading frames (mostly)	3' Untranslated regions (mostly)	3' Untranslated regions (mostly)
Number of miRNA target sites	one (generally)	multiple (generally)	multiple (generally)

[1]Adapted and expanded from reference (62).

a target RNA provides a given miRNA the potential to regulate many targets within a given genome. When the miRNA is able to pair extensively with the target RNA, like siRNAs, it directs target RNA cleavage (dominant mechanism in plants). However, when miRNAs are only partially complementary to their target RNAs, they cannot direct target cleavage, and instead impose a block in translation or cause accelerated deadenylation of their RNA target(s) (14, 17, 18). Therefore, miRNA-programmed RISC can induce RNA degradation, translational inhibition, or accelerated deadenylation, depending on the degree of base complementarity to the target RNA (Figure 1.1). Since miRNAs participate in the regulation of almost every cellular process investigated, it is likely that changes in their expression may underlie plant, invertebrate and mammalian pathologies, such as those associated with viral infections and cancer. Hence miRNAs, like siRNAs, may represent novel therapeutic targets to alter gene expression or modify pathogenesis of infectious and metabolic diseases.

1.3 Viruses and the RNA Silencing Pathway

1.3.1 RNA Silencing is an Antiviral Response in Plants

Early evidence indicating an antiviral role for RNA silencing in plants came from studies of transgenic plants following infection with tobacco etch virus (TEV) from which the transgene was derived (20). The transgenic plants were initially susceptible to TEV infection but later recovered and became resistant to subsequent infection with homologous virus (20). The recovery phenotype and establishment of an antiviral state was associated with a post-transcriptional reduction in the levels of the transgene mRNA. This suggested that the infecting virus induced post-transcriptional gene silencing of the

homologous transgene, which then targeted the viral RNA for silencing, conferring the antiviral state (20, 63). A number of subsequent studies supported this model in both transgenic and wild-type plants and suggested that viral RNAs act as the trigger and the target of RNA silencing in plants (63-67). The antiviral role of RNA silencing in plants is further supported by the demonstration that many essential viral pathogenicity determinants are suppressors of RNA silencing (discussed in more detail in *Chapter 3*).

1.3.2 RNA Silencing and Innate Immunity Against Viruses in Invertebrates

In invertebrates, the first suggestion that RNA silencing played a role in innate immunity against viruses came from the observation that the B2 protein of Flock house virus (FHV) was able to suppress RNA silencing in plants (68). Subsequent studies in cultured *Drosophila* and *Anopheles gambiae* cells, as well as *D. melanogaster* adults, demonstrated that the RNA silencing pathway controls innate immunity against viruses in invertebrates (68-70). In addition, recent studies have demonstrated that viral replication is also able to trigger antiviral RNA silencing immunity in *C. elegans* (71, 72).

1.3.3 RNA Silencing Plays a Role in Host-virus Interactions in Mammalian Cells

It has been well established in plants and invertebrates that RNA silencing plays an important role in both nucleic-acid based immunity against viruses and in the regulation of host gene expression. Although it is clear that RNA silencing plays an important role in the regulation of mammalian gene expression, it is not clear whether RNA silencing plays an antiviral role in mammals (since no virus-derived siRNAs have been demonstrated in mammalian cells to date). However, a number of mammalian

viruses have now been documented to interact with small RNAs and the RNA silencing pathway, underscoring the importance of this pathway in host-pathogen interactions and adding to the growing body of evidence that this pathway plays a role in viral infection, invasion, and/or persistence in mammalian cells.

First of all, mammalian viruses have been demonstrated to have complex interactions with the endogenous miRNA pathway. Several mammalian viruses, including members of the *Herpesvirus* family and human immunodeficiency virus 1 (HIV-1), have been predicted (73, 74), or demonstrated (74-82), to encode viral miRNAs that regulate host or viral gene expression. Using computational prediction, small RNA cloning, and northern blot analyses, several groups have identified virally-encoded pri-miRNAs in structured regions of mRNAs from DNA viruses (e.g. *Herpesviruses*) and retroviruses (e.g. HIV-1) (74-82); however, no virally-encoded miRNAs have been identified in the RNA viruses (74, 75). Virally-encoded pri-miRNAs are processed in the nucleus by Drosha and can then enter into the RNA silencing pathway to silence host or viral gene expression (76-82).

Endogenous cellular miRNAs have also been demonstrated to specifically interact with mammalian viruses. For example, primate foamy virus 1 (PFV-1) replication was shown to be restricted in mammalian cells by the expression of a cellular miRNA (miR-32) with complementarity to the viral RNA genome (83). In addition, Pederson and colleagues demonstrated that interferon (IFN) β signaling was able to induce the expression of cellular miRNAs in a human liver cell line, some of which had direct complementarity to the hepatitis C virus (HCV) genome and were able to limit HCV replication in cell culture (84). In contrast, a highly abundant, liver-specific, human

miRNA, miR-122, has recently been demonstrated to interact with the 5' NCR of HCV, and actually facilitate replication of the viral RNA in cell culture (85, 86).

Finally, a number of mammalian viruses have been demonstrated to encode suppressors of RNA silencing that are pathogenicity determinants (discussed in more detail in *Chapter 3*). Thus, there is accumulating evidence that mammalian viruses, like those that infect plants and invertebrates, have developed strategies to suppress and, in some cases, take advantage of, the RNA silencing machinery. This implicates small RNAs and the RNA silencing pathway as important regulators of viral infection, invasion and persistence in mammalian cells.

1.4 Applications of RNA Silencing and Small RNAs

1.4.1 Investigating Gene Function

Since its description by Fire and Mello in 1998 (1), RNA silencing has evolved into a powerful tool for probing gene function. Prior to the discovery of the RNA silencing pathway, gene knockdown in mammalian cells was primarily confined to the development of knock-out mice or the laborious identification of small molecule inhibitors. With the advent of RNA silencing, gene knockdown is accessible to almost all researchers and has accelerated the process of assessing gene function.

Since RNA silencing is based on pairing between the gene of interest and the siRNA, sequence-specific inhibition can be achieved with only partial sequence information. In addition, closely related isoforms of proteins can be selectively silenced through careful selection of isoform-specific target sequences (87). Because of the small size of siRNAs, and their structural characteristics, sequence-specific inhibition of target

genes can be obtained with minimal off-target effects and without the induction of the IFN response (4, 88, 89). Also, due to the ubiquity of the RNA silencing pathway in eukaryotes, siRNA technology can be applied to a broad range of organisms and cell types for assessing gene function.

1.4.2 Pathway Analysis and Large-scale RNA Silencing Libraries

Another powerful application of RNA silencing is the ability to elucidate signaling pathways (90). By designing siRNAs against a gene of interest and monitoring the expression of other related genes, it is possible to identify networks of genes associated with the gene of interest. The position of each gene within the signaling pathway can then be assigned by sequential knockdown of the genes in the pathway using sequence-specific siRNAs and assaying for the affected genes (90). This approach has already been used to elucidate components of many mammalian receptor signaling pathways (90-93).

Besides functional analyses of individual genes or of signaling pathways, RNA silencing technologies have recently been applied to large-scale, and even genome-wide, surveys of gene function (90). Kamath and colleagues (94) developed a genome-wide RNA silencing screen of *C. elegans*; and since then, RNA silencing libraries have been replicated in nematodes (95-100), *Drosophila* (101), and in the mass-screening of mammalian genes (102-106).

1.4.3 Target Discovery and Validation

Target discovery and validation are the first stages in the long process of drug development. Silencing the expression of a potential therapeutic target and verifying the desired phenotype provides assurance that an inhibitor of the same target gene will have therapeutic value (90). RNA silencing technology has rapidly become useful for identification of target genes associated with disease pathogenesis in inherited diseases, cancer, and infectious disease (107, 108). In addition, large-scale RNA silencing libraries can help narrow down lists of potential drug targets so that the most promising candidates can be followed up.

1.4.4 Therapeutic Applications of RNA Silencing

Since small RNAs can be designed against virtually any gene of interest, RNA silencing can be used to target disease-relevant genes that cannot be shut down with currently available drugs. Several reports have demonstrated the use of RNA silencing to target viral replication or cellular gene expression in both cell culture and in adult organisms (1, 4, 28, 71, 102). The three main areas of human disease that have received the most attention with regards to RNA silencing-based therapy are dominantly-inherited genetic diseases, cancer, and infectious disease (107, 108), each of which will be discussed in more detail.

Dominantly-inherited genetic diseases. People with dominantly-inherited genetic disorders carry one normal allele and one mutant allele of the gene that causes the disease phenotype. The dominant mutant allele could cause disease by loss-of-function, that is,

the mutant allele has lost its function and the normal allele is insufficient to compensate for the mutant allele. Alternatively, the dominant allele could cause disease by gain-of-function, where the mutant allele results in a gain of a novel function or the enhancement of an already existing function. In theory, loss-of-function mutations could be treated by delivery of a normal copy of the gene to the patient. However, until the advent of RNA silencing, a solution to the gain-of-function mutations was less evident. Now it seems likely that RNA silencing can be used to silence the disease-relevant, dominant gain-of-function allele in such cases. Towards this end, many groups have now demonstrated the utility of RNA silencing based approaches to treat dominantly-inherited genetic disorders including neurodegenerative or inflammatory diseases (109, 110). For example, lentiviral delivery of siRNAs targeting the mutant superoxide dismutase 1 (*Sod1*) gene has been used to improve survival of motor neurons and delay the onset of amyotrophic lateral schlerosis in mice (109, 110). These studies have demonstrated the utility of lentiviral delivery methods *in vivo* and the therapeutic effectiveness of siRNA-based treatment strategies without toxic side effects (109, 110).

Cancer. There are many instances during cancer progression that could be envisioned as targets for siRNA-based therapy. RNA silencing has been used to target dominant mutant oncogenes, overexpressed oncogenes, as well as angiogenic, metastatic, and multidrug resistance factors involved in tumor growth or cancer progression (111-115). For example, Brummelkamp and colleagues used retrovirally-delivered siRNA to specifically silence the mutant *K-RAS*^{V12} allele in human pancreatic carcinoma cells, while leaving the wild-type *K-RAS* allele untouched (111). Loss of the mutant *K-RAS*^{V12} led to loss of

tumorigenicity (111). This demonstrates the utility of allele-specific silencing in the treatment of human cancer.

In addition, a number of other cancer-related genes have been successfully targeted in cell culture or in mouse models of human cancer including the tyrosine kinase *EphA2* (116), epidermal growth factor receptor (117), the proto-oncogene *c-Met* (118), and the multidrug resistance gene (115), among others. No matter the approach, it is clear that tumor-specific siRNA-based therapy can be used to reverse the oncogenic phenotype of cancer cells. Hence, RNA silencing-based strategies will likely be an area of great impact for years to come, especially for cancers for which there are few treatment options currently available.

In addition, since abnormal expression of miRNAs has been demonstrated in a number of human cancers, miRNAs themselves may be novel therapeutic targets. For miRNAs whose expression is reduced, re-introduction of the mature miRNA (miRNA mimic) into the cancer tissue could restore proper regulation of the mRNA targets. For those tumors where miRNA expression is increased, sequestration of the miRNA using antisense oligonucleotides or antagomirs (119) could be used to inhibit the overexpressed miRNA. Recently, Elmén *et al.* have demonstrated that PBS-formulated locked-nucleic-acid-modified oligonucleotides were able to effectively antagonize a miRNA in non-human primates for up to 7 weeks (120). This supports the potential of antisense miRNAs as a novel class of therapeutics for disease-associated miRNAs. In addition, since abnormal miRNA expression seems to characterize many human cancers (121, 122), miRNA signatures are likely to be of diagnostic and prognostic significance.

Infectious disease. Since the RNA silencing pathway is an antiviral pathway in plants and invertebrates, commandeering the pathway in mammalian cells for destruction of viral RNAs or viral replicative intermediates is an obvious approach for specific antiviral therapy. For example, synthetic siRNA-induced RNA silencing has already been shown to effectively inhibit many DNA and RNA viruses in mammalian cells, including influenza virus (123), poliovirus (124), human papillomavirus (125), HIV-1 (126-130), hepatitis B virus (HBV) (131, 132), and HCV (133-138), among others (reviewed in (139)). Unfortunately, viruses are often able to overcome siRNA-mediated silencing by accumulating point mutations within the target sequence in the viral RNA. To avoid these escape mutations, siRNAs should be directed against highly conserved regions in the viral genomes and, in addition, multiple siRNAs can be used to knockdown viral targets to decrease the likelihood of accumulating escape mutations. As an alternative approach, cellular factors required for viral entry or replication have also been successfully targeted using RNA silencing, since these targets avoid the problems associated with viral genetic variability or mutability (140, 141).

As discussed previously, viruses are known to encode their own viral miRNAs (73, 75-78, 80, 81), or to take advantage of cellular miRNAs (85, 142), to benefit viral replication (reviewed in (143)). In these cases, sequestration of the miRNAs using antisense oligonucleotides or antagomirs (119) could be an effective therapeutic strategy. For example, HCV has been demonstrated to rely on a highly abundant, liver-specific human miRNA, miR-122, for replication in cell culture (85). Sequestering miR-122 using antagomirs has been shown to inhibit HCV replication in cultured human liver cells (85). The effectiveness of this strategy against viral infections *in vivo* has not yet been

demonstrated; however, silencing of miRNAs in mice and non-human primates using antisense oligonucleotides or antagomirs supports the therapeutic potential of this approach for virus-associated miRNAs (120).

1.5 Tools for the Study of RNA Silencing and Small RNAs

1.5.1 Tools for Analysis of Small RNAs

Experimental detection and expression profiling of small RNAs (siRNAs or miRNAs) is challenging due to their small size, relatively low expression levels, and sequence similarity among members (144-146). Nevertheless, reliable methods for detection, purification, quantification, and identification of small RNAs are essential to the study of RNA silencing pathways and small RNAs.

Small RNA isolation. The first step in obtaining small RNA samples is isolation of the RNA from cells or tissues of the organism in question. Typical RNA isolation procedures rely on organic extraction followed by alcohol precipitation or adsorption of the RNA to silica-based matrices (e.g. *mir*Vana™ miRNA Isolation Kit, Ambion, Austin, Texas). RNA extractions can be enriched for small RNAs (<200 nt) based on differential precipitation of large mRNAs (>200 nt) at alcohol concentrations where the small RNAs remain soluble. This typically results in an RNA preparation highly enriched for tRNAs, 5S rRNA, as well as the small RNAs, including miRNAs and/or siRNAs. Alternatively, small RNAs can also be isolated by size-fractionation using polyacrylamide gel elecrophoresis (PAGE) (38, 146, 147). However, both of these procedures can result in inefficient small RNA recovery, and the small RNA population often includes

contaminant RNAs such as the tRNAs and 5S rRNA, highlighting the need for new methods for isolation of small RNAs (siRNAs and miRNAs).

Small RNA detection and analysis. Several approaches have been used for small RNA detection and analysis, including: Northern blot analyses, RNase protection assay, small RNA cloning, PCR-based approaches, *in situ* hybridization, as well as microarray-based approaches, among others (reviewed in (146, 148)).

Northern blot analysis is widely used to determine the expression level of small RNAs and is the current gold standard for small RNA quantification, validation and confirmation of high-throughput data (37, 38, 147, 149, 150). Northern blot analyses can be used to detect both mature and precursor miRNAs and yields information on both the size and expression level of a given small RNA. However, northern blots are relatively low-throughput, have limited sensitivity for rare small RNAs, and require relatively large amounts of total RNA per sample (37, 38, 147, 149, 150).

Other hybridization techniques include RNase protection assay and *in situ* hybridization. RNase protection assay relies on hybridization of labeled antisense probes complementary to the small RNA of interest to total RNA, followed by treatment with a single-strand-specific RNase to degrade unhybridized target RNA. The protected small RNA:probe duplex can then be detected by PAGE analysis (39). *In situ* hybridization is useful for the detection of small RNAs in cells or tissues (151-155). This method can be used to detect both mature and precursor miRNAs and yields information about expression and localization patterns of small RNAs in fixed cells. However, a major limitation of these hybridization techniques is their low-throughput nature. Additionally,

in situ hybridization is limited in that small RNAs that diffuse quickly could be lost during the fixation and washing of samples (151-155).

Small RNA cloning approaches which involve the random cloning and sequencing of size-fractionated RNA has become the method of choice for small RNA identification (28, 37, 38, 75, 149). Typically, adaptor molecules are ligated to small RNA molecules using T4 RNA ligase, this is followed by reverse transcription and derivation of a complementary DNA (cDNA) library (37, 38, 146, 149). The cDNA is then concatenated, ligated into a plasmid vector, and sequenced (37, 38, 146). This is an excellent approach for identification of novel small RNAs, including viral miRNAs (75); however, ligation to adaptor molecules may introduce bias into the small RNA profile, and sequencing can be costly and time-consuming (156).

PCR-based approaches can also be used that detect specific small RNAs (157, 158). Typically, total RNA is extracted and reverse transcribed to cDNA, then specific small RNAs are amplified and monitored by real-time quantitative PCR (RT-qPCR) (157, 158). PCR-based approaches can detect both mature and precursor miRNAs, are highly sensitive and quantitative, and are able to discriminate between closely related small RNAs (148). However, while large differences in expression levels are maintained in the amplification process using PCR, small differences in expression may be lost (159).

Finally, microarray-based approaches have also been used for the analysis of small RNAs including traditional microarrays (160-164), locked nucleic acid (LNA)-modified microarrays (165-167), and RNA-primed array-based klenow enzyme (RAKE) assay microarrays (145). Microarray-based approaches are attractive due to their high-throughput nature and ability to screen large numbers of small RNAs simultaneously.

However, microarray technologies can be limited due to their requirement for high concentrations of input target for efficient hybridization and signal generation, poor sensitivity to rare targets, cross-hybridization of closely related small RNAs, and their requirement for post-array validation (146).

Other approaches for small RNA detection and analysis include signal-amplifying ribozymes (168) for fluorescence detection of small RNAs *in situ* or *in vivo*, primer-extension analysis (169, 170), and bead-based flow cytometry (121). Although a number of methods have been developed that have advanced the field, the currently available tools are limiting in that they give static information about small RNA profiles, future tools will likely help to address the issue of dynamics in RNA silencing pathways in diverse eukaryotic organisms.

1.5.2 Tools for the Design and Screening of Small RNAs

RNA silencing has also become a mainstream tool for the silencing of target gene(s), and has the potential to be used to silence disease-relevant targets. The first step in successful application of RNA silencing is the design of siRNAs. There are currently a number of design algorithms available that increase the likelihood of designing effective siRNAs (i.e. those capable of silencing gene expression by >50%) (171, 172). These approaches take into account both features of the siRNA duplex (171, 172), and in some cases, the target RNA (173-176). However, computational prediction of large, highly-structured target RNA molecules is not yet amenable to accurate modeling. Hence, there is a need to develop new approaches to analyze the structure of large, highly-structured RNAs, and to screen for effective siRNAs against these targets.

Chapter 2: Materials & Methods

2.1 p19 Methods

2.1.1 Codon Optimization, Plasmids, and Mutagenesis

Codon optimization of Carnation Italian ringspot virus (CIRV) p19 for mammalian and bacterial expression was manually selected according to the codon usage tables for *Homo sapiens* and *Escherichia coli* obtained from the Genbank Codon Usage Database at http://www.kazusa.or.jp/codon/ and the CIRV genome (Genbank Accession #: NC_003500). Chosen codons had a frequency score >10 for both *Homo sapiens* and *Escherichia coli*. The sequence of the codon optimized CIRV p19 used is shown in Figure 2.1. The codon optimized CIRV p19 gene was synthesized by Genescript Corporation (Pistcataway, NJ) in plasmid vector pUC57. CIRV p19 was subsequently subcloned by polymerase chain reaction (PCR) into the pTriEx 4-neo vector (EMD Biosciences, San Diego, CA) by using forward (5'-TAA GCC ATG GAA CGC GCT ATC CAA GG-3') and reverse (5'- CGA CTC GAG CTC GCT TTC TTT CTT GAA GG-3') PCR primers. The CIRV p19 PCR product was digested with *NcoI* and *XhoI* and inserted into the multiple cloning site of pTriEx 4-neo resulting in an octa-Histidine tag (His-tag) at the C-terminus of CIRV p19. The resulting CIRV p19 pTriEx 4-neo (pTriEx-p19) plasmid construct was confirmed by DNA sequencing.

All His-tagged cysteine mutants of CIRV p19 were created using the QuickChange II site-directed mutagenesis Kit (Stratagene, La Jolla, CA) according to the manufacturer's protocol. The template plasmid and the pair of mutagenic primers used to create each of the cysteine mutant constructs are described in Table 2.1. Briefly, for each mutagenesis reaction, the sample contained 50 ng of plasmid and 100 ng of each primer. Sixteen cycles of amplification after denaturing (95 °C), annealing (55 °C), and extension

ATG GAA CGC GCT ATC CAA GGC AAC GAC ACT CGC GAA CAA GCT AAC GGT GAA CGC
TGG GAT GGC GGC TCC GGC GGT ATC ACT TCT CCA TTC AAA CTG CCT GAC GAA AGC
CCA AGC TGG ACT GAG TGG CGC CTG TAT AAC GAT GAG ACC AAT TCC AAT CAA GAT
AAT CCA CTG GGT TTC AAG GAA AGC TGG GGT TTC GGG AAA GTT GTC TTT AAG CGC
TAT CTG CGC TAC GAC CGC ACC GAA GCT TCC CTG CAC CGC GTC CTG GGC TCT TGG
ACC GGC GAT TCC GTT AAC TAT GCA GCA TCT CGC TTT CTG GGT GCC AAC CAG GTC
GGC TGT ACC TAT AGC ATT CGC TTT CGC GGC GTT AGC GTC ACC ATT TCT GGC GGG
TCC CGC ACT CTG CAG CAT CTG TGT GAG ATG GCA ATT CGC TCT AAG CAA GAA CTG
CTG CAG CTG ACC CCA GTC GAA GTG GAA AGC AAT GTG TCC CGC GGC TGC CCT GAA
GGT ATT GAA ACC TTC AAG AAA GAA AGC GAG TAA

Figure 2.1 Sequence of the codon optimized CIRV p19 used in this study. Sequence is written 5' to 3'. Start (AUG) and stop (TAA) codons are underlined.

Table 2.1 DNA templates and mutagenic primers used for site-directed mutagenesis.

Construct	Template	Mutagenic Primer Pair[1]
C110S	pTriEx-p19	5'-AACCAGGTCGGC**A**GTACCTATAGCATTCGC-3'
C134S	pTriEx-p19	5'-CTGCAGCATCTGT**C**TGAGATGGCAATTCGC-3'
C160S	pTriEx-p19	5'-AATGTGTCCCGCGGCT**C**CCCTGAAGGTATT-3'
C110S/C134S	C134S	5'-AACCAGGTCGGC**A**GTACCTATAGCATTCGC-3'
C110S/C160S	C110S	5'-AATGTGTCCCGCGGCT**C**CCCTGAAGGTATT-3'
C134S/C160S	C134S	5'-AATGTGTCCCGCGGCT**C**CCCTGAAGGTATT-3'
C110S/C134S/C160S	C110S/C134S	5'-AATGTGTCCCGCGGCT**C**CCCTGAAGGTATT-3'
C110I	pTriEx-p19	5'-AACCAGGTCGGC**AT**TACCTATAGCATTCGC-3'
C134I	pTriEx-p19	5'-CTGCAGCATCTG**AT**TGAGATGGCAATTCGC-3'
C160I	pTriEx-p19	5'-AATGTGTCCCGCGGC**AT**CCCTGAAGGTATT-3'
C110I/C134I	C110I	5'-CTGCAGCATCTG**AT**TGAGATGGCAATTCGC-3'
C110G	pTriEx-p19	5'-AACCAGGTCGGC**G**GTACCTATAGCATTCGC-3'
C134G	pTriEx-p19	5'-CTGCAGCATCTG**G**GTGAGATGGCAATTCGC-3'
C110G/C134G	C110G	5'-CTGCAGCATCTG**G**GTGAGATGGCAATTCGC-3'
C110A	pTriEx-p19	5'-AACCAGGTCGGC**GC**TACCTATAGCATTCGC-3'

[1]The sequences of the forward and reverse primers are complementary to each other. Only the forward primer sequence is shown for each construct. Mutated nucleotides are in bold.

(68 °C), resulted in nicked circular strands. Following temperature cycling, the product was treated with *DpnI* at 37 °C for 1 h to digest the parental DNA. The nicked vector DNA with the incorporated mutation was then used to transform competent XL-1 Blue sub-cloning grade competent cells (Statagene, La Jolla, CA). The resulting plasmids, prepared from individual colonies, were sequenced to verify the presence of the desired mutations.

2.1.2 siRNA and miRNA Sequences

All siRNAs were duplex RNA unless otherwise indicated and were purchased from Dharmacon (Lafayette, CO). siRNA sequences used in the p19 studies are listed in Table 2.2. All siRNAs were PAGE purified and were demonstrated to be >95% pure according to the manufacturer's specifications. The mir-122 duplex used was also purchased from Dharmacon (Lafayette, CO) with the following sense (guide) and antisense (passenger) sequences, respectively: 5'-UGG AGU GUG ACA AUG GUG UUU G-3' and 5'-AAC GCC AUU AUC ACA CUA AAU A-3'.

2.1.3 Protein Expression and Purification

Bacterial expression of the wild-type His-tagged CIRV p19 and its mutant derivatives was carried out at 37 °C in *E. coli* BL21 (DE3) cells until an OD_{600} of 0.5-0.6 was achieved. Expression of p19 proteins was induced by IPTG at a final concentration of 1 mM. Cultures were then grown for an additional 4-5 h at 30 °C. After harvesting, bacterial pellets were resuspended in lysis buffer (50 mM NaH_2PO_4, 300 mM NaCl,

Table 2.2 siRNA sequences used in the p19 studies.

siRNA	Sequence[1,2,3]	References
CSK	5'-cuaccgcaucauguaccauTT-3' 3'-TTgauggcguaguacauggua-5'	(177-181)
331	5'-ggucucguagaccgugcacTT-3' 3'-TTccagagcaucuggcacgug-5'	(137, 177)
GL3	5'-cuuacgcugaguacuucgaTT-3' 3'-TTgaaugcgagucaugaagcu-5'	(177, 179, 180, 182)
GL2 (19-nt)	5'-uacgcggaauacuucgaTT-3' 3'-TTaugcgccuuaugaagcu-5'	(177, 179)
GL2 (21-nt)	5'-cguacgcggaauacuucgaTT-3' 3'-TTgcaugcgccuaaugaagcu-5'	(177, 179, 180, 182)
GL2 (23-nt)	5'-cguacgcggaauacuucgaaaTT-3' 3'-TTgcaugcgccuuaugaagcuuu-5'	(177, 179)
GL2 (25-nt)	5'-ucacguacgcggaauacuucgaaTT-3' 3'-TTagugcaugcgccuuaugaagcuu-5'	(177, 179)
GL2 (28-nt)	5'-acaucacguacgcggaauacuucgaaTT-3' 3'-TTuguagugcaugcgccuuaugaagcuu-5'	(177, 179, 180)

[1]Uppercase letters denote deoxyribonucleotides; [2]All siRNAs are duplex unless otherwise indicated in the text; [3]Labeled siRNAs are indicated in the text and contain either Cy3 or Dy547 dyes at the 5' end of the anti-sense (guide) strands.

10 mM imidazole, 1 mM dithiothreitol (DTT), 1 mM benzamidine, pH 8.0) supplemented with Complete™ protease inhibitor cocktail (Roche Diagnostics, Penzberg, Germany) and lysed by sonication on an ice-bath. After centrifugation, soluble lysate fraction containing the His-tagged p19 proteins was loaded onto a nickel affinity column (Pharmacia, Peapack, NJ). After protein binding, the resin was washed with wash buffer (50 mM NaH_2PO_4, 300 mM NaCl, 60 mM imidazole, pH 8.0). Elution of the His-tagged p19 proteins was carried out using elution buffer (50 mM NaH_2PO_4, 300 mM NaCl, 250 mM imidazole, pH 8.0) and 10 mM of DTT was added immediately to the eluate. A typical SDS-PAGE gel of the nickel-nitrilotriacetic acid (Ni^{2+}-NTA) column purification is shown in Figure 2.2. The pooled eluates were concentrated to 0.5 mL using the Amicon Ultra-15 10-kDa MWCO centrifugal filter device (Millipore, Concord, MA). The concentrated samples were then injected into Superdex 200 size exclusion column (Pharmacia, Peapack, NJ) at a flow rate of 0.5 mL/min. The p19 proteins elute as stable dimers and are recalcitrant to denaturation even upon boiling for 15-20 min (177, 179, 183). Fractions containing the desired p19 proteins, as determined by SDS-PAGE analyses, were pooled and stored at 4 °C for subsequent assays. Pooled p19 fractions were monitored by SDS-PAGE as a single band and estimated to be >95% pure.

2.1.4 SDS-PAGE and Western Blot Analysis

For SDS-PAGE and Western blot analysis of CIRV p19 expression in *E. coli* BL21 (DE3) cells, 1 mL aliquots were taken at 0.5, 1, 2, and 4 h post-induction with IPTG (Figure 2.3). Cells transformed with the parental pTriEx 4-neo vector were used as a negative control. The pelleted cell aliquots were resuspended with SDS-PAGE loading

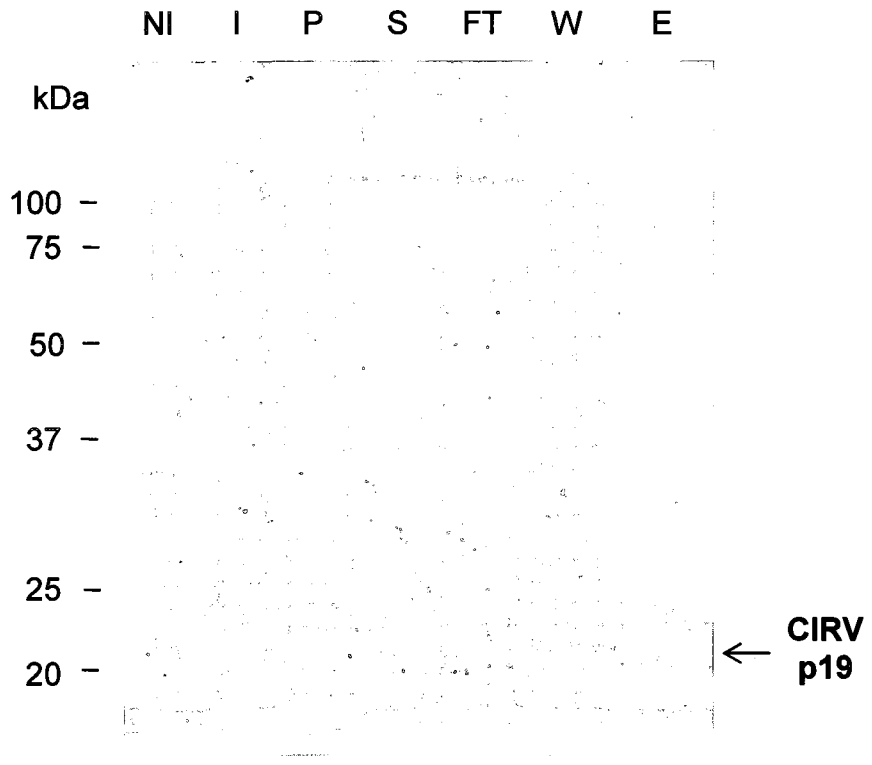

Figure 2.2 SDS-PAGE analysis of protein expression and Ni^{2+}-NTA column purification of CIRV p19. The migration of CIRV p19 protein is indicated. NI, whole cell lysate of non-induced cells; I, whole cell lysates of induced cells; P, insoluble cell fraction (pellet); S, soluble cell fraction; FT, flow-through; W, wash; E, elution.

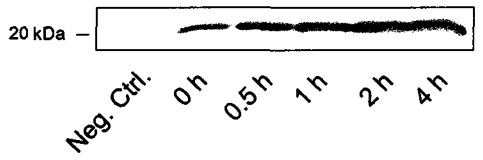

Figure 2.3 Western blot analysis of CIRV p19 expression. Cell aliquots were taken at 0, 0.5, 1, 2 and 4 h post-induction. The negative control (Neg. Ctrl.) is cells transformed with empty vector.

buffer (50 mM Tris-HCl, pH 6.8, 2% SDS, 10% glycerol, 1 mM DTT, 0.1% bromophenol blue), and 25 µL of sample was loaded per well for SDS-PAGE (12% resolving, 4% stacking gel). The resolved proteins were transferred to a Hybond-P polyvinylidene difluoride (PVDF) membrane (Amersham Biosciences, Piscataway, NJ). The membrane was blocked with 5% skim milk in Tris-buffered saline (TBS)–Tween and probed for the C-terminal His-tagged CIRV p19 with a monoclonal anti-polyhistidine primary antibody (1.5 µg/mL; R&D Systems, Minneapolis, MN) followed by a secondary horseradish peroxidase (HRP)-conjugated goat anti-mouse IgG antibody (1:1000 dilution; Jackson ImmunoResearch Laboratories, Westgrove, PA). Protein bands were visualized by using Western Lightning western blot chemiluminescence reagents (PerkinElmer, Boston, MA) according to the manufacturer's protocol.

2.1.5 p19-siRNA Electrophoretic Mobility Shift Assay (EMSA)

For EMSA p19-siRNA binding experiments, samples were prepared by allowing incubation of 200 nM fluorescently-labeled CSK siRNA with various concentrations (1 – 8192 nM) of purified p19, or its mutant derivatives, in buffer containing 20 mM Tris, 100 mM NaCl, 1 mM EDTA, 0.02% v/v TritonX-100, 1 mM Tris(2-carboxyethyl)phosphine (TCEP), pH 7 for 1 h at room temperature. For competitive experiments, 1 µM of CSK siRNA was premixed with the same molar ratio of the p19 dimer at room temperature for 1 h. Samples were then titrated with various concentrations of unlabeled CSK siRNA for 1 h at room temperature. Two microliters of 5X Hi-Density Tris-Borate-EDTA (TBE) sample buffer (Invitrogen, Burlington, ON) was added to 18 µL of binding reaction. Ten microliters of each sample was analyzed by electrophoresis at a constant voltage of 100 V

for 1 h through a 6% TBE DNA retardation gel in 1X TBE running buffer (Invitrogen, Burlington, ON). Band intensities corresponding to bound fluorescently-labeled siRNAs were quantified with a Molecular Dynamics Typhoon phosphorimager (GE Healthcare, Pistcataway, NJ) and the ImageJ software (National Institutes of Health, USA). The data from the direct binding experiments were fitted according to the following equation:

$$\Delta P = \Delta P_{Max}\left(\frac{K_d + np + x}{2np} - \sqrt{\left(\frac{K_d + np + x}{2np}\right)^2 - \frac{x}{np}}\right) \qquad [1]$$

where ΔP denotes the change in fluorescence intensity, ΔP_{Max} is the maximal change in fluorescence intensity, K_d is the dissociation constant, n is the number of equivalent sites on the p19 dimer, p is the concentration of fluorescently-labeled siRNA, and x is the concentration of the p19 dimer.

2.1.6 Fluorescence Detection Assay

Fluorescence detection assays were carried out using 96-well Ni^{2+}-NTA plates (Qiagen, Mississauga, Ontario). With respect to the binding specificity, a small peptide sequence (≈12 kDa) from the parental pTriEx 4-neo vector that corresponded to the multiple cloning site (MCS) of pTriEx 4-neo and included a His-tag at the C-terminus, was expressed and purified as described for CIRV p19. Two-hundred microliters (10 μg/mL) of purified CIRV p19 or the small peptide in 1X PBS, 0.2% bovine serum albumin (BSA), pH 7.2, was pre-bound to the surface of each well of the Ni^{2+}-NTA coated 96-well plate for 1-3 h at room temperature. Wells were then washed twice with

wash buffer (1X PBS, pH 7.2, 0.05% Tween 20, 1 mM ethylenediaminetetraacetic acid (EDTA)). The composition of the wash buffer and washing conditions were optimized to minimize non-specific binding, maximize signal, and lower background fluorescence. Two-hundred microliters of 1X PBS, 0.2% BSA, pH 7.2 was then placed in each well, and the background fluorescence (E_x = 546 nm, E_m = 590 nm) was measured with a Spectramax M2 plate reader (Molecular Devices Corporation, Sunnyvale, CA) for normalization purposes. The wells were then washed once more with wash buffer before the addition of the siRNAs. The fluorescently-labeled siRNAs (0–4 μM, diluted in 1X PBS, 0.2% BSA, pH 7.2) were then added to each well, and the plates were incubated in the dark for 3 h at room temperature. Wells were then washed four times with wash buffer, and 200 μL of 1X PBS, 0.2% BSA, pH 7.2, was placed into each well for fluorescence measurement. Fluorescence detection of bound fluorescently-labeled siRNAs (E_x = 546 nm, E_m = 590 nm) was measured with a Spectramax M2 plate reader. The relative fluorescence of specific binding was calculated by subtracting the non-specific value for the fluorescence of siRNA incubated with the small peptide from the measured fluorescence of siRNA binding to CIRV p19. Although the washing steps were optimized, it is possible that siRNA off rates may contribute to discrepancies between apparent dissociation constants.

In order to verify specific binding of the His-tag of CIRV p19 to the Ni^{2+}-NTA-coated wells, imidazole was added at varying concentrations (0–100 mM) to the Ni^{2+}-NTA-coated wells prior to the addition of CIRV p19 and fluorescently tagged siRNAs. In the presence of 100 mM imidazole, less than 10% total binding of fluorescently-labeled siRNA was detected at saturating siRNA concentrations. To ensure that the fluorescence

measured for siRNA binding was due to a specific interaction with CIRV p19, the ≈12 kDa His-tagged polypeptide was subjected to the same expression, purification, and assay conditions as utilized for CIRV p19. Negligible fluorescence was observed. Additionally, when relative K_d values of binding between different siRNA molecules were compared, experiments were conducted with the same batches of Ni^{2+}-NTA plates and the same stock solution of protein to ensure that the saturation point for each well was the same within experimental error. In some cases, saturation binding (i.e. the determination of $[siRNA]_{max}$) was impossible to achieve as a result of the prohibitively high cost of producing sufficient quantities of siRNA. In these cases, the potential error in the K_d value from this uncertainty in $[siRNA]_{max}$ was evaluated by measuring the saturation binding for a generic siRNA on the same surfaces with the same protein samples. For all reported K_d values, the results obtained from curve fitting, performed with and without the $[siRNA]_{max}$ measured with generic siRNA, were found to be the same within experimental error.

2.1.7 Screening of a Small Molecule Compound Library

The binding of purified CIRV p19 to Ni^{2+}-NTA plates was carried out as described for fluorescence-detection assays. After the washing and normalization steps, compounds from the Tripos Optiverse Panlabs library (NRC-BRI, Montreal, Quebec) were added at 100 μM in 1X PBS to each well (a different compound was added to each well of the plate). The plates were then incubated for 2 h at room temperature in the dark. Wells were then washed four times with wash buffer, and 200 μL of 1X PBS, 0.2% BSA,

pH 7.2, was placed into each well for normalization measurements (E_x = 546 nm, E_m = 590 nm) with a Spectramax M2 plate reader. Fluorescently-labeled siRNAs (CSK siRNA, 1 μM) diluted in 1X PBS, 0.2% BSA, pH 7.2, were then added to each well, and the plates were incubated in the dark for 2 h at room temperature. Wells were then washed four times with wash buffer, and 200 μL of 1X PBS, 0.2% BSA, pH 7.2, was placed into each well for fluorescence measurement. Fluorescence detection of bound fluorescently-labeled siRNAs (E_x = 546 nm, E_m = 590 nm) was measured with a Spectramax M2 plate reader. The increased emission wavelength of E_m = 590 nm rather than the reported E_m = 565 nm for Cy3/Dy547 was used to minimize background fluorescence. Post-incubation experiments in which the treatment with compounds was carried out after siRNA binding were also conducted. All experiments in which compounds of the small molecule library were added were carried out in triplicate. As controls, fluorescence was measured from wells containing CIRV p19 alone, as well as those containing CIRV p19 incubated with unlabeled CSK siRNAs.

2.1.8 MALDI-TOF Mass Spectrometry

For MALDI-TOF (matrix assisted laser desorption/ionization time-of-flight) mass spectrometry (MS) protein analysis, either 0.5 μg of CIRV p19 or CIRV p19 with a 1:1 or 1:10 molar ratio of compound **3** (see Figure 3.7, *Chapter 3*) were incubated for 1–24 h at room temperature prior to analysis. Similar experiments were conducted with 0.5 μg CIRV p19 incubated with compound **1** (see Figure 3.7, *Chapter 3*) in a 1:1 molar ratio. For MALDI-TOF analysis of NEM-modified CIRV p19, 0.5 μg of CIRV p19 was incubated with 50 mM NEM for 2 h at 4 °C. All experiments were performed in 10 mM

CH_3COONH_4 buffer, pH 7.5 and diluted to a final volume of 10 µL for analysis. One microliter of each sample was mixed with sinapinic acid matrix (60 mg/mL in 30% Ethanol; 10 µL), and the resulting mixture was spotted on a steel target plate and air dried at room temperature. Mass spectrometry was performed on a Voyager-DE STR MALDI-TOF instrument (Applied Biosystems, Foster City, CA) operated in the linear/positive mode.

2.1.9 Circular Dichroism and Thermal Melt Analysis

Circular dichroism (CD) spectra were recorded on 15 - 45 µM for wild-type p19, and the cysteine mutants C110I and C110S, in 20 mM Na_2HPO_4 pH 7.2, 25 mM NaCl and 1 mM DTT on a Jasco J-810 spectropolarimeter (Jasco, Easton, MD) with a 1-mm path length quartz cell at 25 °C. Spectra reflect an average of 8 scans recorded from 250 to 190 nm with a 0.2 nm step resolution, response of 1 s, speed of 20 nm/min, and a bandwidth of 1 nm. Following CD spectroscopy, the concentration of the samples used to calculate the molar ellipticity per mean residue was determined using the Bio-Rad Protein Assay (Bio-Rad, Hercules, CA). CD data was analyzed using the CDPro suite of programs (184). Thermal denaturation of the constructs was performed using a Jasco thermal control unit (model PTC-423S; Jasco, Easton, MD) with a heating rate of 1 °C/min from 25 to 95 °C. At each step, the molar ellipticity at 222 nm was recorded.

2.1.10 N-ethylmaleimide (NEM) Treatment

The alkylation experiments were carried out using 96-well Ni^{2+}-NTA-coated plates (Qiagen, Mississauga, Ontario) with the following His-tagged constructs: wild-type p19, C110A, C134S, C160S, C110S/C160S, C134S/C160S, C110I, C134I, C160I and C110I/C134I. Two-hundred microliters of 1 μM CIRV p19 or its mutant derivatives in PBS 0.2% BSA, pH 7.5, were pre-bound to the surface of each well of the Ni^{2+}-NTA-coated 96-well plate for 1 h at room temperature. Wells were then washed three times with wash buffer (1X PBS, 0.05% Tween 20, 1 mM EDTA). Then 200 μL of PBS or 20 mM NEM in PBS was added to each well and incubated for 1 h at room temperature. Wells were washed twice with wash buffer and 200 μL of wash buffer was placed in each well and background fluorescence was measured (E_x = 546 nm and E_m = 590 nm) with a Spectramax M2 Plate Reader (Molecular Devices Corporation, Sunnyvale, CA) for normalization purposes. Two-hundred microliters of 1 μM fluorescently-labeled CSK siRNA in 1X PBS, 0.2% BSA, pH 7.5, was added to each well and incubated in the dark for 1 h at room temperature. Wells were then washed twice with wash buffer and 200 μL of wash buffer was then placed in each well and read for fluorescence detection of bound fluorescently-labeled siRNAs (E_x = 546 nm and E_m = 590 nm). Experiments were performed four times for each construct, with or without NEM treatment.

2.1.11 Fluorescence Polarization and Data Analysis

Samples were prepared by allowing incubation of 2 μM labeled siRNAs or mir-122 with various concentrations of purified p19 in PBS with 10 mM DTT at room temperature for 1 h. Fluorescence polarization measurements were then carried out using

Fluorolog® Tau-3 Lifetime System (HORIBA Jobin Yvon, Edison, NJ) at room temperature. Polarization was monitored at E_m = 560 nm (with a bandwidth of 1 nm) with E_x = 546 nm (with a bandwidth of 6 nm). Polarization is expressed as:

$$P = \frac{I_V - I_H}{I_V + I_H} \qquad [2]$$

where I_V and I_H are the vertically and horizontally polarized emission intensities when linear polarized light was used to excite the sample. The polarization of each sample was calculated from an average of 10 measurements each of I_V and I_H and three replicates of such set of averages were collected. The resulting concentration-dependent increase in polarization was plotted against the concentration of the p19 dimer (since the p19 protein binds to one molecule of siRNA as a dimer) (185, 186) and fitted according to the following equation:

$$\Delta P = \Delta P_{Max}\left(\frac{K_d + np + x}{2np} - \sqrt{\left(\frac{K_d + np + x}{2np}\right)^2 - \frac{x}{np}}\right) \qquad [3]$$

where ΔP_{Max} denotes the maximal change in polarization, K_d is the dissociation constant, n is the number of equivalent sites on the p19 dimer, p is the concentration of labeled small RNA, and x is the concentration of the p19 dimer.

Competitive studies were carried out by pre-mixing 2 μM of CSK siRNA with the same molar ratio of the p19 dimer at room temperature for 1 h. Samples were then titrated with increasing concentration of unlabeled CSK siRNA for 1 h at room temperature and the decrease in fluorescence polarization was measured. The resulting concentration dependent decrease in polarization was fitted to the following equation:

$$\Delta P = \frac{\Delta P_{Max}}{\left(\frac{K_d \cdot (K'_d + x)}{(K'_d + p)}\right) + 1} \qquad [4]$$

where ΔP_{Max} denotes the maximal change in polarization, K_d is the dissociation constant for one small RNA and K'_d is the dissociation constant for the competing small RNA, p is the concentration of labeled small RNA, x is the concentration of the unlabeled small RNA.

2.1.12 Graphs and Data Analysis

All graph analyses were performed using the Graph-Pad Prism (San Diego, CA, USA) or GraFit version 3.0.0.3 (Erithacus Software, Surrey, UK) softwares.

2.2 Target Site Accessibility Methods

2.2.1 Cell Culture

The Huh-7 cell lines used in this study were cultured in Dulbecco's Modified Eagle Medium (DMEM; Invitrogen, Burlington, ON) supplemented with 100 nM nonessential amino acids, 50 U/mL penicillin, 50 mg/mL streptomycin, and 10% fetal bovine serum (FBS; PAA Laboratories, Etobicoke, ON). G418 (Geneticin) was added at a concentration of 250 μg/mL to the Huh-7 cells stably expressing HCV subgenomic replicons. The pFK-I389neo/NS3-3'/5.1 and pFK-I389luc/NS3-3'/5.1 plasmids, which contain HCV subgenomic replicons (genotype 1b, Con1, Genbank Accession # AJ242654), were kindly provided by Ralf Bartenschlager (Institute of Hygiene, University of Heidelberg, Heidelberg, Germany) (187). The replicons harbour either neomycin resistance (neo^R; pFK-I_{389}neo/NS3-3'/5.1) or the firefly luciferase (luc; pFK-I_{389}luc/NS3-3'/5.1) gene at the 5' end (driven by the HCV internal ribosomal entry site (IRES)), but otherwise are identical and express the HCV non-structural proteins (NS3 to NS5B) from the encephalomyocarditis virus (EMCV) IRES and are described in (187).

For siRNA transfections, Huh-7 cells harbouring the subgenomic replicon (pFK-I_{389}neo/NS3-3'/5.1) were seeded in 60-mm dishes (1×10^6 cells) for preparation of whole cell lysates and total RNA extractions. The fluorescently-labeled (Cy3 or Dy547) siRNA duplexes (10-100 nM; described below) were transfected using Lipofectamine™ RNAiMAX Transfection Reagent (Invitrogen, Burlington, ON) according to the manufacturer's protocol. Whole cell lysates and RNA extractions were prepared at 24, 48 and 72 h post-transfection. IFNγ was used as a positive control for knockdown of HCV RNA replication at a concentration of 100 units/mL.

2.2.2 siRNA Sequences

HCV-specific siRNAs were designed based on the HCV subgenomic replicon (Genbank accession #AJ242654) (187). The siRNA design software described in (188) was used for the design of HCV-specific siRNAs and is freely available at http://i.cs.hku.hk/~sirna/software/sirna.php. This software compiles the design softwares of Ambion, Jack, Emboss, MPI, Genscript, Qiagen, Invitrogen, Deqor, and MPI + Rational for siRNA design. The organism that was selected was *Homo sapiens* and output siRNAs were selected that were predicted from at least 4 softwares. The top siRNAs were selected for further analysis and scored according to the design criteria outlined by Reynolds and colleagues (172). The siRNAs that were selected for analysis had scores ≥ 6. The siRNA sequences used to investigate target site accessibility are listed in Table 2.3. Where indicated, duplex siRNAs were formed between the corresponding sense and antisense strands according to the manufacturer's protocol. The 331 (IRES) siRNA and the positive control, NS5B-7256 siRNA (a.k.a. NS5B-6367; (136)), have been previously reported to be functional siRNAs for inhibition of HCV RNA in cell culture (136-138). The SL3.3-8589 siRNA was designed against a known stem-loop in the NS5B coding region of the HCV genome (SL3.3; (189, 190)) as a negative control.

2.2.3 In Vitro Transcription (IVT)

In vitro transcripts were generated using the MEGAscript™ T7 kit (Ambion, Austin, TX) according to the manufacturer's protocol. Briefly, the template DNA was linearized with the restriction enzyme *ScaI* (New England Biolabs, Pickering, ON),

Table 2.3 siRNA sequences used in the target site accessibility studies.

siRNA	Sequence[1,2,3]	References
GL3	5'-cuuacgcugaguacuucgaTT-3' 3'-TTgaaugcgagucaugaagcu-5'	(177, 179, 180, 182)
331 (IRES)	5'-ggucucguagaccgugcacuu-3' 3'-uuccagagcaucuggcacgug-5'	(137, 177)
NS3-2904	5'-ucacccaaauguacaccaaug-3' 3'-uuagugggguuuacaugugguu-5'	
NS4B-5027	5'-cauacccuccuguuuaacauc-3' 3'-uuguaugggaggacaaauugu-5'	
NS5A-5567	5'-ugcacgguguugacugauuuc-3' 3'-auaggugccacaacugacuaa-5'	
NS5B-7256	5'-gacacugagacaccaauugacTT-3' 3'-TTcugugacucugugguuaacug-5'	(136, 138)
NS5B-8136	5'-ggaugauccugaugacucauu-3' 3'-uuccuacuaggacuacugagu-5'	
SL3.3-8589	5'-uguggugccuacuccuacuuu-3' 3'-guacaccacggaucaccauga-5'	

[1]Uppercase letters denote deoxyribonucleotides; [2]All siRNAs were single-stranded guide strand for microarray experiments and duplex for transfection into Huh-7 cells; [3]All siRNAs used were labeled with Cy3 or Dy547 dyes at the 5' end of the anti-sense (guide) strands as indicated in the text.

precipitated for less than 30 min, and resuspended in RNase-free water to a final concentration of 0.5 μg/μL. The IVT reaction was set up in a final volume of 20 μL and incubated at 37 °C for 2 h. In order to degrade the template DNA, 1 μL of *DNase I* was added and the reaction was incubated for an additional 15 min at 37 °C. The *in vitro* transcripts were then cleaned up using the MEGAclear™ kit (Ambion, Austin, TX) according to the manufacturer's protocol. A 20 μL reaction typically produced ~100 μg of RNA. The concentration was determined by measurement of the absorbance at 260 nm with an ND-1000 spectrophotometer (NanoDrop Technologies, Rockland, DE), and RNA integrity was verified by electrophoresis using the Agilent 2100 bioanalyzer with the RNALabChip® kit (Agilent Technologies, Palo Alto, CA) according to the manufacturer's protocol.

2.2.4 Atomic Force Microscopy (AFM)

RNA transcripts were diluted in AFM imaging buffer (20 mM HEPES, 10 mM $MgCl_2$, 3 mM $NiCl_2$, pH 7) to 0.5 to 2 ng/μL. Prior to RNA deposition, freshly cleaved mica (grade V2; Ted Pella Incorporated, Redding, CA) was treated with 4 mM $NiCl_2$ for 1 min at room temperature and washed twice by soaking in 10 mL nuclease-free water for 10 and 1 min, respectively. The $NiCl_2$-treated mica was then dried under a stream of nitrogen. Ten microliters of diluted RNA was dropped on the surface of the $NiCl_2$-treated mica and allowed to adsorb for 5 min at room temperature. Non-adsorbed RNA was removed by two washes with 10 mL of nuclease-free water as described above, after which the sample was dried under a stream of nitrogen and imaged. Imaging was performed at room temperature (22 ± 1 °C) on a PicoSPM atomic force microscope

(Molecular Imaging, Providence, RI) in acoustic (AC) mode using aluminum-coated silicon tips with spring constants of ~40 N/m and resonance frequencies between 250 and 325 kHz. Fields of 0.5 to 3.0 μm were scanned at 1 to 1.5 Hz. Images were flattened, and approximate cluster diameters were determined using PicoScan 5.3.3 software (Molecular Imaging, Providence, RI). Two or three independently prepared samples were imaged for each RNA transcript, and several areas were scanned for each sample.

2.2.5 Microarray Design

A prototype microarray was generated, consisting of a dilution series of HCV subgenomic replicon RNA (5, 25, 100, 125, 250 and 500 ng/uL) as well as *Campylobactor jejuni* positive (Cj0373: 5'-GTA TCC ACG CAC CTT TAA ATG AAA AAA CC-3'; Cj1119c: 5'-GTA CCA TCG CTA TAA CTT TGG CTT-3') and negative (Cj1437c: 5'-GCC AGA GTG TAT GTG ATT TGG TTG AAC-3') control oligonucleotides. Computer-based homology searches using NCBI BLAST was used to ensure that control oligonucleotides contained no homology with the *Homo sapiens* or HCV genomes, or any of the HCV-specific siRNAs. All oligonucleotides were PAGE-purified and spotted at a final concentration of 500 ng/μL (Invitrogen Canada, Burlington, ON). Each sample was spotted in quadrupicate, interspersed by blank spots across the array in order to reduce spatial effects (see Figure 5.10, *Chapter 5*).

2.2.6 Preparation of Microarray Spike-ins

Cy3-labeled short DNA oligonucleotides complementary to the Cj1119c and Cj0373 oligonucleotides spotted on the microarrays were prepared as positive control spike-ins and printing quality controls using the Mirus Label-IT® Cy3 Labeling kit (Fisher Scientific, Ottawa, ON) according to the manufacturer's protocol. For normalization purposes and to account for spot morphology, a DNA probe was designed against the relatively unstructured luciferase region of the HCV replicon (see Figure 5.6, *Chapter 5*). The Luc988-42nt probe (5'-GGA AGG GCC ACA CCC TTA GGT AAC CCA GTA GAT CCA GAG GAA-3') was labeled with Cy5 for cross-channel normalization, using the Mirus Label-IT® Cy5 Labeling kit (Fisher Scientific, Ottawa, ON). All labeling reactions were carried out according to the manufacturer's protocol with the following modifications. Labeling reactions typically contained 5 μg DNA and 2.5 μL of Cy3 or Cy5 label in a 50 μL reaction volume. Reactions were incubated at 37 °C overnight. Unincorporated dye was removed by ethanol precipitation and the Cy3-labeled oligonucleotides were resuspended in RNase-free water. Labeling efficiencies were between 9-20 pg/μL as assessed using an ND-1000 spectrophotometer (NanoDrop Technologies, Rockland, DE). All oligonucleotides were PAGE-purified prior to the labeling reactions.

2.2.7 Microarray Printing and Blocking

Microarray printing was carried out using a Nano-Plotter (NP2.1, GeSiM, Germany) on barcoded Nexterion® slide E, epoxysilane coated substrates (Schott North America, Louisville, KY). All probes were diluted in spotting buffer (20 mM HEPES, 50

nM KCl, 10 mM $MgCl_2$, 1 mM DTT, pH 7.2) and spotted at 18 ± 2 °C and a relative humidity of 50%. Spotting was carried out in one tip mode with the nano tip A. The average drop volume was 140 pL and 7 drops were deposited for a total of approximately 980 pL/spot. The spotting buffer was also printed on the slides as a negative control. Post-printing, the slides were left in the printer for 30 min to dry before storage at -80 °C until use.

2.2.8 Microarray Hybridization and Data Analysis

Microarray hybridizations were performed between single-stranded, fluorophore-labeled antisense (guide) siRNAs and the HCV replicon RNA under native (non-denaturing) conditions in order to maintain the RNA secondary structure. All solutions were prepared with nuclease-free water and all hybridizations were performed at 37 °C, unless otherwise indicated. All slides were blocked in 4× SSC, 0.1% ultrapure non-acetylated BSA (Ambion, Austin, TX) for 15 min at 37 °C and washed five times with nuclease-free water at room temperature for 1 min each. The slides were dryed prior to the hybridization reaction by centrifugation at 200 ×g for 5 min. Hybridizations were performed in 1× Hyb buffer (20 mM HEPES, pH 7.8, 50 mM KCl, 10 mM $MgCl_2$, 1 mM DTT) supplemented with 100 µg/mL yeast tRNAs, 0.625 mg/mL salmon sperm DNA, 40 U RNase-OUT (Invitrogen Canada, Burlington, ON), 300 pg/µL Cy3-Cj1119c spike-in, 900 pg/µL Cy3-Cj0373 spike-in, 30 nM Cy5-Luc988-42nt, and 1 µM siRNA in a 40 µL reaction volume. The hybridization reactions were denatured at 65 °C for 5 min and then incubated at 37 °C for 10 min, prior to application to the microarrays. Both the coverslips and microarray slides were pre-heated to 37 °C for 10 min prior to hybridization.

Hybridizations were performed for 45 min to 1 h at 37 °C under glass coverslips (24 × 20 mm) in a humidified SlideBooster™ hybridization chamber (Olympus Advalytix, Concord, MA). For hybridizations carried out under denaturing conditions, hybridization buffer was replaced with a denaturing 50% DIG Easy Hybridization solution (Roche, Laval, QC) and hybridizations (target microarray + hybridization solution) were initially heated to 65 °C and slowly cooled to 37 °C over the 1 h hybridization period. After hybridization, microarrays were washed twice with 1× SSC + 0.05% SDS, twice with 0.5× SSC, and twice with 0.1× SSC at 45 °C for 5 min each. The slides were spun dry by centrifugation at 200 ×g for 5 min and stored in light-tight containers until they were scanned. Microarrays were scanned using the VersArray Chipreader (Bio-Rad, Hercules, CA), according to the recommendations of the manufacturer.

Spot quantification, signal normalization, and data analysis was performed using the Array-Pro Analyzer image analysis software (version 4.5; MediaCybernetics, Silver Spring, MD). Net signal intensities were obtained by local-ring background subtraction (net intensity = raw intensity – background). For normalization purposes and to account for spot morphology, the ratio of the signal intensities of the siRNAs (Cy3 channel) to that of the Luc988-42-nt spike-in (Cy5 channel) of the spots containing HCV RNA was used for further analysis (normalized net intensity). The Cy3-labeled *Campylobacter jejuni* spike-ins were used to scale the intensities between microarrays. A single HCV replicon RNA concentration was chosen for analysis (125 ng/μL) since it had a greater than 2-fold signal-to-noise ratio without reaching saturation for all HCV-specific siRNAs. Signal intensities for quadruplicate spots were averaged, and all hybridizations were carried out in duplicate or triplicate.

2.2.9 Western Blot Analysis

For detection of HCV proteins, whole cell lysates were prepared from Huh-7 cells harbouring subgenomic replicons after treatment with siRNAs as described for 24, 48 or 72 h. Cells were washed twice with PBS (8 g/L NaCl, 0.2 g/L KCl, 1.44 g/L Na_2HPO_4, 0.24 g/L KH_2PO_4, pH 7.4) and lysed with a lysis buffer consisting of 50 mM Tris-HCl (pH 6.8), 2% SDS, 10% glycerol, 100 mM DTT and 0.1% bromophenol blue (prepared initially without the DTT and bromophenol blue). Complete™ protease inhibitor cocktail (Roche Diagnostics, Penzberg, Germany) was added to each extract to a final concentration of 1X. The protein concentration of each sample was quantified using the Bio-Rad DC protein assay (Bio-Rad, Hercules, CA) according to the manufacturer's protocol. Prior to loading, 10% v/v of DTT and bromophenol blue (1:1) was added to each sample and the samples were heated to 95 °C for 5 min and cooled on ice. Approximately 60 μg of protein per well was loaded for SDS-PAGE (10% resolving, 4% stacking gel). The resolved proteins were transferred to a Hybond-P PVDF membrane (GE Healthcare, Piscataway, NJ). The membrane was blocked for 1 h with 5% skim milk in TBS–Tween and probed for the HCV NS5A protein with a mouse monoclonal anti-NS5A antibody (0.2 μg/mL; Virostat, Portland, ME) followed by a HRP-conjugated goat anti-mouse IgG antibody (1:1000 dilution; Jackson ImmunoResearch Laboratories, Westgrove, PA). As a loading control, the membranes were stripped using Re-blot Plus Strong Solution (Millipore, Concord, MA) according to the manufacturer's protocol, and re-probed with a mouse anti-PTP1D/SHP2 primary antibody (1:1000 dilution; Sigma, Saint Louis, MO) with the same secondary antibody as described above. Protein bands

were visualized by using Western Lightning western blot chemiluminescence reagents (PerkinElmer, Boston, MA) according to the manufacturer's protocol.

2.2.10 RNA Isolation and Northern Blot Analysis

Total RNA was isolated from siRNA-transfected HCV subgenomic replicon-harboring cells at 24, 48 and 72 h post-transfection using the RNeasy extraction kit (Qiagen, Mississauga, ON). Approximately 0.5 μg/well of total RNA was loaded onto a 1% agarose gel. Biotinylated negative-sense probes complementary to the HCV genome NS5B region nts 6648-7770 (Genbank accession #AJ242654) and the β-actin gene (Genbank accession #X00351) were synthesized using the MEGAscript™ T7 kit (Ambion, Austin, TX). *In vitro* transcriptions were performed as described above with the inclusion of biotin-11-UTP and biotin-11-CTP (Perkin Elmer, Boston, MA) at molar ratio of 1:3 with unlabeled UTP and unlabeled CTP, respectively, and were carried out at 37 °C overnight. DNA template was removed by *DNase I* digestion, and biotinylated RNA was purified using the MEGAclear™ kit (Ambion, Austin, TX) with elution in RNase-free water. The biotinylated negative-sense probes were used at a final concentration of 2.2 ng/uL and 0.133 ng/uL for the HCV and β-actin probes, respectively. Northern blotting and hybridization were carried out using the NorthernMAX® kit (Ambion, Austin, TX) and Hybond XL nylon membranes (GE Healthcare, Piscataway, NJ). The bound riboprobes were detected using the Chemiluminescent Nucleic Acid Detection Module (Pierce, Rockford, IL) according to the manufacturer's protocol.

2.2.11 hAGO2:siRNA EMSA

For EMSA of siRNAs bound by hAGO2, purified His_6-tagged hAGO2 was kindly provided by Ian MacRae (The Scripps Reseach Institute, La Jolla, CA) and was purified according to the protocol described in (191). hAGO2 was diluted to 0.66 mg/ml, aliquoted, and stored at -80 °C until use. Samples were prepared by allowing incubation of 40 nM fluorescently labeled single-stranded siRNAs with 0-1000 nM His_6-tagged hAGO2, in slicing buffer (20 nM Tris-HCl, 50 nM KCl, 1.5 mM $MgCl_2$, 5% glycerol, pH 7) supplemented with 2 U RNase-OUT at 37 °C for 30 min. Prior to loading on the gel, 1 µL of 5X Hi-Density TBE sample buffer (Invitrogen, Burlington, ON) was added to the 10 µL reaction. Ten microliters of each sample was analyzed by electrophoresis at a constant voltage of 100 V for 45 min through a 6% TBE DNA retardation gel in 1X TBE running buffer (Invitrogen, Burlington, ON). Bands corresponding to bound fluorescently-labeled single-stranded siRNAs were quantified with a Hitachi FMBIO III Multi-view fluorescent image analyzer (Hitachi Software Engineering) and the ImageJ software (National Institutes of Health, USA).

2.2.12 In Vitro RISC Cleavage Assay

In vitro RISC cleavage assays were performed at 30 °C for 90 min in a reaction volume of 10 µl. Reactions contained 30-60 nM hAGO2, 60 nM fluorescently-labeled single-stranded siRNA, 1 U RNase-OUT, 20 mM Tris-HCl (pH 7), 50 mM KCl, 1.5 mM $MgCl_2$, and 10 ng of *in vitro* transcribed 8858-nt HCV subgenomic replicon RNA (pFK-I_{389}luc/NS3-3'/5.1; described above). One microliter of the reaction was diluted in 5 µl of NorthernMAX® formaldehyde load dye (Ambion, Austin, TX) and was heated at 75 °C for 10 min before samples were analyzed by electrophoresis on a 1% agarose gel.

Northern blotting was performed as described above to detect the HCV RNA 5' and 3' cleavage products.

Chapter 3: Development of a Protein-based Tool for Studying Small RNAs

3.1 Introduction

In plants, RNA silencing is an important host defence pathway against invading pathogens. Both RNA and DNA viruses, which replicate through a dsRNA intermediate in the cytoplasm of host cells, can effectively trigger the RNA silencing pathway (64, 65, 192). Viral invasion and persistence therefore requires evasion or suppression of the RNA silencing surveillance system. As a counter-defensive strategy, several viruses encode suppressors of RNA silencing. Viral suppressors of RNA silencing (VSRs) could be used to directly block specific steps of the RNA silencing pathway and analyze the roles of RNA silencing pathway components, including both the protein and RNA components of the pathway. Specifically, VSR-based tools could be useful to probe the importance of this pathway in the context of host-virus interactions and may be useful in the systematic study of RNA silencing pathways and small RNAs *in vitro* and in diverse eukaryotic organisms. The VSRs identified to date will be reviewed and our efforts at developing protein-based tools for studying RNA silencing and small RNAs are described.

3.1.1 Suppression of RNA Silencing

VSRs can implement diverse mechanisms to target key steps of the RNA silencing pathway, including: (i) recruitment of endogenous suppressors of RNA silencing; (ii) transcriptional modification of positive effectors or endogenous suppressors of RNA silencing; and (iii) direct inhibition of RNA silencing pathway components and/or effectors (i.e. dsRNA, Dicer, siRNA, miRNA, AGOs, or other components of the RISC complex) (63, 193, 194). A summary of the known plant and

animal VSRs identified to date, their proposed effector mechanisms and their other known function(s) in the viral life cycle, are summarized in Table 3.1.

3.1.2 Recruitment of Endogenous Suppressors of RNA Silencing

Endogenous inhibitors of RNA silencing have been identified in plants (260) as well as in *C. elegans* (261). This suggests a mechanism that viruses could take advantage of in order to persist in their hosts. For example, Hc-Pro of potyviruses has been demonstrated to interact with a calmodulin-related protein, rgsCaM (regulator of gene silencing calmodulin) (260). Overexpression of rgsCaM mimics suppression of RNA silencing by Hc-Pro suggesting that rgsCaM is an endogenous suppressor of RNA silencing (260). Hence, one of the mechanisms used by Hc-pro to inhibit RNA silencing may be recruitment of this endogenous cellular suppressor protein (260). In addition, the ERI-1 (enhanced RNA interference-1) protein of *C. elegans* is an evolutionarily conserved nuclease that processes siRNAs into shorter, inactive forms effectively suppressing RNA silencing (261). However, it remains to be seen whether ERI-1 orthologues contribute to suppression of RNA silencing mediated by viruses (194). Endogenous suppressors of RNA silencing have not yet been identified in mammalian cells; however, it would not be surprising that there is some form of cellular regulation of the RNA silencing pathway in mammals.

Table 3.1 **Plant and Animal VSRs.**[1]

Virus genus	Virus Name	VSR[2]	Mechanism of Suppression	Other Functions	References
Plant Viruses					
Aureusvirus	*Pothos latent virus*	P14	dsRNA binding	Pathogenicity determinant	(195)
Begomovirus	*Tomato leaf curl virus*	C2		Pathogenicity determinant	(196)
	Mungbean mosaic virus	AC2	Transcriptional activation	Transcriptional activator	(197)
	African cassava mosaic virus	AC2	Transcriptional activation	Transcriptional activator	(198)
		AC4	miRNA binding[3]	Pathogenicity determinant	(198, 199)
Carmovirus	*Turnip crinkle virus*	CP	dsRNA binding	Coat protein	(200-203)
Closterovirus	*Beet yellow stunt virus*	P22		Major coat protein	(204)
	Beet yellows virus	P21	dsRNA binding[4]	Replication enhancer	(204-208)
	Citrus tristeza virus	P20		Replication enhancer	(209)
		P23		Replication enhancer	(209)
		CP		Coat protein	(209)
	Grapevine leafroll-associated virus-2	P24			(204)
Crinivirus	*Sweet potato chlorotic stunt virus*	P22			(210)
		RNase 3	RNase III		(210)
Comovirus	*Cowpea mosaic virus*	Small CP		Small coat protein	(211)
Cucumovirus	*Cucumber mosaic virus*	2b	dsRNA binding	Host-specific movement protein	(202, 212-214)
	Tomato aspermy virus	2b	dsRNA binding[5]	Host-specific movement protein	(215-217)
Curtovirus	*Beet curly top virus*	L2	ADK binding	Pathogenicity determinant	(218)
Furovirus	*Soilborne wheat mosaic virus*	19K			(219)
Hordeivirus	*Barley stripe mosaic virus*	Γb	RNA binding[6]	Replication enhancer; movement protein; seed transmission; pathogenicity determinant	(203, 220, 221)
Pecluvirus	*Peanut clump virus*	P15	dsRNA binding[7]	Movement protein	(203, 222, 223)
Phytoreovirus	*Rice dwarf virus*	Pns10			(224)
Polerovirus	*Beet western yellows virus, Cucurbit aphid-born yellows virus*	P0	AGO1 binding	Pathogenicity determinant	(225, 226)
Potexvirus	*Potato virus X*	P25		Movement protein	(227)
Potyvirus	*Tobacco etch virus, Potato virus Y, Turnip mosaic virus*	Hc-Pro[8]	dsRNA binding[9,10]	Movement protein; polyprotein processing; aphid transmission; pathogenicity determinant	(203, 208, 212, 228-230)
Sobemovirus	*Rice yellow mottle virus*	P1		Movement protein; pathogenicity determinant	(231, 232)
Tenuivirus	*Rice hoja blanca virus*	NS3	dsRNA binding[11]		(233-235)

***Table 3.1** Continued...*

Virus genus	Virus Name	VSR[2]	Mechanism of Suppression	Other Functions	References
Tobamovirus	*Tobacco mosaic viruses, Tomato mosaic viruses*	P130		Replication	(236)
Tobravirus	*Tobacco rattle virus*	16K			(237-239)
Tombusvirus	*Carnation Italian ringspot virus, Cymbidium ringspot virus, Tomato bushy stunt virus*	p19	dsRNA binding[12]	Movement protein; pathogenicity determinant	(185, 186, 202, 208, 231, 240)
Tospovirus	*Tomato spotted wilt virus*	NSs		Pathogenicity determinant	(233, 241)
Tymovirus	*Turnip yellow mosaic virus*	P69		Movement protein; pathogenicity determinant	(242)
Vitivirus	*Grapevine virus A*	P10	RNA binding[13]	Pathogenicity determinant	(204, 243, 244)
Animal Viruses					
Adenovirus	*Adenovirus*	VA1 RNA	Dicer binding	PKR inhibitor	(245, 246)
Ebolavirus	*Ebola virus*	VP35	dsRNA binding	polymerase cofactor; PKR and RIG-I inhibitor; IFN resistance	(247)
Hepacivirus	*Hepatitis C virus*	core E2	Dicer binding Ago2 binding	capsid protein envelope protein	(248, 249) (250)
Lentivirus	*HIV-1*	Tat	Dicer binding	transcriptional transactivator	(251)
Nodavirus	*Flock house virus, nodamura virus, striped jack nervous necrosis virus, greasy grouper nervous necrosis virus*	B2	dsRNA binding[13]		(68-71, 252-255)
Orthobunyavirus	*La Crosse virus*	NSs		IFN resistance	(256)
Orthomyxovirus	*Influenza virus A*	NS1	dsRNA binding	PKR inhibitor; poly(A) binding; inhibitor of mRNA export	(69, 257, 258)
Orthoreovirus	*Reovirus*	σ3	dsRNA binding[14]	capsid protein	(259)
Poxvirus	*Vaccinia virus*	E3L	dsRNA binding	PKR inhibitor; IFN resistance	(69)
Spumavirus	*PFV-1*	Tas		transcriptional transactivator	(83)

[1]Adapted and expanded from reference (63); [2]VSR, Viral suppressor of RNA silencing; [3]Prefer mature single-stranded miRNAs; [4]Specificity of dsRNA-binding of p21 is controversial, it has been reported that p21 is a general dsRNA-binding protein (206), in contrast, others have reported that p21 binds size-selectively to 21-nt duplex siRNAs (203, 208); [5]Prefer 21-nt or 32-nt duplex siRNAs; [6]Binds both long ssRNA and 21-nt siRNA duplexes; [7]Prefers 21-nt siRNA duplexes with 3' 2-nt overhangs; [8]Hc-Pro, Helper component proteinase; [9]Efficient binding requires an unidentified cellular factor *in vitro*; [10]Some Hc-pro isoforms have been shown to bind with higher affinity to long dsRNA than to siRNA duplexes and numerous dsRNA-binding independent VSR activities have been described for Hc-Pro isoforms (references herein); [11]Prefer 19-nt RNA duplexes; [12]Binds long ssRNA and dsRNA, in addition to siRNA duplexes; [13]Prefer mature single-stranded miRNAs; [14]Prefer dsRNA longer than 30-nt. ADK, Adenosine kinase; AGO1, Argonaute 1; PKR, Protein Kinase R; RIG-I, Retinoic acid inducible gene-I; IFN, interferon.

3.1.3 Transcriptional Modification of Positive Effectors or Endogenous Suppressors of RNA Silencing

A second method for suppression of RNA silencing by viruses involves modification of the host transcriptome (261). This was first described for the begomoviruses which encode transcriptional activator proteins that are suppressors of RNA silencing (262) (Table 3.1). The nuclear localization and DNA-binding activities of the transcriptional activator proteins were required for their suppression of RNA silencing; and transcriptional activator proteins from two different begomoviruses induced a common set of host mRNAs (197). Of these, the WEL-1 (Werner exonuclease-like 1) protein was sufficient to suppress RNA silencing in *Nicotiana benthamiana* (197), demonstrating that VSRs may act by transcriptional modification of positive effectors or endogenous suppressors of RNA silencing. An alternative transcriptional method for suppression of RNA silencing may involve transcriptional downregulation at the promoter level for the Dicer, AGOs, or other RNA silencing pathway components themselves. To date, this has not been demonstrated, but it could represent a novel mode of RNA silencing suppression.

3.1.4 Direct Inhibition of RNA Silencing Pathway Components and/or Effectors

A third strategy for suppression of RNA silencing involves inhibition of key components of RNA silencing pathways, including direct binding to dsRNA, Dicer, siRNAs, miRNAs, AGOs, or other components of the RISC complex. For example, the polerovirus P0 protein has been demonstrated to bind directly to, and destabilize, AGO1 of *Arabidopsis thaliana* (226) (Table 3.1). Silencing suppression could also be RNA-

mediated rather than protein-mediated. This is exemplified in the case of adenovirus VA1 RNA which competes with small RNAs for the exportin 5 receptor and human Dicer (245, 246) (Table 3.1). In addition to binding to the proteins of the RNA silencing pathway, many VSRs have evolved that are able to bind to dsRNAs, or small RNAs, which are the inducers and mediators of the RNA silencing pathway, respectively. These dsRNA-binding VSRs will be discussed in more detail below.

3.1.5 Double-stranded RNA-binding VSRs

A major class of VSRs are dsRNA-binding proteins. A role for dsRNA binding in suppression of RNA silencing was initially proposed by Guo and Ding for the cucumoviral 2b protein (263), and has since grown to include VSRs from diverse classes of both plant and animal viruses (Tables 3.1). In theory, dsRNA-binding VSRs could target the RNA silencing pathway at two key steps: by binding and sequestering the silencing inducer – long viral dsRNA, and/or by binding and sequestering the mediators of RNA silencing – siRNAs (203). Most of the dsRNA-binding VSRs have no sequence similarity to the canonical dsRNA binding motif found in many cellular proteins, such as the *Xenopus laevis* RNA binding protein A (*Xlrbpa2*), *Drosophila* Staufen protein, PKR, Dicer or R2D2 (264-266), suggesting that the distinct protein folds used to bind dsRNA evolved independently in these viruses (63) (Figure 3.1).

Many of the dsRNA-binding VSRs are able to bind to both long dsRNA and the silencing-generated small RNA duplexes. In fact, no size selection in dsRNA-binding has been observed for aureusviral P14 (195), carmoviral CP (200-203), vitiviral P10 (243), ebola virus VP35 (247), influenza NS1 (69, 257), and vaccinia E3L (69); while reovirus

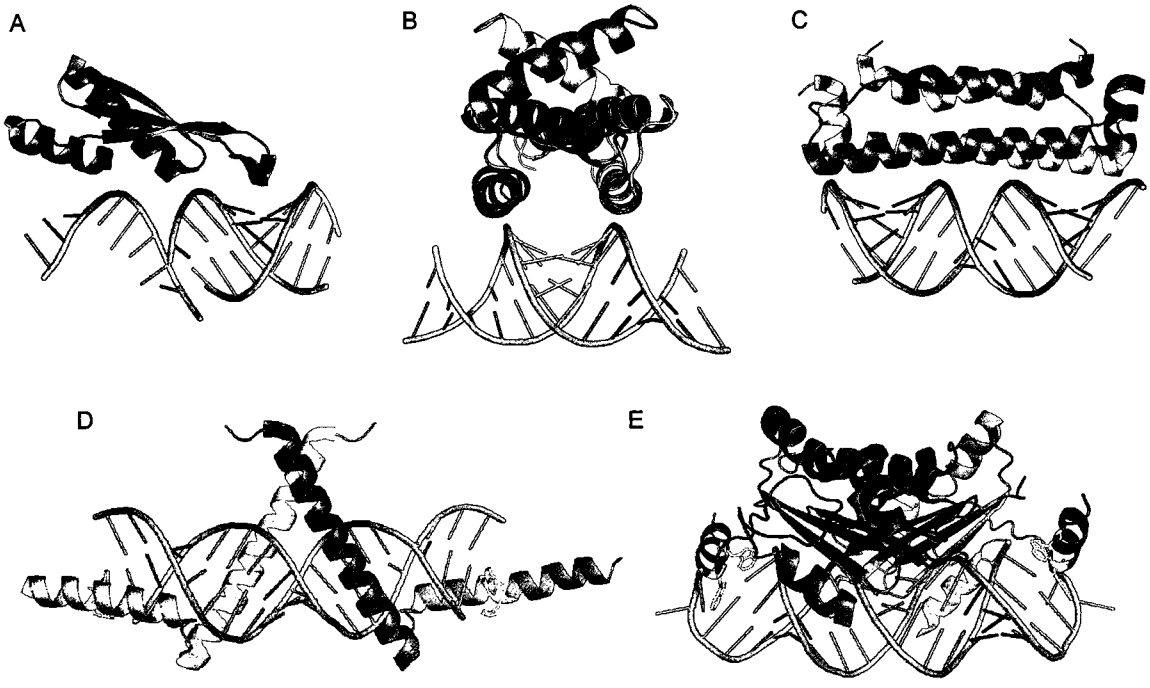

Figure 3.1 Comparison of dsRNA binding motifs between the canonical dsRNA-binding motif and dsRNA-binding VSRs. A) Cartoon view of the canonical dsRNA-binding motif of *Xlrbpa2* in complex with dsRNA (PDB ID: 1D12, reference (264)). B) Cartoon view of the NS1 protein of influenza modeled in complex with dsRNA (PDB ID: 1NS1, reference (267)). C) Cartoon view of flock house virus B2 in complex with dsRNA (PDB ID: 2AZ0, reference (268)). D) Cartoon view of tomato aspermy virus 2b in complex with dsRNA (PDB ID: 2ZI0, reference (216)). The conserved His51 and crucial Trp40 residues are indicated in yellow. E) Cartoon view of the CIRV p19 protein in complex with 21-nt siRNA (PDB ID: 1RPU, reference (185)). The p19 protein end-capping Trp39 and Trp42 residues are indicated in yellow.

σ3 and nodaviral B2 exhibit higher affinities for long dsRNA than for siRNAs (71, 259) (Table 3.1). In contrast, several dsRNA-binding VSRs have been identified that bind with some specificity to silencing-generated small RNA duplexes in a size-selective manner (Table 3.1); these include: *Tobacco etch virus* Hc-Pro (203, 208), *Peanut clump virus* P15 (203), *Barley stripe mosaic virus* γB (203), closteroviral p21 (203, 205, 208), *Rice hoja blanca virus* NS3 (234, 235), *Tomato aspermy virus* 2b (216, 217), and tombusviral p19 (185, 186).

3.1.6 Size-selective, dsRNA-binding VSRs

To date, seven VSRs have been identified that bind with some specificity to 21-nt duplex siRNAs. These siRNA-binding VSRs are from broad classes of viruses suggesting that siRNA binding has evolved independently in several virus families (Table 3.1). The *Tobacco etch virus* Hc-Pro and closteroviral p21 have been demonstrated to bind size-selectively to 21-nt duplex siRNAs and require the 3' 2-nt overhangs for efficient binding (203, 208), suggesting that these proteins interact directly with the 3' 2-nt overhang of the siRNA duplex. Both the *Tobacco etch virus* Hc-Pro and the closteroviral p21 proteins have also been implicated in other activities or mechanisms of RNA silencing suppression, indicating that preferential binding to the siRNA duplex may not be their only mode of RNA silencing suppression (205, 206, 212, 223, 230, 231, 269, 270). In addition, *Tobacco etch virus* Hc-Pro was demonstrated to bind with enhanced efficiency to varying lengths of siRNA duplexes (19- to 24-nt) *in vitro* in the presence of a yet to be identified cellular factor (208), suggesting that *Tobacco etch virus* Hc-Pro's dsRNA-binding activity *in planta* is dependent on a cellular factor. Although the closteroviral p21

protein was demonstrated to bind size-specifically to 21-nt siRNA duplexes (203, 208); Ye and colleagues, who reported the crystal structure of p21, have demonstrated that p21 is able to act as a general dsRNA-binding protein (206). To date, this controversy has not been resolved. The *Peanut clump virus* P15 and *Barley stripe mosaic virus* γB proteins are lesser studied VSRs, but have both been demonstrated to bind size-selectively to 21-nt duplex siRNAs containing 3' 2-nt overhangs, suggesting that they too interact with the 3' 2-nt overhang of the siRNA duplex (203, 208).

In contrast, the *Rice hoja blanca virus* NS3, *Tomato aspermy virus* 2b, and tombusviral p19 proteins all bind preferentially to 21-nt duplex siRNAs in a size-selective manner with no requirement for the 3' 2-nt overhangs (185, 186, 216, 234). Interestingly, although none of them contain any significant sequence similarity, each of these proteins has been demonstrated to be a dimer in its siRNA-binding competent state (185, 186, 216, 234). For *Tomato aspermy virus* 2b, in addition to binding with high affinity to 21-nt duplex siRNAs, this protein also binds with similar affinity to 32-nt duplex siRNAs (216), and has been shown to have some affinity for ssRNA (217). The 21-nt and 32-nt siRNA duplexes correspond to two or three helical turns of the dsRNA, respectively, which reflects the 2b protein's mechanism of dsRNA-binding by wrapping around the major groove of the dsRNA (216) (Figure 3.1D). This is in contrast to the mechanism of dsRNA-binding employed by the tombusviral p19 protein, which binds to the minor groove of the dsRNA (185, 186) (Figure 3.1E). The crystal structure of *Rice hoja blanca virus* NS3 has not yet been reported and hence it's mechanism of dsRNA binding has not yet been elucidated.

Due to their size-selective and sequence-independent binding to silencing-generated small RNA duplexes, and the ubiquity of the RNA silencing pathway in eukaryotes, the *Tomato aspermy virus* 2b, *Rice hoja blanca virus* NS3, and tombusviral p19 proteins are excellent candidates for the development of tools to study RNA silencing and small RNAs in a wide variety of *in vitro* and eukaryotic systems. Of these, the tombusviral p19 protein is the best characterized and has the greatest affinity for 21-nt duplex siRNA (185, 186, 216, 234). In addition, the p19 protein is amenable to overexpression in bacteria and plants and can be readily purified to high and soluble amounts (271, 272). Thus, the tombusviral p19 protein was chosen for development of a protein-based tool for studying RNA silencing and small RNAs.

3.1.7 The Tombusvirus p19 Protein

Tombusviruses are a family of positive-sense, single-stranded RNA viruses of plants (273). Their fifth ORF encodes the 19 kDa (p19) protein which is a siRNA-binding VSR (274). As discussed above, the p19 protein binds to and sequesters siRNAs in a size-selective and relatively sequence-independent manner, preventing their incorporation into RISC, and thereby inhibiting the downstream silencing of target RNAs (185, 186, 240, 275) (Figure 3.2). This inhibition allows persistence of the virus in its host.

The p19 protein acts as a dimer, with two molecules of p19 per siRNA duplex (185, 186) (Figure 3.3). The p19 dimer consists of two main functional domains: the core and the α-helical reading head. The core consists of basic and polar groups which bind to the phosphate backbone of the minor groove of the siRNA duplex. This ensures relatively sequence-independent binding (185, 186, 275). In addition, the critical contribution of the

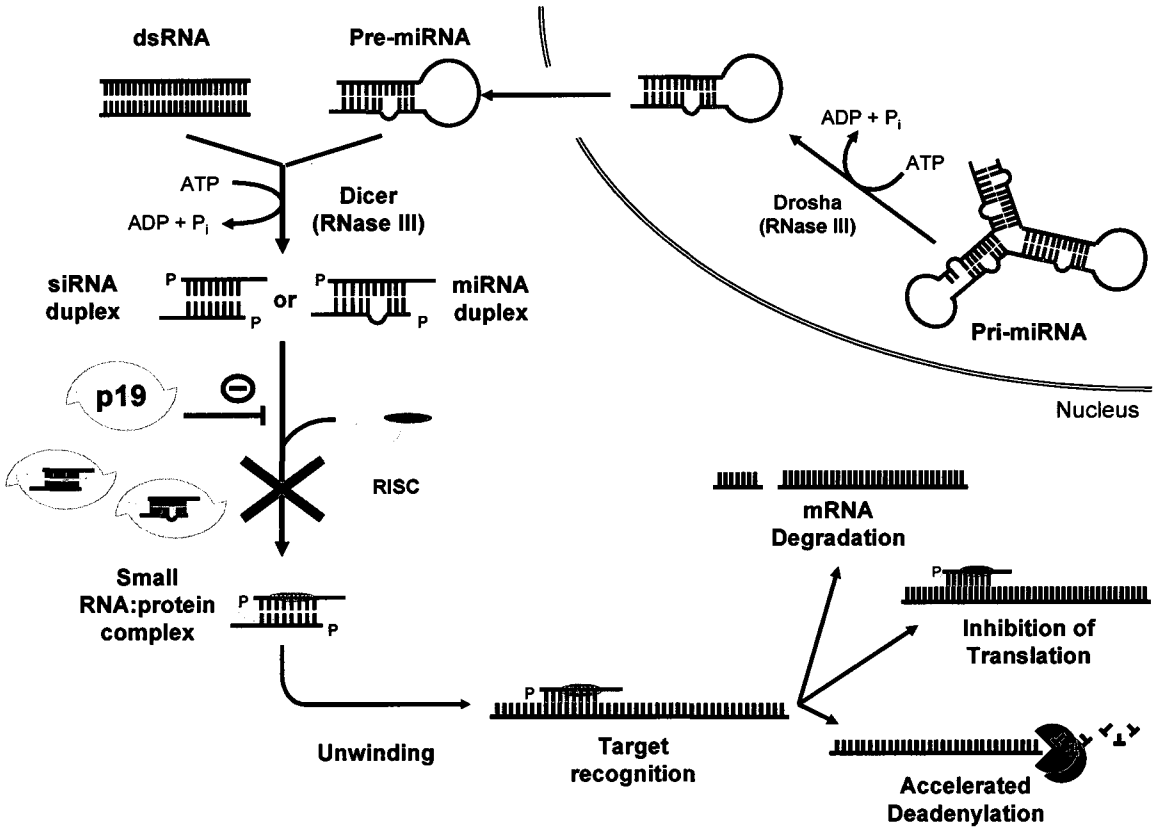

Figure 3.2 Schematic diagram of where the p19 protein acts in the RNA silencing pathway. The p19 protein binds to and sequesters silencing-generated small RNAs, preventing their incorporation into the RISC and downstream silencing of their target genes.

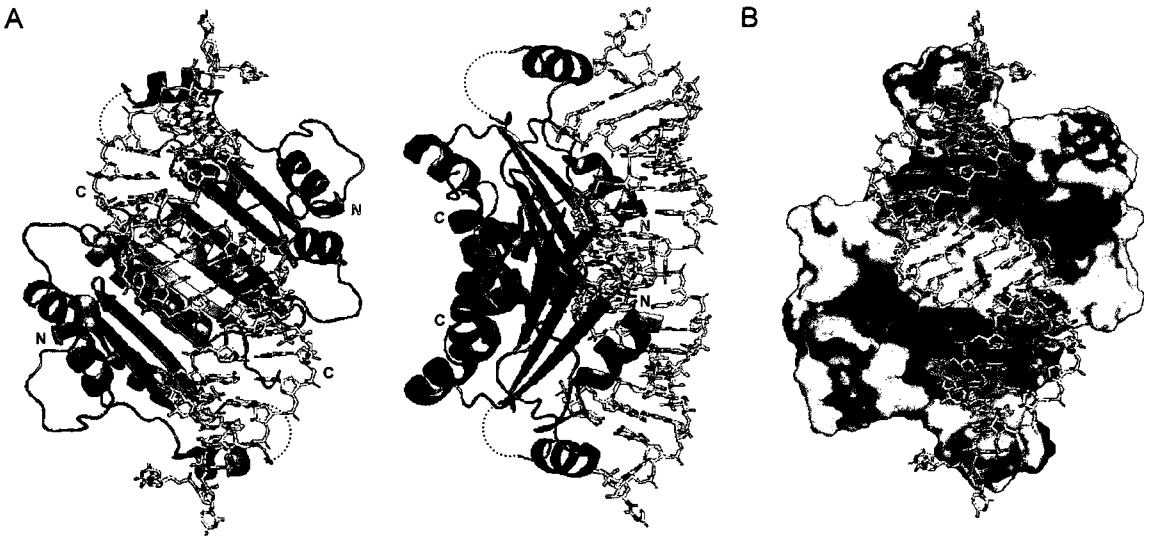

Figure 3.3 Crystal structure of CIRV p19 in complex with 21-nt siRNA (PDB ID: 1RPU, reference (185)). A) Two orientations (related by a 90° rotation about the vertical axis) of the CIRV p19-siRNA complex. Each monomer is indicated (blue, teal), as are their N- and C-termini. The p19 dimer is rendered as a ribbon diagram and the siRNA is rendered as sticks. B) Electrostatic surface representation of CIRV p19 in complex with 21-nt siRNA. Regions of positive potential are shown in blue and negative potential are in red.

2'-OH groups in siRNA duplex recognition allows p19 to distinguish RNA duplexes from DNA duplexes (185, 186). The core domain also contains the dimer interface which consists of hydrogen bonds between four anti-parallel β-sheets (185, 186) (Figure 3.3). The α-helical reading head consists of two important residues: Trp39 and Trp42, which form stacking interactions with the last bases in the siRNA duplex, effectively capping the 5' end of the RNA duplex and forcing the 3' 2-nt overhang out of the way (185, 186) (Figures 3.1E and 3.3). Since this allows the p19 protein to effectively measure RNA duplex length, it binds with high affinity to 21-nt duplex siRNAs, with much less affinity for other nucleic acids including long dsRNA, ssRNA, or siRNA duplexes of greater or shorter lengths (185, 186, 240). In addition, it does not require the 3' 2-nt overhangs for efficient binding; however, binding is enhanced by the presence of the 5' phosphate group(s) (185, 186).

3.1.8 p19-based Tools

As siRNAs are ubiquitously involved in RNA silencing, the p19 protein could be useful to study RNA silencing and small RNAs in an organism- and system-independent manner. The p19 protein is able to function as a suppressor of RNA silencing independently of other viral proteins and siRNA-binding is its sole mechanism of RNA silencing suppression. It is also amenable to overexpression in bacteria and plants, and it can be readily purified to high and soluble amounts (271, 272). In addition, the ability of the p19 protein to act as a molecular ruler allows it to distinguish Dicer products, such as siRNAs and miRNAs, from other small RNAs involved in regulatory aspects of the cell, such as rRNAs and tRNAs. These features make p19 an ideal candidate for the

development of a tool to study small RNAs and for dissecting RNA silencing pathways in a range of organisms and *in vitro* systems.

Given that p19 binds with high affinity to small RNA duplexes, it could be used as a tool for the isolation, purification and quantification of small RNAs. Also, within the context of viral infections, the p19 protein could be used to assess the role of RNA silencing in specific host-virus interactions. Moreover, inhibitors of the p19-small RNA interaction could be used as molecular switches to turn on and off gene expression.

In this chapter, the use of arrayed recombinant p19 of the CIRV for rapid and quantitative detection of CIRV p19-siRNA interactions is described. The p19 protein arrays allow size-selective detection of siRNAs and provide a convenient method for screening small-molecule libraries for compounds that can perturb the protein-RNA interaction. Furthermore, two small molecule inhibitors were identified that act by modification of one or more cysteine residue(s). Mutational analyses revealed the role of these cysteine residues in the overall structure of the p19 protein and may have implications for the design of more specific p19 inhibitors or the regulation of this protein *in vivo*.

3.2 Hypothesis

The p19 protein may be useful in the study of small RNAs and RNA silencing pathways in vitro and in a range of cells/organisms

3.3 Results

3.3.1 Arrayed p19 Retains its Ability to Bind to 21-nt Duplex siRNAs Sequence Independently

In order to obtain optimal expression of the p19 protein, the CIRV p19 sequence was codon optimized for both mammalian and bacterial expression and sub-cloned into the pTriEx 4-neo vector with a C-terminal Histidine (His) tag (see *Chapter 2*). The p19 protein was expressed in *E. coli* BL21 (DE3) cells and was purified on a Ni^{2+}-NTA column. Purified recombinant p19 was then captured on 96-well Ni^{2+}-NTA plates at a binding capacity of approximately 20 pmol/well.

Aliquots of 5'-Cy3-labeled siRNAs were added at increasing concentrations, and the fluorescence of the siRNA that remained bound in each well was measured after a 1-3 h incubation period. The fraction of bound siRNA was calculated by determining the fraction of the original fluorescence intensity that remained after removal of the unbound siRNA (as outlined in Figure 3.4). The fluorescence data was fit to Equation [1] in order to determine the equilibrium dissociation constant (K_d) of p19-siRNA binding. Figure 3.5A depicts a representative graph of the relative fluorescence intensity vs. the concentration of the fluorescently labeled 21-nt siRNA.

$$f = [siRNA]_{max} \cdot \left(\frac{[siRNA]_U}{[siRNA]_U + K_d} \right) \qquad [1]$$

where f denotes the relative fluorescence intensity which is directly proportional to the fractional occupancy of p19; $[siRNA]_{max}$ denotes the maximal binding of siRNA; $[siRNA]_U$, the fraction of unbound siRNA; and K_d, the equilibrium dissociation constant.

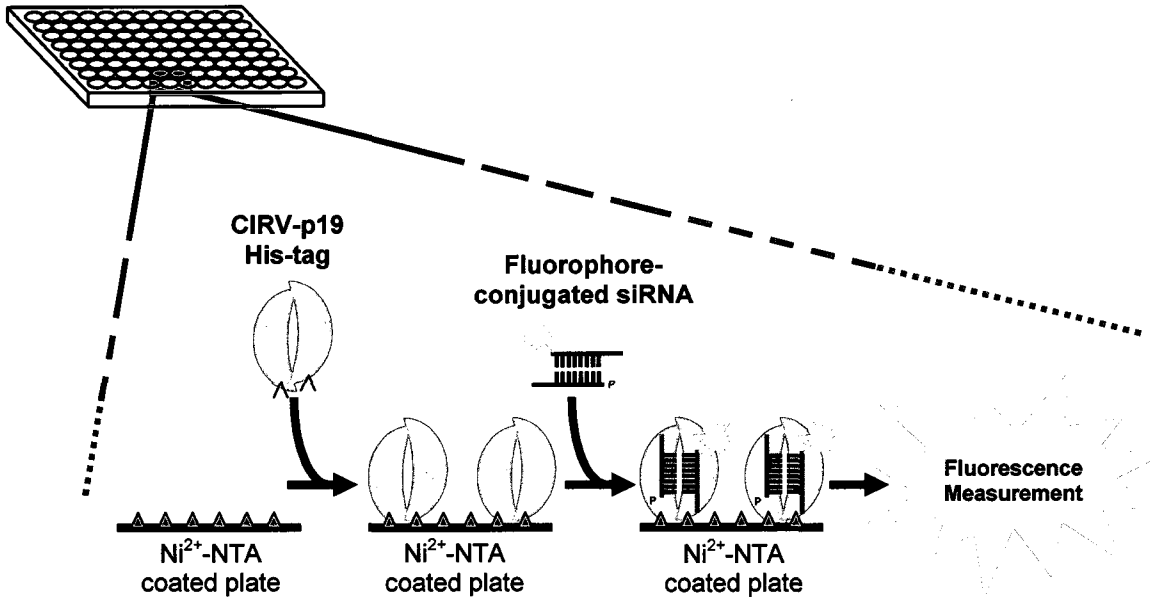

Figure 3.4 Screening method in the form of a fluorescence-detection assay developed using the p19 protein.

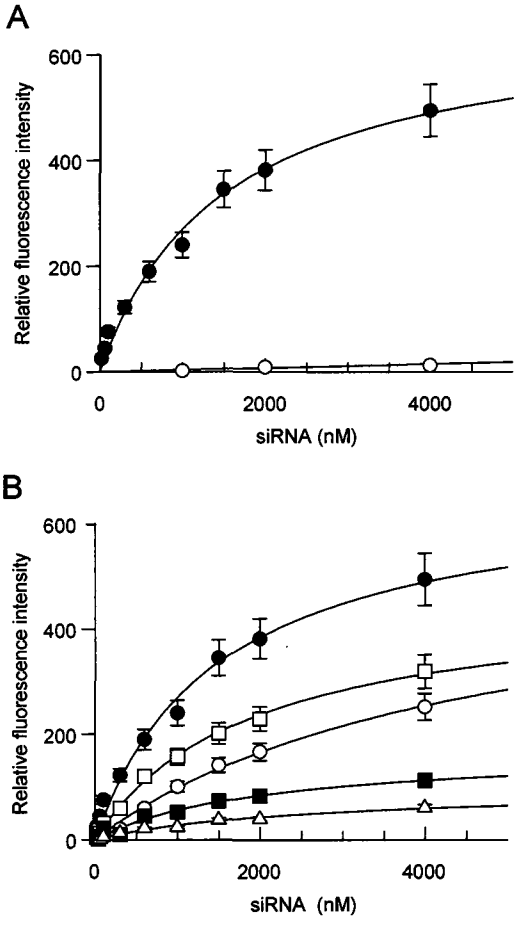

Figure 3.5. Representative plot and overlaid plots of siRNA binding data for p19 fluorescence detection assays. Ninety-six-well microtiter plates containing bound p19 were incubated with the following types of siRNA at varying concentrations (0-4 μM). A) A representative Cy3-labeled 21-nt double-stranded GL2 siRNA (●) and a corresponding Cy3-labeled 21-nt single-stranded GL2 siRNA (○). B) Double-stranded siRNAs of varying lengths: 19-nt GL2 siRNA (○), 21-nt GL2 siRNA (●), 23-nt GL2 siRNA (□), 25-nt GL2 siRNA (■), and 28-nt GL2 siRNA (Δ). Data points represent the average measurement values from triplicate experiments. Best-fit binding hyperboles are shown with the assumption that one p19 dimer binds a single siRNA. All experiments were conducted with the same batch of plates and protein stock solutions to ensure that the saturation point for each well would be the same within experimental error.

In order to verify that the arrayed p19 retained its ability to bind specifically to duplex siRNA, increasing concentrations of fluorescently-labeled single-stranded siRNAs were added to wells with immobilized p19 (Figure 3.5A). Reaction wells containing fluorescently-labeled 21-nt single-stranded GL2 siRNA designed to target the firefly luciferase gene gave very low levels of fluorescence (Figure 3.5A, open circles), whereas a significant fluorescence intensity was attained with fluorescently-labeled 21-nt duplex GL2 siRNA over the range of concentrations tested (Figure 3.5A, closed circles). This illustrates that the arrayed CIRV p19 binds specifically to double-stranded siRNAs rather than to the corresponding single-stranded siRNAs, as previously reported (185).

The size-selectivity of CIRV p19 binding was tested using duplex siRNAs of various lengths (19-, 21-, 23- 25- and 28-nt GL2 targeting siRNAs). Plate-bound p19 showed the highest affinity for 21-nt duplex siRNA with progressively declining affinities for siRNAs of greater or shorter lengths (Figure 3.5B). This is in agreement with the trend observed previously by EMSA using radiolabeled siRNAs of varying lengths (185).

To determine whether the immobilized p19 also binds to siRNAs in a sequence-independent manner, interactions of p19 with a range of 21-nt siRNAs of unrelated sequences were evaluated (see Table 2.2, *Chapter 2*). The apparent K_d values of p19 for 21-nt duplex siRNA molecules that target GL2, CSK (human Src kinase), and 331 (HCV 5' NCR) were determined by fitting the fluorescence versus siRNA concentration data to Equation [1]. The immobilized p19 bound to all duplex 21-nt siRNAs with a similar affinity, exhibiting apparent K_d values of ~600-1200 nM (740 nM, 570 nM, and 1200 nM

for GL2, CSK and 331 siRNAs, respectively). This confirms that arrayed p19 binds to 21-nt double-stranded siRNA in a relatively sequence-independent manner (177, 185).

3.3.2 Library Screen

Next, 500 compounds were screened from the Tripos Optiverse Panlabs library for inhibitors of p19 binding to CSK siRNA, as this siRNA exhibited the highest affinity in the assay. Inhibitors of the p19-siRNA interaction are of interest since they could be used to control suppression of RNA silencing by the p19 protein (i.e. as a molecular switch to turn gene expression on and off). From the library screen, two compounds were found to inhibit p19 interactions with CSK siRNA to a larger degree than the positive control (competition with unlabeled CSK siRNA; Figure 3.6). Further investigation of both compounds showed that they inhibited siRNA binding activity in a concentration-dependent manner with IC_{50} values of 9.2 μM and 45 μM, for compounds **1** and **2** (Figure 3.7), respectively.

3.3.3 Cysteine Alkylation Inhibits siRNA Binding Activity

A mechanism for p19 inhibition can be proposed on the basis of the presence of thiosulfate functional groups in both identified inhibitors (Figure 3.7). Since thiosulfate groups are reactive toward cysteine residues, inhibition of p19-siRNA interactions could be attributed to covalent modification of p19 according to Equation [2].

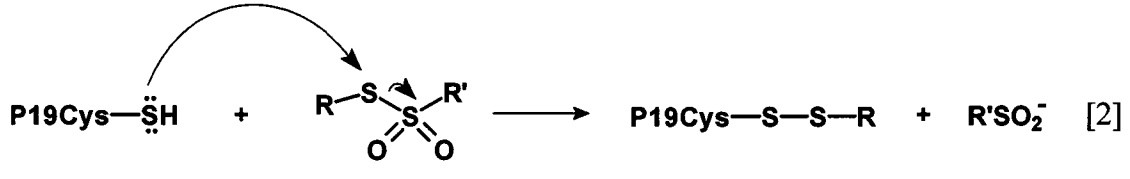

[2]

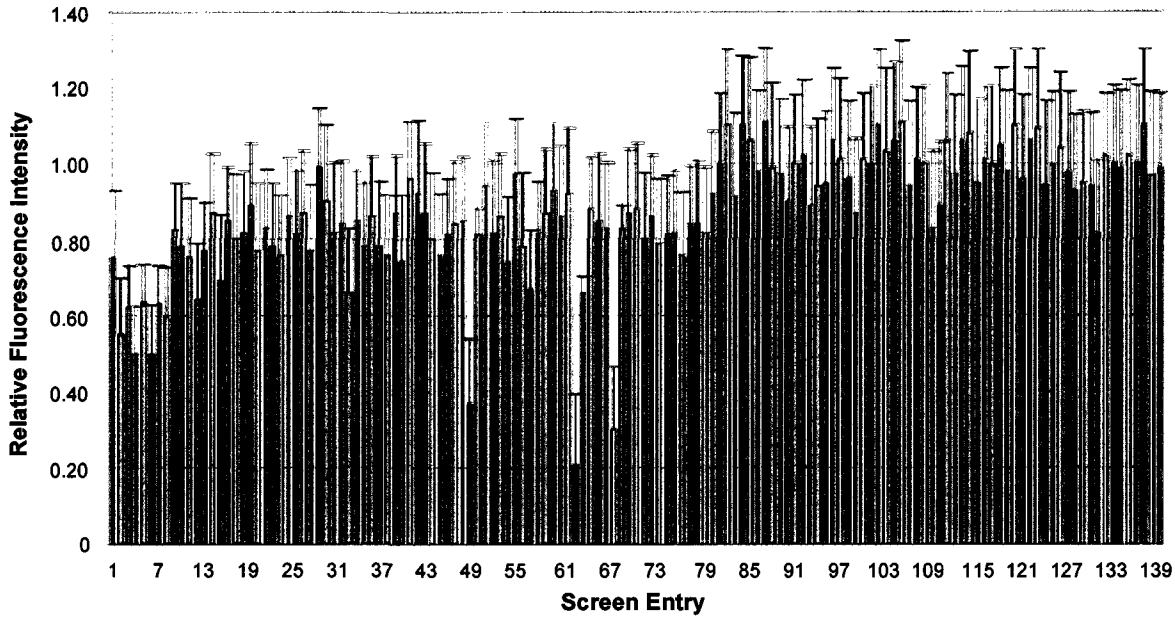

Figure 3.6 Small molecule library screen. Fluorescence measurements for the binding activity of GL2 siRNA to p19 in the presence of a representative sampling of the Tripos Optiverse Panlabs small molecule library are shown. Relative reduction in siRNA binding by each compound was measured upon addition of 100 μM to a well where siRNA was already bound to p19. Each measurement was performed in triplicate. Mean ± SE are presented. Hits were selected based on statistical analyses of fluorescence intensity differences between compound-treated and mock-treated wells (mock-treated samples had a relative fluorescence intensity of 1.0 ± 0.01). Unlabeled siRNA that reduces the fluorescence signal by competitive binding to p19 was used as a positive control (relative fluorescence intensity of 0.5 ± 0.07). Two-tailed *p*-values of *t*-tests for the screening data were determined and *p*-values < 0.05 was set as the threshold of significance. Compounds **1** and **2**, which were further validated, correspond to entries 61 and 67, respectively. Both compounds **1** and **2** had *p*-values < 0.01.

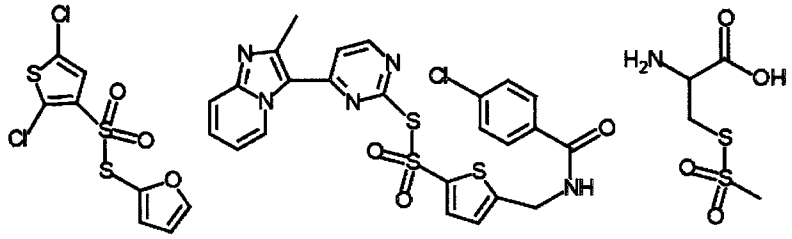

1 2 3

Figure 3.7 Structures of the two thiosulfanates identified from the libaray screen and a model thiosulfanate. Structures of the two thiosulfonates identified from the Tripos Optiverse Panlab library that block p19-siRNA interactions (compounds **1** and **2**), and a model thiosulfonate, (R)-2-amino-2-carboxyethylmethanethiosulfate (compound **3**), used for MALDI-TOF mass spectrometry analyses are shown.

To determine whether covalent modification of cysteine residues could inhibit p19 activity, the effect of cysteine alkylation by *N*-ethylmaleimide (NEM) on p19-siRNA binding was investigated. When the ability of this alkylated sample to bind siRNA was evaluated in the fluorescence detection assay, there was a greater than 10-fold reduction in siRNA binding (Figure 3.8), which suggests the modification of p19 cysteine residues as a mechanism for the inhibition of siRNA binding. By using model compound **3** (Figure 3.9), as well as compound **1** (Figure 3.10), it was established that molecules containing thiosulfonate functional groups can modify p19. Depending on the incubation time and number of equivalents, the mass increases observed by MALDI-TOF MS corresponded to between one and four modifications per p19 dimer (Figures 3.9 and 3.10). Thus, compound **1** is likely a covalent inhibitor.

Inspection of the CIRV p19 crystal structure (185) provides some insight into how the covalent modification of a cysteine residue(s) could inhibit siRNA binding. Since there are three cysteine residues in CIRV p19 (C110, C134 and C160), we sought to determine the sites at which alkylation occurs. According to the crystal structure (Figure 3.11), C160 is located in the flexible C-terminal region of p19 where electron density was not observed (185), suggesting that C160 is probably highly solvent accessible and likely to be alkylated. Nonetheless, the location of C160 is far from the p19-siRNA binding interface and in a highly unstructured region of the protein, suggesting that modification of this cysteine is likely to have a minimal effect on p19 binding to siRNA. The crystal structure also illustrates that the side chains of both C110 and C134 are oriented towards the protein interior, C110 being located within the siRNA-binding interface, and C134 being further from the siRNA-binding interface (Figure 3.11). Therefore, we postulated

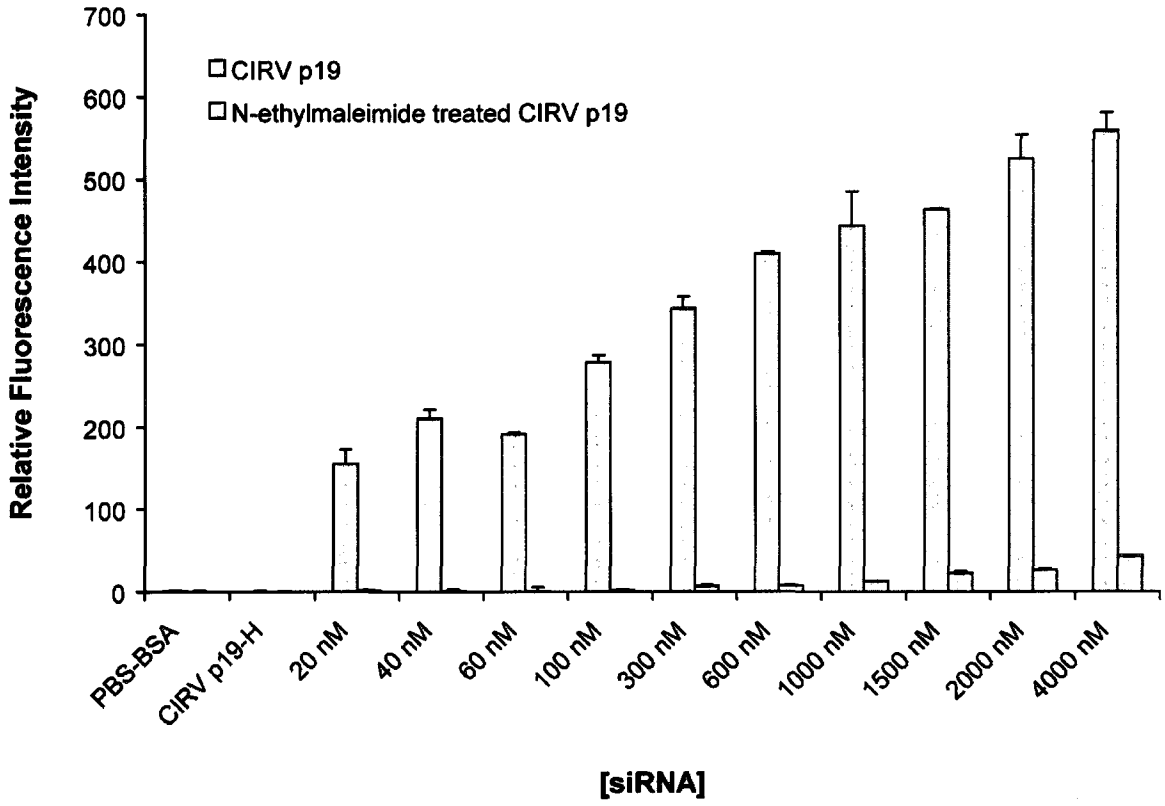

Figure 3.8 Relative fluorescence intensity after treatment with *N*-ethylmaleimide. Relative fluorescence intensity obtained from *N*-ethylmaleimide treated and untreated p19 binding to fluorescently-labeled GL2 21-nt siRNA. Each bar represents the average of three measurements with the error provided by the standard deviation from the mean.

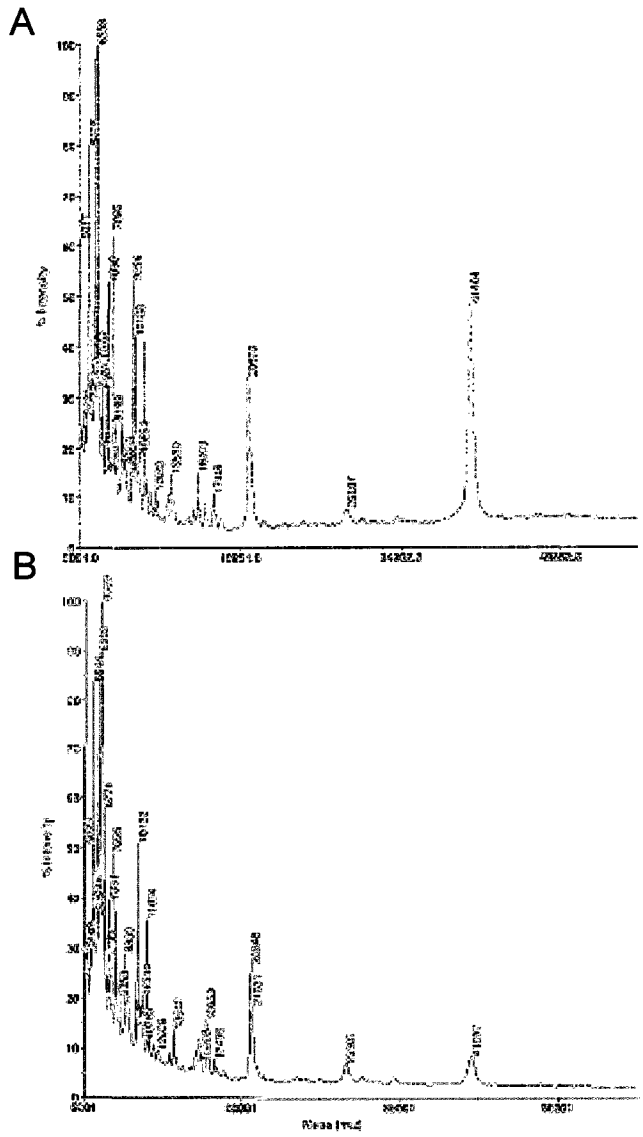

Figure 3.9 MALDI-TOF spectra for p19 treated with compound **3**. A) p19 alone; B) p19 treated with a 10:1 molar ratio of compound **3**:p19. The peak with *m/z* = 41404 corresponds to unmodified p19 (A) and the peak with *m/z* = 41887 corresponds to p19 containing four modifications by compound **3** (two modifications per p19 monomer), within experimental error.

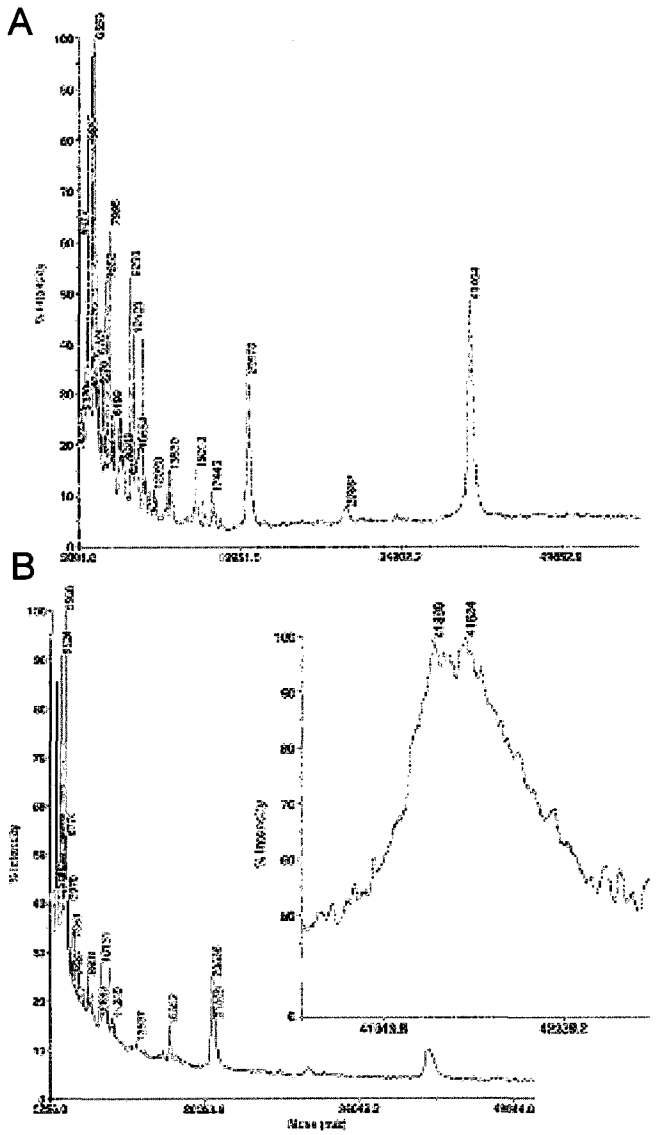

Figure 3.10 MALDI-TOF spectra for p19 treated with compound **1**. A) p19 alone; B) p19 treated with a 1:1 molar ratio of compound **1**:p19; inset shows an expanded mass spectrum for p19 treated with a 1:1 molar ratio of compound **1**: p19. The peak with *m/z* = 41398 corresponds to unmodified p19 and the peak with *m/z* = 41624 corresponds to p19 with two modifications by compound **1**, within experimental error.

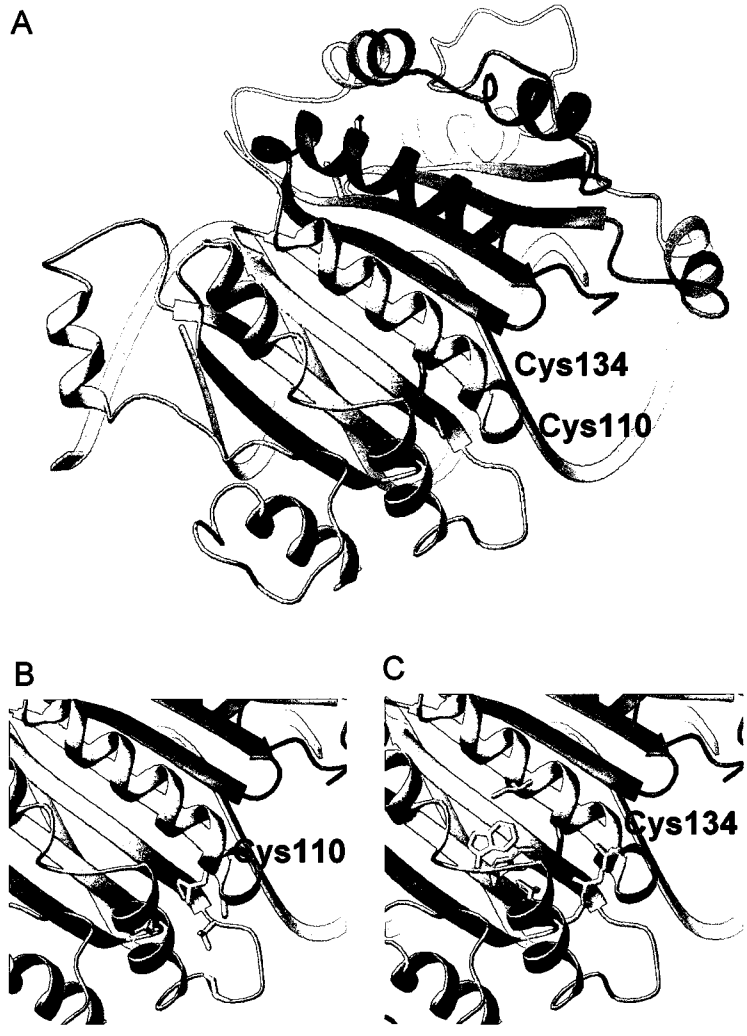

Figure 3.11 CIRV p19 crystal structure A) A ribbon diagram of the CIRV p19 crystal structure (PDB ID: 1RPU, reference (185)) with the side chains of Cys110 and Cys134 highlighted in orange. Cys160 is located in a flexible C-terminal region, which was not resolved in the crystal structure. B) Local environment around Cys110 with residues Ser127, Leu130, Ala99, Leu103, Val108, Phe65, Gly64, and Ty r112 highlighted and C) Cys134 with residues Trp63, Leu130, Val95, Gly92, Gln131, and Asn96 highlighted.

that alkylation of these sites would perturb the chemical and structural properties of p19, affecting its ability to bind to siRNA. We also hypothesized that the p19 apoprotein may adopt an alternate conformation in order for C110 and/or C134 to become solvent accessible so that alkylation can occur at these sites. Moreover, C110 is the only cysteine residue conserved among the entire p19 family, and hence it is likely to be significant with respect to p19 function; and hence, when alkylated, may result in a reduction in p19's siRNA binding activity. In order to determine which of the cysteine residues gave rise to altered p19 function upon alkylation, site-directed mutagenesis and functional studies were performed.

3.3.4 Construction of CIRV p19 Cysteine Mutants

To determine which of the cysteine residues within the p19 protein are sensitive to alkylation, each of the cysteine residues from the CIRV p19 dimer were systematically replaced and the function of each of the mutant p19 proteins was tested. A set of cysteine p19 mutants were constructed from the wild-type p19 construct using site-directed mutagenesis (see Table 2.1, *Chapter 2*). The cysteine residues at positions 110, 134 and 160 were mutated to serine, isoleucine, alanine or glycine. First, the cysteine residues were substituted with serine because the chemical structure of these two residues is very similar. This strategy was chosen so that the substitution of cysteine residues with serine would have a minimal effect on the global structure of the protein, but would prevent alkylation at the site in the presence of a cysteine-specific alkylating agent. Cysteine residues were next substituted for alanine, which is the most common amino acid used for substitution in mutagenesis studies due to its small and relatively unreactive side

chain. In order to observe the effects of a more dramatic change in side chain, cysteines were substituted with glycine, containing no side chain; and with isoleucine, a more hydrophobic and bulkier side chain. Mutation of cysteine residues to glycine or isoleucine were conducted to determine if alkylation and/or substitution could result in structural perturbations in the p19 dimer.

3.3.5 Expression, Purification and Structural Analysis of Cysteine Mutants

The cysteine mutant constructs were prepared from the wild-type CIRV p19 construct in which the p19 sequence was cloned into a vector for heterologous expression in *E. coli* (described above and in *Chapter 2*). All p19 constructs contained a C-terminal His-tag and were purified by nickel affinity chromatography and gel filtration. All constructs expressed well; however, not all of them yielded a quantitative amount of purified soluble protein. When C110 was replaced by either serine or glycine, considerably lower yields of soluble protein were obtained compared with wild-type p19. The C110S and C110S/C160S mutants had typically more than a 10-fold reduction of soluble protein yield than wild-type p19 purified from the same amount of cell culture. In the more extreme cases, expression of the C110G, C110G/C134G, C110S/C134S and C110S/C134S/C160S mutants was only detected in the insoluble cell fraction by western blot analysis using an anti-His-tag antibody. After numerous attempts at optimizing the soluble expression of these constructs by varying the induction temperature, IPTG concentration, and cell density at which protein expression was induced, no soluble expression of the C110G/C134G mutant was observed. By lowering the induction temperature, a small yield of the soluble C110G, C110S/C134S, and

C110S/C134S/C160S mutants was attained, although after extraction and purification only a very small amount of soluble protein was obtained. Attempts to pool and concentrate these samples to practical concentrations typically resulted in protein precipitation. Thus, the latter C110 mutants were not studied any further.

To determine whether there was a structural basis for the low soluble yield for mutants with cysteine to serine but not with cysteine to isoleucine substitutions at position 110, circular dichroism (CD) spectra were acquired for wild-type p19, C110S and C110I. As shown in Figure 3.12A, the far-UV CD spectra all possessed minima at 208 and 222 nm suggesting significant α-helical content that overlapped well amongst the wild-type p19 and the C110S and C110I mutants. This was confirmed by secondary structure deconvolution using the suite of programs provided by CDPro which consistently gave ~22% α-helix and ~26% β-sheet for all three constructs (Table 3.2). This indicates that the secondary structure contents of all three constructs are very similar and that the global structure of the protein was unaltered by the substitutions.

In order to further understand what gave rise to the differences in soluble protein yield between C110S, C110I and the wild-type p19, thermal denaturation was performed and monitored by CD at 222 nm (Figure 3.12B). All three constructs showed a significant loss of CD signal intensity over a narrow range of temperatures, with ellipticity values being close to zero at 90 °C. For wild-type p19, the signal started to decrease at ~50 °C, with half the signal remaining at ~58 °C, while for C110S, denaturation started at a significantly lower temperature of ~38 °C with half the intensity being lost at ~43 °C (Figure 3.12B). Interestingly, for C110I, denaturation did not start until the temperature reached ~58 °C, with half the signal remaining at ~67 °C (Figure 3.12B). The difference

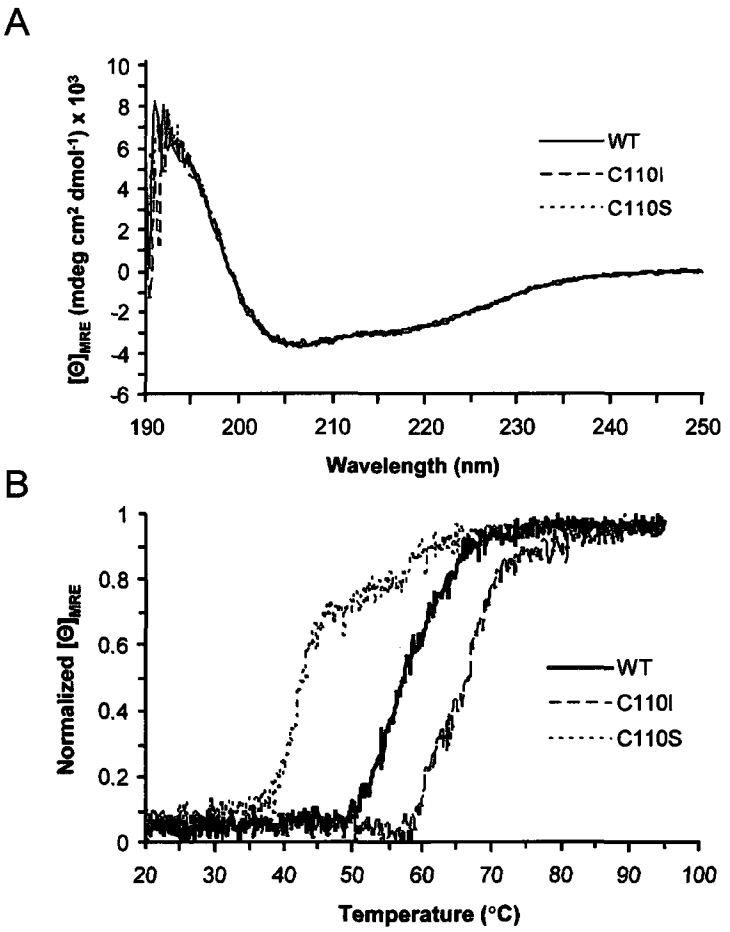

Figure 3.12 Circular dichroism of wild-type p19 and the cysteine mutants C110I and C110S. A) Far UV spectra and B) thermal denaturation profiles monitored at 222 nm. WT, wild-type.

Table 3.2 Secondary structure content of p19 cysteine mutants from CD analysis.

	Secondary Structure Content (%)[1]			
	α-Helix	**β-Sheet**	**Turn**	**Unordered**
WT	21.73	25.88	21.66	30.73
C110I	22.45	25.80	20.06	29.80
C110S	22.30	26.50	21.63	29.57

[1]Secondary structure content was calculated using the CDPro suite of programs. WT, wild-type.

in denaturation temperatures suggests that C110S is less stable, and that C110I is more stable, than the wild-type p19. This implies that the impact on the stability of the p19 protein upon mutation of C110 to serine renders the protein more vulnerable to unfolding and precipitation. Conversely, p19 becomes more thermally stable when C110 is replaced by isoleucine. This may explain why C110S mutants had low or no soluble protein yield but C110I mutants were unaffected.

3.3.6 siRNA Binding Activity of the Cysteine Mutants

EMSA was used to assess the siRNA binding activities of the recombinant p19 cysteine mutants relative to wild-type CIRV p19. This technique is commonly used to assess protein-nucleic acid interactions (276). In previous studies, EMSA has been used to analyze the binding affinity and specificity of CIRV p19 with ^{32}P-radiolabeled (185) and fluorescently-labeled siRNAs (180). The p19 mutant constructs that did not yield soluble purified proteins were not included in this assay. Figure 3.13A illustrates a representative fluorescence image from a typical EMSA experiment showing the interaction between C110S/C160S mutant p19 and the fluorescently-labeled CSK siRNA. The band intensities corresponding to the p19-small RNA complex were measured and plotted as a function of the mutant p19 concentration. Curves corresponding to all p19 constructs show a dose-response relationship between the siRNA and p19 proteins as illustrated in the representative plot in Figure 3.13B.

The dissociation constants determined from each plot for siRNA binding to p19 and its mutant derivatives are listed in Table 3.3. The K_{rel} values represent the relative affinity for the siRNA of the cysteine mutants relative to wild-type p19, and range from

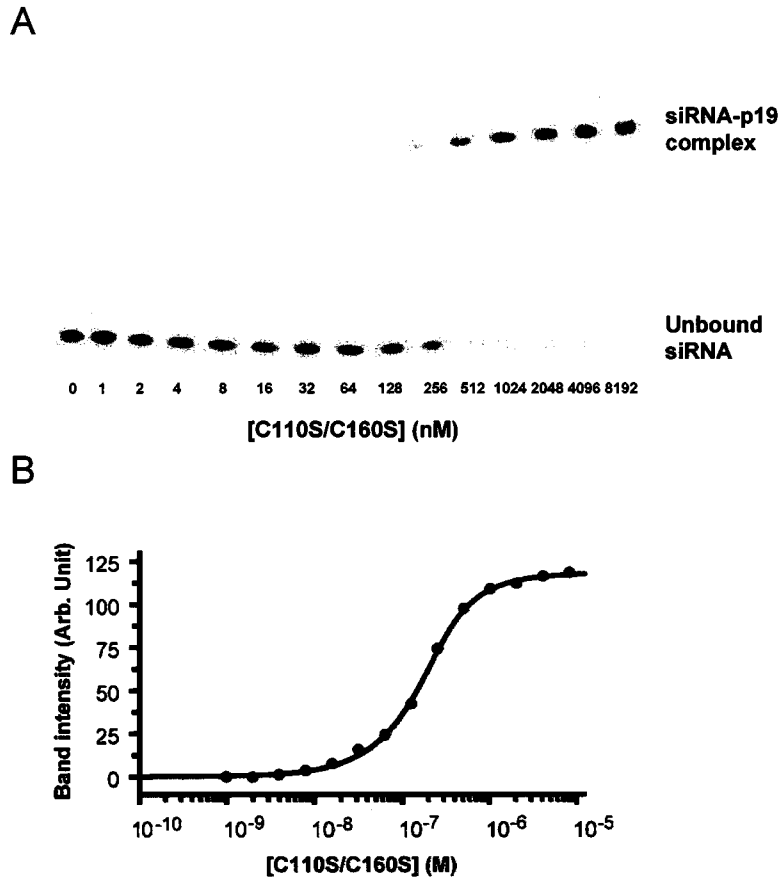

Figure 3.13 Electrophoretic mobility shift assay of p19-siRNA interactions. A) A representative gel determining the dissociation constant for C110S/C160S p19 with siRNA using varying concentrations of the C110S/C160S p19 mutant (0 – 8192 nM) and 200 nM fluorescently-labeled Dy547-CSK siRNA. B) Corresponding curve obtained by plotting the fluorescent band intensities of the p19-siRNA complex (from panel A) as a function of the concentration of the p19 dimer for the labeled siRNA.

Table 3.3 Dissociation constants for siRNA binding to wild-type CIRV p19 and its cysteine mutant derivatives.

Construct	K_d' **(nM)**	K_{rel}[1]
Wild-type	97 ± 29	1
C110S	133 ± 15	0.7
C134S	110 ± 16	0.9
C160S	101 ± 16	1
C110A	101 ± 43	1
C110G[2]	N/A	N/A
C134G	133 ± 12	0.7
C110I	79 ± 33	1.2
C134I	196 ± 46	0.5
C160I	94 ± 44	1
C110G/C134G[2]	N/A	N/A
C110I/C134I	161 ± 11	0.6
C110S/C134S[2]	N/A	N/A
C110S/C160S	72 ± 10	1.3
C134S/C160S	106 ± 16	0.9
C110S/C134S/C160S[2]	N/A	N/A

[1]K_{rel} is the relative affinity of the cysteine mutants for siRNA as compared with wild-type CIRV p19; [2]These constructs did not yield quantitative amount of soluble proteins for the assay.

0.5 to 1.3 for all mutants. The less than two-fold difference between each cysteine mutant with respect to the wild-type p19 suggests that the mutations in these constructs have a minimal effect on p19's siRNA binding activity. The results from binding measurements indicate that the mutants maintain their ability to bind siRNAs with nanomolar affinity (Table 3.3).

3.3.7 Effect of Alkylation on siRNA Binding Activity of the Cysteine Mutants

The p19 mutants C110A, C134S, C160S, C110S/C160S, C134S/C160S, C110I, C134I, C160I, C110I/C134I and wild-type p19 were treated with the alkylating agent NEM to deduce which cysteine residues influence p19 binding to siRNA upon alkylation. Since NEM is reactive towards thiol-containing groups such as cysteine, mutation of cysteine to other residues potentially blocks alkylation at the mutated site. The His-tagged p19 proteins were allowed to bind to the wells of a 96-well Ni^{2+}-NTA coated plate and were incubated in the presence or absence of NEM, prior to addition of fluorescently-labeled CSK siRNA, to facilitate binding. After removal of unbound siRNA and washing, the fluorescence intensity was measured using a plate reader (E_x = 546 nm and E_m = 590 nm). The fluorescence intensity is directly proportional to the fraction of fluorescent siRNA bound to p19. The relative fluorescence intensities obtained from NEM-treated and untreated p19 proteins are represented by a bar graph in Figure 3.14. All measurements were carried out in quadruplicate. The residual siRNA binding activity of NEM-treated relative to untreated samples was expressed as a percentage by taking the ratio of fluorescence intensity of NEM-treated over untreated samples (Figure 3.14).

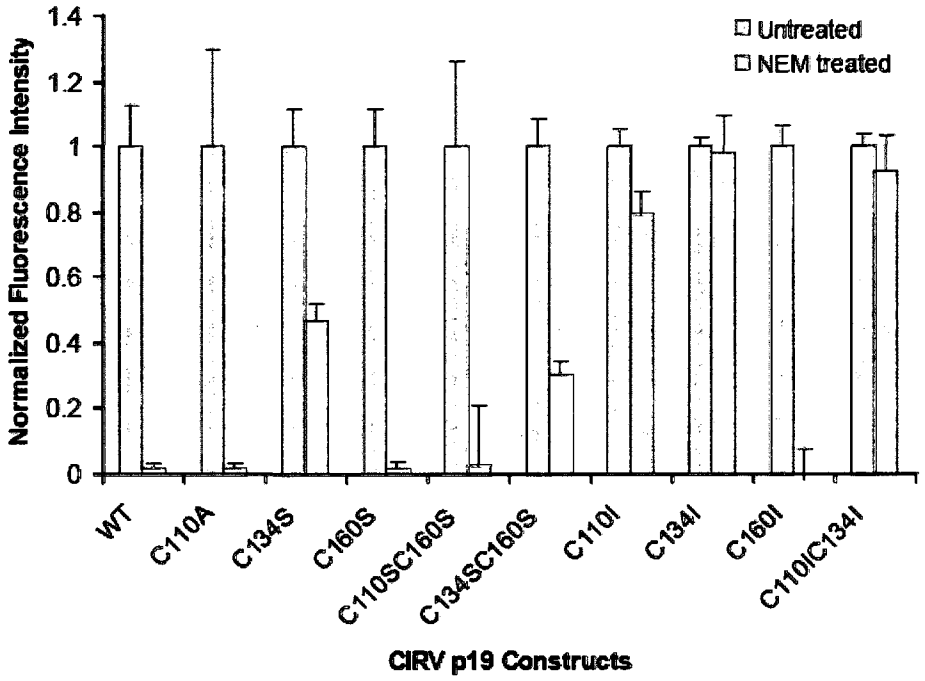

Figure 3.14 Effect of alkylation on siRNA binding activity of wild-type CIRV p19 and its cysteine mutant derivatives. The normalized relative fluorescence intensity obtained from NEM treated and untreated p19 proteins after incubation with 1 μM Dy547-CSK siRNA. Each bar represents the average of four measurements with the error provided by the standard deviation from the mean.

As a positive control, the wild-type p19 was treated with NEM and the siRNA binding activity was reduced by more than 98% compared to the untreated protein (Figure 3.14). For C110I/C134I, most of the siRNA binding activity remained (>92%) after alkylation with NEM. This is not surprising since C160 is the only available site for alkylation in this construct and its location is far from the p19-siRNA binding interface, suggesting that modification of this cysteine likely has a minimal effect on p19 binding to siRNA. In contrast, most of the siRNA binding activity was eliminated for the C160S and C160I mutants indicating that alkylation of C110 and/or C134 had an effect on siRNA binding activity. Alkylation of the cysteine to alanine mutant (C110A) and the cysteine to serine mutant series (C134S, C110S/C160S and C134S/C160S) also reduced p19's ability to bind siRNA by greater than 50% (Figure 3.14). These results imply that both the C110 and C134 positions can be alkylated and that alkylation at either site affects siRNA binding activity.

Intriguingly, most of the siRNA-binding activity of the cysteine to isoleucine mutants (C110I and C134I) was retained after treatment with NEM (79% and 98%, respectively). These isoleucine mutants seemed to be much less sensitive to alkylation in comparison to the cysteine to serine mutant series. A possible explanation may relate to the stability of these mutants. In our thermal denaturation analyses, C110I has a melting temperature of approximately 9 °C higher, and the melting temperature of C110S was approximately 15 °C lower, than wild-type p19, indicating that C110I has a significantly greater thermal stability than C110S. Mutation of cysteine to isoleucine at position 110 could be stabilizing since the side chain at that position is pointing towards the interior of the protein surrounded predominantly by non-polar residues (Figure 3.11B). The

transition from a polar cysteine to a hydrophobic isoleucine side chain may strengthen the Van der Waals interactions of the p19 protein hydrophobic interior, thus further stabilizing the protein. This may also explain why the soluble protein yield was unaffected when C110 was substituted with alanine (C110A), since alanine is also non-polar and its small side chain is unlikely to cause steric effects on the protein structure.

In the case of the cysteine to serine mutant series, it was first predicted that mutation of cysteine to serine would have a minimal effect on the structure of p19 due to the similarity in their side chain structure. However, the reduced stability of the C110S mutant was first evident during protein expression where a low yield of soluble protein was observed. The protein expressed but was almost exclusively targeted to the insoluble cell fraction and readily precipitated in solution after purification. As a protein becomes less stable, it is more susceptible to unfolding and has a greater tendency to aggregate (277-279). Although serine and cysteine differ by only one atom, serine is relatively more polar than cysteine, since the oxygen in the hydroxyl group of the serine side chain is more electronegative than the sulfur in the thiol group of the cysteine side chain. Therefore, substitution of cysteine at position 110 with the more polar serine in the hydrophobic interior of the p19 protein would be less favourable, resulting in a destabilizing effect on the p19 structure. The cysteine to glycine mutants, C110G and C110G/C134G, also demonstrated the impact of the cysteine substitutions on protein stability. These glycine mutants were only expressed in the insoluble fraction even after extensive optimization. Due to the absence of a side chain, substitution of C110 to glycine potentially creates a cavity in the interior of the protein, decreasing protein packing density. Since the packing density of proteins has been reported to correlate with

protein stability (280), this may indicate that the C110G mutation is detrimental to proper folding of the p19 protein.

Given that the side chain of C134 is also pointed towards the interior of the p19 protein according to the crystal structure, it is assumed that there are similar stabilizing or destabilizing effects for mutation to isoleucine or to serine at C134, respectively. As the protein stability decreases, the structural dynamics of the protein increase and the interior of the protein becomes more easily exposed to the aqueous environment (277-279). This may explain why the less stable cysteine to serine mutant series was more susceptible to alkylation at both positions C110 and C134, even though the cysteine residues were located in the interior of the p19 protein. In contrast, the enhanced stability of C110I and C134I mutants makes the p19 protein less susceptible to alkylation at these locations.

According to the crystal structure of the CIRV p19-siRNA complex, none of the cysteine residues has direct contact with the siRNA molecule (185). Consistent with the crystal structure, our EMSA data indicate that mutation of the cysteine residues had minimal effect on p19 binding to siRNA when compared to wild-type. This confirms that each cysteine residue in p19 is not directly involved in siRNA binding; but, is likely important for the overall structural integrity of the protein. This is supported by the results from the thermal denaturation experiment which demonstrated that mutation of C110 affects the thermal stability of the protein. The difference in stability between the cysteine to isoleucine and the cysteine to serine mutant series was also demonstrated in the alkylation experiments illustrating that the cysteine to serine mutant series is much more susceptible to alkylation of the buried C110 and C134 than the cysteine to isoleucine mutant series. In addition, the mode of NEM inhibition on siRNA binding

activity of p19 is likely also a result of protein destabilization. The addition of the NEM group to the C110 and/or C134 side chains likely results in steric hindrance of these bulky groups within the interior of the p19 protein. It is interesting to note that attempts were made to perform the alkylation reaction in solution. The p19 proteins treated with NEM under various solution conditions precipitated out of solution whereas the buffer-treated samples remained soluble. All of these observations suggest that the reduction in siRNA binding activity of p19 after alkylation of the C110 and/or C134 residues is due to disruption of the protein integrity, resulting in a non-functional p19 protein.

3.4 Discussion

In conclusion, the siRNA-suppressor protein CIRV p19 can be arrayed in multi-well plates through interactions of Ni^{2+}-NTA with the His-tag of the recombinant CIRV p19 protein. The arrayed p19 proteins can be used to rapidly determine relative siRNA-binding affinities and arrayed p19 maintains its ability to act as a molecular ruler by binding to siRNAs in a size-selective and relatively sequence-independent manner. Furthermore, screening of a library of small molecules identified two thiosulfonate inhibitors of CIRV p19 activity that may act through the modification of p19 cysteine residues.

In order to determine whether covalent modification of cysteine residues could inhibit p19 activity, the effect of alkylation by a model thiosulfonate (compound **3**, Figure 3.7) and NEM on p19's siRNA binding activity was investigated. In the presence of compound **3**, p19 was modified on average at two sites per monomer. This suggested that the mechanism of inhibition of siRNA binding by the identified inhibitors from our

library screen (compounds **1** and **2**, Figure 3.7) is through modification of cysteine residues. Although these inhibitors are unlikely to act specifically on p19 in the protein-rich environment of the cell, they could represent a starting point for the design of more specific inhibitors of the p19-siRNA interaction in order to regulate gene expression *in vivo*.

To identify which of the three CIRV p19 cysteine residues is susceptible to modification, and how cysteine modification affects the siRNA binding activity of the p19 protein, a series of p19 cysteine mutants were created where the cysteine residues at positions C110, C134 and C160 were replaced by serine, isoleucine, glycine or alanine. The results from binding measurements of the purified and soluble p19 cysteine mutants indicated that the mutant proteins retained their ability to bind siRNAs with nanomolar affinity, but varied in their thermal stabilities according to CD analyses. Functional studies in the presence of the cysteine alkylating agent NEM indicated that p19's siRNA binding activity, and consequently its suppression of RNA silencing, is sensitive to alkylation mainly at C110 and C134. The maximal effects on siRNA binding activity occurred when C110 and C134 were both alkylated. These results suggest that the C160 residue has a minimal involvement in siRNA binding and that the roles of C110 and C134 are likely to preserve the overall structural integrity of the protein in order for it to sustain maximal siRNA binding activity.

Chapter 4: Investigation of p19-small RNA Interactions

4.1 Introduction

The RNA silencing pathway involves the biogenesis of small RNA molecules and is an important antiviral pathway in plants and invertebrates (281-283). As described in *Chapter 3*, Tombusviruses use a 19 kDa protein, p19, that acts as a siRNA inhibitor, to evade the RNA silencing host response (272, 284). The p19 protein selectively binds to siRNAs in a size-selective manner with little dependence on nucleic acid sequence (185, 186, 275). The unique binding properties of p19 have already been exploited for the study of small RNAs in both plant and mammalian systems (83, 183, 208, 223, 275, 285-287). For example, p19-GFP fusion proteins have been used for localization and temporal studies during viral infections in plants (288, 289). The p19 protein has also been used to characterize the small RNAs present in mouse embryonic stem cells (275). In addition, more stable and higher-affinity variants of p19 have also been engineered (179). Thus, p19 may serve as an important tool for studying small RNAs and RNA silencing pathways in a variety of *in vitro* and *in vivo* systems. Hence, a better understanding of the binding properties and selectivity of the p19 protein will aid in its further utility as a tool for probing small RNAs and RNA silencing pathways in a number of eukaryotic systems.

4.1.1 Binding of p19 to Non-canonical Small RNA Duplexes

The small RNA component of a eukaryotic cell can arise transcriptionally (19) as well as from the processing of cytoplasmic dsRNA intermediates by the RNA silencing pathway. The host-encoded miRNAs are generally ~21-25-nt in length, are expressed in a developmental- and tissue-specific manner, and have been found in all metazoa studied to date (19, 290). miRNAs play important roles in regulation of a number of cellular

activities including transcription, chromatin structure, genome integrity, translation, and mRNA stability (19). In addition, a number of viral genomes have even been demonstrated to encode miRNAs that can regulate viral and/or host gene expression (143).

Systemic infection of plants by viruses often results in developmental abnormalities resembling perturbation of miRNA-mediated function (199, 234). This is typically characterized by developmental defects such as loss of leaf polarity, changes in proper control of cell division, and defects in reproduction (291). Such phenotypes are often associated with VSRs or virulence factors, like p19. Expression of the p19 protein in plants results in these developmental phenotypes suggesting that the p19 protein is able to bind to miRNA duplexes in addition to siRNA duplexes *in planta* (208, 223, 292). Naturally, binding to siRNA duplexes serves to inhibit the antiviral arm of the RNA silencing pathway; however, interference with miRNA duplexes may also contribute to establishment of an advantageous environment for the infecting virus in plants and invertebrate cells (234). In addition to miRNA binding activities in plants, it has been demonstrated that miRNA duplexes can also be bound by the p19 protein in mammalian cells (83, 275).

In contrast to the fully-complementary canonical siRNA duplexes, miRNA duplexes are typically derived from imperfectly complementary hairpin dsRNAs. The miRNA duplexes thus often contain mismatches or bulges that distort the canonical A-form dsRNA duplex. Although the p19 protein has been demonstrated to bind to miRNA duplexes *in vitro* and in eukaryotic cells, the extent to which nucleotide mismatches, bulges or distortions to the canonical A-form siRNA duplex are tolerated by the p19

protein has not been investigated in detail. In this chapter, the interaction of p19 with three types of small RNAs is investigated in order to gain a better understanding of the specificity and selectivity of p19 for small RNA duplexes.

4.1.2 Biochemical Techniques Used to Study Protein-RNA Interactions

In this thesis, the fluorescence detection assay described above (see *Chapter 3* and reference (177)), fluorescence-based EMSA, and fluorescence polarization techniques were used to investigate the interaction of p19 with canonical and non-canonical small RNA duplexes. Fluorescence polarization has been used extensively to make detailed and accurate measurements of protein-nucleic acid interactions (293). This technique relies on a change in rotational diffusion upon binding and the decorrelation of polarization in fluorescence. Fluorescence polarization has been used to study the tetramer-dimer equilibrium of the λ repressor (294), aptamer protein interactions (295), domain-domain interactions (296), and DNA-p53 binding through its C-terminal domain (297). Here, this approach is extended to assess protein-RNA interactions between the p19 protein and various small RNAs, including both miRNAs and siRNAs. In principle, the p19 protein can interact with small RNAs derived from both sources and influence the regulatory and/or antiviral roles of these small RNAs. In this study, the binding of the p19 protein to two important small RNAs that influence hepatitis C virus (HCV) replication in human hepatocytes, miR-122 and CSK siRNA was investigated. miR-122 is an endogenous, liver-specific miRNA that comprises approximately 70% of the total miRNAs found in the human liver (147, 298). The level of miR-122 expression correlates positively with HCV replication, and miR-122 has been demonstrated to interact with the 5′-NCR of the

HCV RNA genome, facilitating viral replication (85, 86). Since miR-122 has been demonstrated to have a positive outcome on HCV replication, sequestration of miR-122 could be a novel antiviral strategy. The second small RNA studied, CSK siRNA, is a synthetic siRNA that downregulates carboxyl-terminal Src kinase (CSK) which influences HCV replication by regulating the phosphorylation of a key viral protein, NS5A (181). Herein, it is demonstrated that the p19 protein is able to bind to both of these small RNA species, and detailed binding studies of these interactions using fluorescence polarization and fluorescence-based EMSA are described. The results show that, in principle, p19 may be used to sequester siRNAs and/or miRNAs from diverse sources and has the potential to be used as an antiviral tool to sequester small RNAs that are important for replication or pathogenesis of viruses such as HCV.

4.2 Hypothesis

The p19 protein is likely to be able to bind to both canonical siRNAs and irregularly structured miRNA species.

4.3 Results

4.3.1 Quantification of p19-small RNA Interactions Using Fluorescence Polarization

Fluorescence polarization was used to quantify the binding interactions between the p19 protein and the small RNA species (siRNAs and miRNAs). Fluorescence polarization measurements are based on observations of the rotational motion of fluorescently-labeled molecules in solution and do not require the separation of bound and free ligand. Thus, information about the true equilibrium of the molecular

interactions can be obtained using this technique (293, 299). For example, when linearly polarized light is used to excite a rapidly rotating fluorophore-conjugated small RNA molecule in solution, the emitted light will deviate from the plane of excitation, becoming depolarized (Figure 4.1). However, when the fluorophore-conjugated small RNA molecule is bound by p19, the larger complex tumbles much slower in solution and the emitted light will remain polarized on a longer timescale (Figure 4.1). The change in polarization (ΔP) upon p19 binding to fluorophore-conjugated siRNA can be measured and used to obtain binding constants for the p19-small RNA interaction.

The small RNAs used in the experiments were conjugated to the Cy3 fluorophore; hence, the optimal wavelength for excitation and emission according to the excitation and emission spetra of Cy3 (E_x = 546 nm and E_m = 560 nm) was first established. To determine the minimum concentration of the fluorophore that gives a detectable intensity by the instrument, various concentrations of the Cy3 dye were excited at E_x = 546 nm and the vertical and horizontal components of the emitted light were measured at E_m = 560 nm. It was found that fluorescence could be measured with a sufficient signal-to-noise ratio at concentrations as low as 40 nM. Similar experiments were performed on the Cy3-conjugated small RNA samples. The measurements taken with the Cy3-conjugated small RNAs verified that conjugation of the Cy3-fluorophore to the small RNA did not result in a change in the excitation and emission spectra of Cy3. In addition, varying the concentration of the Cy3-conjugated small RNA did not have a significant effect on polarization. However, as expected, the polarization of the Cy3-conjugated small RNA was significantly greater than that of the Cy3 fluorophore alone, due to the overall increase in molecular weight.

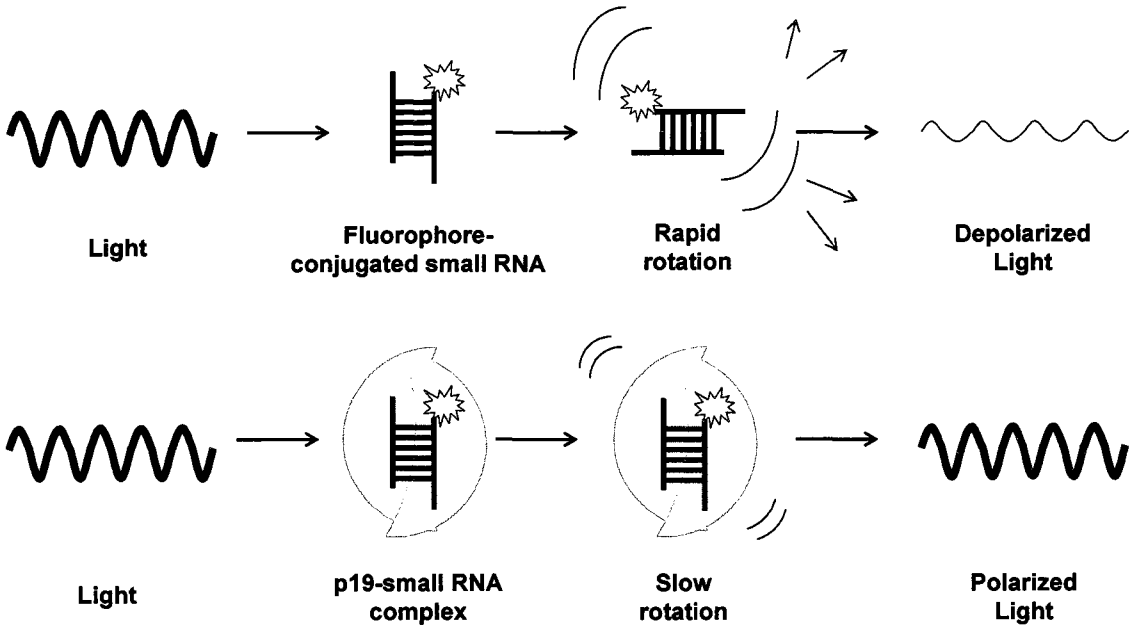

Figure 4.1 Schematic diagram of fluorescence polarization. When a fluorophore-conjugated small RNA molecule is in solution by itself, due to its relatively small size, it tumbles relatively rapidly in solution. Therefore, when it is excited with linearly polarized light, the emitted light will deviate from the plane of excitation, and become rapidly depolarized. On the other hand, if the siRNA is bound by p19, this larger complex tumbles much slower in solution, and the emitted light remains polarized on a much longer timescale. The change in polarization upon p19 binding can then be measured and used to obtain binding curves and determine the binding constants of p19 with various small RNAs.

Next, the dependence of fluorescence polarization of Cy3-conjugated CSK siRNA in the presence of p19 was investigated. All fluorescence polarization measurements were carried out in buffer containing PBS, designed to mimic physiological conditions, and 10 mM DTT, used to prevent aggregation of p19 due to non-specific disulfide linkage of p19 cysteine residues. The total fluorescence intensity was monitored and remained constant throughout the duration of each experiment. With the increase in the concentration of p19 in the samples containing a constant concentration of CSK siRNA (Figure 4.2A), there was a gradual increase in polarization implying that binding had occurred between the p19 protein and the siRNA. By plotting the change in polarization as a function of the concentration of p19, a sigmoidal curve was obtained (Figure 4.2B) signifying a dose-response relationship between the p19 protein and the siRNA. Analysis of the curve indicates a dissociation constant for the p19-CSK siRNA interaction of 15 ± 7 nM. The presence of the Cy3 fluorophore on the 5′ end of the siRNA may impede its ability to bind p19 due to steric hindrance and hence may account for the slightly larger dissociation constant than previously reported by others (0.17 ± 0.02 nM (185) or 15.24 ± 2.3 nM (208)). The dissociation constant determined by fluorescence polarization in this study is much smaller, however, than the value determined from our previous studies using a fluorescence detection method on Ni^{2+}-NTA-coated plates (177, 179) (Table 4.1). The lower affinity obtained from the fluorescence detection method on Ni^{2+}-NTA-coated plates may be due to the conformational restriction of p19 as a result of surface binding which may hinder its ability to bind to the siRNA.

To be certain that the observed change in polarization was due to the binding of functional p19 with the target CSK siRNA, the dependence of the change in fluorescence

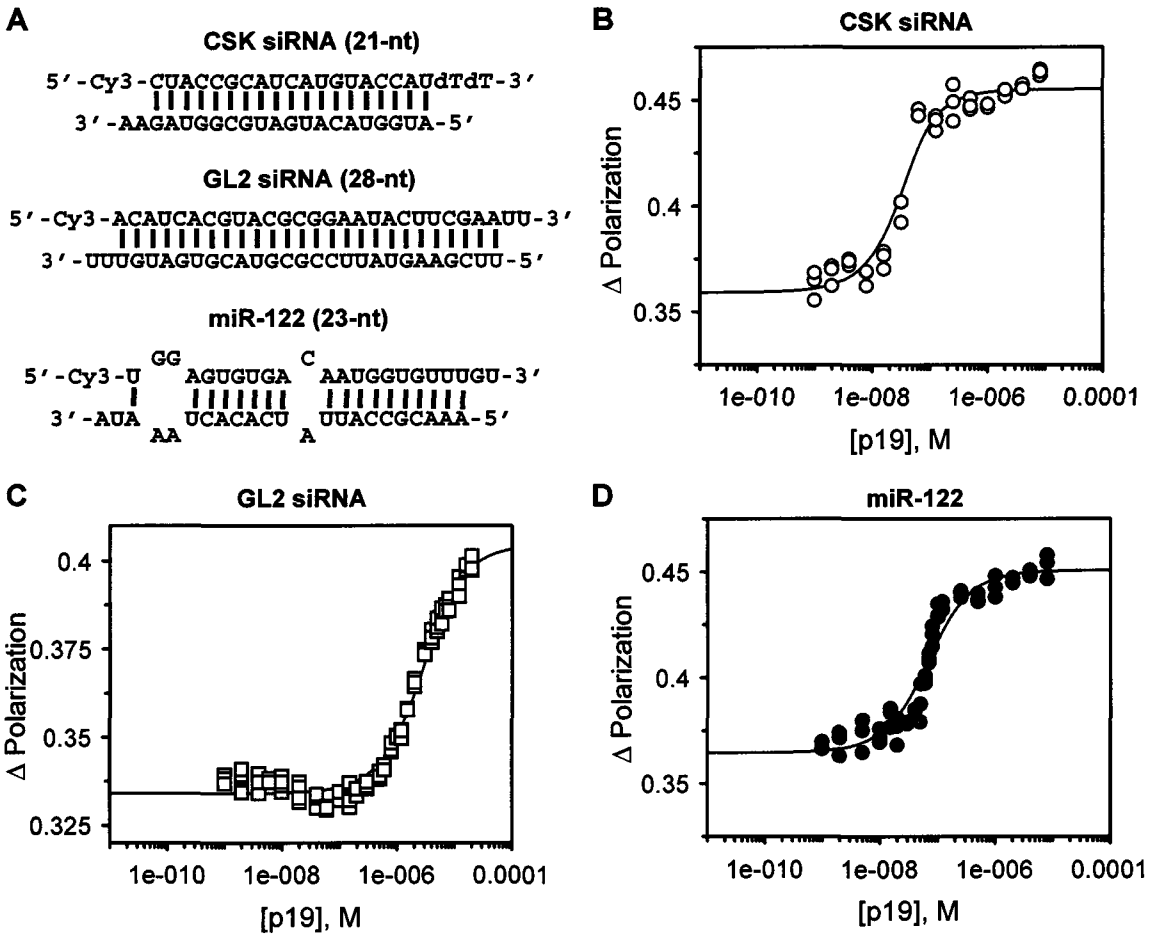

Figure 4.2 Binding curve analyses of p19 with various small RNAs obtained from fluorescence polarization. (A) Structures of small RNA duplexes. The mispairing of bases in the 23-nt duplex of miR-122 is illustrated showing the bulges in the structure of the miRNA. The binding curves for B) CSK siRNA (21-nt), C) GL2 siRNA (28-nt), and D) miR-122, are shown. The curves were obtained by plotting the change in polarization as a function of the concentration of the p19 dimer using 40 nM small RNA (CSK and miR-122) or 2 μM (GL2). All measurements were carried out in triplicate.

Table 4.1 Dissociation constants for CIRV p19 and small RNAs.

	K_d (nM)		
	Ni-NTA[1]	**Florescence Polarization**	**EMSA[2]**
CSK siRNA (21-nt)	450 ± 91	15 ± 7	21 ± 3
GL2 siRNA (28-nt)	~35 000[3]	1790 ± 182	~20 000[3]
miR-122 (23-nt)	N/A	47 ± 7	223 ± 43[4]
			199 ± 186[5]
unlabeled CSK siRNA (21-nt)	N/A	12 ± 2	7 ± 3

[1]Fluorescence detection with a 96-well Ni^{2+}-NTA-coated plate. [2]Electrophoretic mobility shift assay performed at 40 nM small RNA. [3]Binding experiments were performed at 200 nM siRNA and were not able to reach saturation. [4]Performed with 5'-sense-labeled miR-122. [5]Performed with 5'-antisense-labeled miR-122. Similar values were determined at 200 nM miR-122.

polarization in the presence of a longer duplex siRNA was investigated. The curve obtained from the fluorescence polarization experiment with the 28-nt GL2 siRNA (Figure 4.2A) is shown in Figure 4.2C. The dissociation constant was estimated to be approximately 1790 ± 182 nM, an almost 120-fold decrease in affinity compared to that of the 21-nt CSK siRNA (Table 4.1). This is consistent with previous results obtained by our group (177), and others (185), in which p19 was demonstrated to bind with decreasing affinities to siRNAs of increasing length from 21- to 28-nt. Saturation was not reached using the 28-nt GL2 siRNA due to the solubility limitations of concentrations of p19 > 20 μM. Nonetheless, this demonstrates the size-selective binding of p19 to siRNA using the fluorescence polarization method which is consistent with the known binding behavior of CIRV p19 from previous studies (177, 179, 185).

4.3.2 p19 is Able to Bind to a Human miRNA, miR-122, with Nanomolar Affinity

The binding of p19 to miR-122 was also investigated by fluorescence polarization. miR-122 is a 23-nt miRNA containing several mismatched base pairs resulting in structural irregularities or bulges in the dsRNA duplex when compared to the perfectly complementary, canonical CSK siRNA duplex (Figure 4.2A). Plotting the data from the polarization measurements of miR-122 with varying concentrations of p19 also resulted in a sigmoidal curve (Figure 4.2D) with a dissociation constant of 47 ± 7 nM (Table 4.1). The binding affinity of p19 for miR-122 shows an approximately 3-fold decrease in affinity when compared with that for CSK siRNA. The decreased affinity is most likely due to the steric hindrance imposed on the p19 protein because of the bulges arising from mismatched base pairs in the miRNA duplex. However, the affinity did not

decrease to the same degree as that of the 28-nt GL2 siRNA, perhaps due to the less dramatic length difference of the 23-nt miR-122 compared to the 21-nt CSK siRNA. The mismatches in the miR-122 structure may also compress the actual length of the 23-nt miRNA duplex so that it appears slightly shorter, similar to the canonical 21-nt siRNA molecule. As a result, the p19 dimer may be able to accommodate the miR-122 duplex between the two end-capping helices (see *Discussion*).

4.3.3 Fluorescence-based EMSA as an Alternative Method for Assessing p19-small RNA Interactions

The binding behaviors of p19 with the fluorophore-labeled small RNAs examined by fluorescence polarization were also investigated with EMSA. This technique is also commonly used to assess protein-nucleic acid interactions (276). In previous studies, EMSA has been used to analyze the binding affinity and specificity of CIRV p19 with ^{32}P-radiolabeled siRNAs (185, 208). For comparison with the fluorescence-based techniques, similar EMSA experiments were performed with fluorophore-labeled small RNAs. In addition, the use of fluorescence labeling as the detection marker for EMSA in place of ^{32}P-radiolabeling can avoid the use of radioactivity while retaining similar sensitivities with the use of modern laser-based scanners.

The EMSA experiments were performed by allowing binding of the small RNA samples with various concentrations of p19 in solution under conditions similar to those of the fluorescence polarization experiments before gel electrophoresis. A representative EMSA experiment showing the interaction between p19 and the CSK siRNA is shown in Figure 4.3A. There was a gradual increase in the fluorescence intensity of the slower

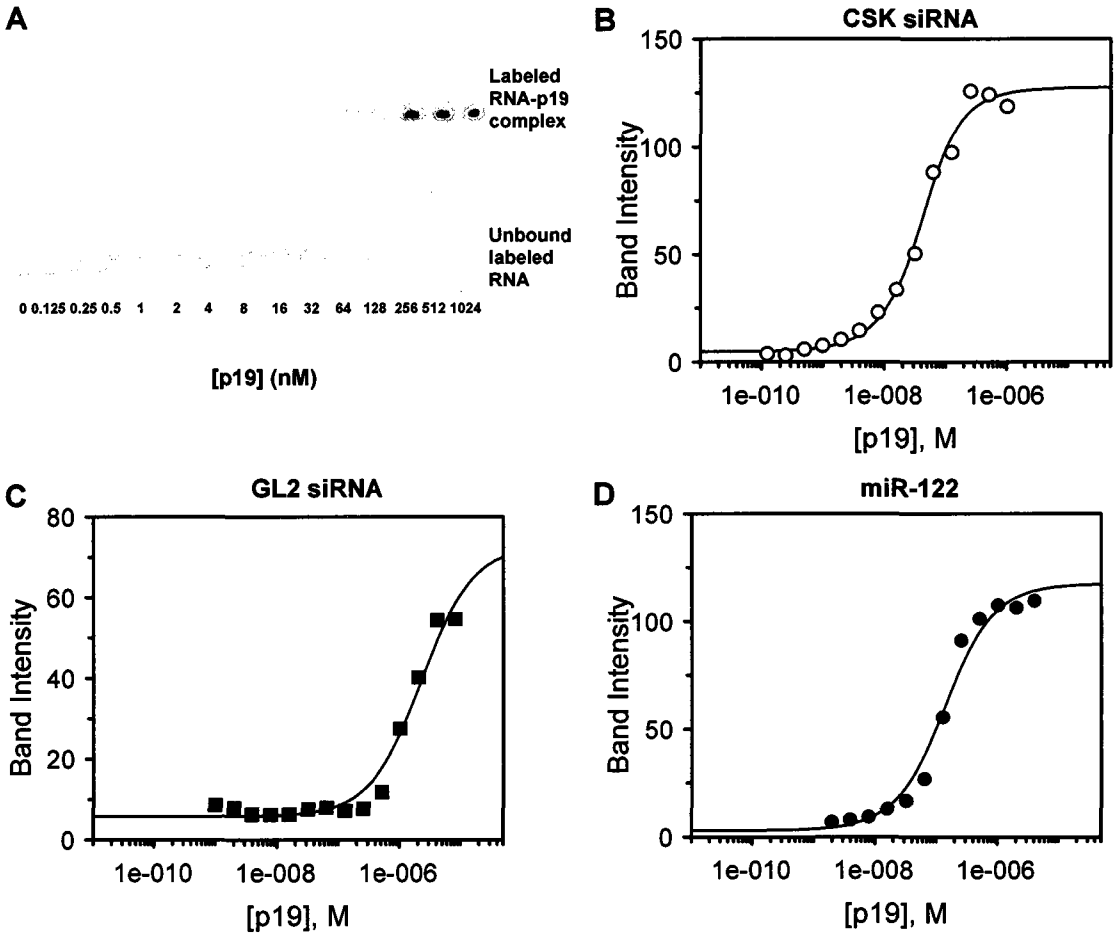

Figure 4.3 Electrophoretic mobility shift assays of p19-small RNA interactions. A) A representative gel for determining the dissociation constant for p19 and CSK siRNA performed with 40 nM CSK siRNA (21-nt) with varying concentrations (0-512 nM) of the p19 dimer. Curves in panels B) and C) were obtained by plotting the normalized fluorescent band intensities as a function of the concentration of the p19 dimer for the labeled small RNAs (40 nM CSK siRNA and miR-122; 200 nM GL2 siRNA). The binding curves for B) CSK siRNA (21-nt), C) GL2 siRNA (28-nt), and D) miR-122, are shown.

migrating bands with an increase in p19 concentration, corresponding to the labeled CSK siRNA population in complex with p19 (Figure 4.3A). In contrast, there was a gradual decrease in intensity of the faster migrating bands corresponding to unbound labeled siRNA, indicating an increase in the size of the population of labeled siRNA molecules in complex with p19 (Figure 4.3A). The band intensities corresponding to the p19-small RNA complex were measured and plotted as a function of p19 concentration. Curves corresponding to 21-nt CSK siRNA (Figure 4.3B), 28-nt GL2 siRNA (Figure 4.3C), and miR-122 (Figure 4.3D) all show a dose-response relationship between small RNA complex formation and p19 concentration. The dissociation constant of p19 in complex with CSK siRNA (21-nt) obtained from EMSA (21 ± 3 nM) was comparable to that from fluorescence polarization (15 ± 7 nM; Table 4.1). However, the EMSA binding curve for miR-122 (23-nt) demonstrated a larger dissociation constant than that obtained by fluorescence polarization (223 ± 43 nM and/or 199 ± 186 nM; Table 4.1). For GL2 siRNA (28-nt), the EMSA binding curve did not reach saturation; however, the estimated dissociation constant values are consistent with those obtained by fluorescence polarization (Table 4.1). This indicates that the binding affinities of p19 in complex with small RNAs obtained by fluorescence polarization and EMSA measurements are consistent with one another.

4.3.4 The 5'-Cy3 Fluorophore has a Minimal Effect on p19-small RNA Interactions

To determine whether the presence of the Cy3 fluorophore on the small RNAs used in this study had any effect on p19 binding, competition experiments were conducted with the Cy3-labeled CSK siRNA and unlabeled CSK siRNA for p19 binding

using both the fluorescence polarization and EMSA methods. The competition experiments were carried out by allowing incubation of a 1:1 molar ratio of p19 with Cy3-CSK siRNA and then titrating with increasing concentrations of unlabeled CSK siRNA. Fluorescence polarization was measured at each concentration of unlabeled small RNA. Likewise, the competition experiment was conducted by EMSA under similar conditions except that the samples were loaded onto a gel and examined by in-gel fluorescence. As the unlabeled siRNA concentration was increased, there was a gradual decrease in the fluorescence intensity of the bands corresponding to the labeled small RNA population in complex with p19 as seen in Figure 4.4A. In contrast, there was a gradual increase in the intensity of the bands corresponding to unbound labeled siRNA, demonstrating the competition between labeled and unlabeled CSK siRNA for binding with p19. Measurements from back-titration experiments for both fluorescence polarization and EMSA methods were plotted as a function of unlabeled CSK siRNA concentration (Figure 4.4B,C). The dissociation constant for p19 binding to unlabeled CSK siRNA was calculated according to Equation [4] (see *Chapter 2*) for the fluorescence polarization (12 ± 2 nM) and EMSA (7 ± 3 nM) experiments, as summarized in Table 4.1. The values of the Cy3-labeled and unlabeled CSK siRNAs were similar in magnitude, indicating that the presence of the Cy3-fluorophore has a minimal effect on the binding of p19 to the siRNA. These results also confirm that the lower affinity obtained with the fluorescence detection method on the Ni^{2+}-NTA-coated plate (177, 179) was not due to the presence of the Cy3 fluorophore, but was likely a result of surface effects. However, the latter fluorescence detection method using 96-well

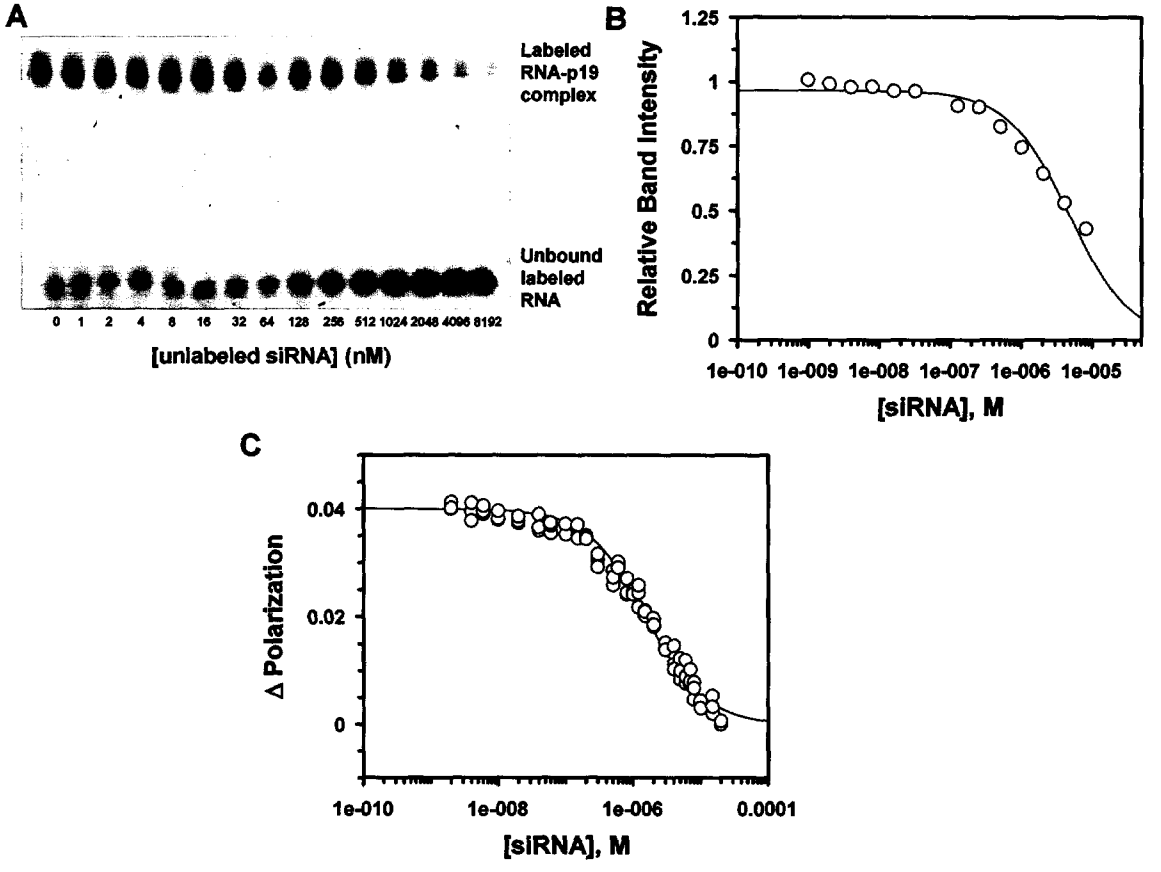

Figure 4.4 Competition experiments with labeled and unlabeled small RNAs. A) Gel from an EMSA performed with a 1:1 molar ratio of the p19 dimer to CSK siRNA (21-nt) with varying concentrations (1-8000 nM) of competitor unlabeled CSK siRNA (21-nt). B) Competition binding curve obtained by plotting the normalized fluorescent band intensities from panel (A) as a function of the concentration of competitor unlabeled CSK siRNA. C) Competition experiment between labeled and unlabeled CSK siRNA with p19 as measured by fluorescence polarization. The competition binding curve was obtained by plotting the change in polarization as a function of the concentration of competitor (unlabeled CSK siRNA). All measurements were carried out in triplicate.

Ni^{2+}-NTA-coated plates is still a useful high-throughput method for screening p19-small RNA interactions.

4.4 Discussion

4.4.1 Interactions of p19 with Small RNA Duplexes

The ability of p19 to bind to various classes of small RNAs, from perfectly complementary siRNAs to more irregularly structured miRNAs, makes it an important tool for studying these broad classes of small RNAs in a variety of *in vitro* and *in vivo* systems. It has previously been demonstrated that p19 has the ability to bind miRNAs in mammalian cells (83, 275), as well as the ability to bind siRNAs of differing lengths with varying affinities (177, 185). Since the large class of miRNAs identified to date have a wide degree of secondary structures (300), it is expected that the degree of complementarity and the varying lengths of the miRNAs will result in a wide degree of p19 binding affinities. In this study, the interactions of p19 with a specific, irregularly-structured miRNA, miR-122, was further characterized by fluorescence polarization and fluorescence-based EMSA. The results indicated that the p19 protein can bind miR-122 with nanomolar affinity (47 ± 7 nM; Table 4.1). The approximately 3-fold reduction in affinity in comparison with p19's interaction with a canonical 21-nt siRNA (CSK siRNA) is likely due to perturbations to the known p19-siRNA interactions as a result of the structural irregularities arising from the base pair mismatches in the miR-122 duplex. Assuming the 23-nt miR-122 duplex, in complex with CIRV p19, adopts a slightly compressed conformation similar in length to that of a perfectly complementary A-form 21-nt siRNA duplex (as in reference (185)), it is likely that the miRNA docks into the

protein in a fashion similar to that of the canonical CSK siRNA duplex (Figure 4.5A). If this is the case, the presence of the asymmetric bulges in the miR-122 duplex results in two possible orientations of the miR-122 molecule within the CIRV p19 dimer (Figure 4.5B,C). Since the interactions of the siRNA molecule with the p19 dimer involve interactions with amino acid residues from both monomer subunits, the residues of one p19 monomer will be differentiated from the other by designating them A and B.

In the first orientation (Figure 4.5B), the bigger (2-nt) bulge will likely affect the interactions of Lys60(A) and Arg18(A) with the miR-122 phosphate backbone. The compression in the length of the miRNA molecule due to the bulges may result in a significant shift in the phosphate backbone which could also have an effect on the interaction with Gln107(A). The smaller (1-nt) bulge is likely to overlap with the position of the central nucleotide (nucleotide 10 from the 5′ end of the sense strand) of CSK siRNA (Figure 4.5A), as observed in the crystal structure of the CIRV p19-bound siRNA complex (185). In this position, the smaller (1-nt) bulge is likely to disrupt the interaction of Ser120(B) and Ser113(B) with the sugar groups of miR-122. Interactions of the Lys67(A), Arg11(A), Arg115(B), and Ser62(B) residues with the miR-122 phosphate backbone are also likely to be at least partially disrupted.

In the second orientation of miR-122 docked into p19 (Figure 4.5C), the bigger (2-nt) bulge will likely affect the interaction of the Lys60(B) and Arg18(B) residues with the miR-122 phosphate backbone. Since the position of the bigger (2-nt) bulge is opposite to that of the first orientation, a shift in the miR-122 backbone is likely to affect the interaction of the miR-122 sugar and phosphate groups with Gln107(B). In addition, like in the first orientation (Figure 4.5B), the overlap between the smaller (1-nt) bulge with

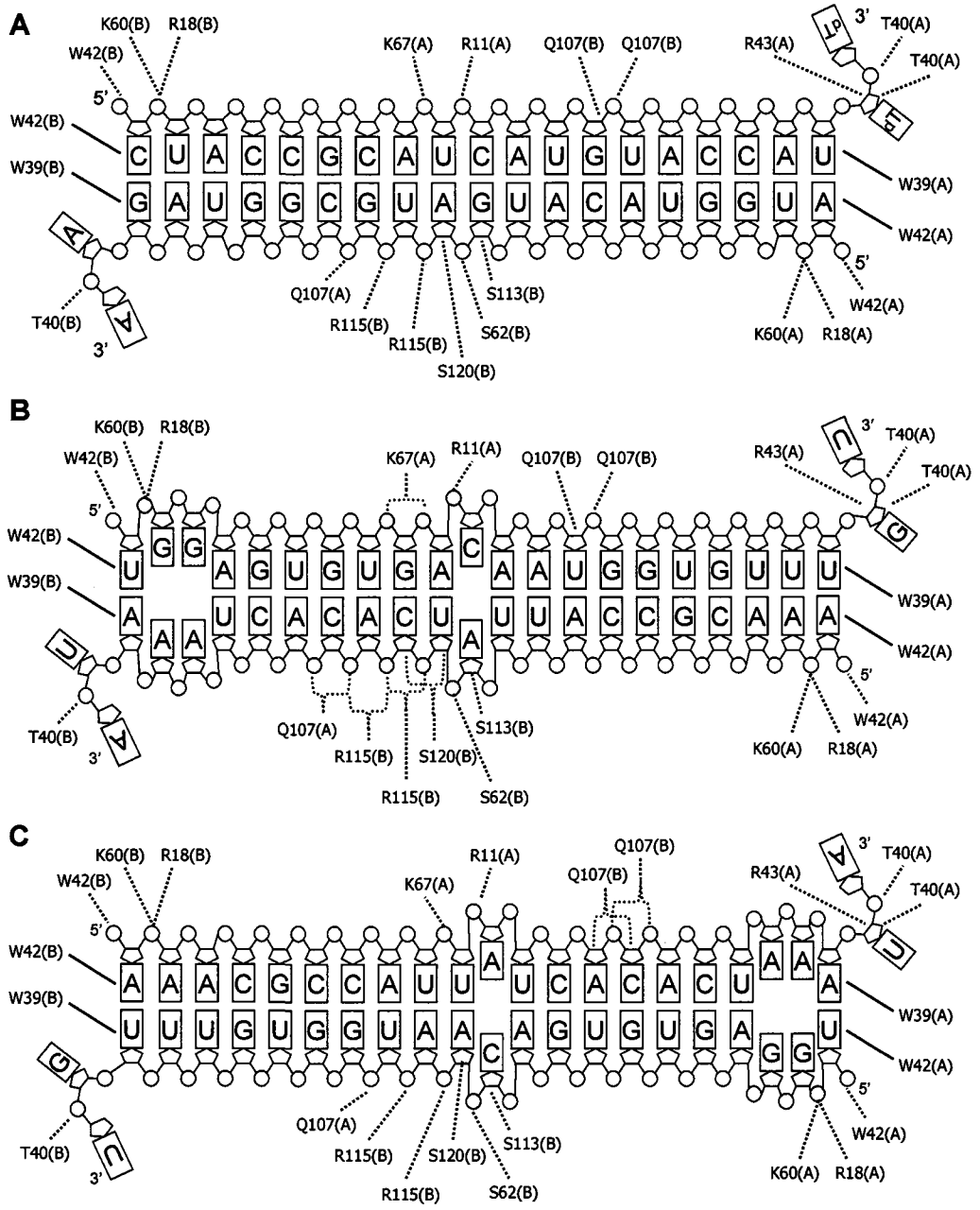

Figure 4.5 Schematic representation of p19–small RNA contacts. A) Interaction of p19 with CSK siRNA based on the crystal structure of the CIRV p19-siRNA complex described in reference (185). The proposed interactions between CIRV p19 and miR-122 in orientation 1 and orientation 2 are shown in panels (B) and (C), respectively. The p19 amino acid residues from each monomer subunit are distinguished as dashed lines, and stacking interactions are shown as solid lines. The phosphate and sugar group contacts predicted to be disrupted due to the irregular bulges in the miR-122 duplex are indicated [phosphate groups (green); sugar residues (blue)].

the position of the central nucleotide (nucleotide 10 from the 5′ end of the sense strand) of the CSK siRNA (Figure 4.5A) is also likely to be slightly shifted. In this case, interactions between the Ser120(B) and Ser113(B) residues and the miR-122 sugar groups and the interaction of the Lys67(A), Arg11(A), and Ser62(B) residues with the phosphate backbone will likely be affected, but the interaction with Arg115(B) is likely to be partially recovered (Figure 4.5C). The predicted perturbations to the interaction of the p19 residues, known to interact with canonical siRNAs (185), with the asymmetric and irregular miR-122 molecule described here, are likely to account for the approximately 3-fold decrease in affinity of p19 for the miR-122 molecule that was observed by fluorescence polarization (Figure 4.2 and Table 4.1).

The capacity of p19 to bind to miR-122 with nanomolar affinity requires the retention of key interactions between p19 and the miR-122 molecule. Electrostatic interactions between the miR-122 phosphate groups and p19 residues Gln107(B), Lys60(A), Arg18(A), Thr40(A), and Trp42(A) and interactions between the sugar groups and Gln107(B), Thr40(A), Thr40(B), and Arg43(A) in the first orientation are far from the bulges, and these contacts are hypothesized to be sustained (Figure 4.5B). Similarly, interactions between the phosphate groups and Lys60(B), Arg18(B), Thr40(A), Thr40(B), Gln107(A), and Arg115(B) and interactions between the sugar groups and Arg43(A) and Thr40(A) in the second orientation are also likely to remain intact (Figure 4.5C). Moreover, it is anticipated that the end-capping interactions with Trp39 and Trp42 are also maintained and probably account for the bulk of the binding affinity of p19 for miR-122 (Figure 4.5B,C). As seen in Figure 4.5A, both ends of the 19 base pair (bp) duplex region of the 21-nt siRNA are capped by key contacts between the Trp39 and

Trp42 residues on each monomer of the p19 dimer. In addition, as demonstrated by Vargason and colleagues, there is a 22-fold decrease in the affinity of p19 for a 23-nt siRNA in comparison with that for a canonical 21-nt siRNA (185). However, greater differences in length result in magnitude order decreases in affinity (185). Since miR-122 is 23-nt in length, and the bulges are expected to slightly compress the length of the molecule, this could allow the duplex region to adopt a length closer to that of the standard 19 bp A-form dsRNA duplex (206) to fit between the two end-capping helices of the p19 dimer. Therefore, it is anticipated that the p19 end-capping interactions with miR-122 are similar to those with conventional 21-nt siRNA and largely account for the p19:miR-122 binding affinity.

Protein-nucleic acid interactions often involve conformational changes to both the apoprotein and nucleic acid ligand upon binding (301-304). These conformational changes facilitate binding by maximizing the number of interactions at the protein-nucleic acid interface. Many nucleic acid binding proteins alter the shape of their targets upon binding, demonstrating a close relationship between the conformational changes of the nucleic acid with complex formation and binding specificity (185, 186, 305-308). For example, in the crystal structure of the *Drosophila* sex-lethal protein-RNA complex, the RNA target is sharply bent into a V-shaped conformation within the protein's binding cleft (308). More specifically, in the crystal structures of p19-siRNA complexes, there is a 40° bend in the siRNA molecule when bound by p19 (185, 186). This bending seems to maximize the contacts between the siRNA sugar-phosphate backbone and the concave binding surface of the p19 dimer. The conformation of the miR-122 molecule may also be adjusted in a similar fashion to maximize its interaction with the p19 protein.

Ligand-induced conformational changes in protein structure are also widely recognized in protein-nucleic acid interactions (309-313). For example, conformational flexibility is thought to be important for binding of Ro protein to its RNA target (313). In addition, in the model of the Dicer-dsRNA complex, the flexible hinges of the protein are suggested to be crucial for dsRNA binding and processing (312). The inherent flexibility of the p19 protein dimer therefore should allow it to tolerate the irregular structure of the miR-122 molecule.

In addition, RNA binding proteins often contain arginine-rich motifs (ARMs) that are able to cross-recognize diverse RNA ligands (314). This results from different combinations of electrostatic interactions between multiple Arg residues and the RNA phosphate backbone (314). For the p19 protein, the presence of multiple Arg residues in the RNA binding surface (178, 179, 185), combined with the inherent flexibility of the protein and nucleic acid ligands, may allow p19 to form new contacts with the miR-122 molecule. These new contacts may compensate for the loss of interactions arising from the bulges in the miR-122 molecule.

4.4.2 Conclusion

In conclusion, fluorescence polarization and fluorescence-based EMSA experiments can be applied to the study of p19-small RNA interactions. The detailed binding studies of p19 with miR-122 indicate that p19 binds to the miRNA with nanomolar affinity. The binding interactions can be understood by the orientations of the miR-122 bulges relative to the key amino acid residues in p19 that interact with a canonical 21-nt siRNA. The ability of p19 to bind to miR-122 and to other irregularly-

structured miRNAs (83, 223, 275) gives it the potential to be used as a versatile tool for the investigation of small RNA function in eukaryotes.

Chapter 5: *In Vitro* Screening for High Affinity siRNA Interactions with Native Hepatitis C Virus RNA

5.1 Introduction

The first step in any successful RNA silencing experiment is the design of highly effective siRNAs. Current design algorithms typically focus on siRNA sequence and, though they greatly increase the probability of selecting an effective siRNA, many siRNAs designed accordingly still fail to silence their target gene(s). Thus, additional parameters, like the accessibility of the target RNA or the presence of RNA-binding proteins, are likely to be important factors for successful RNA silencing. Herein, the importance of target site accessibility in the silencing efficiency of siRNAs against highly-structured RNA targets is investigated using the HCV replicon RNA genome as a model. As will be addressed in this chapter, target site accessibility may be a particularly important parameter for the design of effective siRNAs against the large, highly-structured genomes of postitive-sense RNA viruses, such as HCV.

5.1.1 Importance of RNA Secondary Structure in the Life Cycle of RNA Viruses

Despite its limited functional group diversity, RNA forms a wide variety of complex structures capable of highly specific ligand recognition and catalysis. RNA secondary and higher ordered structures are also known to play a fundamental role in the life cycle of RNA viruses. For example, translation of viral proteins often involves IRES elements that function in ribosome recruitment and initiation of translation (315-317). Replication of the viral RNA genome also involves recognition of *cis*-acting RNA elements that direct the viral polymerase to initiate positive- and negative-strand synthesis (318-321). And finally, packaging involves recognition of RNA structures for encapsidation of the RNA genome into progeny particles (322, 323). Recently,

Simmonds and colleagues have provided evidence for evolutionarily conserved, defined RNA structures of yet unknown function, in diverse RNA viruses from plants and animals, using increasingly advanced computational approaches (324).

5.1.2 Genome-scale Ordered RNA Structures (GORS)

Target site accessibility can be governed by secondary and higher-ordered intramolecular RNA structures within viral genomes. In an investigation of the distribution of RNA secondary structure in viral genomes, Simmonds and colleagues used MFOLD thermodynamic analysis to estimate the minimum free energy (MFE) of folding and Z-scores of virus genomes and control sequences (324-326). MFOLD is an energy minimization algorithm used to predict optimal and suboptimal secondary structures of RNA molecules based on empirically determined values for the various base pairs that form simple stem loops (325-327). Examination of aligned viral genome fragments using MFOLD indicated the existence of a widely distributed predicted RNA structure, termed genome-scale ordered RNA structures (GORS), throughout the genomes of virus groups, such as the aphthoviruses and hepaciviruses (324). In contrast, there was no evidence of GORS upon examination of other genera within the *Flaviviridae* or *Picornaviridae* families, the large DNA viruses, as well as among the bacterial and mammalian coding sequences analyzed (324).

GORS were widely distributed in many animal and plant RNA virus families, but there was remarkable variability in the occurrence of GORS in different viral genera (Figure 5.1A). For example, HCV (genus *Hepacivirus*), of the family *Flaviviridae*, had

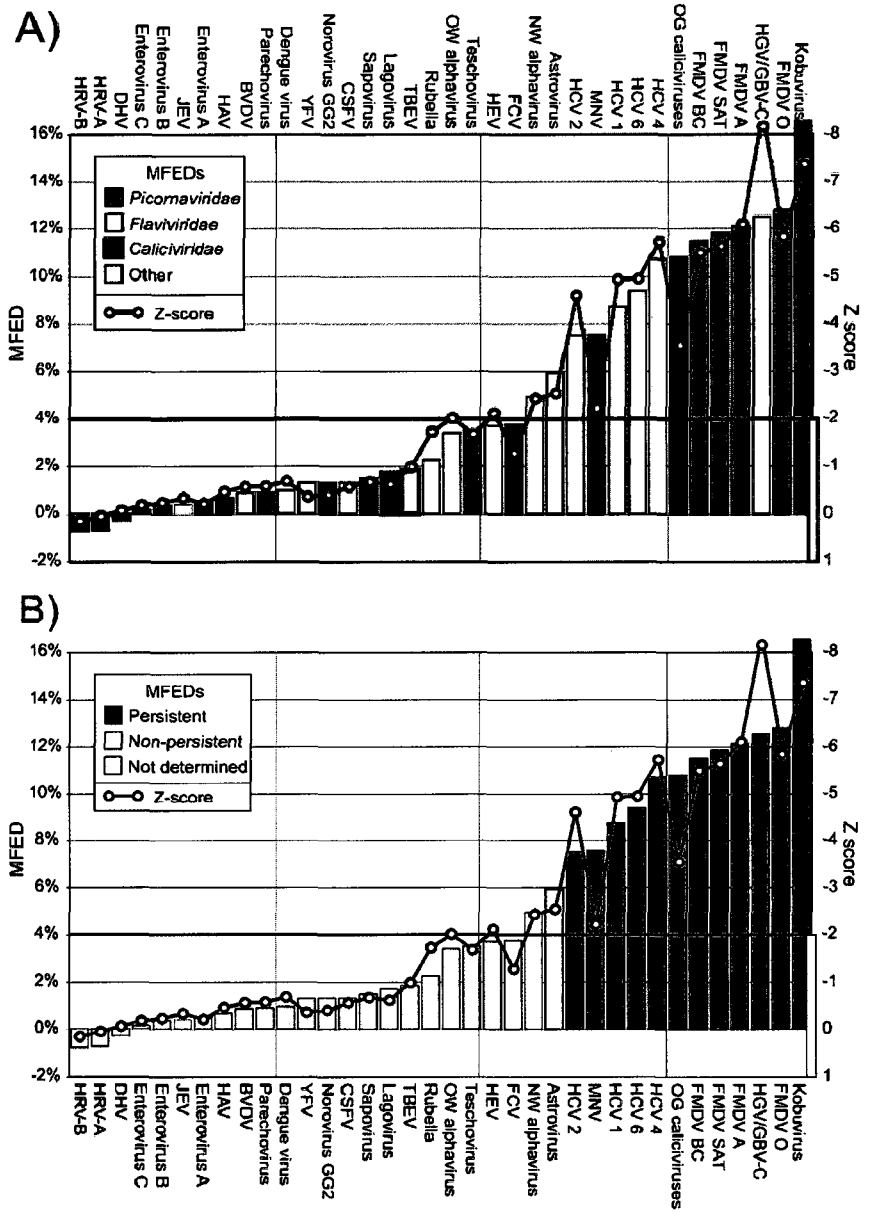

Figure 5.1 Prediction of GORS in the genomes of RNA viruses. RNA structure prediction in alignments of native sequences for 36 RNA virus groups. Alignments are ordered left-to-right by ascending MFEDs. MFEDs are coloured based on virus family (A) or by persistence (B), as indicated in the insets. HRV, human rhinovirus; DHV, duck hepatitis virus; JEV, Japan encephalitis virus; HAV, hepatitis A virus; BVDV, bovine viral diarrhoea virus; YFV, yellow fever virus; CSFV, classical swine fever virus; TBEV, tick-borne encephalitis virus; OW, old-world; HEV, hepatitis E virus; FCV, feline calicivirus; NW, new world; HCV, hepatitis C virus; MNV, murine norovirus; OG, ocean group; FMDV, foot-and-mouth disease virus; HGV/GBV-C, hepatitis C virus/GB virus C. Figure adapted from reference (328).

thermodynamic evidence of extensive RNA structure throughout the coding region of the genome, whereas this was absent in the closely related *Pestivirus* and *Flavivirus* genera (324, 328). Similar genus-associated variability was seen within the *Picornaviridae* and *Caliciviridae* (Figure 5.1A), as well as within many plant virus families. As such, it is unlikely that GORS functions in fundamentally conserved aspects of viral replication or encapsidation strategies (324, 328). However, the existence of GORS correlated strongly with the ability of each virus to persist in their natural hosts (Figure 5.1B), suggesting a role for GORS in modulating innate intracellular defence mechanisms (324, 328).

To provide biophysical evidence for the existence of GORS, Simmonds and colleagues performed hybridization accessibility assays and atomic force microscopy (AFM) of RNA virus genomes from viruses with and without GORS (328). In the hybridization accessibility assay, oligonucleotide probes were selected every 200-300 base pairs (bp) down the genomes of each virus investigated. The duplex regions were specifically selected to have similar G+C contents in order to ensure equal binding strengths, irrespective of the overall base composition of each transcript (328). Full-length, biotin-labeled viral genomes were then hybridized under native conditions at 37 °C to the oligonucleotide probes (324). As shown in Figure 5.2, for the predicted structured viruses, hepatitis G virus/GB virus-C (HGV/GBV-C), HCV, and murine norovirus (MNV), most probes failed to hybridize to their target sequences within the viral transcripts (Figure 5.2A). In contrast, in the predicted unstructured viruses, enterovirus C, tick-borne encephalitis virus (TBEV), rubella virus, and bunyavirus (BV), hybridization intensities were much more uniform, with the majority of the probes hybridizing efficiently to their targets (Figure 5.2B). Low or absent binding of the viral

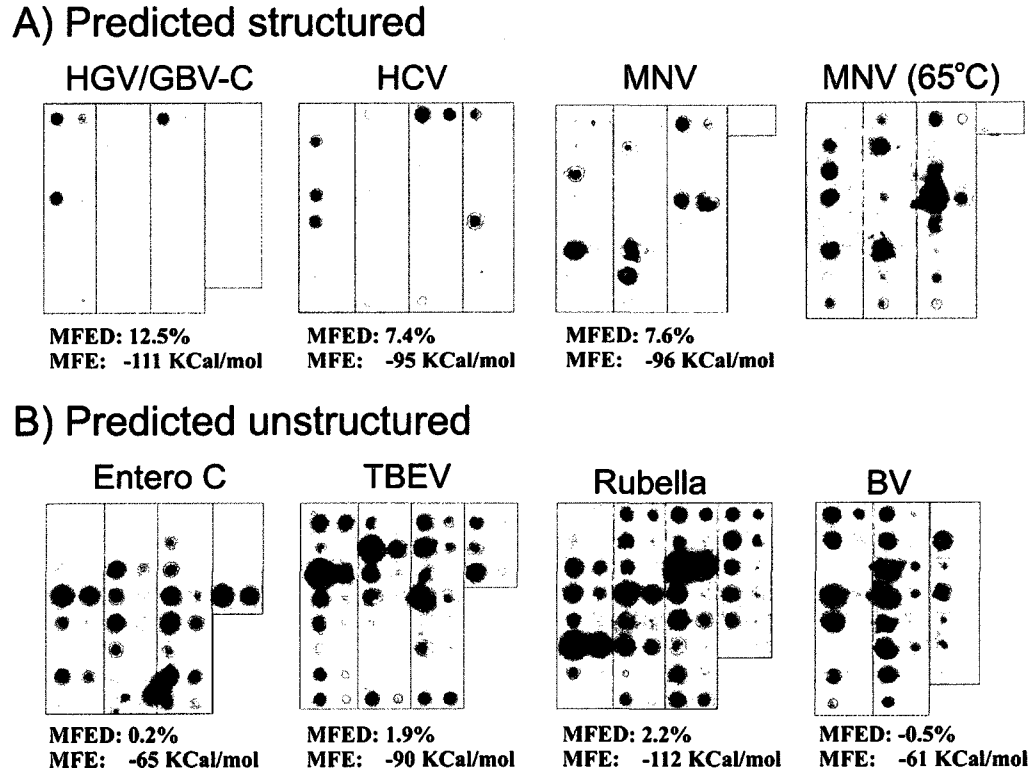

Figure 5.2 Reverse hybridization of filter-immobilized oligonucleotides to RNA transcripts of predicted structured and unstructured genomes of RNA viruses. The reverse hybridizations of biotin-labeled RNA transcripts from predicted structured (A) and unstructured (B) virus genomes to filter immobilized probes (left 50 pmol; right 5 pmol) are shown. Probes proceed down the viral genomes from the 5'-end (upper left corner) to the 3'-end (lower left corner). HGV/GBV-C, hepatitis C virus/GB virus C; HCV, hepatitis C virus; MNV, murine norovirus; Entero C, enterovirus species C; TBEV, tick-borne encephalitis virus; OW, old-world; HEV, hepatitis E virus; FCV, feline calicivirus; NW, new world; BV, bunyavirus. Figure adapted from reference (328).

genome transcripts to their complementary probes suggests that the structure of the viral genomes makes the transcripts inaccessible to hybridization. To confirm that internal base-pairing of the viral transcripts indeed prevented hybridization, viral transcripts were hybridized at an elevated temperature (65 °C), selected to disrupt secondary structure but retain hybridization of the viral RNAs to the oligonucleotide probes. The elevated temperature of hybridization had little effect on the hybridization of the predicted unstructured viral transcripts; however, there was an increased frequency of hybridization of the predicted structured viruses (see the MNV transcript at 65 °C vs. 37 °C; Figure 5.2A) (328). This is consistent with the bioinformatic prediction of GORS in the structured and unstructured viral RNA genomes (324, 328).

In order to further investigate the physical nature of GORS, AFM was performed to directly visualize the predicted structured and unstructured viral RNA transcripts (328). AFM is a high resolution, scanning probe microscopy that is able to determine the surface topography of native biomolecules at sub-nanometer resolution (329-331). To achieve atomic scale resolution, a sharp tip attached to a cantilever is tapped across the surface of a sample and allows point-by-point contouring while a small constant force is applied. The extremely high resolution of this technique allows direct visualization of the viral RNA transcripts at the molecular level (328, 332-336). When examined using AFM, the predicted structured viruses, HGV/GBV-C and HCV, uniformly adopted a tightly packed, condensed state that was largely maintained during the deposition process (Figure 5.3A and insets) (328). While the predicted unstructured viruses, rubella and poliovirus, appeared as pleomorphic clusters with frequently observed protrusions of what appears to be single-stranded RNA, often hundreds of nanometers in length (Figure

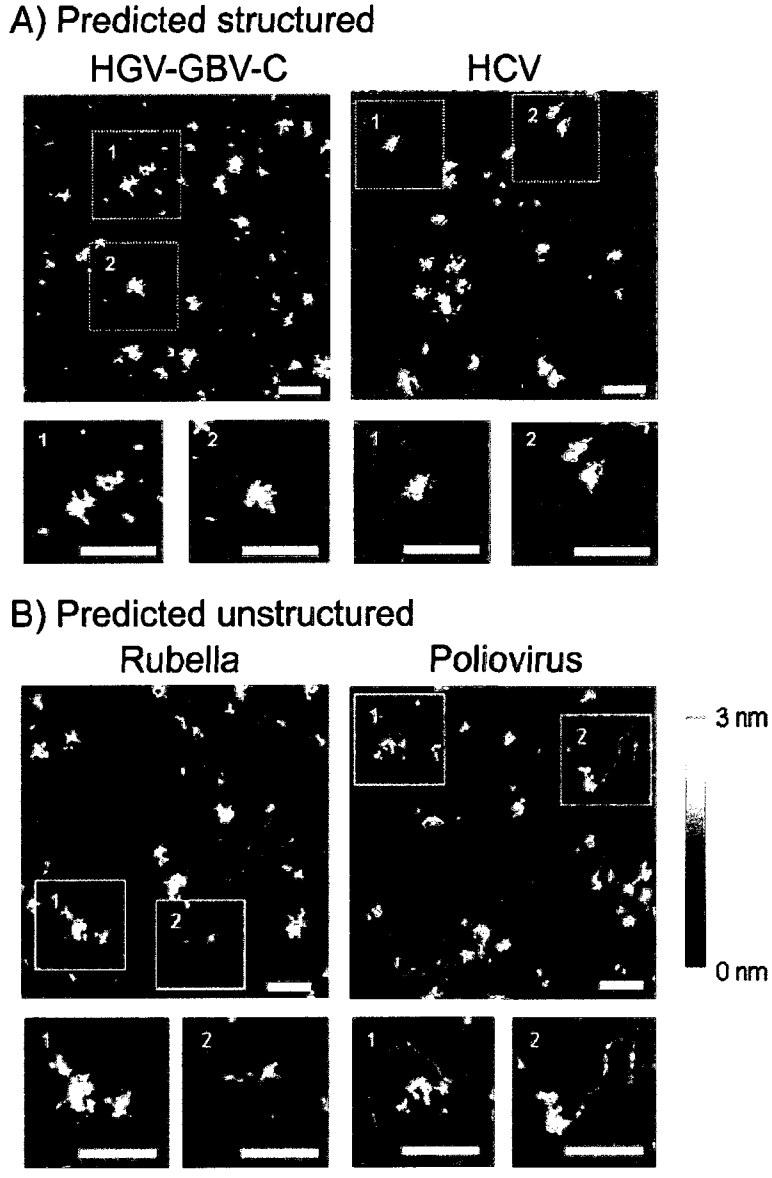

Figure 5.3 AFM images of predicted structured and unstructured genomes of RNA viruses. Analysis of RNA transcripts of A) predicted structured (HGV/GBV-C and HCV) and B) unstructured (Rubella virus and Poliovirus) viral RNA genomes. HGV/GBV-C, hepatitis C virus/GB virus C; HCV, hepatitis C virus. All scale bars are 200 nm and the Z-scale ranges from 0-3 nm. Figure adapted from reference (328).

5.3B and insets) (328). The AFM images revealed the overall structural differences between the predicted structured and unstructured viral RNA transcripts, and further supported the bioinformatic prediction of GORS.

The existence of GORS must influence the accessibility of certain regions of viral RNA transcripts (328). This suggests that target site accessibility may be an important factor when designing therapeutics that target viral genomes, including small RNA species such as siRNA. This chapter outlines the importance of target RNA structure on the effectiveness of siRNAs directed against the highly-structured genome of HCV.

5.1.3 Hepatitis C Virus

Hepatitis C virus (HCV) infection is a rapidly increasing global health concern, with over 200 million people infected worldwide, including 251 000 Canadians (337-339). In most infected individuals, HCV establishes a chronic infection that can lead to cirrhosis, hepatocellular carcinoma, and death. Currently, there is no vaccine available and the antiviral therapy, which consists of combination therapy with pegylated-IFNα 2a and ribavirin, achieves sustained response rates in only approximately 50% of infected patients (340). Although new antiviral agents are in development, the rapid development of resistance suggests that multiple drugs may be needed to limit the emergence of drug-resistant strains (135). There is thus an urgent need to develop effective preventative and alternative therapeutic strategies for HCV infection. The pursuit of new HCV therapies has led to significant advances in the understanding of basic HCV molecular virology. This effort has been focused on elucidating the structural and functional components of

the genome and viral proteins that mediate the viral life cycle, as well as in identifying host-virus interactions required for viral entry, replication and propagation.

5.1.4 HCV Genome Structure and Organization

HCV is a positive-sense RNA virus that replicates through a dsRNA intermediate in the cytoplasm of host cells. Its 9.6-kb genome encodes a single ORF that results in an approximately 3000 amino acid polyprotein. The HCV polyprotein is cleaved post-translationally, by host and viral proteases, into three structural proteins (core, E1, and E2) and seven non-structural proteins (p7, NS2, NS3, NS4A, NS4B, NS5A, and NS5B) (Figure 5.4). The core (C) protein and the envelope glycoproteins (E1 and E2) compose the physical virion, while the non-structural proteins carry out viral replication, assembly and egress. The NS2 and NS3 proteins are responsible for liberating the non-structural proteins from the polyprotein, and the NS5B protein is the RdRp, responsible for genome replication. The NS4A protein forms a cofactor for NS3 (protease and helicase), while the functions of the p7 (ion channel), NS2 following autoproteolysis, NS4B, and NS5A proteins remain unclear. The NS3-5B proteins comprise the HCV replication complex and are sufficient for replication of the viral genome. As for all positive-sense RNA viruses, HCV replication takes place in association with altered cytoplasmic membrane structures termed the 'membranous web' (341, 342). Transcription proceeds through a negative-strand intermediate, which serves as a template for production of positive-strand genomic RNA that can either be translated, serve as a template for negative-strand synthesis, or be packaged into virions (Figure 5.5). Since HCV is a cytoplasmically

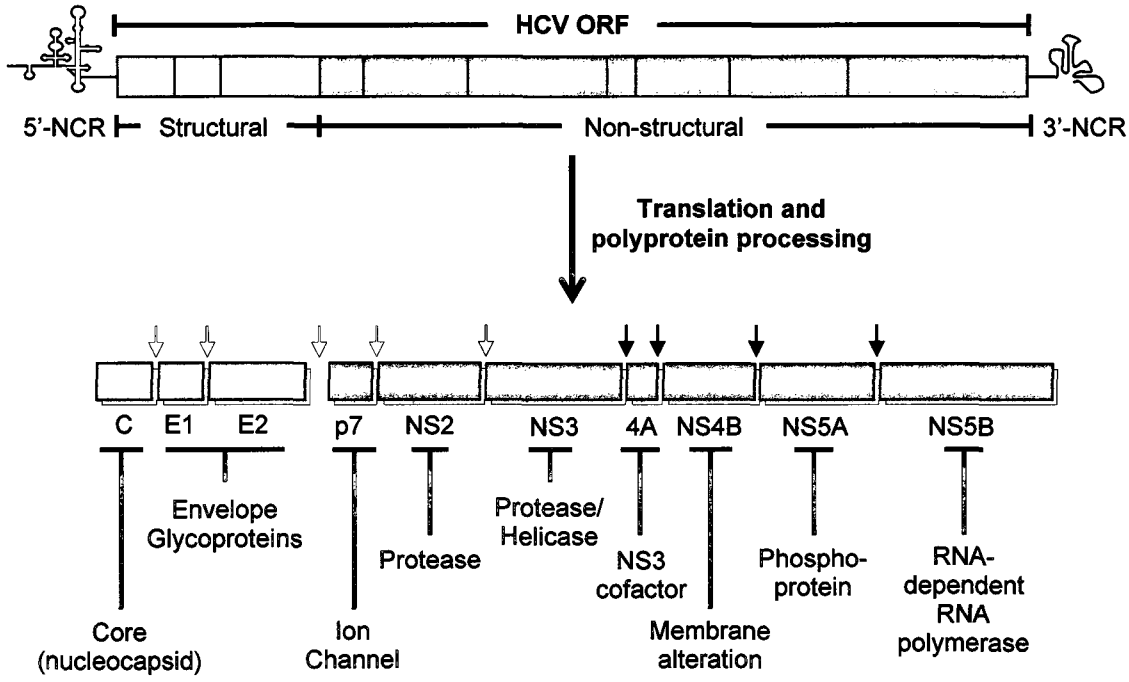

Figure 5.4 HCV genome organization and viral proteins. The 5'-NCR of the HCV genome contains an IRES that drives translation of the HCV polyprotein. The terminal loop of the 5'-NCR is also implicated in viral replication. Following translation, the HCV polyprotein is cleaved into ten unique viral proteins via host (structural) and viral (non-structural) proteases. The red arrows indicate cleavage by host signal peptidases and the blue and black arrows indicate cleavage by the NS2/NS3 cysteine protease and the NS3/NS4A serine proteases, respectively. The primary functions of each of the mature viral proteins are indicated. The 3'-NCR contains three distinct domains: a poly(U/UC) tract, a highly conserved 98-nt sequence, and a variable region that coordinate to direct HCV RNA replication. In addition, a *cis*-acting RNA element has been described within the NS5B coding sequence that forms a kissing-loop interaction with the 3'-NCR to modulate viral replication.

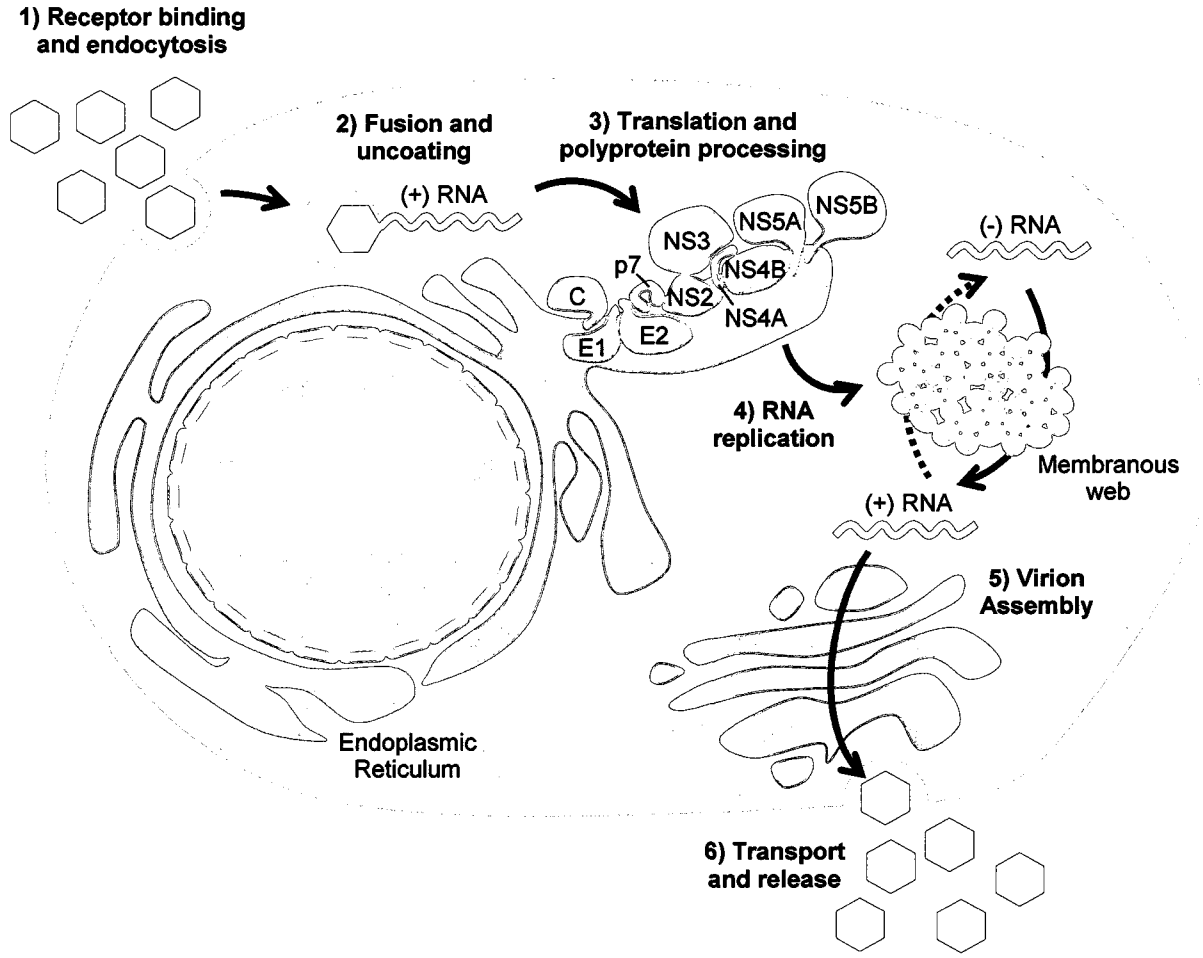

Figure 5.5 The life cycle of HCV. The HCV life cycle consists of the following steps outlined in the schematic: 1) Receptor binding and internalization; 2) fusion and uncoating of the viral genome; 3) IRES-mediated translation and polyprotein processing; 4) RNA replication; 5) packaging and virion assembly; and 6) transport and release of mature HCV virions. HCV RNA replication occurs in a membranous web composed of lipid droplets and altered ER-derived membranes.

replicating single-stranded RNA virus whose genome functions as both an mRNA and the template for replication, it is an attractive target for siRNA-based antiviral therapy.

5.1.5 Replicon Model of HCV Replication

For many years, the study of the molecular virology of HCV was hampered by the extremely restricted host range and inefficiency of *in vitro* models based on culturing primary cells isolated from persistently HCV-infected patients or infection of cultured cells with sera from HCV-infected patients (104, 343). Hence, the establishment of the replicon model of HCV replication was a major milestone in HCV research (187).

Lohmann and colleagues established a non-infectious subgenomic replicon where the structural region of the HCV ORF was replaced with a reporter gene (luciferase) or a selection gene (neomycin phosphotransferase) (Figure 5.6). Expression of the non-structural proteins (NS3-5B) is driven by a heterologous encephalomyocarditis virus (EMCV) IRES element. After transfection into a human hepatoma cell line (Huh-7), the transfected cells contain self-replicating HCV subgenomic replicon RNA (104, 187, 343). HCV subgenomic replicons harbouring the neomycin phosphotransferase gene can be selected for G418 resistance to establish cell lines stably replicating HCV replicon RNA (104, 187, 343). The replicons can support robust replication in cell culture, but do not produce infectious virions; and, efficient replication in cell culture is due to a series of cell culture adaptive mutations (344). Initially, subgenomic replicons that expressed only the NS3-5B proteins were constructed (Figure 5.6); however, replicons have since been created that contain the entire HCV polyprotein (345, 346). HCV replicons are useful tools for the study of HCV replication, viral protein function, and provide an excellent

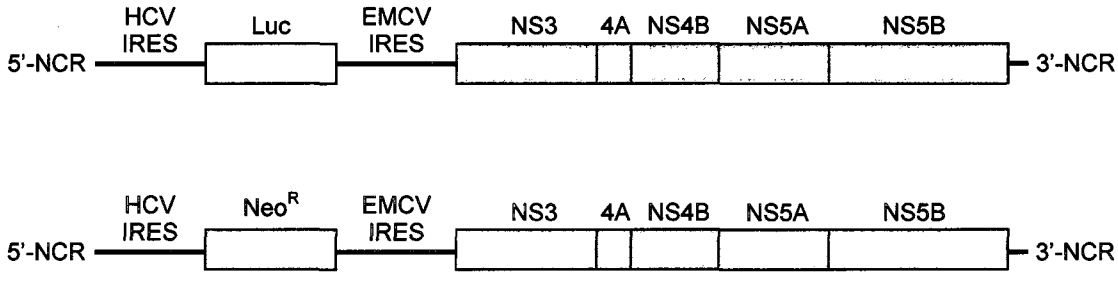

Figure 5.6 Schematic organization of the HCV subgenomic replicons used in this study. The 5'- and 3'-NCRs and the NS3 to NS5B proteins are required for viral RNA replication. Expression of the HCV non-structural proteins is driven by the encephalomyocarditis virus (EMCV) IRES and the expression of the luciferase (Luc) reporter gene (top) or the neomycin resistance (Neo^R) selection gene (bottom) are driven by the HCV IRES.

system for the evaluation of antiviral agents in cell culture, including small RNA species targeting the HCV genome (135).

5.1.6 Secondary Structure of the HCV RNA Genome

As for all positive-sense RNA viruses, the HCV genome contains many *cis*-acting RNA elements that drive translation, replication and packaging. The large size of the HCV genome is prohibitive to using standard computational and experimental methods for identifying *cis*-acting RNA elements. As such, the known *cis*-acting RNA elements have largely been identified through phylogenic comparison and local thermodynamic RNA structure modeling (347-350), followed by structural probing and functional studies.

The HCV ORF is flanked by 5' and 3' NCRs that contain *cis*-acting RNA elements important for viral translation and replication (351). The 5' NCR contains the IRES element that is responsible for cap-independent translation of the HCV polyprotein (352-355). A stem-loop element upstream of the IRES in the 5' NCR has also been identified that plays a role in viral replication (356, 357). The 3' NCR of the genome contains three distinct domains important for viral replication: a variable region, a poly(U/UC) tract, and a highly conserved 98-nt sequence known as the 3' X tail (358-362).

In addition to the *cis*-acting RNA elements in the 5' and 3' NCRs of the viral genome, there is evidence that additional RNA structures exist within the polyprotein coding sequence (189, 190, 347, 363-366). This includes well-defined conserved stem-loop structures in the core and NS5B-coding regions (189, 190, 347, 363-366); as well as

the less well-defined, extensive large-scale secondary structure collectively known as GORS (discussed above), that spans the entire coding region of the HCV genome (324, 328). Reverse genetic analyses have also identified multiple long-range RNA-RNA interactions between stem-loops in the NS5B-coding region and sequences in the downstream 3' X tail that seem to be essential for viral replication (189, 190, 366).

The complex and highly structured nature of the HCV genome could preclude the design of effective nucleic acid-based therapeutics targeting the viral RNA, including small RNA species such as siRNAs. In fact, a number of reports have already suggested that target site accessibility can hamper efficient siRNA knockdown (367-372). For example, a number of groups were largely unsuccessful in generating efficient siRNAs against the regions of the highly-conserved IRES elements of various RNA viruses (373-376), including HCV (136, 377); suggesting that the complex structure of the viral RNA makes targeting these regions especially difficult (378). Despite this, computational methods cannot easily assess target site accessibility of large RNA targets and few siRNA design algorithms currently account for target site accessibility.

5.1.7 siRNA Design

Many factors contribute to the overall efficiency of RNA silencing. Recent studies have led to the establishment of eight parameters that, when incorporated into a rational siRNA design algorithm, increase the probability of selecting an effective siRNA (i.e. one capable of silencing gene expression by >50%) (171, 172) (Table 5.1).

Firstly, siRNAs should have a G+C content between 30-52% (171, 172, 367). A high G+C content can inhibit duplex unwinding, whereas a low G+C content is

Table 5.1 siRNA design criteria.

Criterion[1,2]	**Reference(s)**
30 - 52% G+C content	(171, 172)
Three or more 'A/U' bases at positions 15-19 (sense strand[3])	(12, 13, 172)
Lack of internal repeats (potential hairpin structure has $T_m < 20$ °C)	(12, 13, 172)
'A' base at position 19 (sense strand[3])	(12, 13, 172)
'A' base at position 3 (sense strand[3])	(172)
'U' base at position 10 (sense strand[3])	(28, 172, 380, 381)
A base other than 'G' or 'C' at position 19 (sense strand[3])	(12, 13, 172)
A base other than 'G' at position 13 (sense strand[3])	(172)

[1]Adapted from reference (172). [2]All criteria assume siRNAs are 21-nt in length with a 19-nt duplex region and 3' 2-nt overhanging ends. [3]Sense strand and antisense strand refer to the passenger and guide strands, respectively.

associated with decreased functionality, likely due to lower target affinity and specificity (172, 379). Additionally, G+C contents between 30-64% have been demonstrated to correlate with accessibility (171, 172), although relying on G+C content alone results in a large number of predicted false negatives (173).

Designed siRNAs should also have a low internal stability of the 3' terminus of the sense (passenger) strand since this will determine which strand of the duplex is incorporated into RISC to target complementary RNAs for degradation (12, 13, 172) (Figure 5.7). In addition, siRNAs should lack inverted repeat sequences since palindromes may foster internal secondary structures that could result in poor RISC loading (172).

Finally, effective siRNAs have been demonstrated to have sense (passenger) strand base preferences at positions 3 (A), 10 (U), 13 (≠G) and 19 (A/U) (172). The preference for a U at position 10 likely reflects the RISC endonuclease' preference to cleave the 3' end of U over A, G, or to a lesser extent, C (28, 172), like other endonucleases (380). The preference for an A/U at position 19 likely reflects which strand is incorporated into the RISC (12, 13, 172).

However, despite a rational approach to siRNA design, only a fraction of siRNAs are effective at reducing the expression of their RNA targets and, the efficiency of different siRNAs directed against the same target often varies significantly (129, 367). Additional parameters must therefore affect the effiency of siRNAs, such as target site accessibility or the presence of RNA-binding proteins (Figure 5.7). These parameters are not taken into account by many currently available siRNA design algorithms, despite the fact that target site accessibility is

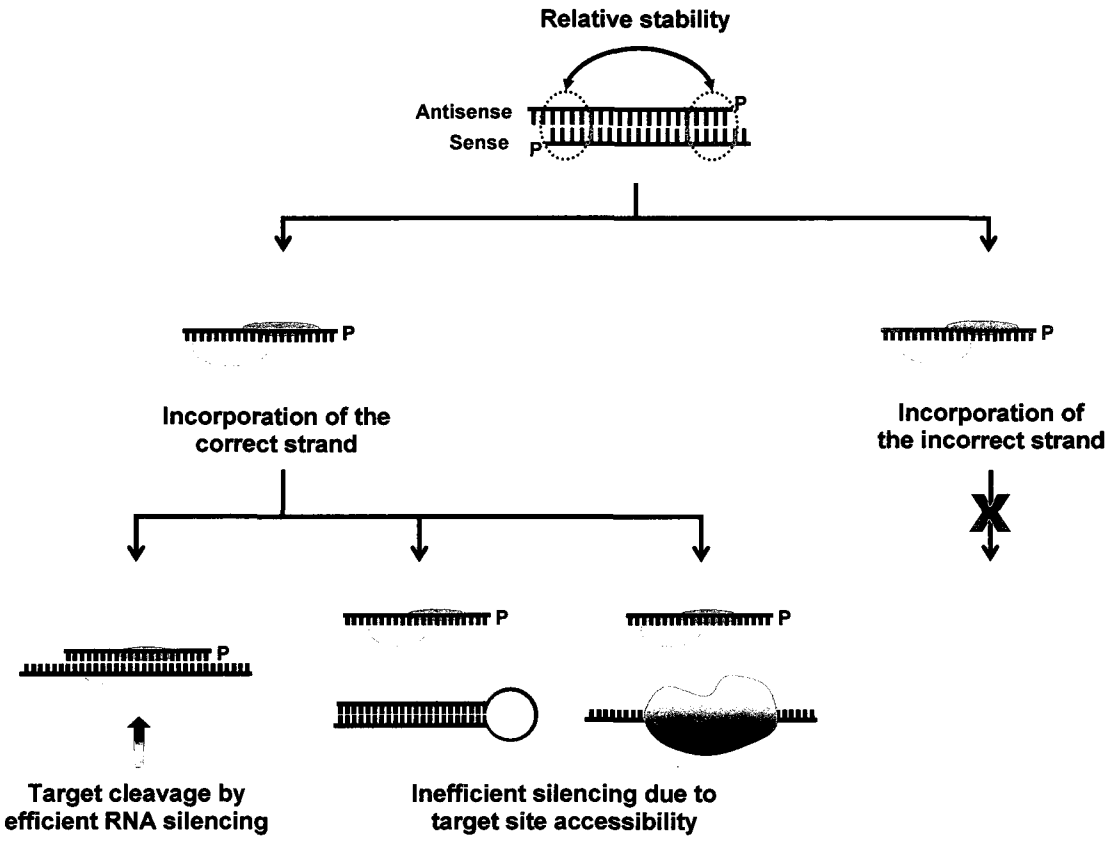

Figure 5.7 A model for efficient RNA silencing. Depending on the relative stability of the two ends of a siRNA duplex, one of the two strands in preferentially incorporated into the RNA-induced silencing complex (RISC). Incorporation of the correct (antisense) strand can be achieved through selection of a suitable target sequence and siRNA duplex design. The local structure or the presence of RNA binding proteins can also influence silencing. Target RNAs that are inaccessible impede silencing even if the correct (antisense) strand has been incorporated into RISC. Figure adapted and expanded from references (87, 378).

known to hamper efficient siRNA knockdown (367-372). This may not be an important parameter for design of siRNAs targeting the ORFs of relatively unstructured cellular mRNAs, but for RNA viruses, such as HCV, that have been demonstrated to have a complex and highly-structured genome, target site accessibility may be an important consideration.

A few groups have now described algorithms that take into account local secondary structure prediction in siRNA design that have greatly improved the probability of designing effective siRNAs (173-176). However, for long RNA targets, the prediction accuracy of currently available computational algorithms is still very low, generating numerous alternative structures (378, 382). In addition, the prevalence of long range RNA-RNA interactions in the genomes of RNA viruses is not yet amenable to accurate modeling. Hence, reliable results of analysis based on target RNA secondary structure prediction methods cannot be guaranteed for such targets (382). Also, for long RNA targets, the demands on the computer are high, and in lieu of the long running time needed to predict the secondary structure of large target RNAs, many siRNA design algorithms still rely solely on the siRNA sequence characteristics described above.

Thus, there is a need for a high-throughput approach to screen for effective siRNAs against long, highly-structured target RNAs. In this chapter, native target RNA microarrays are used to probe the accessibility of HCV replicon RNA to siRNA hybridization. By spotting HCV replicon RNA in a native confirmation, hybridization of the HCV-specific siRNAs (target site accessibility) can be correlated to their silencing efficiency in cell culture. The technique described could be useful for screening highly effective siRNAs against the highly-structured HCV RNA genome and has the potential

to be applied to other RNA-RNA interactions, including the genomes of other highly-structured positive-sense RNA viruses.

5.2 Hypothesis

Native target RNA microarrays may represent a high-throughput approach to screen for high affinity siRNA interactions.

5.3 Results

5.3.1 Atomic Force Microscopy (AFM)

To investigate the physical nature of the highly-structured HCV replicon RNA, the HCV replicon RNA transcripts were directly visualized by AFM. AFM has been extensively used in the study of DNA (383-385) and, more recently, has been extended by us (328, 336) and others (333-335, 385-388), to the investigation of large-scale secondary structure of RNAs. In order to facilitate adhesion of the polyanionic HCV replicon RNA to the anionic surface of freshly cleaved mica, a high concentration of Ni^{2+} was used to overcome the coulombic repulsion between the like charges (389, 390). The Ni^{2+}-treated mica was then incubated with 0.5 to 2.0 ng/μL of HCV RNA in a buffer containing sufficient quantities of Mg^{2+} to facilitate folding of the RNA. It is assumed that the HCV replicon RNAs take on random orientations upon deposition. Upon imaging, the HCV replicon RNA transcripts uniformly adopted a tightly packed condensed state that was largely maintained during the deposition process (Figure 5.8). HCV replicon RNAs had a regular unit size with a mean radii for the x and y axes of approximately 30 nm and mean heights of 3.9 ± 1.0 nm ($n = 10$). This indicates that,

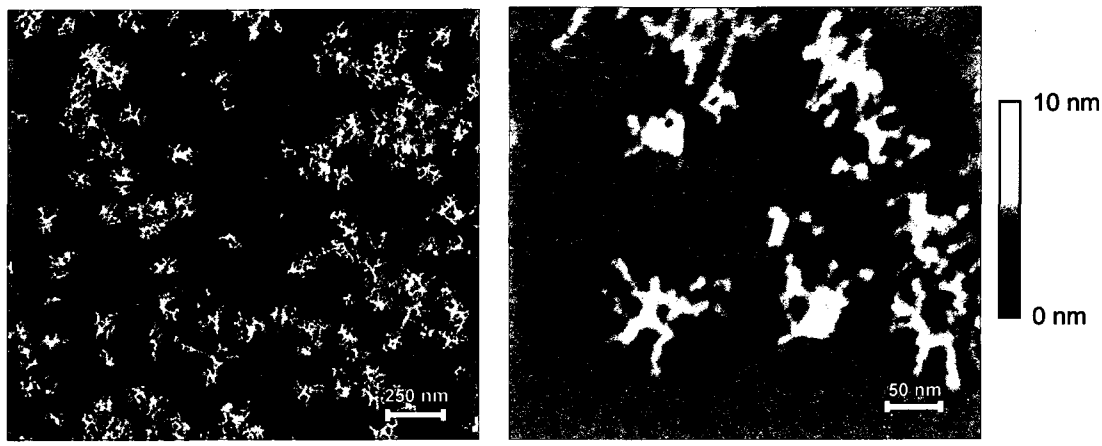

Figure 5.8 AFM of HCV RNA. HCV RNAs appeared as tightly packed clusters upon deposition indicating that the tertiary interactions remain intact in the collapsed state. HCV RNAs had diameters of approximately 80-120 nm. The Z-scale ranges from 0-10 nm.

under appropriate conditions, HCV replicon RNA can be spotted onto surfaces in a complex, highly folded conformation that may be representative of the native conformation.

5.3.2 Design of siRNAs Against HCV Replicon RNA

Once it was demonstrated that the HCV replicon RNA could be spotted in a native conformation, we wanted to further investigate whether hybridization to spotted HCV replicon RNAs could be used to predict the potency of HCV replicon-specific siRNAs. Synthetic siRNAs were thus designed targeting different regions of the HCV replicon RNA (Figure 5.9). siRNAs were designed using the rules outlined by Reynolds and colleagues (172) (described above) and had similar G+C contents to ensure equal binding strengths irrespective of the overall base composition of the siRNAs. siRNAs were named according to their nucleotide location in the subgenomic replicon RNA (Figure 5.9). As controls, two previously characterized HCV-specific siRNAs were used: 331 (IRES) siRNA directed against the IRES region of the HCV replicon RNA (137), and NS5B-7256 siRNA, a highly potent siRNA directed against the NS5B region of the replicon RNA (136). As a negative control, GL3 siRNA was used which has no sequence complimentarity to the HCV replicon RNA. Finally, as a control for target site accessibility, an siRNA (SL3.3-8589) was designed against the 5' arm of a known stem-loop region (SL3.3) in the NS5B ORF (189, 190). All siRNAs were fluorophore-conjugated at the 5'-end of their antisense (guide) strands so that hybridization to target RNA microarrays could be monitored by fluorescence.

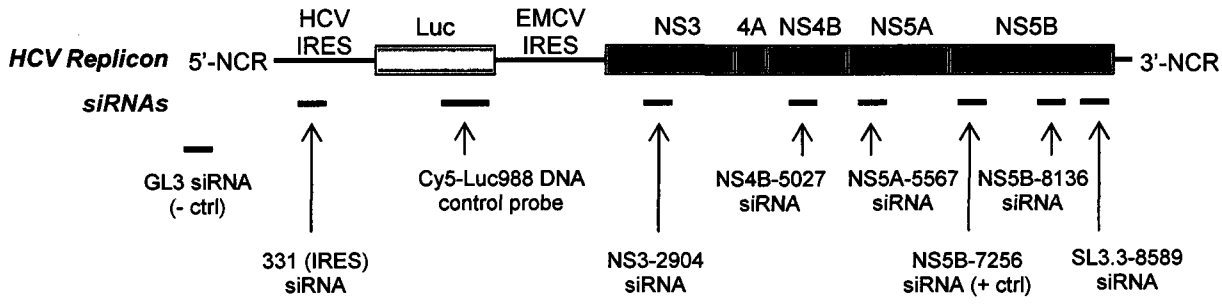

Figure 5.9 Schematic diagram of the HCV subgenomic replicon showing the approximate location of the HCV-specific siRNAs. The Cy5-labeled Luc988 DNA control probe location is indicated in purple.

5.3.3 Preparation of Native Target RNA Microarrays

Native target RNA microarrays were prepared by spotting the HCV replicon RNA under native conditions on epoxysilane-coated glass slides using a Nano-Plotter (NP2.1, GeSiM, Germany). The target RNA was diluted in native spotting buffer and was printed at room temperature. The HCV replicon RNA was spotted in quadruplicate in increasing concentrations on the microarray from 5 to 500 ng/μL (Figure 5.10). As negative and positive controls, oligonucleotides complementary to *Campylobacter jejuni* genes were spotted in duplicate (negative control) or quadruplicate (positive controls) in the microarrays at a concentration of 500 ng/μL (Figure 5.10). The average volume printed was ~980 pL per spot. A representative image of hybridization of the NS5B-7256 siRNA to the native HCV replicon RNA is shown in Figure 5.10. The Cy3 channel represents the *Campylobacter jejuni* spike-ins and hybridization of the NS5B-7256 siRNA to the HCV replicon RNA; whereas the Cy5 channel represents hybridization of the Luc988-42nt DNA control probe to the HCV replicon RNA (Figure 5.10).

5.3.4 Validation of Native Target RNA Microarrays as an Assessment of Target Site Accessibility

In order to investigate the ability of hybridization to native HCV replicon RNA microarrays to differentiate between accessible and inaccessible target RNA sequences, hybridization of the positive and negative control single-stranded fluorophore-labeled antisense (guide) siRNAs was carried out under native and denaturing conditions (Figure 5.11). Under native conditions, regions of the HCV replicon RNA with a high degree of stable internal base-pairing should adopt a closed configuration and be relatively

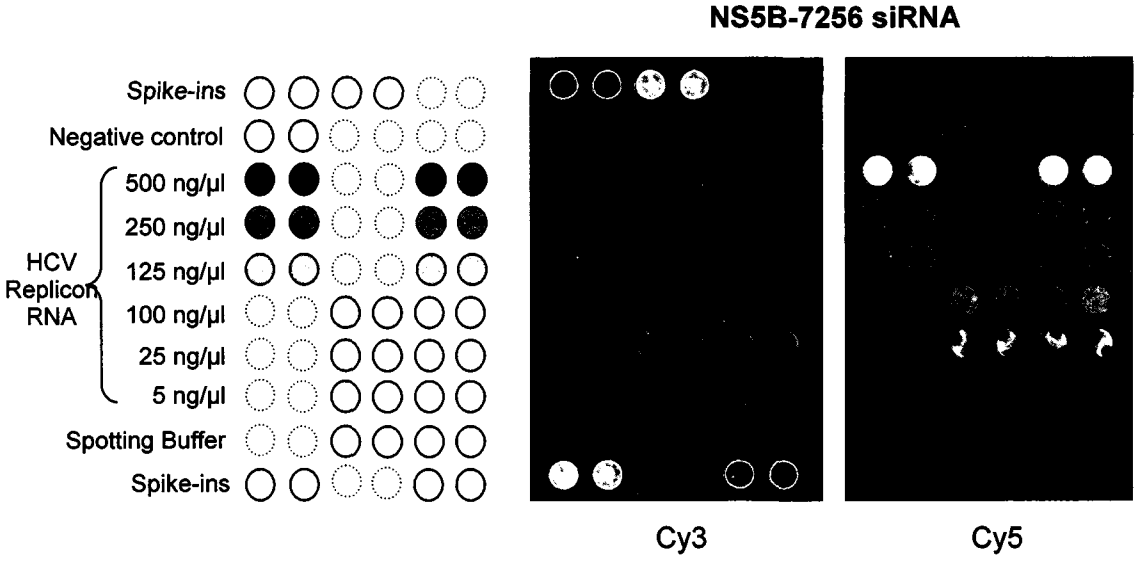

Figure 5.10 Schematic diagram of microarray design and a representative HCV replicon RNA microarray hybridization. After hybridization reactions containing HCV-specific siRNAs, slides were scanned using a microarray scanner, resulting in images of the siRNA and positive controls (spike-ins) in the Cy3 channel (middle) and the Luc988-42nt control probe in the Cy5 channel (right). A representative hybridization of the NS5B-7256 siRNA is shown.

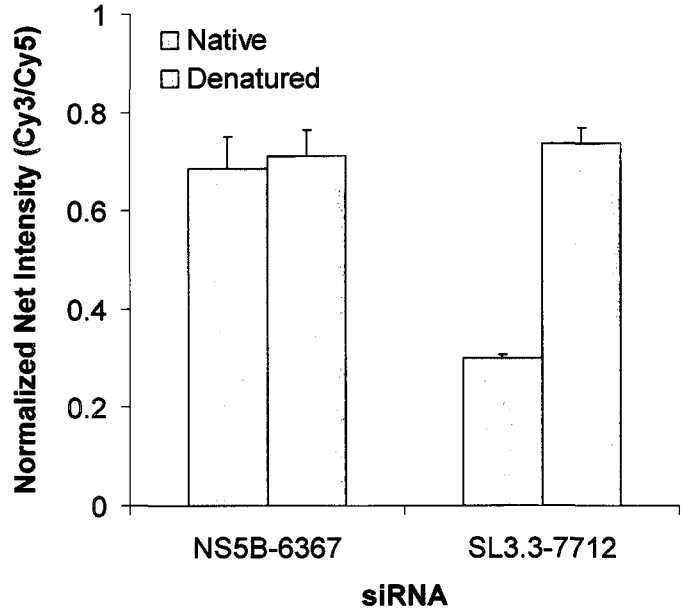

Figure 5.11 Native versus denaturing hybridization to HCV replicon RNA microarrays. The normalized net intensities (Cy3/Cy5) of the positive control NS5B-7256 siRNA and the negative control SL3.3-8589 siRNA are shown. Error bars represent SE.

inaccessible to siRNA hybridization. In contrast, the relatively unstructured regions of the HCV replicon RNA should be relatively accessible and lead to a greater degree of hybridization under native conditions. Under denaturing conditions, the inaccessible regions should become unpaired resulting in an open conformation that should have a similar degree of hybridization to the accessible regions.

The NS5B-7256 siRNA has previously been described as a highly potent siRNA against HCV replicon RNA (>90% reduction in HCV replicon RNA 72 h post-transfection, (136)); as such, it is likely to have a highly accessible target in the native HCV replicon RNA. In agreement with this, hybridization of this siRNA to the native HCV replicon RNA microarray yielded similar normalized net intensities under native and denaturing conditions (Figure 5.11). In contrast, the SL3.3-8589 siRNA, which was designed against the 5' arm of a known stem-loop region (SL3.3) in the HCV replicon RNA (189, 190), should be largely inaccessible to hybridization. This was confirmed by the hybridizations under native and denaturing conditions (Figure 5.11). Under native conditions the normalized net intensities of SL3.3-8589 siRNA hybridization was approximately 40% of that observed under denaturing conditions (Figure 5.11), suggesting that hybridization of single-stranded siRNAs to HCV replicon RNA microarrays is restricted by target site accessibility under native conditions.

5.3.5 Native Target RNA Hybridization and Image Analysis

Using the native target RNA microarrays, the accessibility of all of the HCV-specific siRNAs were analyzed by quantifying their hybridization to the HCV replicon RNA microarrays under native conditions (Figure 5.12). Hybridization intensities of the

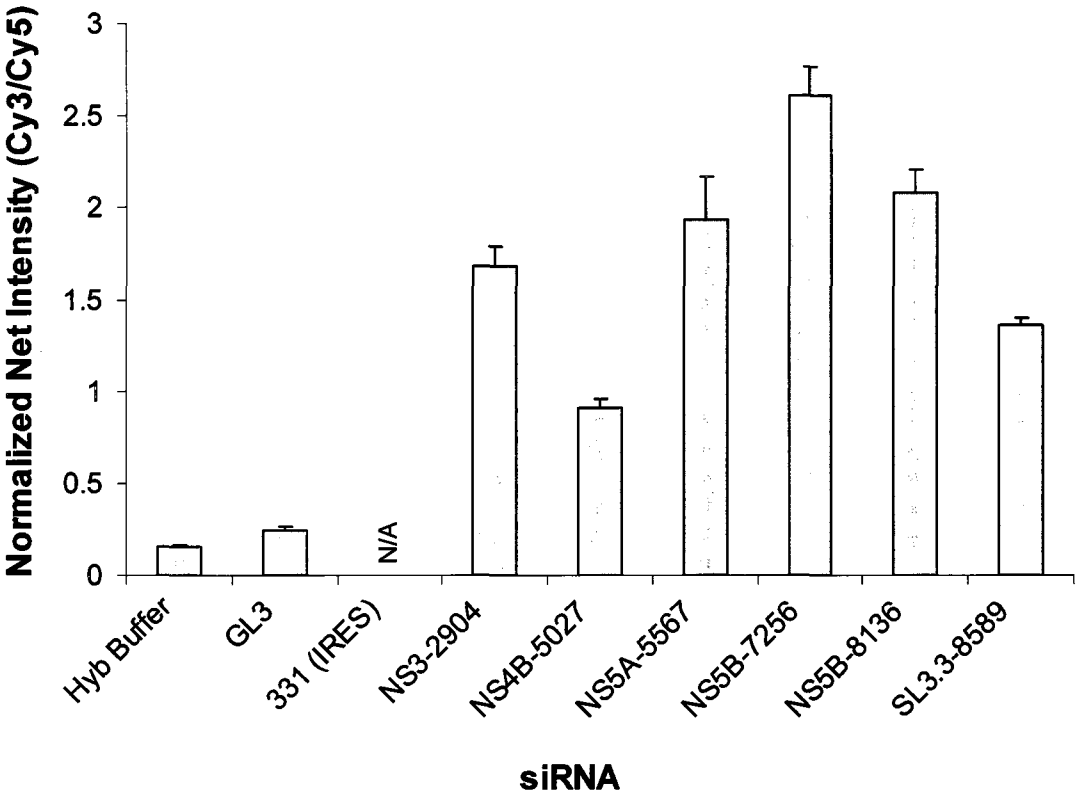

Figure 5.12 Hybridization of the HCV-specific siRNAs to native HCV replicon RNA microarrays. The data represents the average of two independent hybridizations and normalized net intensities (Cy3/Cy5) from a single HCV replicon RNA concentration (125 ng/μL) are shown. Error bars represent SE.

different siRNAs were scaled according to standard amounts of DNA oligonucleotide spike-in controls to give the normalized net intensities. All siRNAs were hybridized in triplicate. The positive-control NS5B-7256 siRNA gave the highest signal intensity, while the negative control GL3 siRNA, with no sequence complementarity to the HCV replicon RNA, had negligible signal intensity similar to background (see Hyb Buffer, Figure 5.12). The NS5B-8136, NS5A-5567 and NS3-2904 siRNAs had the next highest signal intensities, with normalized net intensities 78.7%, 72.6% and 62.2% of the positive control NS5B-7256 siRNA, respectively. This was followed by the negative control for target site accessibility SL3.3-8589 siRNA (49.2%) and the NS4B-5027 siRNA (30.3%). The low signal intensity of the NS4B-5027 siRNA suggests that this siRNA is against an inaccessible target site within the HCV replicon RNA.

5.3.6 Assessment of the Potency of the HCV-specific siRNAs in Cell Culture

In order to correlate the target site accessibility predictions from the native target RNA microarrays to siRNA silencing in cell culture, the effect of each of the HCV-specific siRNAs on HCV protein and replicon RNA levels was examined by Western and Northern blot analyses from siRNA transfection of Huh-7 cells stably harbouring the HCV subgenomic (neo^R) replicon (Figure 5.13). Densitometry of three individual replicate Western and Northern blots indicated that the patterns of silencing of the HCV-specific siRNAs were consistent at the protein and RNA levels (Figure 5.14). Of the eight siRNAs tested, the NS3-2904, NS5B-7256, and NS5B-8136 siRNAs were the most potent, decreasing HCV replicon RNA levels by 96.8%, 93.2% and 96.8%, respectively, when compared with the levels of HCV replicon RNA in control cells transfected in the

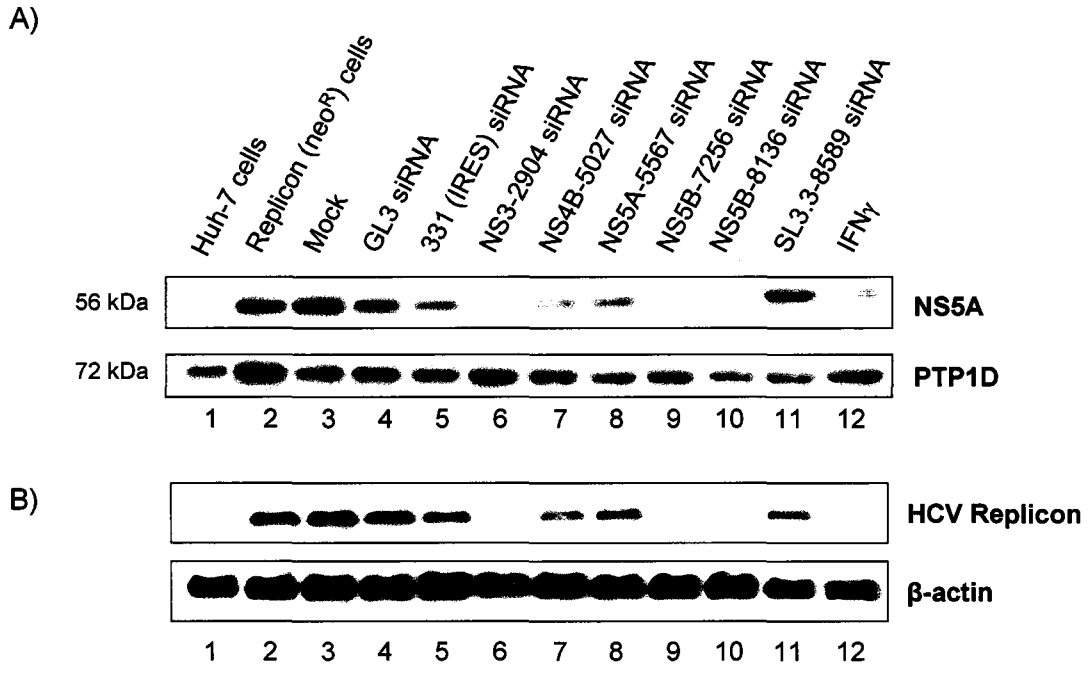

Figure 5.13 Western and Northern blot analyses of siRNA knockdown in cell culture. A) Western blot analysis of HCV NS5A protein levels in HCV subgenomic replicon-harbouring cells 48 h post-transfection with HCV-specific siRNAs. A sample from the parental Huh-7 cells (lane 1) and replicon-harbouring cells (lane 2) are shown. Mock transfected samples (lane 3, transfection reagent only) and samples transfected with the negative control (GL3, lane 4) and HCV-specific siRNAs (lanes 6-11) are shown. IFNγ was used as a positive control for knockdown of HCV NS5A protein and replicon RNA. B) Northern blot analysis of HCV replicon RNA levels in HCV subgenomic replicon-harbouring cells 48 h post-transfection with HCV-specific siRNAs. The samples analyzed by Northern blot are identical to those described for (A).

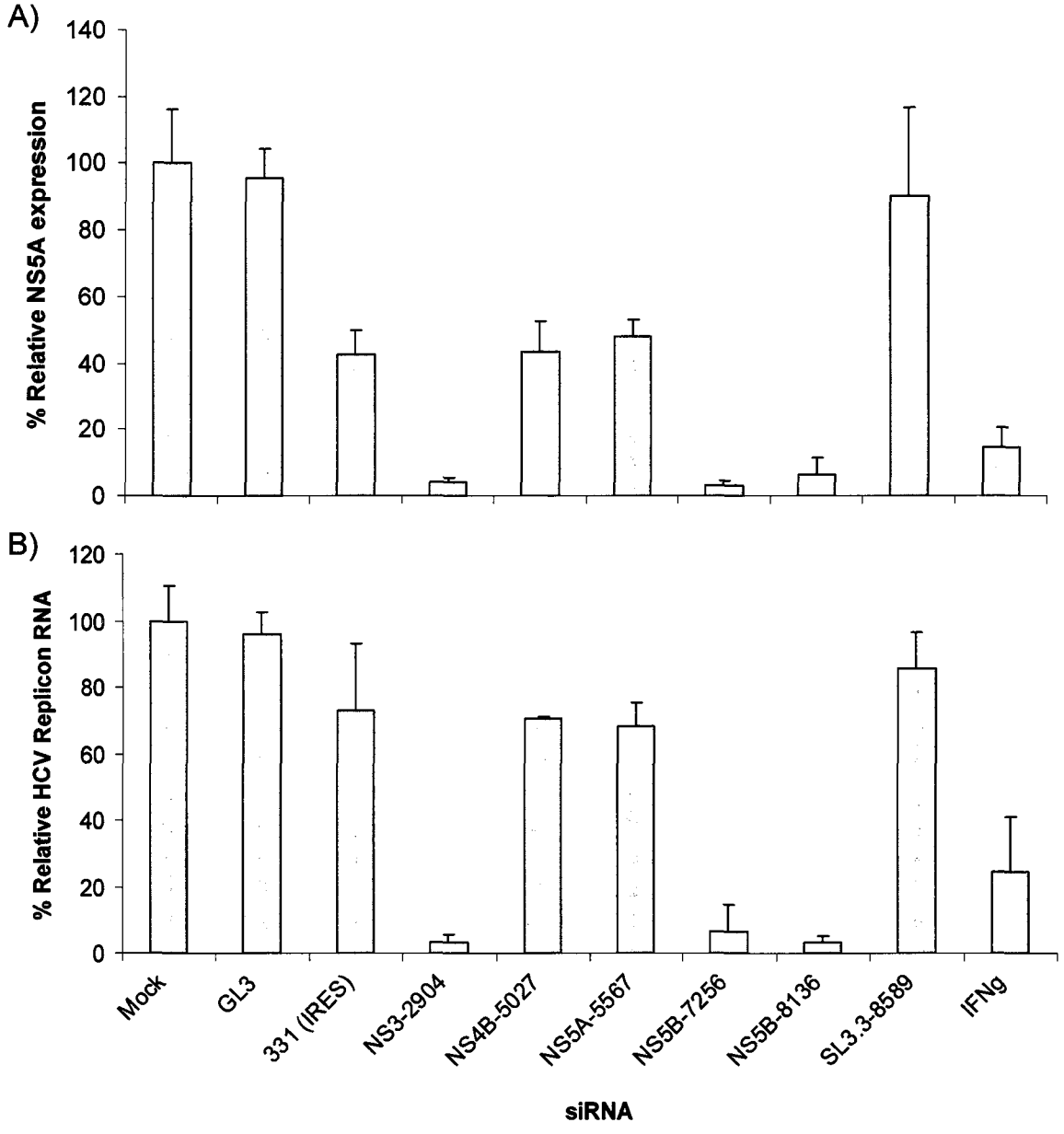

Figure 5.14 The effect of HCV-specific siRNAs on HCV protein and replicon RNA expression in cell culture. A) Percentage of relative NS5A expression and B) HCV replicon RNA expression from densitometry of Western and Northern blots is shown. The cells transfected with transfection reagent only (Mock) were defined as 100%, and the NS5A (A) and HCV replicon RNA (B) levels are expressed as relative percentages. The data represent the average of three independent experiments, and error bars represent SD.

absence of siRNA (Figures 5.13B and 5.14B). The 331 (IRES), NS4B-5027, and NS5A-5567 siRNAs reduced HCV replicon RNA levels only moderately by approximately 27.1%, 29.3% and 31.8%, respectively (Figure 5.14B). Not surprisingly, the SL3.3-8589 siRNA, also resulted in only a minor reduction in HCV replicon RNA levels of approximately 14.7% (Figure 5.14). The negative control (GL3) siRNA did not have a significant effect on the levels of HCV replicon RNA or the levels of the HCV NS5A protein (Figures 5.13 and 5.14), indicating that the effects of the siRNAs on HCV protein and RNA levels are sequence-specific and are not caused by induction of the non-specific IFN response (Figures 5.13 and 5.14). This is consistent with other findings that dsRNAs < 30-nt do not induce IFN responses (391, 392). Thus, the effects of the designed siRNAs on HCV protein and RNA levels seem to be the result of siRNA-directed degradation of the HCV replicon RNA by HCV-specific siRNA-loaded RISC.

5.3.7 Assessment of RISC Loading of HCV-specific siRNAs

The variations in silencing efficiency among the HCV-specific siRNAs could be due to variations in their RISC-loading efficiencies. To test this, single-stranded fluorophore-labeled HCV-specific siRNAs were incubated with recombinant affinity-purified human AGO2 (191). Human AGO2 and siRNA have previously been demonstrated to form a minimal human RISC (11, 191). The HCV-specific siRNAs were incubated with or without recombinant hAGO2 for 30 min at 37 °C to allow complexes to form, and the reactions were analyzed by EMSA (Figure 5.15). After the 30 min incubation period, the percentage of siRNAs bound by hAGO2 was >75% for all of the HCV-specific siRNAs except for the NS5B-7256 siRNA, of which 46% was bound by

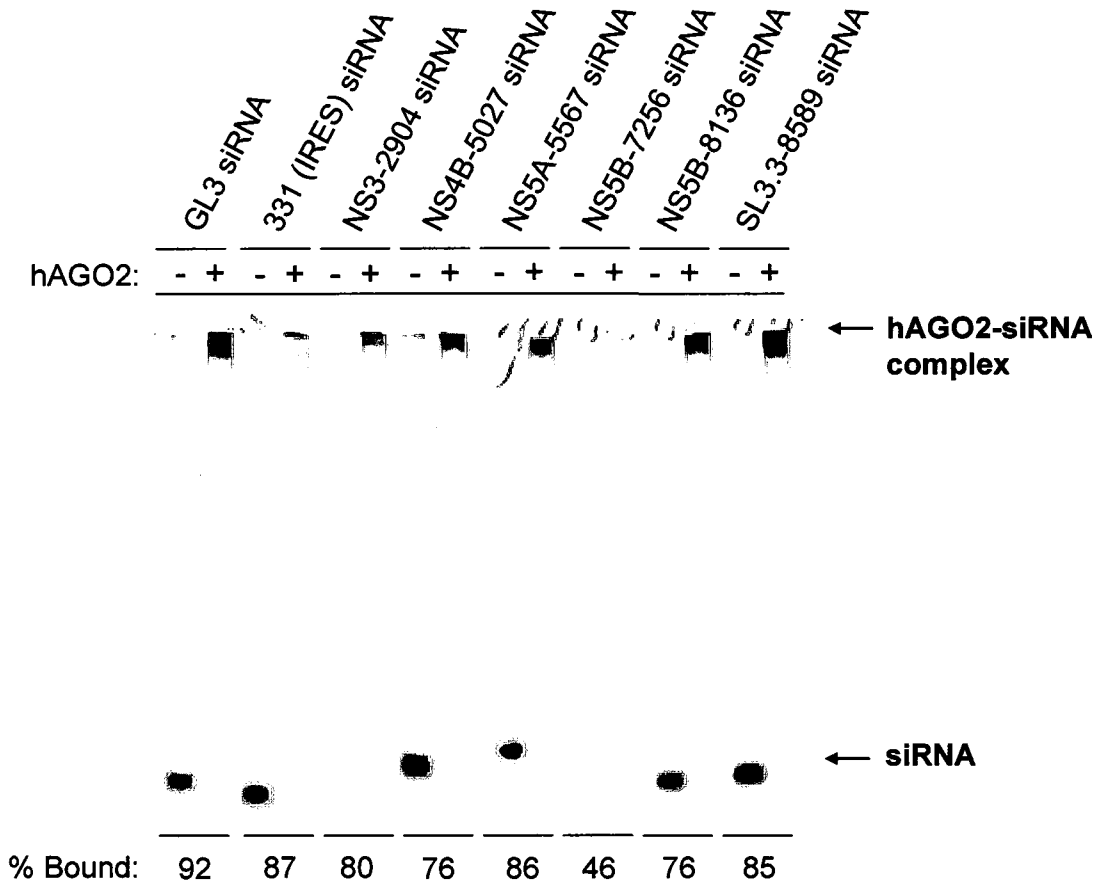

Figure 5.15 HCV-specific siRNAs have similar efficiencies of RISC loading. Single-stranded Cy3-labeled, HCV-specific siRNAs were incubated with or without recombinant HA-tagged hAGO2 at 37 °C for 30 min. Samples were then analyzed by EMSA to visualize complex formation. Gels were scanned using a fluorescent image analyzer and the bands were quantified by densitometry. % Bound indicates the percentage of siRNA in complex with hAGO2 after the 30 min incubation period. The EMSA was carried out in duplicate and a representative image is shown.

hAGO2 (Figure 5.15). This may be due to the slightly larger length of the NS5B-7256 siRNA (23-nt) as opposed to the other HCV-specific siRNAs (21-nt) (see Table 2.3, *Chapter 2*). Despite the fact that the environment within the cytoplasm of the cell is much more complex, in this minimal *in vitro* system, the majority of the siRNAs were efficiently loaded into the RISC after a 30 min incubation period, suggesting that variations in silencing efficiency are unlikely to be explained by differences in RISC loading efficiency.

5.4 Discussion

5.4.1 HCV Replicon RNA Retains a Complex Folded Structure Upon Deposition

The high resolution possible with AFM provides a means to directly visualize deposited HCV replicon RNA at the molecular level (332-336). Previous studies have used AFM analyses to visualize specific RNA-RNA interactions such as kissing-loop interactions (333) or RNA virus genome circularization (334), and more recently, we and others have used it to visualize the larger-scale shape of RNA molecules (328, 335, 336) (Figure 5.3). In the current study, it was demonstrated that the HCV RNA can be spotted in a very regular, tightly-packed condensed state (Figure 5.8).

Despite the high resolution of this technique, AFM does introduce artefacts associated with the deposition process, most notably the flattened appearance of the RNAs (i.e. the measured x and y diameters are approximately 15 times greater than their height) (332, 333). This is likely due to the partial dissolution of the condensed state due to interactions with the surface divalent metal ions that become energetically more favourable as the buffer is removed (328, 336). Nevertheless, the AFM imaging revealed

a regular, tightly packed condensed structure of the HCV replicon RNA with many of the tertiary structures remaining intact, despite the likely shape distortions arising from the AFM method.

5.4.2 Native Target RNA Microarrays are Restricted by Target Site Accessibility

Traditional microarray experiments are based on duplex stability (thermodynamics) between the nucleic acid probe and its target. They are typically carried out close to the melting temperature of the specific nucleic acid probe-target interaction under conditions which destroy less-stringent secondary structures that may be present in the target. The native target RNA microarrays described herein differ from traditional microarrays in that they are carried out under physiological conditions meant to preserve the native structure of the target RNA. In this way, the native target microarrays are a measure of hybridization speed (kinetics) of the siRNA-target interaction and reflect the accessibility of the folded state of the RNA target.

In this study, HCV replicon RNAs were spotted into native target RNA microarrays and the hybridization of HCV-specific siRNAs was used as a measure of target site accessibility. The ability of the native HCV replicon RNA microarrays to distinguish between known accessible and inaccessible sites within the viral RNA was tested using two siRNAs: NS5B-7256 and SL3.3-8589. The NS5B-7256 siRNA was previously demonstrated to be a highly potent siRNA against the HCV replicon (136), and is therefore likely to be against an accessible region of the viral RNA; while SL3.3-8589 siRNA, an siRNA directed against the 5' arm of a known stem-loop region (189, 190), targets an inaccessible site. Hybridization under native conditions was restricted by

target site accessibility, with the SL3.3-8589 siRNA hybridizing much less efficiently than the NS5B-7256 siRNA (Figure 5.11); however, under denaturing conditions, both the SL3.3-8589 and NS5B-7529 siRNAs hybridized with similar efficiencies (Figure 5.11). This indicates that the native target RNA microarrays are restricted by target site accessibility under native conditions. Subsequent hybridization of the HCV-specific siRNAs demonstrated that three of the siRNAs (NS3-2904, NS5A-5567, and NS5B-8136) had relatively high hybridization intensities under native conditions, similar to the hybridization intensity of the NS5B-7256 siRNA (positive control), suggesting that their target sites are likely to be relatively accessible in the native HCV replicon RNA (Figure 5.12). In contrast, the NS4B-5027 siRNA had a relatively low hybridization intensity similar to that of the SL3.3-8589 siRNA, suggesting that it is likely to have a relatively inaccessible target site within the native HCV replicon RNA (Figure 5.12).

The minimal hybridization seen with the NS4B-5027 siRNA is likely to be due to the highly-structured nature of the HCV replicon RNA. Alternatively, it cannot be ruled out that the apparent inaccessibility of this siRNA could be a result of a 'shell' of folded RNA shielding an unfolded core of unstructured RNA within the 3D conformation of the HCV replicon RNA. However, Simmonds and colleagues investigated this possibility for the HCV RNA genome in their investigation of GORS (328). By creating chimeric viral RNAs where a region of the relatively unstructured Bunyavirus (BV) RNA was inserted into the HCV viral RNA, they were able to demonstrate that insertions into the RNA genome did not affect the accessibility of the surrounding regions to probe hybridization (328). The same was true for the reverse chimera (i.e. where regions of the HCV RNA

genome were inserted into the BV RNA genome) (328); arguing against the 'shell' hypothesis.

5.4.3 Correlating Target Site Accessibility to Silencing in Cell Culture

The results from the native target RNA microarrays largely correlate with the potency of siRNAs in cell culture (at least qualitatively; Figures 5.13 and 5.14). The pattern of potency of the siRNAs is unlikely to be due to the kinetics of silencing since Western and Northern blots prepared from 24, 48, and 72 h post-transfection resulted in similar patterns of siRNA silencing (data not shown). The HCV-specific siRNAs with high target site accessibility tended to silence HCV protein expression and replicon RNA levels quite efficiently, while those predicted to be target inaccessible tended to have little effect on HCV protein and replicon RNA levels (Figures 5.13 and 5.14; summarized in Table 5.2).

A notable exception is the NS5A-5567 siRNA (Table 5.2). This siRNA was predicted to have a relatively accessible target site based on native target RNA microarray hybridization (Figure 5.12); however, it exhibited little silencing in cell culture (Figure 5.13 and 5.14). This may indicate that the NS5A-5567 siRNA target site is occupied by a novel protein-RNA or RNA-RNA interaction within the context of the mammalian cell. Indeed, protein-RNA interactions have been suggested to preclude the efficacy of siRNAs against HIV-1 (128) and human Tissue Factor (367). Thus, this technique could be used as a starting point for the development of nucleic acid-based probes to identify novel protein-RNA or RNA-RNA interactions within the HCV replicon RNA genome. Notwithstanding this notable exception, the intensity of array

Table 5.2 Summary of siRNA target site accessibility and silencing in cell culture.

siRNA	Position (nt)	G+C content (%)	Basic Tm (°C)	Target site accessibility[1] (%)	Relative NS5A expression[2] (%)	Relative Replicon RNA level[3] (%)	RISC loading[4] (%)
GL3	-	42.9	49	3.5	95.4	95.8	91.8
331 (IRES)	320-331	57.1	55	N/A	42.4	72.9	87.2
NS3-2904	2886-2904	38.1	47	62.2	4.0	3.2	80.1
NS4B-5027	5006-5027	38.1	47	30.3	43.6	70.7	76.0
NS5A-5567	5546-5567	42.9	49	72.6	47.9	68.2	85.9
NS5B-7256	7235-7256	43.5	52	100.0	3.2	6.8	46.1
NS5B-8136	8115-8136	42.9	49	78.7	6.3	3.2	76.1
SL3.3-8589	8568-8589	52.4	51	49.2	90.2	85.5	85.5

[1]Target site accessibility is based on hybridization intensities to native target RNA microarrays and is expressed as a percentage of the highly potent NS5B-7256 siRNA hybridization intensity. [2]Relative NS5A expression levels are based on Western blot densitometry of siRNA knockdowns in cell culture and is expressed as a percentage of mock-transfected cells. [3]Relative replicon RNA levels are based on Northern blot densitometry of siRNA knockdowns in cell culture and is expressed as a percentage of mock-transfected cells. [4]RISC loading is expressed as a percentage of siRNA complexed to the hAGO2 protein after a 30 min incubation at 37 °C. N/A, Not Available.

hybridization under native conditions generally predicted the silencing of HCV protein and replicon RNA levels in cell culture. Interestingly, preliminary results from native hybridization of the HCV-specific siRNAs to HCV replicon RNA in a solution-based system resulted in the same trend observed for the native target RNA microarrays (*personal communication, Neda Nasheri-Ardakan*). This is despite the fact that in both cases the composition of the hybridization buffer does not reflect the protein- rich cytosolic environment of the cell. As a future direction, it may be interesting to include host or viral proteins in the hybridization reactions to identify specific protein-RNA interactions.

5.4.4 Kinetics of RISC Loading

Efficiency of loading into the RISC could potentially contribute to differences in silencing efficiency of the HCV-specific siRNAs. To investigate this possibility, the ability of hAGO2 to load the HCV-specific siRNAs *in vitro* was explored (Figure 5.15). The majority of the siRNAs were efficiently loaded into hAGO2 after a 30 min incubation period (>75% for 7 of the 8 siRNAs; Figure 5.15) and the slight variations in loading did not correlate with silencing efficacy (Table 5.2), arguing against the efficiency of RISC loading as a contributing factor to silencing efficacy in this case. However, the contribution of other cellular RNA silencing pathway components on the efficiency of RISC loading cannot be ruled out within the cell. Interestingly, the NS5B-7256 siRNA, which was one of the most potent siRNAs in cell culture, was loaded much less efficiently than the other siRNAs (Figure 5.15 and Table 5.2). This may be due to the longer length (23-nt) of this siRNA, when compared to the other siRNA duplexes used in

this study (21-nt). This seeming paradox, poor RISC loading but high silencing efficacy, may be accounted for by recent studies which demonstrated that longer siRNA duplexes (~27-nt) are up to 10-100-fold more potent than the canonical 21-nt siRNAs (393, 394). This is thought to be due to the fact that these siRNAs, like miRNAs and shRNAs, are initially processed by Dicer to give 21-nt siRNA duplexes and that the association with the processing machinery aids in RISC loading. Co-purification experiments have indeed indicated that Dicer is involved in the loading of siRNAs into RISC explaining the improved potency of longer siRNA duplexes or shRNAs (395). However, this does not suggest that shRNAs (or miRNA mimics) are preferable to siRNAs since the requirement for Dicer cleavage can inhibit natural miRNA processing, altering cellular gene expression in the affected cell(s) or organism (396).

Due to the relatively fast kinetics of loading of the 5' fluorophore-labeled siRNAs used in this study, we anticipate that the presence of the 5' fluorophore is unlikely to inhibit RISC loading or cleavage. In agreement with this, Harborth and colleagues demonstrated that silencing is not perturbed by conjugation of fluorescent chromophores to the 5'- or 3'-end of the sense strand or to the 5'-end of the antisense strand, although conjugation to the 3'-end of the antisense strand of the siRNA abolished gene silencing (397). Additionally, the fact that the HCV-specific siRNAs were functional in cell culture further supports the notion that the 5' fluorophore does not affect RISC cleavage activity (Figure 5.13 and 5.14). Also, due to the rational design of the siRNAs with similar G+C contents, it is unlikely that there are dramatic differences in the ability of the RISC to unwind the siRNA duplexes in cell culture (Table 5.2).

It has been previously demonstrated that hAGO2 alone can be programmed for targeted RNA cleavage by pre-incubation with a single-stranded antisense (guide) siRNA (11, 191). Attempts to perform *in vitro* RISC cleavage assays using recombinant affinity-purified, His-tagged hAGO2, HCV-specific siRNAs, and *in vitro* transcribed HCV replicon target RNA resulted in either no detectable cleavage products or, after longer incubation periods, significant non-specific degradation of the HCV replicon RNA. There are a few possible explanations for these observations. First of all, the encounter between siRNA-loaded RISC and target RNA occurs through a diffusion controlled mechanism whereby the complex binds to and dissociates from non-specific sequences until the correct target sequence is found (372). The long length of the HCV replicon RNA (8858-nt) and its highly-structured nature could therefore impede the capacity of siRNA-loaded RISC to identify target sites through this mechanism (372). This suggests that long incubation times may be required to facilitate specific cleavage of long, highly-structured target RNAs. Additionally, a few groups have recently demonstrated that the minimal RISC cannot resolve secondary structure on its own (14, 398-400), and that the overall rate of structure displacement and product release can be dramatically affected by secondary or higher-ordered structure of the target RNA (400). Unfortunately, longer incubation times led to significant non-specific degradation of the target HCV replicon RNA, suggesting the presence of a low level of contaminating RNase in the hAGO2 preparations (191). In the cell, the 3' and 5' cleavage products are readily degraded by 3' and 5' exonucleases in the cytoplasm since they lack the stabilizing 5' cap or poly(A) tail (29). The presence of a contaminating RNase in the preparations may have impeded our ability to observe these cleavage products for the long, highly-structured HCV replicon

RNA and may have resulted in the non-specific degradation observed. As a future direction, a RISC cleavage product trapping technique may be used to increase the likelihood of detecting the cleavage products once they are released from the RISC (16).

5.4.5 Conclusion

Under appropriate conditions, the HCV replicon RNA can be spotted onto surfaces in a conformation that appears to be representative of the native conformation. Using native target RNA microarrays, hybridization efficiency (target site accessibility) of HCV-specific siRNAs was correlated to their silencing in cell culture. The parallels observed between native target RNA microarray hybridization and siRNA efficiency suggest that secondary structure in the HCV replicon RNA is a major factor in determining the efficiency of synthetic siRNAs. The technique described here represents a rapid, high-throughput approach to screen for effective siRNAs directed against the large, highly-structured HCV replicon RNA genome, based on target site accessibility. This technique also has the potential to be applied to other RNA-RNA interactions, including the highly-structured genomes of other important human pathogens.

Chapter 6: Discussion and Future Directions of Protein- and RNA-based Tools for RNA Silencing

6.1 Development of Protein-based Tools for Studying RNA Silencing and Small RNAs Using the Tombusvirus p19 Protein

Despite the importance of the RNA silencing pathway to molecular biology and medicine, the underlying mechanisms and principles guiding efficient RNA silencing are not yet fully understood. Since siRNAs are ubiquitously involved in RNA silencing, development of novel tools for the detection, purification and quantification of small RNAs are required. Additionally, the development of tools to facilitate the identification of low abundance small RNAs are likely to be necessary to gain a more complete understanding of RNA silencing in a wide range of organisms.

VSRs are a unique class of proteins that can be harnessed for their ability to specifically inhibit the RNA silencing pathway. The ability of the *Tombusvirus* p19 protein to function as a VSR independently (in the absence of other viral proteins), and also to sequester siRNAs size-selectively and relatively sequence-independently, in a system- and/or organism-independent manner, makes it well suited for biotechnology applications. Consequently, in this thesis, the *Tombusviral* p19 VSR was developed as a tool to study small RNAs and RNA silencing. The recent use of p19 in a variety of applications will be discussed as well as potential future directions regarding the use of p19 as a tool in molecular biology and biotechnology.

6.1.1 p19-siRNA Binding Interactions and Purification of siRNAs

In *Chapter 3*, the siRNA binding properties of p19 were investigated by arraying p19 onto the surface of multi-well Ni^{2+}-NTA plates using a fluorescence detection assay. The arrayed p19 maintained the ability to bind to siRNAs in a size-selective and

relatively sequence-independent manner. In addition to its siRNA binding activity, the results described in *Chapter 4*, and elsewhere (83, 180, 223, 275), indicated that p19 is able to bind to irregularly-structured miRNAs in addition to the canonical 21-nt siRNAs, albeit with a lower affinity. This indicates that p19 could be an attractive tool for the isolation and purification of silencing-generated small RNAs, including both siRNAs and miRNAs.

Current small RNA isolation procedures typically involve organic extraction and enrichment of small RNAs based on differential precipitation of large RNAs (>200 nt) at alcohol concentrations where the small RNAs (<200 nt) remain soluble. This typically results in enrichment of small RNAs <200 nt in size including silencing-generated small RNAs, tRNAs, rRNAs and other classes of small regulatory RNAs. By using p19 to purify small RNAs, preparations should contain a more homogeneous population of silencing-generated small RNAs with little contamination from other classes of RNA species (<200 nt). Indeed, immunoprecipitations from p19 transgenic plants are highly enriched for the silencing-generated small RNAs (siRNAs and miRNAs) (205, 223, 240); indicating that p19 may be a useful tool for purifying endogenous small RNAs from a variety of sources. In accordance with this, a few groups have now demonstrated that expression of epitope-tagged p19 proteins can be used to immunoprecipitate silencing-generated small RNA duplexes in transgenic plants (205, 223, 240, 292) as well as in insect (69) and mammalian cells (223, 275). More recently, *New England Biolabs* (Ipswitch, MA) has also developed a p19-based magnetic affinity purification system for isolation of small RNAs from cellular extracts. This suggests that, in the future, p19 may

be a useful tool for the identification and purification of small RNAs from diverse sources, including those present in mammalian cells.

6.1.2 Development of Molecular Switches

In *Chapter 3*, arrayed p19 was used to screen a small molecule library to identify inhibitors that may permit p19 to be used as a molecular switch. Two thiosulfanate inhibitors were identified that act through the modification of one or more p19 cysteine residues. These inhibitors could serve as a starting point for the development of reversible inhibitors of p19 activity with enhanced target selectivity. The design of specific inhibitors of the p19-small RNA interaction could permit p19 to be used as a molecular switch to control the RNA silencing pathway. The RNA silencing pathway could be turned off using p19, and a specific inhibitor could be used to control p19 activity, turning the RNA silencing pathway back on. This may be useful in elucidating the importance of the pathway in response to viruses (siRNA pathway) and in regulation of gene expression and development (miRNA pathway) in diverse systems and under various experimental conditions.

6.1.3 p19 Cysteine Residues and Regulation of p19 Activity

Interestingly, the library screen unexpectedly revealed novel postulates regarding the role of cysteine residues within the p19 protein. Mutational analyses indicated that the cysteine residues of p19 participate in maintaining the overall structural integrity of the protein. Since Cys110 is highly conserved across the entire p19 family and isoleucine was capable of fulfilling the structural role of this residue, it is possible that Cys110 is

required for a different type of biological function. In addition to its siRNA binding activity, the p19 protein has been demonstrated to interact with a family of RNA processing factors known as the ALY/REF proteins in plants (271, 288, 289). It is hypothesized that interactions between p19 and ALY/REF proteins may result in processing of siRNA bound by p19, resulting in p19 turnover, or effects on viral transport and defence-related gene silencing (271, 272, 288, 289). It is possible that the Cys110 residue is involved in this interaction, or yet undefined host-virus interactions, since our results suggest that the cysteine residues are likely exposed in the apoprotein form. Interestingly, plant viruses containing class I triple gene blocks of cell-to-cell movement proteins (found in *Peanut clump virus*, several fungus-transmitted viruses, and the *Hordeiviruses*), typically encode 14-20 kDa cysteine-rich proteins that have VSR activity (222). This indicates that cysteine residues may play an important role in suppression of RNA silencing by VSRs from distantly-related viruses. Alternatively, since the p19 ORF is completely embedded within the cell-to-cell movement protein (p22) gene of tombusviruses, it is possible that the cysteine conservation is due to sequence or amino acid conservation of one or more residues of the tombusviral cell-to-cell movement protein (274).

Additionally, modification of cysteine residues is a common post-translational modification which occurs in plants. Disulfide bond formation, as well as glutathionylation, play key roles in protein folding and in modulating plant stress responses (401, 402), respectively. The presence of glutathione (and possibly other physiological thiols) in plants could thus affect the p19-siRNA interaction within the context of viral infections. This could lead to the reversible inactivation of p19 since our

findings demonstrate that p19 function is compromised at high levels of thiol alkylation or in an oxidizing environment. Such regulation could influence the site of action of p19 or its siRNA binding activity. In future, it will be interesting to test the importance of the cysteine residues in the regulation of the p19 protein *in planta.*

6.1.4 Probing RNA Silencing Pathways

The unique binding properties of the p19 protein have already led to its widespread use for probing RNA silencing pathways in diverse eukaryotic organisms from plants to mammals (83, 183, 208, 223, 275, 285-287). Since p19 provides the ability to specifically block RNA silencing between Dicer processing and RISC assembly, p19 could be used to demonstrate the precise contribution of each of these components to RNA silencing in various organisms under different experimental conditions. In addition, using p19 in conjunction with other VSRs that target distinct steps of the pathway could increase our understanding of the pathway and its components.

The p19 protein could also be used as a cellular imaging tool. In fact, p19-GFP fusion proteins have already been used for localization and temporal studies during viral infections in plants (288, 289). In addition, Förster resonance energy transfer (FRET)-based p19 probes have recently been developed in our lab and can be used to detect p19-siRNA interactions in solution (403). This represents a novel strategy for siRNA sensing, and a starting point for the development of other FRET-based tools to report on siRNAs without the necessity for labeling of the siRNA *in vivo.*

6.1.5 Enhancement of Foreign Gene Expression and Elucidating Host-virus Interactions

Currently, transient gene expression in plants is limited by the induction of the RNA silencing pathway (287, 404). In theory, the p19 protein could be used to prevent the onset of RNA silencing and increase the expression of foreign genes. In agreement with this, Voinnet and colleagues found that co-expression with the p19 protein resulted in >50-fold enhancement of foreign gene expression in *Nicotiana benthamiana* plants (287). This suggests that p19 will be a useful tool for the high level expression of a broad range of proteins without the need for generation of stably transformed plants. However, a major hurdle may be the requirement of p19 to be expressed at relatively high levels for VSR activity and the fact that in many plants, p19 is a pathogenicity determinant (240, 272, 286, 292).

In addition to enhancement of foreign gene expression, p19 could be used to increase the production of viruses defective in their own innate antiviral suppressor genes. This could allow increased production of attenuated vaccine strains or viruses that are currently difficult to culture. In accordance with this, Li and colleagues have demonstrated that virus titres can be increased in insect cells by complementation with cross-kingdom suppressor proteins, such as p19 (69); and this has recently been extended to mammalian cells (83, 405). Lecellier and colleagues used p19 to demonstrate that a cellular miRNA (miR-32) was able to restrict the accumulation of PFV-1 in human 293T cells (83). More recently, Qian and colleagues used the p19 protein to demonstrate that RNA silencing limits translation of the HIV-1 Gag protein and consequently restricts the production of viral particles (405). This suggests that the p19 protein may not only be

useful for enhancement of foreign gene expression, or for production of viruses defective in their own innate antiviral suppressor genes, but may be helpful for elucidating novel host-virus interactions involving the RNA silencing pathway.

6.1.6 Developing p19 Proteins with Substrate Specificity

It is obvious that the unique properties of the p19 protein make it a useful tool for a broad range of applications. Interestingly, future biotechnology efforts might benefit from p19 protein-engineering to introduce sequence-specificity or to create p19 variants specific for different size classes of small RNAs. In this way, p19 could be used to sequence-specifically suppress RNA silencing of target genes without interfering with the regulation of host gene expression by miRNAs (406).

In *Chapter 4*, it was demonstrated that the p19 protein is able to bind to irregularly structured miRNAs in addition to canonical 21-nt siRNAs. Since a number of viruses have been demonstrated to encode their own viral miRNAs or interact with cellular miRNAs (81, 82, 85), sequestration and silencing of specific miRNAs *in vivo* could be a novel approach to inhibiting viral replication. The use of p19 in this way would effectively turn a viral protein into an antiviral agent. This would necessitate site-directed engineering of the p19 protein for introduction of greater specificity and higher affinity for specific miRNAs. In addition, the suppression of specific miRNAs by p19 may serve as a unique approach to understanding the roles of miRNAs in development and disease. Thus, it seems likely that a greater understanding of the p19 protein and its further characterization will make it an increasingly valuable tool in molecular biology and biotechnology.

6.2 Developing an RNA-based Screening Tool to Predict the Efficiency of siRNAs Against Highly-structured RNA Targets

The first step in designing successful RNA silencing approaches is the identification of highly efficient siRNAs. The results presented in this thesis and elsewhere suggest that target site accessibility is an important factor in the design of siRNAs against large, highly-structured target RNAs (367-372). In accordance with this, many groups have started to apply local target structure prediction algorithms in the design of synthetic siRNAs (173-176). However, due to the highly-structured nature of positive-sense RNA viruses, the presence of GORS, and the prevalence of long-range RNA-RNA interactions in the genomes of viruses such as HCV, local structure prediction may not yet be sufficient to predict the accessibility of these targets.

In *Chapter 5*, the importance of target site accessibility in the design of effective siRNAs against the highly-structured HCV replicon RNA was investigated. A native HCV replicon RNA microarray-based *in vitro* screening tool was described that was able to correlate hybridization efficiency (target site accessibility) of HCV-specific siRNAs to their silencing efficiency in cell culture. Although a relatively small number of siRNAs were screened, target site accessibility was found to be an important factor in determining the efficacy of siRNAs against the HCV replicon RNA. The screening of a greater number of siRNAs in the future will help validate this approach and improve the predictive capacity of the native target RNA microarrays. Nonetheless, this represents a rapid, high-throughput approach to screen for effective siRNAs against highly-structured target RNAs *in vitro*. This technique also has the potential to be applied to other highly-

structured RNAs, and in the investigation of protein-RNA and RNA-RNA interactions as described below.

6.2.1 Targeting HCV Using RNA Silencing

HCV is a highly-structured positive-sense RNA virus that replicates in the cytoplasm of host cells. This makes HCV susceptible to regulation by the RNA silencing pathway. Indeed, a number of groups have already demonstrated the antiviral potential of RNA silencing using the HCV replicon system (133, 135-137, 407). However, success rates varied widely between studies and only approximately half of the siRNAs were at least partially effective at silencing HCV, despite a rational approach to siRNA design (133, 135-137, 407). This suggests that additional factors, such as the complex and highly-structured nature of the HCV RNA genome could impede silencing.

The HCV sequences targeted in this thesis were not completely conserved across HCV genotypes. With the exception of the 331 (IRES) siRNA, all of the HCV-specific siRNAs were directed against the coding region of the HCV replicon RNA. Since a single nucleotide mismatch can affect the specificity with which siRNAs bind their targets, for therapeutic applications, it will be important to identify optimal target sites with high sequence conservation across the HCV genotypes. Additionally, because of the error-prone HCV RdRp and the rapid evolution of quasispecies, it may be necessary to use multiple siRNAs targeting different regions of the viral RNA to decrease the likelihood of developing escape mutations, as was recently demonstrated (138). However, the use of two highly active siRNAs simultaneously dramatically reduced the emergence of escape mutations in HCV replicons (138).

Interestingly, sequence divergence may not be the only route for resistance to RNA silencing by HCV. Recently, the viral gene products core and E2 have been suggested to be VSRs, inhibiting Dicer and hAGO2 activities, respectively (248-250). In contrast, there exists a genetic interaction between the highly abundant cellular miR-122 and the HCV RNA genome, which is required for viral replication in cell culture (85, 86). This suggests that HCV may have two interactions with the RNA silencing machinery, an inhibitory interaction through the core and E2 gene products (248-250), and a miRNA interaction that facilitates viral replication (85, 86). However, recent studies using siRNA knockdown of RNA silencing pathway components in full-length replicon harbouring cells, and the recently described infectious model of HCV (408, 409), suggest that the requirement for functional RNA silencing for replication (i.e. miR-122 biogenesis and action) is dominant over any inhibitory action of the HCV gene product(s) (141). In agreement with this, previous reports have demonstrated no differences in the susceptibility of HCV genomic and subgenomic replicons to RNA silencing, suggesting that the core and E2 gene products do not have a major affect on the susceptibility of HCV to RNA silencing (135, 138, 377). Further studies will be needed to corroborate these findings and clarify the effects of the core and E2 proteins on the RNA silencing pathway within the context of HCV infection, since this may have implications for RNA silencing-based therapy for HCV.

Despite obstacles associated with escape mutations and the need for effective delivery strategies for siRNAs *in vivo*, RNA silencing represents an exciting new approach for the treatment of HCV and potentially other viral diseases. The highly-structured nature of many RNA viral genomes suggests that the method described here to

screen for highly effective siRNAs based on target site accessibility will be useful in selecting siRNAs for therapeutic applications that are capable of inducing extensive silencing of their targets at low doses.

6.2.2 Investigating Protein-RNA and RNA-RNA Interactions

The HCV RNA genome is likely to have a dynamic structure able to readily accommodate unwinding, elongation and exposure of different regions of the RNA to viral and cellular proteins for translation and replication of the viral genome. As a future direction, it may be interesting to look at how specific viral or cellular proteins affect the accessibility of the HCV replicon RNA *in vitro*. Addition of purified viral or cellular proteins to the *in vitro* hybridization reactions could yield new information about direct interactions with the viral genome. For example, addition of siRNA-hAGO2 complexes could help us gain information on the accessibility of the HCV RNA to the larger RISC rather than the just the siRNA itself. In addition, viral proteins could be added to identify novel RNA-interacting domains. This could be particularly important for the elucidation of packaging signals within the HCV genome since none have been identified to date. However, the addition of proteins to the hybridization reactions may require a solution-based approach to screening target site accessibility which would represent a more native, less conformationally-restrained environment for protein-RNA interactions. Interestingly, our lab has already extended this approach to a solution-based system whereby fluorophore-labeled small RNAs are hybridized to 3' biotinylated HCV RNA in solution, and then the complex is conjugated to streptavidin microbeads for measurement of the relative fluorescence. This may represent a useful solution-based approach more

amenable to addition of proteins that can avoid the surface effects that might result in conformational restriction of protein-RNA interactions in the microarray-based approach.

Information gained from structural probing by native hybridization of nucleic acids may also serve as a starting point for the design of nucleic-acid based probes to pull-down or titrate out novel interacting partners with the viral RNA genome. For example, where the hybridization of the siRNA probes *in vitro* disagrees with the silencing efficiency in cell culture, this may indicate that the siRNA target site is occupied by a novel protein-RNA or RNA-RNA interaction *in vivo*. RNA-based probes could then be designed to pull-down or titrate out the interacting partners in the context of viral replication. RNA-based probes have already been demonstrated to be useful for elucidating protein-RNA or RNA-RNA interactions in a number of cellular systems (reviewed in (410)). In fact, 3' biotinylated siRNA probes were used to pull-down the human RISC and identify the AGO proteins as being at the center of RNA silencing (411). Thus, structural probing and correlation with silencing efficiency may represent a starting point for the design of RNA-based probes to identify novel protein-RNA or RNA-RNA interactions with the HCV RNA genome *in vivo*. The native target RNA microarray approach could also be extended to other RNA molecules, including cellular mRNAs or the RNA genomes of other important human pathogens.

6.2.3 Elucidating miRNA-target RNA Interactions

The results presented here and elsewhere clearly demonstrate that target RNA folding has major consequences for siRNA-induced gene silencing (367-372). Recent studies have demonstrated that the structure of the target RNA or the binding of proteins

can also dramatically affect miRNA recognition of RNA targets (412-416). Since miRNA-target recognition is thought to require as little as 7-nt for targeting (seed region) (47), hybridization of miRNAs to native target RNA microarrays may also be useful for elucidation of the strict rules governing miRNA target site recognition as well as conformation of *bona fide* miRNA target sites.

6.3 Conclusions

In this thesis, protein- and RNA-based tools were developed for studying the RNA silencing pathway and small RNAs based on *Tombusvirus* p19 and native target RNA microarrays. The p19 protein has the potential to be used in a number of molecular biology and biotechnology applications to enhance foreign gene expression, dissect RNA silencing pathways, investigate host-virus interactions, and for the study of small RNAs in diverse *in vitro* and eukaryotic systems. The native target RNA microarray approach described here can be used to predict highly effective siRNAs based on target site accessibility. This approach has the potential to be applied to other RNA-RNA interactions and for the identification of novel protein-RNA and RNA-RNA interactions with large RNAs, such as the RNA genomes of important human pathogens.

Bibliography

1. Fire, A., S.Q. Xu, M.K. Montgomery, S.A. Kostas, S.E. Driver, and C.C. Mello. 1998. Potent and specific genetic interference by double-stranded RNA in Caenorhabditis elegans. *Nature* 391:806-811.

2. Rana, T.M. 2007. Illuminating the silence: understanding the structure and function of small RNAs. *Nat Rev Mol Cell Biol* 8:23-36.

3. Bernstein, E., A.A. Caudy, S.M. Hammond, and G.J. Hannon. 2001. Role for a bidentate ribonuclease in the initiation step of RNA interference. *Nature* 409:363-366.

4. Elbashir, S.M., J. Harborth, W. Lendeckel, A. Yalcin, K. Weber, and T. Tuschl. 2001. Duplexes of 21-nucleotide RNAs mediate RNA interference in cultured mammalian cells. *Nature* 411:494-498.

5. Nykanen, A., B. Haley, and P.D. Zamore. 2001. ATP requirements and small interfering RNA structure in the RNA interference pathway. *Cell* 107:309-321.

6. Hammond, S.M., E. Bernstein, D. Beach, and G.J. Hannon. 2000. An RNA-directed nuclease mediates post-transcriptional gene silencing in Drosophila cells. *Nature* 404:293-296.

7. Janowski, B.A., K.E. Huffman, J.C. Schwartz, R. Ram, R. Nordsell, D.S. Shames, J.D. Minna, and D.R. Corey. 2006. Involvement of AGO1 and AGO2 in mammalian transcriptional silencing. *Nat Struct Mol Biol* 13:787-792.

8. Kim, D.H., L.M. Villeneuve, K.V. Morris, and J.J. Rossi. 2006. Argonaute-1 directs siRNA-mediated transcriptional gene silencing in human cells. *Nat Struct Mol Biol* 13:793-797.

9. Liu, J.D., M.A. Carmell, F.V. Rivas, C.G. Marsden, J.M. Thomson, J.J. Song, S.M. Hammond, L. Joshua-Tor, and G.J. Hannon. 2004. Argonaute2 is the catalytic engine of mammalian RNAi. *Science* 305:1437-1441.

10. Meister, G., M. Landthaler, A. Patkaniowska, Y. Dorsett, G. Teng, and T. Tuschl. 2004. Human Argonaute2 mediates RNA cleavage targeted by miRNAs and siRNAs. *Mol Cell* 15:185-197.

11. Rivas, F.V., N.H. Tolia, J.J. Song, J.P. Aragon, J.D. Liu, G.J. Hannon, and L. Joshua-Tor. 2005. Purified Argonaute2 and an siRNA form recombinant human RISC. *Nat Struct Mol Biol* 12:340-349.

12. Schwarz, D.S., G. Hutvagner, T. Du, Z.S. Xu, N. Aronin, and P.D. Zamore. 2003. Asymmetry in the assembly of the RNAi enzyme complex. *Cell* 115:199-208.

13. Khvorova, A., A. Reynolds, and S.D. Jayasena. 2003. Functional siRNAs and miRNAs exhibit strand bias. *Cell* 115:209-216.

14. Haley, B., and P.D. Zamore. 2004. Kinetic analysis of the RNAi enzyme complex. *Nat Struct Mol Biol* 11:599-606.

15. Matranga, C., Y. Tomari, C. Shin, D.P. Bartel, and P.D. Zamore. 2005. Passenger-strand cleavage facilitates assembly of siRNA into Ago2-containing RNAi enzyme complexes. *Cell* 123:607-620.

16. Rand, T.A., S. Petersen, F.H. Du, and X.D. Wang. 2005. Argonaute2 cleaves the anti-guide strand of siRNA during RISC activation. *Cell* 123:621-629.

17. Hutvagner, G., and P.D. Zamore. 2002. A microRNA in a multiple-turnover RNAi enzyme complex. *Science* 297:2056-2060.

18. Wu, L., J. Fan, and J.G. Belasco. 2006. MicroRNAs direct rapid deadenylation of mRNA. *Proc Natl Acad Sci U.S.A.* 103:4034-4039.

19. Zamore, P.D., and B. Haley. 2005. Ribo-gnome: The big world of small RNAs. *Science* 309:1519-1524.

20. Lindbo, J.A., L. Silvarosales, W.M. Proebsting, and W.G. Dougherty. 1993. Induction of a highly specific antiviral state in transgenic plants - implications for regulation of gene-expression and virus-resistance. *Plant Cell* 5:1749-1759.

21. Cogoni, C., and G. Macino. 1999. Gene silencing in Neurospora crassa requires a protein homologous to RNA-dependent RNA polymerase. *Nature* 399:166-169.

22. Smardon, A., J.M. Spoerke, S.C. Stacey, M.E. Klein, N. Mackin, and E.M. Maine. 2000. EGO-1 is related to RNA-directed RNA polymerase and functions in germ-line development and RNA interference in C. elegans. *Curr Biol* 10:169-178.

23. Mourrain, P., C. Beclin, T. Elmayan, F. Feuerbach, C. Godon, J.B. Morel, D. Jouette, A.M. Lacombe, S. Nikic, N. Picault, K. Remoue, M. Sanial, T.A. Vo, and H. Vaucheret. 2000. Arabidopsis SGS2 and SGS3 genes are required for posttranscriptional gene silencing and natural virus resistance. *Cell* 101:533-542.

24. Dalmay, T., A. Hamilton, S. Rudd, S. Angell, and D.C. Baulcombe. 2000. An RNA-dependent RNA polymerase gene in Arabidopsis is required for posttranscriptional gene silencing mediated by a transgene but not by a virus. *Cell* 101:543-553.

25. Lippman, Z., A.V. Gendrel, M. Black, M.W. Vaughn, N. Dedhia, W.R. McCombie, K. Lavine, V. Mittal, B. May, K.D. Kasschau, J.C. Carrington, R.W. Doerge, V. Colot, and R. Martienssen. 2004. Role of transposable elements in heterochromatin and epigenetic control. *Nature* 430:471-476.

26. Sijen, T., and R.H.A. Plasterk. 2003. Transposon silencing in the Caenorhabditis elegans germ line by natural RNAi. *Nature* 426:310-314.

27. Hakim, S.T., M. Alsayari, D.C. McLean, S. Saleem, K.C. Addanki, M. Aggarwal, K. Mahalingam, and O. Bagasra. 2008. Large number of the human microRNAs target lentiviruses, retroviruses, and endogenous retroviruses. *Biochem Biophys Res Commun* 369:357-362.

28. Elbashir, S.M., W. Lendeckel, and T. Tuschl. 2001. RNA interference is mediated by 21-and 22-nucleotide RNAs. *Genes Dev* 15:188-200.

29. Orban, T.I., and E. Izaurralde. 2005. Decay of mRNAs targeted by RISC requires XRN1, the Ski complex, and the exosome. *RNA* 11:459-469.

30. Voinnet, O. 2005. Non-cell autonomous RNA silencing. *FEBS Lett* 579:5858-5871.

31. Timmons, L., and A. Fire. 1998. Specific interference by ingested dsRNA. *Nature* 395:854.

32. Jose, A.M., J.J. Smith, and C.P. Hunter. 2009. Export of RNA silencing from C. elegans tissues does not require the RNA channel SID-1. *Proc Natl Acad Sci U.S.A* 106:2283-2288.

33. Berezikov, E., V. Guryev, J. van de Belt, E. Wienholds, R.H.A. Plasterk, and E. Cuppen. 2005. Phylogenetic shadowing and computational identification of human microRNA genes. *Cell* 120:21-24.

34. Krek, A., D. Grun, M.N. Poy, R. Wolf, L. Rosenberg, E.J. Epstein, P. MacMenamin, I. da Piedade, K.C. Gunsalus, M. Stoffel, and N. Rajewsky. 2005. Combinatorial microRNA target predictions. *Nat Genet* 37:495-500.

35. Xie, X.H., J. Lu, E.J. Kulbokas, T.R. Golub, V. Mootha, K. Lindblad-Toh, E.S. Lander, and M. Kellis. 2005. Systematic discovery of regulatory motifs in human promoters and 3 ' UTRs by comparison of several mammals. *Nature* 434:338-345.

36. Sood, P., A. Krek, M. Zavolan, G. Macino, and N. Rajewsky. 2006. Cell-type-specific signatures of microRNAs on target mRNA expression. *Proc Natl Acad Sci U.S.A.* 103:2746-2751.

37. Lau, N.C., L.P. Lim, E.G. Weinstein, and D.P. Bartel. 2001. An abundant class of tiny RNAs with probable regulatory roles in Caenorhabditis elegans. *Science* 294:858-862.

38. Lagos-Quintana, M., R. Rauhut, W. Lendeckel, and T. Tuschl. 2001. Identification of novel genes coding for small expressed RNAs. *Science* 294:853-858.

39. Lee, Y., K. Jeon, J.T. Lee, S. Kim, and V.N. Kim. 2002. MicroRNA maturation: stepwise processing and subcellular localization. *EMBO J* 21:4663-4670.

40. Lee, Y., C. Ahn, J.J. Han, H. Choi, J. Kim, J. Yim, J. Lee, P. Provost, O. Radmark, S. Kim, and V.N. Kim. 2003. The nuclear RNase III Drosha initiates microRNA processing. *Nature* 425:415-419.

41. Yi, R., Y. Qin, I.G. Macara, and B.R. Cullen. 2003. Exportin-5 mediates the nuclear export of pre-microRNAs and short hairpin RNAs. *Genes Dev* 17:3011-3016.

42. Lund, E., S. Guttinger, A. Calado, J.E. Dahlberg, and U. Kutay. 2004. Nuclear export of microRNA precursors. *Science* 303:95-98.

43. Bohnsack, M.T., K. Czaplinski, and D. Gorlich. 2004. Exportin 5 is a RanGTP-dependent dsRNA-binding protein that mediates nuclear export of pre-miRNAs. *RNA* 10:185-191.

44. Berezikov, E., W.J. Chung, J. Willis, E. Cuppen, and E.C. Lai. 2007. Mammalian mirtron genes. *Mol Cell* 28:328-336.

45. Rhoades, M.W., B.J. Reinhart, L.P. Lim, C.B. Burge, B. Bartel, and D.P. Bartel. 2002. Prediction of plant microRNA targets. *Cell* 110:513-520.

46. Enright, A., B. John, U. Gaul, T. Tuschl, C. Sander, and D. Marks. 2003. MicroRNA targets in Drosophila. *Genome Biol* 5:R1.

47. Lewis, B.P., I.H. Shih, M.W. Jones-Rhoades, D.P. Bartel, and C.B. Burge. 2003. Prediction of mammalian microRNA targets. *Cell* 115:787-798.

48. Stark, A., J. Brennecke, R.B. Russell, and S.M. Cohen. 2003. Identification of Drosophila MicroRNA targets. *PLoS Biol* 1:397-409.

49. Bonnet, E., J. Wuyts, P. Rouze, and Y. Van de Peer. 2004. Detection of 91 potential conserved plant microRNAs in Arabidopsis thaliana and Oryza sativa identifies important target genes. *Proc Natl Acad Sci U.S.A.* 101:11511-11516.

50. Wang, X.J., J.L. Reyes, N.H. Chua, and T. Gaasterland. 2004. Prediction and identification of Arabidopsis thaliana microRNAs and their mRNA targets. *Genome Biol* 5:R65.

51. John, B., A.J. Enright, A. Aravin, T. Tuschl, C. Sander, and D.S. Marks. 2004. Human MicroRNA targets. *PLoS Biol* 2:1862-1879.

52. Doench, J.G., and P.A. Sharp. 2004. Specificity of microRNA target selection in translational repression. *Genes Dev* 18:504-511.

53. Kiriakidou, M., P.T. Nelson, A. Kouranov, P. Fitziev, C. Bouyioukos, Z. Mourelatos, and A. Hatzigeorgiou. 2004. A combined computational-experimental approach predicts human microRNA targets. *Genes Dev* 18:1165-1178.

54. Rajewsky, N., and N.D. Socci. 2004. Computational identification of microRNA targets. *Dev Biol* 267:529-535.

55. Rehmsmeier, M., P. Steffen, M. Hochsmann, and R. Giegerich. 2004. Fast and effective prediction of microRNA/target duplexes. *RNA* 10:1507-1517.

56. Li, X., and Y.Z. Zhang. 2005. Computational detection of microRNAs targeting transcription factor genes in Arabidopsis thaliana. *Comput Biol Chem* 29:360-367.

57. Brennecke, J., A. Stark, R.B. Russell, and S.M. Cohen. 2005. Principles of MicroRNA-target recognition. *PLoS Biol* 3:404-418.

58. Lewis, B.P., C.B. Burge, and D.P. Bartel. 2005. Conserved seed pairing, often flanked by adenosines, indicates that thousands of human genes are microRNA targets. *Cell* 120:15-20.

59. Grimson, A., K.K.H. Farh, W.K. Johnston, P. Garrett-Engele, L.P. Lim, and D.P. Bartel. 2007. MicroRNA targeting specificity in mammals: Determinants beyond seed pairing. *Mol Cell* 27:91-105.

60. Nielsen, C.B., N. Shomron, R. Sandberg, E. Hornstein, J. Kitzman, and C.B. Burge. 2007. Determinants of targeting by endogenous and exogenous microRNAs and siRNAs. *RNA* 13:1894-1910.

61. Millar, A.A., and P.M. Waterhouse. 2005. Plant and animal microRNAs: similarities and differences. *Funct Integr Genomics* 5:129-135.

62. Shabalina, S.A., and E.V. Koonin. 2008. Origins and evolution of eukaryotic RNA interference. *Trends Ecol Evol* 23:578-587.

63. Li, F., and S.W. Ding. 2006. Virus counterdefense: Diverse strategies for evading the RNA-silencing immunity. *Annu Rev Microbiol* 60:503-531.

64. Covey, S.N., N.S. AlKaff, A. Langara, and D.S. Turner. 1997. Plants combat infection by gene silencing. *Nature* 385:781-782.

65. Ratcliff, F., B.D. Harrison, and D.C. Baulcombe. 1997. A similarity between viral defense and gene silencing in plants. *Science* 276:1558-1560.

66. Hamilton, A.J., and D.C. Baulcombe. 1999. A species of small antisense RNA in posttranscriptional gene silencing in plants. *Science* 286:950-952.

67. Molnar, A., T. Csorba, U. Lakatos, E. Varallyay, C. Lacomme, and J. Burgyan. 2005. Plant virus-derived small interfering RNAs originate predominantly from highly structured single-stranded viral RNAs. *J Virol* 79:7812-7818.

68. Li, H., W. Li, and S. Ding. 2002. Induction and suppression of RNA silencing by an animal virus. *Science* 296:1319-1321.

69. Li, W., H. Li, R. Lu, F. Li, M. Dus, P. Atkinson, E. Brydon, K. Johnson, A. Garcia-Sastre, L. Ball, P. Palese, and S. Ding. 2004. Interferon antagonist proteins of influenza and vaccinia viruses are suppressors of RNA silencing. *Proc Natl Acad Sci U.S.A.* 101:1350-1355.

70. Wang, X.H., R. Aliyari, W.X. Li, H.W. Li, K. Kim, R. Carthew, P. Atkinson, and S.W. Ding. 2006. RNA interference directs innate immunity against viruses in adult Drosophila. *Science* 312:452-454.

71. Lu, R., M. Maduro, F. Li, H.W. Li, G. Broitman-Maduro, W.X. Li, and S.W. Ding. 2005. Animal virus replication and RNAi-mediated antiviral silencing in Caenorhabditis elegans. *Nature* 436:1040-1043.

72. Wilkins, C., R. Dishongh, S.C. Moore, M.A. Whitt, M. Chow, and K. Machaca. 2005. RNA interference is an antiviral defence mechanism in Caenorhabditis elegans. *Nature* 436:1044-1047.

73. Bennasser, Y., S.-Y. Le, M. Yeung, and K.-T. Jeang. 2004. HIV-1 encoded candidate micro-RNAs and their cellular targets. *Retrovirology* 1:43.

74. Pfeffer, S., A. Sewer, M. Lagos-Quintana, R. Sheridan, C. Sander, F.A. Grasser, L.F. van Dyk, C.K. Ho, S. Shuman, M.C. Chien, J.J. Russo, J.Y. Ju, G. Randall, B.D. Lindenbach, C.M. Rice, V. Simon, D.D. Ho, M. Zavolan, and T. Tuschl. 2005. Identification of microRNAs of the herpesvirus family. *Nat Methods* 2:269-276.

75. Pfeffer, S., M. Zavolan, F.A. Grasser, M.C. Chien, J.J. Russo, J.Y. Ju, B. John, A.J. Enright, D. Marks, C. Sander, and T. Tuschl. 2004. Identification of virus-encoded microRNAs. *Science* 304:734-736.

76. Cai, X., S. Lu, Z. Zhang, C.M. Gonzalez, B. Damania, and B.R. Cullen. 2005. Kaposi's sarcoma-associated herpesvirus expresses an array of viral microRNAs in latently infected cells. *Proc Natl Acad Sci U.S.A.* 102:5570-5575.

77. Samols, M.A., J. Hu, R.L. Skalsky, and R. Renne. 2005. Cloning and Identification of a MicroRNA Cluster within the Latency-Associated Region of Kaposi's Sarcoma-Associated Herpesvirus. *J Virol* 79:9301-9305.

78. Grey, F., A. Antoniewicz, E. Allen, J. Saugstad, A. McShea, J.C. Carrington, and J. Nelson. 2005. Identification and Characterization of Human Cytomegalovirus-Encoded MicroRNAs. *J Virol* 79:12095-12099.

79. Omoto, S., M. Ito, Y. Tsutsumi, Y. Ichikawa, H. Okuyama, E. Brisibe, N. Saksena, and Y. Fujii. 2004. HIV-1 nef suppression by virally encoded microRNA. *Retrovirology* 1:44.

80. Omoto, S., and Y.R. Fujii. 2005. Regulation of human immunodeficiency virus 1 transcription by nef microRNA. *J Gen Virol* 86:751-755.

81. Sullivan, C.S., A.T. Grundhoff, S. Tevethia, J.M. Pipas, and D. Ganem. 2005. SV40-encoded microRNAs regulate viral gene expression and reduce susceptibility to cytotoxic T cells. *Nature* 435:682-686.

82. Gupta, A., J.J. Gartner, P. Sethupathy, A.G. Hatzigeorgiou, and N.W. Fraser. 2006. Anti-apoptotic function of a microRNA encoded by the HSV-1 latency-associated transcript. *Nature* 442:82-85.

83. Lecellier, C.H., P. Dunoyer, K. Arar, J. Lehmann-Che, S. Eyquem, C. Himber, A. Saib, and O. Voinnet. 2005. A cellular MicroRNA mediates antiviral defense in human cells. *Science* 308:557-560.

84. Pedersen, I.M., G. Cheng, S. Wieland, S. Volinia, C.M. Croce, F.V. Chisari, and M. David. 2007. Interferon modulation of cellular microRNAs as an antiviral mechanism. *Nature* 449:919-922.

85. Jopling, C.L., M.K. Yi, A.M. Lancaster, S.M. Lemon, and P. Sarnow. 2005. Modulation of hepatitis C virus RNA abundance by a liver-specific microRNA. *Science* 309:1577-1581.

86. Jopling, C.L., S. Schuetz, and P. Sarnow. 2008. Position-dependent function for a tandem microRNA miR-122-binding site located in the hepatitis C virus RNA genome. *Cell Host Microbe* 4:77-85.

87. Kurreck, J. 2009. RNA interference: from basic research to therapeutic applications. *Angew Chem Int Ed* 48:1378-1398.

88. Caplen, N.J., S. Parrish, F. Imani, A. Fire, and R.A. Morgan. 2001. Specific inhibition of gene expression by small double-stranded RNAs in invertebrate and vertebrate systems. *Proc Natl Acad Sci U.S.A.* 98:9742-9747.

89. Marques, J.T., T. Devosse, D. Wang, M. Zamanian-Daryoush, P. Serbinowski, R. Hartmann, T. Fujita, M.A. Behlke, and B.R.G. Williams. 2006. A structural basis for discriminating between self and nonself double-stranded RNAs in mammalian cells. *Nat Biotechnol* 24:559-565.

90. Zhou, D., Q.S. He, C. Wang, J. Zhang, and F. Wong-Staal. 2006. RNA interference and potential applications. *Curr Top Med Chem* 6:901-911.

91. Levy, L., and C.S. Hill. 2005. Smad4 dependency defines two classes of transforming growth factor {beta} (TGF-{beta}) target genes and distinguishes TGF-{beta}-induced epithelial-mesenchymal transition from its antiproliferative and migratory responses. *Mol Cell Biol* 25:8108-8125.

92. Shyu, K.G., W.H. Ko, W.S. Yang, B.W. Wang, and P. Kuan. 2005. Insulin-like growth factor-1 mediates stretch-induced upregulation of myostatin expression in neonatal rat cardiomyocytes. *Cardiovasc Res* 68:405-414.

93. Colland, F., X. Jacq, V. Trouplin, C. Mougin, C. Groizeleau, A. Hamburger, A. Meil, J. Wojcik, P. Legrain, and J.M. Gauthier. 2004. Functional proteomics mapping of a human signaling pathway. *Genome Res* 14:1324-1332.

94. Kamath, R.S., and J. Ahringer. 2003. Genome-wide RNAi screening in Caenorhabditis elegans. *Methods* 30:313-321.

95. Ashrafi, K., F.Y. Chang, J.L. Watts, A.G. Fraser, R.S. Kamath, J. Ahringer, and G. Ruvkun. 2003. Genome-wide RNAi analysis of Caenorhabditis elegans fat regulatory genes. *Nature* 421:268-272.

96. Lee, S.S., R.Y. Lee, A.G. Fraser, R.S. Kamath, J. Ahringer, and G. Ruvkun. 2003. A systematic RNAi screen identifies a critical role for mitochondria in C. elegans longevity. *Nat Genet* 33:40-48.

97. Pothof, J., G. van Haaften, K. Thijssen, R.S. Kamath, A.G. Fraser, J. Ahringer, R.H. Plasterk, and M. Tijsterman. 2003. Identification of genes that protect the C. elegans genome against mutations by genome-wide RNAi. *Genes Dev* 17:443-448.

98. Simmer, F., C. Moorman, A.M. van der Linden, E. Kuijk, P.V. van den Berghe, R.S. Kamath, A.G. Fraser, J. Ahringer, and R.H. Plasterk. 2003. Genome-wide RNAi of C. elegans using the hypersensitive rrf-3 strain reveals novel gene functions. *PLoS Biol* 1:77-84.

99. Lettre, G., E.A. Kritikou, M. Jaeggi, A. Calixto, A.G. Fraser, R.S. Kamath, J. Ahringer, and M.O. Hengartner. 2004. Genome-wide RNAi identifies p53-dependent and -independent regulators of germ cell apoptosis in C. elegans. *Cell Death Differ* 11:1198-1203.

100. Kim, J.K., H.W. Gabel, R.S. Kamath, M. Tewari, A. Pasquinelli, J.F. Rual, S. Kennedy, M. Dybbs, N. Bertin, J.M. Kaplan, M. Vidal, and G. Ruvkun. 2005. Functional genomic analysis of RNA interference in C. elegans. *Science* 308:1164-1167.

101. Kiger, A.A., B. Baum, S. Jones, M.R. Jones, A. Coulson, C. Echeverri, and N. Perrimon. 2003. A functional genomic analysis of cell morphology using RNA interference. *J Biol* 2:27.

102. Paddison, P.J., J.M. Silva, D.S. Conklin, M. Schlabach, M. Li, S. Aruleba, V. Balija, A. O'Shaughnessy, L. Gnoj, K. Scobie, K. Chang, T. Westbrook, M. Cleary, R. Sachidanandam, W.R. McCombie, S.J. Elledge, and G.J. Hannon. 2004. A resource for large-scale RNA-interference-based screens in mammals. *Nature* 428:427-431.

103. Berns, K., E.M. Hijmans, J. Mullenders, T.R. Brummelkamp, A. Velds, M. Heimerikx, R.M. Kerkhoven, M. Madiredjo, W. Nijkamp, B. Weigelt, R. Agami, W. Ge, G. Cavet, P.S. Linsley, R.L. Beijersbergen, and R. Bernards. 2004. A large-scale RNAi screen in human cells identifies new components of the p53 pathway. *Nature* 428:431-437.

104. Brass, A.L., D.M. Dykxhoorn, Y. Benita, N. Yan, A. Engelman, R.J. Xavier, J. Lieberman, and S.J. Elledge. 2008. Identification of Host Proteins Required for HIV Infection Through a Functional Genomic Screen. *Science* 319:921-926.

105. Schlabach, M.R., J. Luo, N.L. Solimini, G. Hu, Q. Xu, M.Z. Li, Z. Zhao, A. Smogorzewska, M.E. Sowa, X.L. Ang, T.F. Westbrook, A.C. Liang, K. Chang, J.A. Hackett, J.W. Harper, G.J. Hannon, and S.J. Elledge. 2008. Cancer proliferation gene discovery through functional genomics. *Science* 319:620-624.

106. Wajapeyee, N., R.W. Serra, X. Zhu, M. Mahalingam, and M.R. Green. 2008. Oncogenic BRAF induces senescence and apoptosis through pathways mediated by the secreted protein IGFBP7. *Cell* 132:363-374.

107. Kim, V.N. 2003. RNA interference in functional genomics and medicine. *J Korean Med Sci* 18:309-318.

108. Campbell, T.N., and F.Y. Choy. 2005. RNA interference: past, present and future. *Curr Issues Mol Biol* 7:1-6.

109. Ralph, G.S., P.A. Radcliffe, D.M. Day, J.M. Carthy, M.A. Leroux, D.C. Lee, L.F. Wong, L.G. Bilsland, L. Greensmith, S.M. Kingsman, K.A. Mitrophanous, N.D. Mazarakis, and M. Azzouz. 2005. Silencing mutant SOD1 using RNAi protects against neurodegeneration and extends survival in an ALS model. *Nat Med* 11:429-433.

110. Raoul, C., T. Abbas-Terki, J.C. Bensadoun, S. Guillot, G. Haase, J. Szulc, C.E. Henderson, and P. Aebischer. 2005. Lentiviral-mediated silencing of SOD1 through RNA interference retards disease onset and progression in a mouse model of ALS. *Nat Med* 11:423-428.

111. Brummelkamp, T.R., R. Bernards, and R. Agami. 2002. Stable suppression of tumorigenicity by virus-mediated RNA interference. *Cancer Cell* 2:243-247.

112. Zhang, L., N. Yang, A. Mohamed-Hadley, S.C. Rubin, and G. Coukos. 2003. Vector-based RNAi, a novel tool for isoform-specific knock-down of VEGF and anti-angiogenesis gene therapy of cancer. *Biochem Biophys Res Commun* 303:1169-1178.

113. Santel, A., M. Aleku, O. Keil, J. Endruschat, V. Esche, G. Fisch, S. Dames, K. Loffler, M. Fechtner, W. Arnold, K. Giese, A. Klippel, and J. Kaufmann. 2006. A novel siRNA-lipoplex technology for RNA interference in the mouse vascular endothelium. *Gene Ther* 13:1222-1234.

114. Subramanian, R., C.S. Gondi, S.S. Lakka, A. Jutla, and J.S. Rao. 2006. siRNA-mediated simultaneous downregulation of uPA and its receptor inhibits angiogenesis and invasiveness triggering apoptosis in breast cancer cells. *Int J Oncol* 28:831-839.

115. Wu, H., W.N. Hait, and J.M. Yang. 2003. Small interfering RNA-induced suppression of MDR1 (P-glycoprotein) restores sensitivity to multidrug-resistant cancer cells. *Cancer Res* 63:1515-1519.

116. Landen, C.N., Jr., A. Chavez-Reyes, C. Bucana, R. Schmandt, M.T. Deavers, G. Lopez-Berestein, and A.K. Sood. 2005. Therapeutic EphA2 gene targeting in vivo using neutral liposomal small interfering RNA delivery. *Cancer Res* 65:6910-6918.

117. Saydam, O., D.L. Glauser, I. Heid, G. Turkeri, M. Hilbe, A.H. Jacobs, M. Ackermann, and C. Fraefel. 2005. Herpes simplex virus 1 amplicon vector-mediated siRNA targeting epidermal growth factor receptor inhibits growth of human glioma cells in vivo. *Mol Ther* 12:803-812.

118. Zhang, S.Z., F.Y. Pan, J.F. Xu, J. Yuan, S.Y. Guo, G. Dai, B. Xue, W.G. Shen, C.J. Wen, D.H. Zhao, and C.J. Li. 2005. Knockdown of c-Met by adenovirus-delivered small interfering RNA inhibits hepatocellular carcinoma growth in vitro and in vivo. *Mol Cancer Ther* 4:1577-1584.

119. Krutzfeldt, J., N. Rajewsky, R. Braich, K.G. Rajeev, T. Tuschl, M. Manoharan, and M. Stoffel. 2005. Silencing of microRNAs in vivo with 'antagomirs'. *Nature* 438:685-689.

120. Elmen, J., M. Lindow, S. Schutz, M. Lawrence, A. Petri, S. Obad, M. Lindholm, M. Hedtjarn, H.F. Hansen, U. Berger, S. Gullans, P. Kearney, P. Sarnow, E.M. Straarup, and S. Kauppinen. 2008. LNA-mediated microRNA silencing in non-human primates. *Nature* 452:896-899.

121. Lu, J., G. Getz, E.A. Miska, E. Alvarez-Saavedra, J. Lamb, D. Peck, A. Sweet-Cordero, B.L. Ebert, R.H. Mak, A.A. Ferrando, J.R. Downing, T. Jacks, H.R. Horvitz, and T.R. Golub. 2005. MicroRNA expression profiles classify human cancers. *Nature* 435:834-838.

122. Calin, G.A., and C.M. Croce. 2006. MicroRNA signatures in human cancers. *Nat Rev Cancer* 6:857-866.

123. Ge, Q., M.T. McManus, T. Nguyen, C.H. Shen, P.A. Sharp, H.N. Eisen, and J.Z. Chen. 2003. RNA interference of influenza virus production by directly targeting mRNA for degradation and indirectly inhibiting all viral RNA transcription. *Proc Natl Acad Sci U.S.A.* 100:2718-2723.

124. Gitlin, L., S. Karelsky, and R. Andino. 2002. Short interfering RNA confers intracellular antiviral immunity in human cells. *Nature* 418:430-434.

125. Jiang, M., and J. Milner. 2002. Selective silencing of viral gene expression in HPV-positive human cervical carcinoma cells treated with siRNA, a primer of RNA interference. *Oncogene* 21:6041-6048.

126. Coburn, G.A., and B.R. Cullen. 2002. Potent and specific inhibition of human immunodeficiency virus type 1 replication by RNA interference. *J Virol* 76:9225-9231.

127. Jacque, J.M., K. Triques, and M. Stevenson. 2002. Modulation of HIV-1 replication by RNA interference. *Nature* 418:435-438.

128. Lee, N.S., T. Dohjima, G. Bauer, H. Li, M.J. Li, A. Ehsani, P. Salvaterra, and J. Rossi. 2002. Expression of small interfering RNAs targeted against HIV-1 rev transcripts in human cells. *Nat Biotechnol* 20:500-505.

129. Novina, C.D., M.F. Murray, D.M. Dykxhoorn, P.J. Beresford, J. Riess, S.K. Lee, R.G. Collman, J. Lieberman, P. Shankar, and P.A. Sharp. 2002. siRNA-directed inhibition of HIV-1 infection. *Nat Med* 8:681-686.

130. Surabhi, R.M., and R.B. Gaynor. 2002. RNA interference directed against viral and cellular targets inhibits human immunodeficiency virus type 1 replication. *J Virol* 76:12963-12973.

131. McCaffrey, A.P., H. Nakai, K. Pandey, Z. Huang, F.H. Salazar, H. Xu, S.F. Wieland, P.L. Marion, and M.A. Kay. 2003. Inhibition of hepatitis B virus in mice by RNA interference. *Nat Biotechnol* 21:639-644.

132. Morrissey, D.V., J.A. Lockridge, L. Shaw, K. Blanchard, K. Jensen, W. Breen, K. Hartsough, L. Machemer, S. Radka, V. Jadhav, N. Vaish, S. Zinnen, C. Vargeese, K. Bowman, C.S. Shaffer, L.B. Jeffs, A. Judge, I. MacLachlan, and B. Polisky. 2005. Potent and persistent in vivo anti-HBV activity of chemically modified siRNAs. *Nat Biotechnol* 23:1002-1007.

133. Kapadia, S.B., A. Brideau-Andersen, and F.V. Chisari. 2003. Interference of hepatitis C virus RNA replication by short interfering RNAs. *Proc Natl Acad Sci U.S.A.* 100:2014-2018.

134. McCaffrey, A.P., L. Meuse, T.T.T. Pham, D.S. Conklin, G.J. Hannon, and M.A. Kay. 2002. Gene expression - RNA interference in adult mice. *Nature* 418:38-39.

135. Randall, G., A. Grakoui, and C.M. Rice. 2003. Clearance of replicating hepatitis C virus replicon RNAs in cell culture by small interfering RNAs. *Proc Natl Acad Sci U.S.A.* 100:235-240.

136. Wilson, J.A., S. Jayasena, A. Khvorova, S. Sabatinos, I.G. Rodrigue-Gervais, S. Arya, F. Sarangi, M. Harris-Brandts, S. Beaulieu, and C.D. Richardson. 2003. RNA interference blocks gene expression and RNA synthesis from hepatitis C replicons propagated in human liver cells. *Proc Natl Acad Sci U.S.A.* 100:2783-2788.

137. Yokota, T., N. Sakamoto, N. Enomoto, Y. Tanabe, M. Miyagishi, S. Maekawa, L. Yi, M. Kurosaki, K. Taira, M. Watanabe, and H. Mizusawa. 2003. Inhibition of intracellular hepatitis C virus replication by synthetic and vector-derived small interfering RNAs. *EMBO Rep* 4:602-608.

138. Wilson, J.A., and C.D. Richardson. 2005. Hepatitis C virus replicons escape RNA interference induced by a short interfering RNA directed against the NS5b coding region. *J Virol* 79:7050-7058.

139. Haasnoot, J., E.M. Westerhout, and B. Berkhout. 2007. RNA interference against viruses: strike and counterstrike. *Nat Biotechnol* 25:1435-1443.

140. Anderson, J., and R. Akkina. 2007. Complete knockdown of CCR5 by lentiviral vector-expressed siRNAs and protection of transgenic macrophages against HIV-1 infection. *Gene Ther* 14:1287-1297.

141. Randall, G., M. Panis, J.D. Cooper, T.L. Tellinghuisen, K.E. Sukhodolets, S. Pfeffer, M. Landthaler, P. Landgraf, S. Kan, B.D. Lindenbach, M. Chien, D.B. Weir, J.J. Russo, J. Ju, M.J. Brownstein, R. Sheridan, C. Sander, M. Zavolan, T. Tuschl, and C.M. Rice. 2007. Cellular cofactors affecting hepatitis C virus infection and replication. *Proc Natl Acad Sci U.S.A.* 104:12884-12889.

142. Jopling, C.L., K.L. Norman, and P. Sarnow. 2006. Positive and negative modulation of viral and cellular mRNAs by liver-specific microRNA miR-122. *Cold Spring Harb Symp On Quant Biol* 71:369-376.

143. Sarnow, P., C.L. Jopling, K.L. Norman, S. Schutz, and K.A. Wehner. 2006. MicroRNAs: expression, avoidance and subversion by vertebrate viruses. *Nat Rev Microbiol* 4:651-659.

144. Triboulet, R., B. Mari, Y.L. Lin, C. Chable-Bessia, Y. Bennasser, K. Lebrigand, B. Cardinaud, T. Maurin, P. Barbry, V. Baillat, J. Reynes, P. Corbeau, K.T. Jeang, and M. Benkirane. 2007. Suppression of microRNA-silencing pathway by HIV-1 during virus replication. *Science* 315:1579-1582.

145. Nelson, P.T., D.A. Baldwin, L.M. Scearce, J.C. Oberholtzer, J.W. Tobias, and Z. Mourelatos. 2004. Microarray-based, high-throughput gene expression profiling of microRNAs. *Nat Methods* 1:155-161.

146. Einat, P. 2006. Methodologies for high-throughput expression profiling of microRNAs. *Methods Mol Biol* 342:139-157.

147. Lagos-Quintana, M., R. Rauhut, A. Yalcin, J. Meyer, W. Lendeckel, and T. Tuschl. 2002. Identification of tissue-specific microRNAs from mouse. *Curr Biol* 12:735-739.

148. Mora, J.R., and R.C. Getts. 2007. High-sensitivity detection methods for low-abundance RNA species: applications for functional genomics research. *Expert Rev Mol Diagn* 7:775-785.

149. Lee, R.C., and V. Ambros. 2001. An extensive class of small RNAs in Caenorhabditis elegans. *Science* 294:862-864.

150. Calin, G.A., C.D. Dumitru, M. Shimizu, R. Bichi, S. Zupo, E. Noch, H. Aldler, S. Rattan, M. Keating, K. Rai, L. Rassenti, T. Kipps, M. Negrini, F. Bullrich, and C.M. Croce. 2002. Frequent deletions and down-regulation of micro- RNA genes miR15 and miR16 at 13q14 in chronic lymphocytic leukemia. *Proc Natl Acad Sci U.S.A.* 99:15524-15529.

151. Wienholds, E., W.P. Kloosterman, E. Miska, E. Alvarez-Saavedra, E. Berezikov, E. de Bruijn, H.R. Horvitz, S. Kauppinen, and R.H. Plasterk. 2005. MicroRNA expression in zebrafish embryonic development. *Science* 309:310-311.

152. Kloosterman, W.P., F.A. Steiner, E. Berezikov, E. de Bruijn, J. van de Belt, M. Verheul, E. Cuppen, and R.H. Plasterk. 2006. Cloning and expression of new microRNAs from zebrafish. *Nucleic Acids Res* 34:2558-2569.

153. Kloosterman, W.P., E. Wienholds, E. de Bruijn, S. Kauppinen, and R.H. Plasterk. 2006. In situ detection of miRNAs in animal embryos using LNA-modified oligonucleotide probes. *Nat Methods* 3:27-29.

154. Nelson, P.T., D.A. Baldwin, W.P. Kloosterman, S. Kauppinen, R.H.A. Plasterk, and Z. Mourelatos. 2006. RAKE and LNA-ISH reveal microRNA expression and localization in archival human brain. *RNA* 12:187-191.

155. Pena, J.T., C. Sohn-Lee, S.H. Rouhanifard, J. Ludwig, M. Hafner, A. Mihailovic, C. Lim, D. Holoch, P. Berninger, M. Zavolan, and T. Tuschl. 2009. miRNA in situ hybridization in formaldehyde and EDC-fixed tissues. *Nat Methods* 6:139-141.

156. Meyers, B.C., F.F. Souret, C. Lu, and P.J. Green. 2006. Sweating the small stuff: microRNA discovery in plants. *Curr Opin Biotechnol* 17:139-146.

157. Schmittgen, T.D., J.M. Jiang, Q. Liu, and L.Q. Yang. 2004. A high-throughput method to monitor the expression of microRNA precursors. *Nucleic Acids Res* 32.

158. Jiang, J., E.J. Lee, Y. Gusev, and T.D. Schmittgen. 2005. Real-time expression profiling of microRNA precursors in human cancer cell lines. *Nucleic Acids Res* 33:5394-5403.

159. Mathieu-Daude, F., R. Cheng, J. Welsh, and M. McClelland. 1996. Screening of differentially amplified cDNA products from RNA arbitrarily primed PCR fingerprints using single strand conformation polymorphism (SSCP) gels. *Nucleic Acids Res* 24:1504-1507.

160. Liu, C.G., G.A. Calin, B. Meloon, N. Gamliel, C. Sevignani, M. Ferracin, C.D. Dumitru, M. Shimizu, S. Zupo, M. Dono, H. Alder, F. Bullrich, M. Negrini, and C.M. Croce. 2004. An oligonucleotide microchip for genome-wide microRNA profiling in human and mouse tissues. *Proc Natl Acad Sci U.S.A.* 101:9740-9744.

161. Babak, T., W. Zhang, Q. Morris, B.J. Blencowe, and T.R. Hughes. 2004. Probing microRNAs with microarrays: Tissue specificity and functional inference. *RNA* 10:1813-1819.

162. Liang, R.Q., W. Li, Y. Li, C.Y. Tan, J.X. Li, Y.X. Jin, and K.C. Ruan. 2005. An oligonucleotide microarray for microRNA expression analysis based on labeling RNA with quantum dot and nanogold probe. *Nucleic Acids Res* 33:e17.

163. Thomson, J.M., J. Parker, C.M. Perou, and S.M. Hammond. 2004. A custom microarray platform for analysis of microRNA gene expression. *Nat Methods* 1:47-53.

164. Miska, E.A., E. Alvarez-Saavedra, M. Townsend, A. Yoshii, N. Sestan, P. Rakic, M. Constantine-Paton, and H.R. Horvitz. 2004. Microarray analysis of microRNA expression in the developing mammalian brain. *Genome Biol* 5:R68.

165. Castoldi, M., S. Schmidt, V. Benes, M. Noerholm, A.E. Kulozik, M.W. Hentze, and M.U. Muckenthaler. 2006. A sensitive array for microRNA expression profiling (miChip) based on locked nucleic acids (LNA). *RNA* 12:913-920.

166. Fang, S., H.J. Lee, A.W. Wark, and R.M. Corn. 2006. Attomole microarray detection of microRNAs by nanoparticle-amplified SPR imaging measurements of surface polyadenylation reactions. *J Am Chem Soc* 128:14044-14046.

167. Castoldi, M., V. Benes, M.W. Hentze, and M.U. Muckenthaler. 2007. miChip: a microarray platform for expression profiling of microRNAs based on locked nucleic acid (LNA) oligonucleotide capture probes. *Methods* 43:146-152.

168. Hartig, J.S., I. Grune, S.H. Najafi-Shoushtari, and M. Famulok. 2004. Sequence-specific detection of microRNAs by signal-amplifying ribozymes. *J Am Chem Soc* 126:722-723.

169. Zeng, Y., and B.R. Cullen. 2003. Sequence requirements for micro RNA processing and function in human cells. *RNA* 9:112-123.

170. Seitz, H., H. Royo, M.L. Bortolin, S.P. Lin, A.C. Ferguson-Smith, and J. Cavaille. 2004. A large imprinted microRNA gene cluster at the mouse Dlk1-Gtl2 domain. *Genome Res* 14:1741-1748.

171. Elbashir, S.M., J. Harborth, K. Weber, and T. Tuschl. 2002. Analysis of gene function in somatic mammalian cells using small interfering RNAs. *Methods* 26:199-213.

172. Reynolds, A., D. Leake, Q. Boese, S. Scaringe, W.S. Marshall, and A. Khvorova. 2004. Rational siRNA design for RNA interference. *Nat Biotechnol* 22:326-330.

173. Heale, B.S.E., H.S. Soifer, C. Bowers, and J.J. Rossi. 2005. siRNA target site secondary structure predictions using local stable substructures. *Nucleic Acids Res* 33:e30.

174. Overhoff, M., M. Alken, R.K.K. Far, M. Lemaitre, B. Lebleu, G. Sczakiel, and I. Robbins. 2005. Local RNA target structure influences siRNA efficacy: A systematic global analysis. *J Mol Biol* 348:871-881.

175. Tafer, H., S.L. Ameres, G. Obernosterer, C.A. Gebeshuber, R. Schroeder, J. Martinez, and I.L. Hofacker. 2008. The impact of target site accessibility on the design of effective siRNAs. *Nat Biotechnol* 26:578-583.

176. Varekova, R.S., I. Bradac, M. Plchut, M. Skrdla, M. Wacenovsky, H. Mahr, G. Mayer, H. Tanner, H. Brugger, J. Withalm, P. Lederer, H. Huber, G. Gierlinger, R. Graf, H. Tafer, I. Hofacker, P. Schuster, and M. Polcik. 2008. www.rnaworkbench.com: A new program for analyzing RNA interference. *Comput Methods Programs Biomed* 90:89-94.

177. Sagan, S.M., R. Koukiekolo, E. Rodgers, N.K. Goto, and J.P. Pezacki. 2007. Inhibition of siRNA binding to a p19 viral suppressor of RNA silencing by cysteine alkylation. *Angew Chem Int Ed* 46:2005-2009.

178. Koukiekolo, R., S.M. Sagan, and J.P. Pezacki. 2007. Effects of pH and salt concentration on the siRNA binding activity of the RNA silencing suppressor protein p19. *FEBS Lett* 581:3051-3056.

179. Cheng, J., S.M. Sagan, N. Assem, R. Koukiekolo, N.K. Goto, and J.P. Pezacki. 2007. Stabilized recombinant suppressors of RNA silencing: Functional effects of linking monomers of Carnation Italian Ringspot virus p19. *Biochim Biophys Acta* 1774:1528-1535.

180. Cheng, J., S.M. Sagan, Z.J. Jakubek, and J.P. Pezacki. 2008. Studies of the interaction of the viral suppressor of RNA silencing protein p19 with small RNAs using fluorescence polarization. *Biochemistry* 47:8130-8138.

181. Supekova, L., F. Supek, J. Lee, S. Chen, N. Gray, J.P. Pezacki, A. Schlapbach, and P.G. Schultz. 2008. Identification of Human Kinases Involved in Hepatitis C Virus Replication by Small Interference RNA Library Screening. *J Biol Chem* 283:29-36.

182. Rakic, B., S.M. Sagan, M. Noestheden, S. Belanger, X.L. Nan, C.L. Evans, X.S. Xie, and J.P. Pezacki. 2006. Peroxisome proliferator-activated receptor alpha antagonism inhibits hepatitis C virus replication. *Chem Biol* 13:23-30.

183. Omarov, R., K. Sparks, L. Smith, J. Zindovic, and H.B. Scholthof. 2006. Biological relevance of a stable biochemical interaction between the tombusvirus-encoded P19 and short interfering RNAs. *J Virol* 80:3000-3008.

184. Sreerama, N., and R.W. Woody. 2000. Estimation of protein secondary structure from circular dichroism spectra: Comparison of CONTIN, SELCON, and CDSSTR methods with an expanded reference set. *Anal Biochem* 287:252-260.

185. Vargason, J.M., G. Szittya, J. Burgyan, and T.M.T. Hall. 2003. Size selective recognition of siRNA by an RNA silencing suppressor. *Cell* 115:799-811.

186. Ye, K.Q., L. Malinina, and D.J. Patel. 2003. Recognition of small interfering RNA by a viral suppressor of RNA silencing. *Nature* 426:874-878.

187. Lohmann, V., F. Korner, J.O. Koch, U. Herian, L. Theilmann, and R. Bartenschlager. 1999. Replication of subgenomic hepatitis C virus RNAs in a hepatoma cell line. *Science* 285:110-113.

188. Yiu, S.M., P.W. Wong, T.W. Lam, Y.C. Mui, H.F. Kung, M. Lin, and Y.T. Cheung. 2005. Filtering of ineffective siRNAs and improved siRNA design tool. *Bioinformatics* 21:144-151.

189. You, S.Y., D.D. Stump, A.D. Branch, and C.M. Rice. 2004. A cis-acting replication element in the sequence encoding the NS5B RNA-dependent RNA polymerase is required for hepatitis C virus RNA replication. *J Virol* 78:1352-1366.

190. Friebe, P., J. Boudet, J. Simorre, and R. Bartenschlager. 2005. Kissing-Loop Interaction in the 3' End of the Hepatitis C Virus Genome Essential for RNA Replication. *J Virol* 79:380-392.

191. MacRae, I.J., E. Ma, M. Zhou, C.V. Robinson, and J.A. Doudna. 2008. In vitro reconstitution of the human RISC-loading complex. *Proc Natl Acad Sci U.S.A.* 105:512-517.

192. Ratcliff, F.G., S.A. MacFarlane, and D.C. Baulcombe. 1999. Gene silencing without DNA: RNA-mediated cross-protection between viruses. *Plant Cell* 11:1207-1215.

193. Lecellier, C.H., and O. Voinnet. 2004. RNA silencing: no mercy for viruses? *Immunol Rev* 198:285-303.

194. Voinnet, O. 2005. Induction and suppression of RNA silencing: Insights from viral infections. *Nat Rev Genet* 6:206-220.

195. Merai, Z., Z. Kerenyi, A. Molnar, E. Barta, A. Valoczi, G. Bisztray, Z. Havelda, J. Burgyan, and D. Silhavy. 2005. Aureusvirus P14 is an efficient RNA silencing suppressor that binds double-stranded RNAs without size specificity. *J Virol* 79:7217-7226.

196. Cui, X.F., G.X. Li, D.W. Wang, D.W. Hu, and X.P. Zhou. 2005. A begomovirus DNA beta-encoded protein binds DNA, functions as a suppressor of RNA silencing, and targets the cell nucleus. *J Virol* 79:10764-10775.

197. Trinks, D., R. Rajeswaran, P.V. Shivaprasad, R. Akbergenov, E.J. Oakeley, K. Veluthambi, T. Hohn, and M.A. Pooggin. 2005. Suppression of RNA silencing by a geminivirus nuclear protein, AC2, correlates with Transactivation of host genes. *J Virol* 79:2517-2527.

198. Vanitharani, R., P. Chellappan, J.S. Pita, and C.M. Fauquet. 2004. Differential roles of AC2 and AC4 of cassava geminiviruses in mediating synergism and suppression of posttranscriptional gene silencing. *J Virol* 78:9487-9498.

199. Chellappan, P., R. Vanitharani, and C.M. Fauquet. 2005. MicroRNA-binding viral protein interferes with Arabidopsis development. *Proc Natl Acad Sci U.S.A.* 102:10381-10386.

200. Qu, F., T. Ren, and T.J. Morris. 2003. The coat protein of turnip crinkle virus suppresses posttranscriptional gene silencing at an early initiation step. *J Virol* 77:511-522.

201. Thomas, C.L., V. Leh, C. Lederer, and A.J. Maule. 2003. Turnip crinkle virus coat protein mediates suppression of RNA silencing in Nicotiana benthamiana. *Virology* 306:33-41.

202. Qi, Y.J., X.H. Zhong, A. Itaya, and B. Ding. 2004. Dissecting RNA silencing in protoplasts uncovers novel effects of viral suppressors on the silencing pathway at the cellular level. *Nucleic Acids Res* 32:e179.

203. Merai, Z., Z. Kerenyi, S. Kertesz, M. Magna, L. Lakatos, and D. Silhavy. 2006. Double-stranded RNA binding may be a general plant RNA viral strategy to suppress RNA silencing. *J Virol* 80:5747-5756.

204. Reed, J.C., K.D. Kasschau, A.I. Prokhnevsky, K. Gopinath, G.P. Pogue, J.C. Carrington, and V.V. Dolja. 2003. Suppressor of RNA silencing encoded by Beet yellows virus. *Virology* 306:203-209.

205. Chapman, E.J., A.I. Prokhnevsky, K. Gopinath, V.V. Dolja, and J.C. Carrington. 2004. Viral RNA silencing suppressors inhibit the microRNA pathway at an intermediate step. *Genes Dev* 18:1179-1186.

206. Ye, K.Q., and D.J. Patel. 2005. RNA silencing suppressor p21 of beet yellows virus forms an RNA binding octameric ring structure. *Structure* 13:1375-1384.

207. Chiba, M., J.C. Reed, A.I. Prokhnevsky, E.J. Chapman, M. Mawassi, E.V. Koonin, J.C. Carrington, and V.V. Dolja. 2006. Diverse suppressors of RNA silencing enhance agroinfection by a viral replicon. *Virology* 346:7-14.

208. Lakatos, L., T. Csorba, V. Pantaleo, E.J. Chapman, J.C. Carrington, Y.P. Liu, V.V. Dolja, L.F. Calvino, J.J. Lopez-Moya, and J. Burgyan. 2006. Small RNA binding is a common strategy to suppress RNA silencing by several viral suppressors. *EMBO J* 25:2768-2780.

209. Lu, R., A. Folimonov, M. Shintaku, W.X. Li, B.W. Falk, W.O. Dawson, and S.W. Ding. 2004. Three distinct suppressors of RNA silencing encoded by a 20-kb viral RNA genome. *Proc Natl Acad Sci U.S.A.* 101:15742-15747.

210. Kreuze, J.F., E.I. Savenkov, W. Cuellar, X.D. Li, and J.P.T. Valkonen. 2005. Viral class 1 RNase III involved in suppression of RNA silencing. *J Virol* 79:7227-7238.

211. Liu, L., J. Grainger, M.C. Canizares, S.M. Angell, and G.P. Lomonossoff. 2004. Cowpea mosaic virus RNA-1 acts as an amplicon whose effects can be counteracted by a RNA-2-encoded suppressor of silencing. *Virology* 323:37-48.

212. Brigneti, G., O. Voinnet, W.X. Li, L.H. Ji, S.W. Ding, and D.C. Baulcombe. 1998. Viral pathogenicity determinants are suppressors of transgene silencing in Nicotiana benthamiana. *EMBO J* 17:6739-6746.

213. Li, H.W., A.P. Lucy, H.S. Guo, W.X. Li, L.H. Ji, S.M. Wong, and S.W. Ding. 1999. Strong host resistance targeted against a viral suppressor of the plant gene silencing defence mechanism. *EMBO J* 18:2683-2691.

214. Goto, K., T. Kobori, Y. Kosaka, T. Natsuaki, and C. Masuta. 2007. Characterization of silencing suppressor 2b of cucumber mosaic virus based on examination of its small RNA-Binding abilities. *Plant Cell Physiol* 48:1050-1060.

215. Lucy, A., H. Guo, W. Li, and S. Ding. 2000. Suppression of post-transcriptional gene silencing by a plant viral protein localized in the nucleus. *EMBO J* 19:1672-1680.

216. Chen, H.Y., J. Yang, C.Q. Lin, and Y. AdamYuan. 2008. Structural basis for RNA-silencing suppression by Tomato aspermy virus protein 2b. *EMBO Rep* 9:754-760.

217. Rashid, U.J., J. Hoffmann, B. Brutschy, J. Piehler, and J.C.H. Chen. 2008. Multiple Targets for Suppression of RNA Interference by Tomato Aspermy Virus Protein 2B. *Biochemistry* 47:12655-12657.

218. Wang, H., K.J. Buckley, X.J. Yang, R.C. Buchmann, and D.M. Bisaro. 2005. Adenosine kinase inhibition and suppression of RNA silencing by geminivirus AL2 and L2 proteins. *J Virol* 79:7410-7418.

219. Te, J., U. Melcher, A. Howard, and J. Verchot-Lubicz. 2005. Soilborne wheat mosaic virus (SBWMV) 19K protein belongs to a class of cysteine rich proteins that suppress RNA silencing. *Virology J* 2:18.

220. Donald, R.G.K., and A.O. Jackson. 1996. RNA-binding activities of barley stripe mosaic virus gamma b fusion proteins. *J Gen Virol* 77:879-888.

221. Yelina, N.E., E.I. Savenkov, A.G. Solovyev, S.Y. Morozov, and J.P.T. Valkonen. 2002. Long-distance movement, virulence, and RNA silencing suppression controlled by a single protein in hordei- and potyviruses: Complementary functions between virus families. *J Virol* 76:12981-12991.

222. Dunoyer, P., S. Pfeffer, C. Fritsch, O. Hemmer, O. Voinnet, and K. Richards. 2002. Identification, subcellular localization and some properties of a cysteine-rich suppressor of gene silencing encoded by peanut clump virus. *Plant J* 29:555 - 567.

223. Dunoyer, P., C.H. Lecellier, E.A. Parizotto, C. Himber, and O. Voinnet. 2004. Probing the microRNA and small interfering RNA pathways with virus-encoded suppressors of RNA silencing. *Plant Cell* 16:1235-1250.

224. Cao, X.S., P. Zhou, X.M. Zhang, S.F. Zhu, X.H. Zhong, Q. Xiao, B. Ding, and Y. Li. 2005. Identification of an RNA silencing suppressor from a plant double-stranded RNA virus. *J Virol* 79:13018-13027.

225. Pfeffer, S., P. Dunoyer, F. Heim, K.E. Richards, G. Jonard, and V. Ziegler-Graff. 2002. P0 of beet western yellows virus is a suppressor of posttranscriptional gene silencing. *J Virol* 76:6815-6824.

226. Bortolamiol, D., M. Pazhouhandeh, K. Marrocco, P. Genschik, and V. Ziegler-Graff. 2007. The polerovirus F box protein PO targets ARGONAUTE1 to suppress RNA silencing. *Curr Biol* 17:1615-1621.

227. Voinnet, O., C. Lederer, and D.C. Baulcombe. 2000. A viral movement protein prevents spread of the gene silencing signal in Nicotiana benthamiana. *Cell* 103:157-167.

228. Anandalakshmi, R., G. Pruss, X. Ge, R. Marathe, A. Mallory, T. Smith, and V. Vance. 1998. A viral suppressor of gene silencing in plants. *Proc Natl Acad Sci U.S.A.* 95:13079-13084.

229. Kasschau, K., and J. Carrington. 1998. A counterdefensive strategy of plant viruses: suppression of posttranscriptional gene silencing. *Cell* 95:461-470.

230. Kasschau, K.D., Z.X. Xie, E. Allen, C. Llave, E.J. Chapman, K.A. Krizan, and J.C. Carrington. 2003. P1/HC-Pro, a viral suppressor of RNA silencing, interferes with Arabidopsis development and miRNA function. *Dev Cell* 4:205-217.

231. Voinnet, O., Y. Pinto, and D. Baulcombe. 1999. Suppression of gene silencing: a general strategy used by diverse DNA and RNA viruses of plants. *Proc Natl Acad Sci U.S.A.* 96:14147-14152.

232. Sire, C., M. Bangratz-Reyser, D. Fargette, and C. Brugidou. 2008. Genetic diversity and silencing suppression effects of Rice yellow mottle virus and the P1 protein. *Virology J* 5:55.

233. Bucher, E., T. Sijen, P. de Haan, R. Goldbach, and M. Prins. 2003. Negative-strand tospoviruses and tenuiviruses carry a gene for a suppressor of gene silencing at analogous genomic positions. *J Virol* 77:1329-1336.

234. Hemmes, H., L. Lakatos, R. Goldbach, J. Burgyan, and M. Prins. 2007. The NS3 protein of Rice hoja blanca tenuivirus suppresses RNA silencing in plant and insect hosts by efficiently binding both siRNAs and miRNAs. *RNA* 13:1079-1089.

235. Schnettler, E., H. Hemmes, R. Goldbach, and M. Prins. 2008. The NS3 protein of rice hoja blanca virus suppresses RNA silencing in mammalian cells. *J Gen Virol* 89:336-340.

236. Kubota, K., S. Tsuda, A. Tamai, and T. Meshi. 2003. Tomato mosaic virus replication protein suppresses virus-targeted posttranscriptional gene silencing. *J Virol* 77:11016-11026.

237. Liu, H., B. Reavy, M. Swanson, and S. MacFarlane. 2002. Functional replacement of the tobacco rattle virus cysteine-rich protein by pathogenicity proteins from unrelated plant viruses. *Virology* 298:232-239.

238. Martin-Hernandez, A.M., and D.C. Baulcombe. 2008. Tobacco rattle virus 16-kilodalton protein encodes a suppressor of RNA silencing that allows transient viral entry in meristems. *J Virol* 82:4064-4071.

239. Martinez-Priego, L., L. Donaire, D. Barajas, and C. Llave. 2008. Silencing suppressor activity of the Tobacco rattle virus-encoded 16-kDa protein and interference with endogenous small RNA-guided regulatory pathways. *Virology* 376:346-356.

240. Silhavy, D., A. Molnar, A. Lucioli, G. Szittya, C. Hornyik, M. Tavazza, and J. Burgyan. 2002. A viral protein suppresses RNA silencing and binds silencing-generated, 21-to 25-nucleotide double-stranded RNAs. *EMBO J* 21:3070-3080.

241. Takeda, A., K. Sugiyama, H. Nagano, M. Mori, M. Kaido, K. Mise, S. Tsuda, and T. Okuno. 2002. Identification of a novel RNA silencing suppressor, NSs protein of Tomato spotted wilt virus. *FEBS Lett* 532:75-79.

242. Chen, J., W.X. Li, D.X. Xie, J.R. Peng, and S.W. Ding. 2004. Viral virulence protein suppresses RNA silencing-mediated defense but upregulates the role of MicroRNA in host gene expression. *Plant Cell* 16:1302-1313.

243. Galiakparov, N., E. Tanne, M. Mawassi, R. Gafny, and I. Sela. 2003. ORF 5 of grapevine virus A encodes a nucleic acid-binding protein and affects pathogenesis. *Virus Genes* 27:257-262.

244. Zhou, Z.S., M. Dell'Orco, P. Saldarelli, C. Turturo, A. Minafra, and G.P. Martelli. 2006. Identification of an RNA-silencing suppressor in the genome of Grapevine virus A. *J Gen Virol* 87:2387-2395.

245. Lu, S.H., and B.R. Cullen. 2004. Adenovirus VA1 noncoding RNA can inhibit small interfering RNA and microRNA biogenesis. *J Virol* 78:12868-12876.

246. Andersson, M.G., P.C.J. Haasnoot, N. Xu, S. Berenjian, B. Berkhout, and G. Akusjarvi. 2005. Suppression of RNA interference by adenovirus virus-associated RNA. *J Virol* 79:9556-9565.

247. Haasnoot, J., W. de Vries, E.J. Geutjes, M. Prins, P. de Haan, and B. Berkhout. 2007. The Ebola virus VP35 protein is a suppressor of RNA silencing. *PLoS Pathog* 3:794-803.

248. Wang, Y., N. Kato, A. Jazag, N. Dharel, M. Otsuka, H. Taniguchi, T. Kawabe, and M. Omata. 2006. Hepatitis C virus core protein is a potent inhibitor of RNA silencing-based antiviral response. *Gastroenterology* 130:883-892.

249. Chen, W.X., Z.Z. Zhang, J. Chen, J. Zhang, Y. Wu, Y. Huang, X.F. Cai, and A.L. Huang. 2008. HCV core protein interacts with Dicer to antagonize RNA silencing. *Virus Res* 133:250-258.

250. Ji, J., A. Glaser, M. Wernli, J.M. Berke, D. Moradpour, and P. Erb. 2008. Suppression of short interfering RNA-mediated gene silencing by the structural proteins of hepatitis C virus. *J Gen Virol* 89:2761-2766.

251. Bennasser, Y., S.Y. Le, M. Benkirane, and K.T. Jeang. 2005. Evidence that HIV-1 encodes an siRNA and a suppressor of RNA silencing. *Immunity* 22:607-619.

252. Johnson, K.L., B.D. Price, L.D. Eckerle, and L.A. Ball. 2004. Nodamura virus nonstructural protein B2 can enhance viral RNA accumulation in both mammalian and insect cells. *J Virol* 78:6698-6704.

253. Sullivan, C.S., and D. Ganem. 2005. A virus-encoded inhibitor that blocks RNA interference in mammalian cells. *J Virol* 79:7371-7379.

254. Iwamoto, T., K. Mise, A. Takeda, Y. Okinaka, K.I. Mori, M. Arimoto, T. Okuno, and T. Nakai. 2005. Characterization of Striped jack nervous necrosis virus subgenomic RNA3 and biological activities of its encoded protein B2. *J Gen Virol* 86:2807-2816.

255. Fenner, B.J., R. Thiagarajan, H.K. Chua, and J. Kwang. 2007. Betanodavirus B2 is an RNA interference antagonist that facilitates intracellular viral RNA accumulation (vol 80, pg 85, 2006). *J Virol* 81:4909-4909.

256. Soldan, S.S., M.L. Plassmeyer, M.K. Matukonis, and F. Gonzalez-Scarano. 2005. La Crosse virus nonstructural protein NSs counteracts the effects of short interfering RNA. *J Virol* 79:234-244.

257. Bucher, E., H. Hemmes, P. de Haan, R. Goldbach, and M. Prins. 2004. The influenza A virus NS1 protein binds small interfering RNAs and suppresses RNA silencing in plants. *J Gen Virol* 85:983-991.

258. Delgadillo, M.O., P. Saenz, B. Salvador, J.A. Garcia, and C. Simon-Mateo. 2004. Human influenza virus NS1 protein enhances viral pathogenicity and acts as an RNA silencing suppressor in plants. *J Gen Virol* 85:993-999.

259. Lichner, Z., D. Silhavy, and J. Burgyan. 2003. Double-stranded RNA-binding proteins could suppress RNA interference-mediated antiviral defences. *J Gen Virol* 84:975-980.

260. Anandalakshmi, R., R. Marathe, X. Ge, J.M. Herr, Jr., C. Mau, A. Mallory, G. Pruss, L. Bowman, and V.B. Vance. 2000. A calmodulin-related protein that suppresses posttranscriptional gene silencing in plants. *Science* 290:142-144.

261. Kennedy, S., D. Wang, and G. Ruvkun. 2004. A conserved siRNA-degrading RNase negatively regulates RNA interference in C. elegans. *Nature* 427:645-649.

262. Hartitz, M.D., G. Sunter, and D.M. Bisaro. 1999. The tomato golden mosaic virus transactivator (TrAP) is a single-stranded DNA and zinc-binding phosphoprotein with an acidic activation domain. *Virology* 263:1-14.

263. Guo, H.S., and S.W. Ding. 2002. A viral protein inhibits the long range signaling activity of the gene silencing signal. *EMBO J* 21:398-407.

264. Ryter, J.M., and S.C. Schultz. 1998. Molecular basis of double-stranded RNA-protein interactions: structure of a dsRNA-binding domain complexed with dsRNA. *EMBO J* 17:7505-7513.

265. Bycroft, M., S. Grunert, A.G. Murzin, M. Proctor, and D. Stjohnston. 1995. Nmr Solution Structure of a Dsrna Binding Domain from Drosophila Staufen Protein Reveals Homology to the N-Terminal Domain of Ribosomal-Protein S5. *EMBO J* 14:3563-3571.

266. Nanduri, S., B.W. Carpick, Y.W. Yang, B.R.G. Williams, and J. Qin. 1998. Structure of the double-stranded RNA-binding domain of the protein kinase PKR reveals the molecular basis of its dsRNA-mediated activation. *EMBO J* 17:5458-5465.

267. Chien, C.Y., Y. Xu, R. Xiao, J.M. Aramini, P.V. Sahasrabudhe, R.M. Krug, and G.T. Montelione. 2004. Biophysical characterization of the complex between double-stranded RNA and the N-terminal domain of the NS1 protein from influenza A virus: evidence for a novel RNA-binding mode. *Biochemistry* 43:1950-1962.

268. Chao, J.A., J.H. Lee, B.R. Chapados, E.W. Debler, A. Schneemann, and J.R. Williamson. 2005. Dual modes of RNA-silencing suppression by Flock House virus protein B2. *Nat Struct Mol Biol* 12:952-957.

269. Llave, C., K.D. Kasschau, and J.C. Carrington. 2000. Virus-encoded suppressor of posttranscriptional gene silencing targets a maintenance step in the silencing pathway. *Proc Natl Acad Sci U.S.A.* 97:13401-13406.

270. Mallory, A.C., B.J. Reinhart, D. Bartel, V.B. Vance, and L.H. Bowman. 2002. A viral suppressor of RNA silencing differentially regulates the accumulation of short interfering RNAs and micro-RNAs in tobacco. *Proc Natl Acad Sci U.S.A.* 99:15228-15233.

271. Park, J.W., S. Faure-Rabasse, M.A. Robinson, B. Desvoyes, and H.B. Scholthof. 2004. The multifunctional plant viral suppressor of gene silencing P19 interacts with itself and an RNA binding host protein. *Virology* 323:49-58.

272. Scholthof, H.B. 2006. Timeline - The Tombusvirus-encoded P19: from irrelevance to elegance. *Nat Rev Microbiol* 4:405-411.

273. Russo, M., J. Burgyan, and G.P. Martelli. 1994. Molecular Biology of Tombusviridae. *Adv Virus Res* 44:381-428.

274. Scholthof, H.B., B. Desvoyes, J. Kuecker, and E. Whitehead. 1999. Biological activity of two tombusvirus proteins translated from nested genes is influenced by dosage control via context-dependent leaky scanning. *Mol Plant Microbe Interact* 12:670-679.

275. Calabrese, J.M., and P.A. Sharp. 2006. Characterization of the short RNAs bound by the P19 suppressor of RNA silencing in mouse embryonic stem cells. *RNA* 12:2092-2102.

276. Lane, D., P. Prentki, and M. Chandler. 1992. Use of Gel Retardation to Analyze Protein-Nucleic Acid Interactions. *Microbiol Rev* 56:509-528.

277. Dumoulin, M., D. Canet, A.M. Last, E. Pardon, D.B. Archer, S. Muyldermans, L. Wyns, A. Matagne, C.V. Robinson, C. Redfield, and C.M. Dobson. 2005. Reduced global copperativity is a common feature underlying the amyloidogenicity of pathogenic lysozyme mutations. *J Mol Biol* 346:773-788.

278. Fandrich, M., V. Forge, K. Buder, M. Kittler, C.M. Dobson, and S. Diekmann. 2003. Myoglobin forms amyloid fibrils by association of unfolded polypeptide segments. *Proc Natl Acad Sci U.S.A.* 100:15463-15468.

279. Chiti, F., M. Stefani, N. Taddei, G. Ramponi, and C.M. Dobson. 2003. Rationalization of the effects of mutations on peptide and protein aggregation rates. *Nature* 424:805-808.

280. Eriksson, A.E., W.A. Baase, X.J. Zhang, D.W. Heinz, M. Blaber, E.P. Baldwin, and B.W. Matthews. 1992. Response of a Protein-Structure to Cavity-Creating Mutations and Its Relation to the Hydrophobic Effect. *Science* 255:178-183.

281. Hannon, G.J. 2002. RNA interference. *Nature* 418:244-251.

282. Baulcombe, D. 2004. RNA silencing in plants. *Nature* 431:356-363.

283. Burgyan, J. 2006. Virus induced RNA silencing and suppression: Defence and counter defence. *J Plant Pathol* 88:233-244.

284. White, K.A., and P.D. Nagy. 2004. Advances in the molecular biology of tombusviruses: Gene expression, genome replication, and recombination. *Prog Nucleic Acid Res Mol Biol* 78:187-226.

285. Havelda, Z., C. Hornyik, A. Crescenzi, and J. Burgyan. 2003. In situ characterization of Cymbidium Ringspot tombusvirus infection-induced posttranscriptional gene silencing in Nicotiana benthamiana. *J Virol* 77:6082-6086.

286. Havelda, Z., C. Hornyik, A. Valoczi, and J. Burgyan. 2005. Defective interfering RNA hinders the activity of a tombusvirus-encoded posttranscriptional gene silencing suppressor. *J Virol* 79:450-457.

287. Voinnet, O., S. Rivas, P. Mestre, and D. Baulcombe. 2003. An enhanced transient expression system in plants based on suppression of gene silencing by the p19 protein of tomato bushy stunt virus. *Plant J* 33:949-956.

288. Uhrig, J.F., T. Canto, D. Marshall, and S.A. MacFarlane. 2004. Relocalization of nuclear ALY proteins to the cytoplasm by the tomato bushy stunt virus P19 pathogenicity protein. *Plant Physiol* 135:2411-2423.

289. Canto, T., J.F. Uhrig, M. Swanson, K.M. Wright, and S.A. MacFarlane. 2006. Translocation of Tomato bushy stunt virus P19 protein into the nucleus by ALY proteins compromises its silencing suppressor activity. *J Virol* 80:9064-9072.

290. Ambros, V. 2004. The functions of animal microRNAs. *Nature* 431:350-355.

291. Mallory, A.C., and H. Vaucheret. 2006. Functions of microRNAs and related small RNAs in plants. *Nat Genet* 38:S31-36.

292. Lakatos, L., G. Szittya, D. Silhavy, and J. Burgyan. 2004. Molecular mechanism of RNA silencing suppression mediated by p19 protein of tombusviruses. *EMBO J* 23:876-884.

293. Lundblad, J.R., M. Laurance, and R.H. Goodman. 1996. Fluorescence polarization analysis of protein-DNA and protein-protein interactions. *Mol Endocrinol* 10:607-612.

294. Banik, U., N.C. Mandal, B. Bhattacharyya, and S. Roy. 1993. A Fluorescence Anisotropy Study of Tetramer-Dimer Equilibrium of Lambda-Repressor and its Implication for Function. *J Biol Chem* 268:3938-3943.

295. Rusinova, E., J.B.A. Ross, T.M. Laue, L.C. Sowers, and D.F. Senear. 1997. Linkage between operator binding and dimer to octamer self-assembly of bacteriophage lambda cI repressor. *Biochemistry* 36:12994-13003.

296. Huang, Y.T., E. Rusinova, J.B.A. Ross, and D.F. Senear. 1997. An aromatic stacking interaction between subunits helps mediate DNA sequence specificity: Operator site discrimination by phage lambda cl repressor. *J Mol Biol* 267:403-417.

297. Weinberg, R.L., S.M.V. Freund, D.B. Veprintsev, M. Bycroft, and A.R. Fersht. 2004. Regulation of DNA binding of p53 by its C-terminal domain. *J Mol Biol* 342:801-811.

298. Chang, J., E. Nicolas, D. Marks, C. Sander, A. Lerro, M.A. Buendia, C. Xu, W.S. Mason, T. Moloshok, R. Bort, K.S. Zaret, and J.M. Taylor. 2004. miR-122, a Mammalian Liver-Specific microRNA, is Processed from hcr mRNA and May Downregulate the High Affinity Cationic Amino Acid Transporter CAT-1. *RNA Biol* 1:106-113.

299. Checovich, W.J., R.E. Bolger, and T. Burke. 1995. Fluorescence Polarization - a New Tool for Cell and Molecular Biology. *Nature* 375:254-256.

300. Griffiths-Jones, S., H.K. Saini, S. van Dongen, and A.J. Enright. 2008. miRBase: tools for microRNA genomics. *Nucleic Acids Res* 36:D154-D158.

301. Steitz, T.A. 1990. Structural Studies of Protein Nucleic-Acid Interaction - the Sources of Sequence-Specific Binding. *Q Rev Biophys* 23:205-280.

302. Tjian, R., and T. Maniatis. 1994. Transcriptional activation - a complex puzzle with few easy pieces. *Cell* 77:5-8.

303. Williamson, J.R. 2000. Induced fit in RNA-protein recognition. *Nat Struct Biol* 7:834-837.

304. Leulliot, N., and G. Varani. 2001. Current topics in RNA-protein recognition: Control of specificity and biological function through induced fit and conformational capture. *Biochemistry* 40:7947-7956.

305. Werner, M.H., A.M. Gronenborn, and G.M. Clore. 1996. Intercalation, DNA kinking, and the control of transcription. *Science* 271:778-784.

306. Hard, T., and T. Lundback. 1996. Thermodynamics of sequence-specific protein-DNA interactions. *Biophys Chem* 62:121-139.

307. Dworkin, J., A.J. Ninfa, and P. Model. 1998. A protein-induced DNA bend increases the specificity of a prokaryotic enhancer-binding protein. *Genes Dev* 12:894-900.

308. Handa, N., O. Nureki, K. Kurimoto, I. Kim, H. Sakamoto, Y. Shimura, Y. Muto, and S. Yokoyama. 1999. Structural basis for recognition of the tra mRNA precursor by the sex-lethal protein. *Nature* 398:579-585.

309. Najmanovich, R., J. Kuttner, V. Sobolev, and M. Edelman. 2000. Side-chain flexibility in proteins upon ligand binding. *Proteins* 39:261-268.

310. Ma, B., M. Shatsky, H.J. Wolfson, and R. Nussinov. 2002. Multiple diverse ligands binding at a single protein site: A matter of pre-existing populations. *Protein Sci* 11:184-197.

311. Gutteridge, A., and J. Thornton. 2005. Conformational changes observed in enzyme crystal structures upon substrate binding. *J Mol Biol* 346:21-28.

312. MacRae, I.J., F. Li, K. Zhou, W.Z. Cande, and J.A. Doudna. 2006. Structure of Dicer and mechanistic implications for RNAi. *Cold Spring Harb Symp Quant Biol* 71:73-80.

313. Ramesh, A., C.G. Savva, A. Holzenburg, and J.C. Sacchettini. 2007. Crystal structure of Rsr, an ortholog of the antigenic Ro protein, links conformational flexibility to RNA binding activity. *J Biol Chem* 282:14960-14967.

314. Bayer, T.S., L.N. Booth, S.M. Knudsen, and A.D. Ellington. 2005. Arginine-rich motifs present multiple interfaces for specific binding by RNA. *RNA* 11:1848-1857.

315. Pelletier, J., and N. Sonenberg. 1988. Internal initiation of translation of eukaryotic mRNA directed by a sequence derived from poliovirus RNA. *Nature* 334:320-325.

316. Tsukiyama-Kohara, K., N. Iizuka, M. Kohara, and A. Nomoto. 1992. Internal ribosome entry site within hepatitis C virus RNA. *J Virol* 66:1476-1483.

317. Belsham, G.J., and N. Sonenberg. 1996. RNA-protein interactions in regulation of picornavirus RNA translation. *Microbiol Rev* 60:499-511.

318. Xiang, W.K., A.V. Paul, and E. Wimmer. 1997. RNA signals in entero- and rhinovirus genome replication. *Semin Virol* 8:256-273.

319. Goodfellow, I., Y. Chaudhry, A. Richardson, J. Meredith, J.W. Almond, W. Barclay, and D.J. Evans. 2000. Identification of a cis-acting replication element within the poliovirus coding region. *J Virol* 74:4590-4600.

320. Haasnoot, P.C., R.C. Olsthoorn, and J.F. Bol. 2002. The Brome mosaic virus subgenomic promoter hairpin is structurally similar to the iron-responsive element and functionally equivalent to the minus-strand core promoter stem-loop C. *RNA* 8:110-122.

321. Mason, P.W., S.V. Bezborodova, and T.M. Henry. 2002. Identification and characterization of a cis-acting replication element (cre) adjacent to the internal ribosome entry site of foot-and-mouth disease virus. *J Virol* 76:9686-9694.

322. Schlesinger, S., S. Makino, and M.L. Linial. 1994. Cis-acting genomic elements and trans-acting proteins involved in the assembly of RNA viruses. *Semin Virol* 5:39-49.

323. Huthoff, H., and B. Berkhout. 2002. Multiple secondary structure rearrangements during HIV-1 RNA dimerization. *Biochemistry* 41:10439-10445.

324. Simmonds, P., A. Tuplin, and D.J. Evans. 2004. Detection of genome-scale ordered RNA structure (GORS) in genomes of positive-stranded RNA viruses: Implications for virus evolution and host persistence. *RNA* 10:1337-1351.

325. Zuker, M. 1989. On finding all suboptimal foldings of an RNA molecule. *Science* 244:48-52.

326. Zuker, M. 2003. Mfold web server for nucleic acid folding and hybridization prediction. *Nucleic Acids Res* 31:3406-3415.

327. Mathews, D.H., J. Sabina, M. Zuker, and D.H. Turner. 1999. Expanded sequence dependence of thermodynamic parameters improves prediction of RNA secondary structure. *J Mol Biol* 288:911-940.

328. Davis, M., S.M. Sagan, J.P. Pezacki, D.J. Evans, and P. Simmonds. 2008. Bioinformatic and physical characterizations of genome-scale ordered RNA structure in mammalian RNA viruses. *J Virol* 82:11824-11836.

329. Muller, D.J., G. Buldt, and A. Engel. 1995. Force-induced conformational change of bacteriorhodopsin. *J Mol Biol* 249:239-243.

330. Schabert, F.A., C. Henn, and A. Engel. 1995. Native Escherichia coli OmpF porin surfaces probed by atomic force microscopy. *Science* 268:92-94.

331. Shao, Z., and Y. Zhang. 1996. Biological cryo atomic force microscopy: a brief review. *Ultramicroscopy* 66:141-152.

332. Rivetti, C., M. Guthold, and C. Bustamante. 1996. Scanning force microscopy of DNA deposited onto mica: equilibration versus kinetic trapping studied by statistical polymer chain analysis. *J Mol Biol* 264:919-932.

333. Hansma, H.G., E. Oroudjev, S. Baudrey, and L. Jaeger. 2003. TectoRNA and 'kissing-loop' RNA: atomic force microscopy of self-assembling RNA structures. *J Microsc* 212:273-279.

334. Alvarez, D.E., M.F. Lodeiro, S.J. Luduena, L.I. Pietrasanta, and A.V. Gamarnik. 2005. Long-range RNA-RNA interactions circularize the dengue virus genome. *J Virol* 79:6631-6643.

335. Kuznetsov, Y.G., S. Daijogo, J. Zhou, B.L. Semler, and A. McPherson. 2005. Atomic force microscopy analysis of icosahedral virus RNA. *J Mol Biol* 347:41-52.

336. Noestheden, M., Q.Y. Hu, A.M. Tonary, L.L. Tay, and J.P. Pezacki. 2007. Evaluation of chemical labeling strategies for monitoring HCV RNA using vibrational microscopy. *Org Biomol Chem* 5:2380-2389.

337. Reed, K.E., and C.M. Rice. 2000. Overview of hepatitis C virus genome structure, polyprotein processing, and protein properties. *Curr Top Microbiol Immunol* 242:55-84.

338. Thomson, B.J., and R.G. Finch. 2005. Hepatitis C virus infection. *Clin Microbiol Infect* 11:86-94.

339. Zou, S., M. Tepper, and S. El Saadany. 2000. Prediction of hepatitis C burden in Canada. *Can J Gastroenterol* 14:575-580.

340. McHutchison, J.G., R. Bartenschlager, K. Patel, and J.M. Pawlotsky. 2006. The face of future hepatitis C antiviral drug development: recent biological and virologic advances and their translation to drug development and clinical practice. *J Hepatol* 44:411-421.

341. Egger, D., B. Wolk, R. Gosert, L. Bianchi, H.E. Blum, D. Moradpour, and K. Bienz. 2002. Expression of hepatitis C virus proteins induces distinct membrane alterations including a candidate viral replication complex. *J Virol* 76:5974-5984.

342. Gosert, R., D. Egger, V. Lohmann, R. Bartenschlager, H.E. Blum, K. Bienz, and D. Moradpour. 2003. Identification of the hepatitis C virus RNA replication complex in Huh-7 cells harboring subgenomic replicons. *J Virol* 77:5487-5492.

343. Bartenschlager, R., and V. Lohmann. 2001. Novel cell culture systems for the hepatitis C virus. *Antiviral Res* 52:1-17.

344. Krieger, N., V. Lohmann, and R. Bartenschlager. 2001. Enhancement of hepatitis C virus RNA replication by cell culture-adaptive mutations. *J Virol* 75:4614-4624.

345. Pietschmann, T., V. Lohmann, A. Kaul, N. Krieger, G. Rinck, G. Rutter, D. Strand, and R. Bartenschlager. 2002. Persistent and transient replication of full-length hepatitis C virus genomes in cell culture. *J Virol* 76:4008-4021.

346. Ikeda, M., M. Yi, K. Li, and S.M. Lemon. 2002. Selectable subgenomic and genome-length dicistronic RNAs derived from an infectious molecular clone of the HCV-N strain of hepatitis C virus replicate efficiently in cultured Huh7 cells. *J Virol* 76:2997-3006.

347. Tuplin, A., J. Wood, D.J. Evans, A.H. Patel, and P. Simmonds. 2002. Thermodynamic and phylogenetic prediction of RNA secondary structures in the coding region of hepatitis C virus. *RNA* 8:824-841.

348. Walewski, J.L., J.A. Gutierrez, W. Branch-Elliman, D.D. Stump, T.R. Keller, A. Rodriguez, G. Benson, and A.D. Branch. 2002. Mutation Master: profiles of substitutions in hepatitis C virus RNA of the core, alternate reading frame, and NS2 coding regions. *RNA* 8:557-571.

349. Pedersen, J.S., I.M. Meyer, R. Forsberg, P. Simmonds, and J. Hein. 2004. A comparative method for finding and folding RNA secondary structures within protein-coding regions. *Nucleic Acids Res* 32:4925-4936.

350. Simmonds, P. 2004. Genetic diversity and evolution of hepatitis C virus--15 years on. *J Gen Virol* 85:3173-3188.

351. Smith, D.B., and P. Simmonds. 1997. Characteristics of nucleotide substitution in the hepatitis C virus genome: constraints on sequence change in coding regions at both ends of the genome. *J Mol Evol* 45:238-246.

352. Le, S.Y., N. Sonenberg, and J.V. Maizel, Jr. 1995. Unusual folding regions and ribosome landing pad within hepatitis C virus and pestivirus RNAs. *Gene* 154:137-143.

353. Wang, C., S.Y. Le, N. Ali, and A. Siddiqui. 1995. An RNA pseudoknot is an essential structural element of the internal ribosome entry site located within the hepatitis C virus 5' noncoding region. *RNA* 1:526-537.

354. Wang, C., and A. Siddiqui. 1995. Structure and function of the hepatitis C virus internal ribosome entry site. *Curr Top Microbiol Immunol* 203:99-115.

355. Otto, G.A., and J.D. Puglisi. 2004. The pathway of HCV IRES-mediated translation initiation. *Cell* 119:369-380.

356. Friebe, P., V. Lohmann, N. Krieger, and R. Bartenschlager. 2001. Sequences in the 5' Nontranslated Region of Hepatitis C Virus Required for RNA Replication. *J Virol* 75:12047-12057.

357. Kim, Y.K., C.S. Kim, S.H. Lee, and S.K. Jang. 2002. Domains I and II in the 5' nontranslated region of the HCV genome are required for RNA replication. *Biochem Biophys Res Commun* 290:105-112.

358. Tanaka, T., N. Kato, M.J. Cho, and K. Shimotohno. 1995. A novel sequence found at the 3' terminus of hepatitis C virus genome. *Biochem Biophys Res Commun* 215:744-749.

359. Tanaka, T., N. Kato, M.J. Cho, K. Sugiyama, and K. Shimotohno. 1996. Structure of the 3' terminus of the hepatitis C virus genome. *J Virol* 70:3307-3312.

360. Kolykhalov, A.A., S.M. Feinstone, and C.M. Rice. 1996. Identification of a highly conserved sequence element at the 3' terminus of hepatitis C virus genome RNA. *J Virol* 70:3363-3371.

361. Blight, K.J., and C.M. Rice. 1997. Secondary structure determination of the conserved 98-base sequence at the 3' terminus of hepatitis C virus genome RNA. *J Virol* 71:7345-7352.

362. You, S., and C.M. Rice. 2008. 3 ' RNA elements in hepatitis C virus replication: Kissing partners and long poly(U). *J Virol* 82:184-195.

363. Tuplin, A., D.J. Evans, and P. Simmonds. 2004. Detailed mapping of RNA secondary structures in core and NS5B-encoding region sequences of hepatitis C virus by RNase cleavage and novel bioinformatic prediction methods. *J Gen Virol* 85:3037-3047.

364. Lee, H., H. Shin, E. Wimmer, and A.V. Paul. 2004. cis-Acting RNA signals in the NS5B c-terminal coding sequence of the hepatitis C virus genome. *J Virol* 78:10865-10877.

365. McMullan, L.K., A. Grakoui, M.J. Evans, K. Mihalik, M. Puig, A.D. Branch, S.M. Feinstone, and C.M. Rice. 2007. Evidence for a functional RNA element in the hepatitis C virus core gene. *Proc Natl Acad Sci U.S.A.* 104:2879-2884.

366. Diviney, S., A. Tuplin, M. Struthers, V. Armstrong, R.M. Elliott, P. Simmonds, and D.J. Evans. 2008. A hepatitis C virus cis-acting replication element forms a long-range RNA-RNA interaction with upstream RNA sequences in NS5B. *J Virol* 82:9008-9022.

367. Holen, T., M. Amarzguioui, M.T. Wiiger, E. Babaie, and H. Prydz. 2002. Positional effects of short interfering RNAs targeting the human coagulation trigger Tissue Factor. *Nucleic Acids Res* 30:1757-1766.

368. Vickers, T.A., S. Koo, C.F. Bennett, S.T. Crooke, N.M. Dean, and B.F. Baker. 2003. Efficient reduction of target RNAs by small interfering RNA and RNase H-dependent antisense agents. A comparative analysis. *J Biol Chem* 278:7108-7118.

369. Bohula, E.A., A.J. Salisbury, M. Sohail, M.P. Playford, J. Riedemann, E.M. Southern, and V.M. Macaulay. 2003. The efficacy of small interfering RNAs targeted to the type 1 insulin-like growth factor receptor (IGF1R) is influenced by secondary structure in the IGF1R transcript. *J Biol Chem* 278:15991-15997.

370. Xu, Y., H.Y. Zhang, D. Thormeyer, O. Larsson, Q. Du, J. Elmen, C. Wahlestedt, and Z. Liang. 2003. Effective small interfering RNAs and phosphorothioate antisense DNAs have different preferences for target sites in the luciferase mRNAs. *Biochem Biophys Res Commun* 306:712-717.

371. Kretschmer-Kazemi Far, R., and G. Sczakiel. 2003. The activity of siRNA in mammalian cells is related to structural target accessibility: a comparison with antisense oligonucleotides. *Nucleic Acids Res* 31:4417-4424.

372. Brown, K.M., C.Y. Chu, and T.M. Rana. 2005. Target accessibility dictates the potency of human RISC. *Nat Struct Mol Biol* 12:469-470.

373. Haasnoot, J., D. Cupac, and B. Berkhout. 2003. Inhibition of virus replication by RNA interference. *J Biomed Sci* 10:607-616.

374. Phipps, K.M., A. Martinez, J. Lu, B.A. Heinz, and G.S. Zhao. 2004. Small interfering RNA molecules as potential anti-human rhinovirus agents: in vitro potency, specificity, and mechanism. *Antiviral Res* 61:49-55.

375. Yuan, J., P.K.A. Cheung, H.M. Zhang, D. Chau, and D. Yang. 2005. Inhibition of coxsackievirus B3 replication by small interfering RNAs requires perfect sequence match in the central region of the viral positive strand. *J Virol* 79:2151-2159.

376. Schubert, S., H.P. Grunert, H. Zeichhardt, D. Werk, V.A. Erdmann, and J. Kurreck. 2005. Maintaining inhibition: siRNA double expression vectors against coxsackieviral RNAs. *J Mol Biol* 346:457-465.

377. Kronke, J., R. Kittler, F. Buchholz, M.P. Windisch, T. Pietschmann, R. Bartenschlager, and M. Frese. 2004. Alternative approaches for efficient inhibition of hepatitis C virus RNA replication by small interfering RNAs. *J Virol* 78:3436-3446.

378. Schubert, S., A. Grunweller, V.A. Erdmann, and J. Kurreck. 2005. Local RNA target structure influences siRNA efficacy: systematic analysis of intentionally designed binding regions. *J Mol Biol* 348:883-893.

379. Birmingham, A., E. Anderson, K. Sullivan, A. Reynolds, Q. Boese, D. Leake, J. Karpilow, and A. Khvorova. 2007. A protocol for designing siRNAs with high functionality and specificity. *Nat Protoc* 2:2068-2078.

380. Donis-Keller, H. 1979. Site specific enzymatic cleavage of RNA. *Nucleic Acids Res* 7:179-192.

381. Elbashir, S.M., J. Martinez, A. Patkaniowska, W. Lendeckel, and T. Tuschl. 2001. Functional anatomy of siRNAs for mediating efficient RNAi in Drosophila melanogaster embryo lysate. *EMBO J* 20:6877-6888.

382. Luo, K.Q., and D.C. Chang. 2004. The gene-silencing efficiency of siRNA is strongly dependent on the local structure of mRNA at the targeted region. *Biochem Biophys Res Commun* 318:303-310.

383. Umemura, K., F. Nagami, T. Okada, and R. Kuroda. 2000. AFM characterization of single strand-specific endonuclease activity on linear DNA. *Nucleic Acids Res* 28:E39.

384. Liu, Z., Z. Li, H. Zhou, G. Wei, Y. Song, and L. Wang. 2005. Imaging DNA molecules on mica surface by atomic force microscopy in air and in liquid. *Microsc Res Tech* 66:179-185.

385. Hansma, H.G., K. Kasuya, and E. Oroudjev. 2004. Atomic force microscopy imaging and pulling of nucleic acids. *Curr Opin Struct Biol* 14:380-385.

386. Drygin, Y.F., O.A. Bordunova, M.O. Gallyamov, and I.V. Yaminsky. 1998. Atomic force microscopy examination of tobacco mosaic virus and virion RNA. *FEBS Lett* 425:217-221.

387. Hansma, H.G., R. Golan, W. Hsieh, S.L. Daubendiek, and E.T. Kool. 1999. Polymerase activities and RNA structures in the atomic force microscope. *J Struct Biol* 127:240-247.

388. Giro, A., A. Bergia, G. Zuccheri, H.H. Bink, C.W. Pleij, and B. Samori. 2004. Single molecule studies of RNA secondary structure: AFM of TYMV viral RNA. *Microsc Res Tech* 65:235-245.

389. Draper, D.E., D. Grilley, and A.M. Soto. 2005. Ions and RNA folding. *Annu Rev Biophys Biomol Struct* 34:221-243.

390. Sushko, M.L., A.L. Shluger, and C. Rivetti. 2006. Simple model for DNA adsorption onto a mica surface in 1:1 and 2:1 electrolyte solutions. *Langmuir* 22:7678-7688.

391. Minks, M.A., D.K. West, S. Benvin, and C. Baglioni. 1979. Structural requirements of double-stranded RNA for the activation of 2',5'-oligo(A) polymerase and protein kinase of interferon-treated HeLa cells. *J Biol Chem* 254:10180-10183.

392. Manche, L., S.R. Green, C. Schmedt, and M.B. Mathews. 1992. Interactions between double-stranded RNA regulators and the protein kinase DAI. *Mol Cell Biol* 12:5238-5248.

393. Kim, D.H., M.A. Behlke, S.D. Rose, M.S. Chang, S. Choi, and J.J. Rossi. 2005. Synthetic dsRNA Dicer substrates enhance RNAi potency and efficacy. *Nat Biotechnol* 23:222-226.

394. Siolas, D., C. Lerner, J. Burchard, W. Ge, P.S. Linsley, P.J. Paddison, G.J. Hannon, and M.A. Cleary. 2005. Synthetic shRNAs as potent RNAi triggers. *Nat Biotechnol* 23:227-231.

395. Gregory, R.I., T.P. Chendrimada, N. Cooch, and R. Shiekhattar. 2005. Human RISC couples microRNA biogenesis and posttranscriptional gene silencing. *Cell* 123:631-640.

396. Grimm, D., K.L. Streetz, C.L. Jopling, T.A. Storm, K. Pandey, C.R. Davis, P. Marion, F. Salazar, and M.A. Kay. 2006. Fatality in mice due to oversaturation of cellular microRNA/short hairpin RNA pathways. *Nature* 441:537-541.

397. Harborth, J., S.M. Elbashir, K. Vandenburgh, H. Manninga, S.A. Scaringe, K. Weber, and T. Tuschl. 2003. Sequence, chemical, and structural variation of small interfering RNAs and short hairpin RNAs and the effect on mammalian gene silencing. *Antisense Nucleic Acid Drug Dev* 13:83-105.

398. Yuan, Y.R., Y. Pei, J.B. Ma, V. Kuryavyi, M. Zhadina, G. Meister, H.Y. Chen, Z. Dauter, T. Tuschl, and D.J. Patel. 2005. Crystal structure of A. aeolicus argonaute, a site-specific DNA-guided endoribonuclease, provides insights into RISC-mediated mRNA cleavage. *Mol Cell* 19:405-419.

399. Ameres, S.L., J. Martinez, and R. Schroeder. 2007. Molecular basis for target RNA recognition and cleavage by human RISC. *Cell* 130:101-112.

400. Rudnick, S.I., J. Swaminathan, M. Sumaroka, S. Liebhaber, and A.M. Gewirtz. 2008. Effects of local mRNA structure on posttranscriptional gene silencing. *Proc Natl Acad Sci U.S.A.* 105:13787-13792.

401. Michelet, L., M. Zaffagnini, C. Marchand, V. Collin, P. Decottignies, P. Tsan, J.M. Lancelin, P. Trost, M. Miginiac-Maslow, G. Noctor, and S.D. Lemaire. 2005. Glutathionylation of chloroplast thioredoxin f is a redox signaling mechanism in plants. *Proc Natl Acad Sci U.S.A.* 102:16478-16483.

402. Noguera-Mazon, V., J. Lemoine, O. Walker, N. Rouhier, A. Salvador, J.P. Jacquot, J.M. Lancelin, and I. Krimm. 2006. Glutathionylation induces the dissociation of 1-Cys D-peroxiredoxin non-covalent homodimer. *J Biol Chem* 281:31736-31742.

403. Koukiekolo, R., Z.J. Jakubek, J. Cheng, S.M. Sagan, and J.P. Pezacki. 2009. Studies of a viral suppressor of RNA silencing p19-CFP fusion protein: A FRET-based probe for sensing double-stranded fluorophore-tagged small RNAs. *Biophys Chem. Accepted for Publication.*

404. Johansen, L.K., and J.C. Carrington. 2001. Silencing on the spot. Induction and suppression of RNA silencing in the Agrobacterium-mediated transient expression system. *Plant Physiol* 126:930-938.

405. Qian, S., X. Zhong, L. Yu, B. Ding, P. de Haan, and K. Boris-Lawrie. 2009. HIV-1 Tat RNA silencing suppressor activity is conserved across kingdoms and counteracts translational repression of HIV-1. *Proc Natl Acad Sci U.S.A.* 106:605-610.

406. Scholthof, H.B. 2007. Heterologous expression of viral RNA interference suppressors: RISC management. *Plant Physiol* 145:1110-1117.

407. Seo, M.Y., S. Abrignani, M. Houghton, and J.H. Han. 2003. Small interfering RNA-mediated inhibition of hepatitis C virus replication in the human hepatoma cell line Huh-7. *J Virol* 77:810-812.

408. Wakita, T., T. Pietschmann, T. Kato, T. Date, M. Miyamoto, Z.J. Zhao, K. Murthy, A. Habermann, H.G. Krasslich, M. Mizokami, R. Bartenschlager, and T.J. Liang. 2005. Production of infectious hepatitis C virus in tissue culture from a cloned viral genome. *Nat Med* 11:905-905.

409. Zhong, J., P. Gastaminza, G. Cheng, S. Kapadia, T. Kato, D.R. Burton, S.F. Wieland, S.L. Uprichard, T. Wakita, and F.V. Chisari. 2005. Robust hepatitis C virus infection in vitro. *Proc Natl Acad Sci U.S.A.* 102:9294-9299.

410. Srisawat, C., and D.R. Engelke. 2002. RNA affinity tags for purification of RNAs and ribonucleoprotein complexes. *Methods* 26:156-161.

411. Martinez, J., A. Patkaniowska, H. Urlaub, R. Luhrmann, and T. Tuschl. 2002. Single-stranded antisense siRNAs guide target RNA cleavage in RNAi. *Cell* 110:563-574.

412. Kertesz, M., N. Iovino, U. Unnerstall, U. Gaul, and E. Segal. 2007. The role of site accessibility in microRNA target recognition. *Nat Genet* 39:1278-1284.

413. Long, D., R. Lee, P. Williams, C.Y. Chan, V. Ambros, and Y. Ding. 2007. Potent effect of target structure on microRNA function. *Nat Struct Mol Biol* 14:287-294.

414. Hofacker, I.L. 2007. How microRNAs choose their targets. *Nat Genet* 39:1191-1192.

415. Obernosterer, G., H. Tafer, and J. Martinez. 2008. Target site effects in the RNA interference and microRNA pathways. *Biochem Soc Trans* 36:1216-1219.

416. Kedde, M., M.J. Strasser, B. Boldajipour, J.A. Oude Vrielink, K. Slanchev, C. le Sage, R. Nagel, P.M. Voorhoeve, J. van Duijse, U.A. Orom, A.H. Lund, A. Perrakis, E. Raz, and R. Agami. 2007. RNA-binding protein Dnd1 inhibits microRNA access to target mRNA. *Cell* 131:1273-1286.

Contributions of Collaborators

I have been very fortunate to be able to study in a highly collaborative environment; and hence, much of the work in this thesis was drawn from collaborative research with talented researchers both locally and internationally. I would like to acknowledge their contributions here.

In *Chapter 3: Development of Protein-based Tools for Studying Small RNAs*, Roger Koukiekolo (National Research Council of Canada) aided in the development of the fluorescence detection assay and cloning of the cysteine mutants. Elisabeth Rodgers (University of Ottawa) aided in the library screen and Katarzyna Kieliszkiewicz (National Research Council of Canada) aided in preparation of some of the cysteine mutant cultures. Jenny Cheng (National Research Council of Canada) aided in CD and cysteine mutant analyses. Results from this chapter have been published, and are reproduced in part with permission from: **Sagan SM**, Koukiekolo R, Rodgers E, Goto NK, and Pezacki JP. Inhibition of siRNA binding to a p19 viral suppressor of RNA silencing by cysteine alkylation. *Angew. Chem. Int. Ed. Engl.* 2007 46 (12): 2005-2009; © Wiley-VCH Verlag GmbH & Co. KGaA; and in Cheng J, Koukiekolo R, Kieliszkiewicz K, **Sagan SM**, and Pezacki JP. Cysteine residues of Carnation Italian ringspot virus p19 suppressor of RNA silencing maintain global structural integrity and stability for siRNA binding. *Biochim Biophys Acta., In Press*, © 2009 with permission from Elsevier.

In *Chapter 4: Investigation of p19-small RNA Interactions,* Jenny Cheng aided in the preparation of the p19 protein, EMSA experiments and fluorescence polarization measurements. Results from this chapter have been published, and are reproduced with

permission from: **Sagan SM**, Cheng J, Jakubek Z, and Pezacki JP. Fluorescence anisotropy studies of the dissociation constants for the protein-RNA interactions of Carnation Italian Ringspot Virus p19 with microRNAs. *Biochemistry.* 2008 Aug; 47(31):8130-8138; © 2008 American Chemical Society.

In *Chapter 5: In Vitro Screening for High Affinity siRNA Interactions with Native Hepatitis C Virus RNA*, Christian Luebbert (National Research Council of Canada) aided in design, printing and analysis of the native target RNA microarrays. Malgosia Pakulska (University of Ottawa) and Jenny Cheng aided in the *in vitro* RISC cleavage assays. The genome-scale ordered RNA structures (GORS) work was carried out in collaboration with Peter Simmonds (University of Edinburgh), Matthew Davis (University of Edinburgh), and David J. Evans (University of Warwick). Figures 4.1, 4.2 and 4.3 have been reproduced in part with permission from: Davis M, **Sagan SM**, Pezacki JP, Evans DJ, and Simmonds P. Bioinformatic and Physical Characterisation of Genome-Scale Ordered RNA Structure (GORS) in Mammalian RNA Viruses. *J. Virol.* 2008 Sep; 82 (23): 11824-11836; © 2008 American Society for Microbiology.

Curriculum Vitae

Dr. Selena M. Sagan

Department of Biochemistry, Microbiology & Immunology, University of Ottawa

And

Steacie Institute for Molecular Sciences, National Research Council of Canada
100 Sussex Drive, Room 2108 Ottawa, ON, K1A 0R6, CANADA
Selena.Sagan@nrc.ca; Tel: (613) 998-9470; Fax: (613) 952-0068

EDUCATION

Degree	*Name of Discipline*	*Institution*	*Country*	*Date*
Bachelor's	Microbiology & Immunology (Min. Pharmacology)	McGill University	Canada	*Sep 2000 – Apr 2004*
Doctorate	Microbiology & Immunology	University of Ottawa	Canada	*Sep 2004 – Jul 2009*

RESEARCH INTERESTS

My principal research focus has centered on the interaction of viruses with the RNA silencing pathway and small RNAs. My research experience thus far has included the development of suppressors of RNA silencing as research tools, micro-RNA (miRNA) profiling, and the development of techniques used to screen for high affinity small-interfering RNAs (siRNAs). This research has entailed the use of a variety of molecular biology laboratory methods and bioinformatics analysis techniques and has led to a number of publications. Currently, my research interests lie within host-virus interactions, particularly in the context of the RNA silencing pathway and the structure of viral RNAs. This includes such questions as:

- How do miRNAs regulate gene expression?
- How do viruses interact with the RNA silencing pathway and/or small RNAs?
- What is the role of miRNA(s) in HCV replication?
- How does the secondary and tertiary structure of viral RNAs influence the viral life cycle and pathogenesis?

- **National Canadian Research Training Program in Hepatitis C virus (NCRTP-HepC) Trainee** (Postdoctoral Fellow) valued at $5 000.00 per year *(Sep 2009 – Aug 2011)*
- **Natural Sciences and Engineering Research Council of Canada (NSERC) Postdoctoral Fellowship (PDF)** valued at $40 000.00 per year *(Sep 2009 – Aug 2011)*
- **15th International Symposium on Hepatitis C virus and Related Viruses Travel Grant** for the cost of travel to the conference in San Antonio, Texas, Oct. 5th-9th, 2008, valued at $800.00 *(Oct 2008)*
- **National Canadian Research Training Program in Hepatitis C virus (NCRTP-HepC) Trainee** (Graduate Student) valued at $23 300.00 per year *(Jul 2008 – Jun 2009)*
- **University of Ottawa Faculty of Medicine Awards of Excellence – Graduate Studies** *(Dec 2007)*
- **Faculty of Graduate and Postdoctoral Studies (FGPS) Travel Grant** for the cost of transportation to the 13th International Meeting on Hepatitis C Virus & Related Viruses, Cairns, Australia. Aug. 27th-31st, 2006, valued at $500.00 *(Sep 2006)*
- **National Research Council of Canada (NRC) Graduate Student Scholarship Supplement Program (GSSSP)** valued at $7 500.00 per year *(Sep 2006 – Aug 2008)*
- **University of Ottawa National Excellence Scholarship** (Tuition, *Sep 2006 – Aug 2008 and Sep 2004 – Aug 2006*)
- **Natural Sciences and Engineering Research Council of Canada (NSERC) Post-graduate scholarship Ph.D. (PGS-D2)** valued at $21 000.00 per year *(Sep 2006 – Aug 2008)*
- **National Research Council of Canada (NRC) Graduate Student Scholarship Supplement Program (GSSSP)** valued at $5 000.00 per year *(Sep 2004 - Aug 2006)*
- **Ontario Graduate Scholarship (OGS)** valued at $15 000 per year *(Declined)*
- **Natural Sciences and Engineering Research Council of Canada (NSERC) Post-graduate scholarship Master's (PGS-M) and PGS-M Extension** valued at $17 300.00 per year *(Sep 2004 - Aug 2005 and Sep 2005 - Aug 2006)*

- **National Research Council of Canada (NRC) Summer Employment Program** (Salaried, *May - Aug 2004 and May - Aug 2003)*
- **Natural Sciences and Engineering Research Council of Canada (NSERC) Undergraduate Student Research Award (USRA)** valued at $4000.00 *(May - Aug 2002 and May - Aug 2001)*

EMPLOYMENT HISTORY

2004, 2003	Summer Research Student, National Research Council of Canada (NRC) Summer Employment Program, Steacie Institute for Molecular Sciences, National Research Council of Canada, Ottawa, Canada
2003-2004	Honours Research Student, McGill University, Montreal, Canada
2002, 2001	Summer Research Student, Adherex Technologies Inc., Ottawa, Canada, Natural Sciences and Engineering Research Council of Canada (NSERC) Undergraduate Student Research Award (USRA) in Industry Student
2000	Summer Research Student, Adherex Technologies Inc., Ottawa, Canada

SCHOLARLY AND ACADEMIC ACTIVITIES

- ***Guest Lecturer*, BCH 3125 - Protein Structure and Function, Department of Biochemistry, University of Ottawa**, Ottawa, Canada *(Spring 2008)*
- **Mentoring**
  - Matthew Goodmurphy *(Summer Student, 2007/2008)*
  - Malgosia Pakulska *(Co-op/Honours Student 2007-2009)*
  - Alison Muir *(Summer Student, 2007)*
  - Naila Assem *(Honours Student, 2006-2007)*
  - Elisabeth Rodgers *(Honours Student, 2005-2006)*
  - Mimi Wang *(Summer Student, 2004)*
- **National Research Council of Canada (NRC) Partners in Education Program**, Ottawa, Canada *(Spring 2006 and 2004)*

- **National Canadian Training Program in Hepatitis C virus (NCRTP-HepC)**
  - NCRTP-HepC trainees participate in the following activities as part of this multidisciplinary program:
    - Webconferenced course: MSC8000Y, Transdisciplinary Studies in Infectious Disease (using hepatitis C virus as a model)
    - Webconferenced Seminar Series
    - Online Journal Club
    - Knowledge Translation
    - Research Electives
    - Liver Clinic Observations
    - Annual Trainee Retreat
    - National and International Conferences

PUBLICATIONS

---

1) Koukiekolo, R., Z.J. Jakubek, J. Cheng, S.M. Sagan, and J.P. Pezacki. Studies of a viral suppressor of RNA silencing p19-CFP fusion protein: A FRET-based probe for sensing double-stranded fluorophore-tagged small RNAs. *Biophys Chem.* 2009 Aug; 143 (3):166-169.

2) Cheng J, Koukiekolo R, Kieliszkiewicz K, **Sagan SM**, and Pezacki JP. Cysteine residues of Carnation Italian ringspot virus p19 suppressor of RNA silencing maintain global structural integrity and stability for siRNA binding. *Biochim. Biophys Acta.* 2009. Aug; 1794 (8): 1197-1203.

3) Pezacki JP, **Sagan SM**, Tonary AM, Rouleau Y, Belanger S, Supekova L, and Su AI. Transcriptional profiling of the effects of 25-hydroxycholesterol on human hepatocyte metabolism and the antiviral state it conveys against the hepatitis C virus. *BMC Chem. Biol.* 2009 Jan; 16 (9): 2.

4) Davis M, **Sagan SM**, Pezacki JP, Evans DJ, and Simmonds P. Bioinformatic and Physical Characterisation of Genome-Scale Ordered RNA Structure (GORS) in Mammalian RNA Viruses. *J. Virol.* 2008 Sep; 82 (23):11824-11836.

5) **Sagan SM**, Cheng J, Jakubek Z, and Pezacki JP. Fluorescence anisotropy studies of the dissociation constants for the protein-RNA interactions of Carnation Italian Ringspot Virus p19 with microRNAs. *Biochemistry.* 2008 Aug; 47(31):8130-8138.

6) Cheng J, **Sagan SM**, Assem N, Koukiekolo R, Goto NK, and Pezacki JP. Stabilized recombinant suppressors of RNA silencing: Functional effects of

linking monomers of Carnation Italian Ringspot virus p19. *Biochim. Biophys. Acta.* 2007 Dec; 1774 (12):1528-1535.

7) Koukiekolo R, **Sagan SM**, and Pezacki JP. Effects of pH and salt concentration on the siRNA binding actitivy of the RNA silencing suppressor protein p19. *FEBS Lett.* 2007 Jun; 581 (16):3051-3056.

8) **Sagan SM**, Koukiekolo R, Rodgers E, Goto NK, and Pezacki JP. Inhibition of siRNA binding to a p19 viral suppressor of RNA silencing by cysteine alkylation. *Angew. Chem. Int. Ed. Engl.* 2007 46 (12):2005-2009

9) **Sagan SM**, Rouleau Y, Leggiadro C, Supekova L, Schultz PG, Su AI, and Pezacki JP. The Influence of Cholesterol and Lipid Metabolism on Host Cell Structure and Hepatitis C Virus Replication. *Biochem. Cell Biol.* 2006 Feb; 84 (1):67-69.

10) Rakic B, **Sagan SM**, Noestheden M, Belanger S, Nan X, Evans CL, Xie XS, and Pezacki JP. Peroxisome Proliferator-activated Receptor α/γ Antagonism Inhibits Hepatitis C Virus Replication through Post-transcriptional Effects. *Chem. Biol.* 2006 Jan; 13 (1):23-30.

ORAL AND POSTER PRESENTATIONS

---

1) **Sagan SM**, Luebbert C, Pakulska M, Cheng J, and Pezacki JP. "Examining the influence of genome structure on siRNA target site accessibility using native hepatitis C virus RNA." *Poster Presentation.* Canadian Association for the Study of the Liver (CASL) 2009 Winter meeting, Banff, AB, *Feb 27th-Mar 1st, 2009.*

2) **Sagan SM**, Luebbert C, Pakulska MM, Cheng J, and Pezacki JP. "Investigating Viral Genome Structure and siRNA Target Site Accessibility Using Native Hepatitis C Virus RNA Microarrays." 15th International Symposium on Hepatitis C Virus and Related Viruses, San Antonio, TX, *Oct 5-9th, 2008.*

3) **Sagan SM**, Luebbert C, and Pezacki JP. "Investigating the microRNA signature of Hepatitis C virus." 15th International Symposium on Hepatitis C Virus and Related Viruses, San Antonio, TX, *Oct 5-9th, 2008.*

4) **Sagan SM**, Luebbert C, Pakulska MM, Cheng J, and Pezacki JP. "Hepatitis C virus and small RNAs: from siRNA design to miRNA profiling." *Oral Presentation.* Invited Lecture, Vaccine and Infectious Disease Organization (VIDO), Saskatoon, SK, *Sep 26th, 2008.*

5) **Sagan SM**, Luebbert C, Pakulska MM, Cheng J, and Pezacki JP. "The microRNA Signature of Hepatitis C Virus: from Pathogenesis to Chronic Disease." *Oral*

Presentation. NRC Genomic and Health Initiative 8th Annual General Meeting, Saskatoon, SK, *Sep 21-25th, 2008.*

6) **Sagan SM** and Pezacki JP. "HCV RNA Microarrays: An *In Vitro* Approach to Screen for High Affinity siRNA Interactions with the HCV Genomic RNA." *Poster Presentation.* Annual Canadian Association for the Study of the Liver (CASL) 2008 Winter Meeting, Montreal, Canada. *Feb 29th-Mar 3rd, 2008.*

7) **Sagan SM**, and Pezacki JP. "*In Vitro* Screening for High Affinity siRNA Interactions with Hepatitis C Virus RNA." *Poster Presentation.* 14th International Symposium on Hepatitis C Virus & Related Viruses, Glasgow, Scotland, UK. *Sep 9-13th, 2007.*

8) **Sagan SM**, Goto NK, and Pezacki JP. "Profiling the Cellular Small RNA Milieu During Hepatitis C virus Replication." *Poster Presentation.* 14th International Symposium on Hepatitis C Virus & Related Viruses, Glasgow, Scotland, UK. *Sep 9-13th, 2007.*

9) **Sagan SM**, Goto NK, and Pezacki JP. "Investigating the Influence of Small RNAs on Hepatitis C Virus Replication." *Poster Presentation.* BMI Student Poster Day, Ottawa, Canada. *May 17th, 2007.*

10) **Sagan SM**, Koukiekolo R, Goto NK, and Pezacki JP. "Small RNA Profiling: The Influence of Small RNAs on Hepatitis C Virus Replication." *Poster Presentation.* 13th International Meeting on Hepatitis C Virus & Related Viruses, Cairns, Australia. *Aug 27-31st, 2006.*

11) **Sagan SM**, Goto NK, and Pezacki JP. "siRNA Suppressor Proteins as Tools for Interrogating Host-Pathogen Interactions." *Oral Presentation.* BMI Graduate Student Seminar Day, Ottawa, Canada. *Feb 22nd, 2006.*

12) **Sagan SM**, Koukiekolo R, Goto NK, and Pezacki JP. "siRNA Suppressor Proteins As Tools For Interrogating Host-Pathogen Interactions." *Poster Presentation.* Ottawa Institute of Systems Biology "Progress in Systems Biology" Symposium, Ottawa, Canada. *Nov 17-18th, 2005.*

13) Rakic B, **Sagan SM**, Noestheden M, Bélanger S, Nan X, Evans C, Xie SX, and Pezacki JP. "Peroxisome Proliferator-activated Receptor α Antagonism Inhibits Hepatitis C Virus Replication through Post-transcriptional Effects." *Poster Presentation.* 12th International Symposium on Hepatitis C Virus and Related Viruses, Montreal, Canada. *Oct 2-6th, 2005.*

14) **Sagan SM**, Goto NK, and Pezacki JP. "Harnessing a Plant Virus siRNA Suppressor Protein for use in Mammalian Cells." *Poster Presentation.* BMI Graduate Student Poster Day, Ottawa, Canada. *Mar 31st, 2005.*